Application of turbulent convection theories for stellar structure and evolution models

Felix Ahlborn

München 2022

Application of turbulent convection theories for stellar structure and evolution models

Felix Ahlborn

Dissertation
der Fakultät für Physik
der Ludwig-Maximilians-Universität
München

vorgelegt von
Felix Ahlborn
aus Witzenhausen

München, den 31.05.2022

Erstgutachter: Prof. Dr. Achim Weiß
Zweitgutachter: Prof. Dr. Rolf-Peter Kudritzki
Tag der mündlichen Prüfung: 01.09.2022

Contents

List of Figures

List of Tables

Zusammenfassung

Die Ausdehnung stellarer Konvektionszonen hat einen tiefgreifenden Einfluss auf die Struktur und Entwicklung von Sternen. Die Größe des konvektiven Kerns wirkt sich direkt auf Altersschätzungen, Leuchtkraft oder nukleosynthetische Erträge von Sternen aus. Die theoretische Beschreibung der Konvektion ist aufgrund der turbulenten Natur der Strömungen jedoch mit großen Unsicherheiten behaftet. Eigentlich sind die physikalischen Prozesse im Sterninneren dreidimensionaler Natur. In eindimensionalen Sternmodellen werden sie jedoch oft durch weitreichende Annahmen über die zugrunde liegende Physik angenähert. Beobachtungen von Sternen mit konvektiv brennenden Kernen haben gezeigt, dass die Größe dieser Kerne durch die sogenannte Mischungswegtheorie, die am häufigsten verwendete Theorie zur Beschreibung der Konvektion in Sternmodellen, erheblich unterschätzt wird. Um die Unterschätzung der Ausdehnung der konvektiven Regionen zu berücksichtigen, wird ad hoc zusätzliches Mischen an den konvektiven Grenzen angewandt, was gemeinhin als Überschießen bezeichnet wird. Das unterstreicht die Notwendigkeit für eine physikalisch vollständigere Theorie der stellaren Konvektion.

In dieser Arbeit wenden wir eine turbulente Konvektionstheorie auf Berechnungen der Sternstruktur und -entwicklung an. Eine turbulente Konvektionstheorie beschreibt die Auswirkungen der Turbulenz auf konvektive Strömungen, ohne die Details der Turbulenz selbst aufzulösen. Wir erörtern zunächst die Bedeutung der Dissipation der kinetischen Energie und entwickeln eine neue Schließbedingung, die die Dissipation durch Schwerewellen mit einbezieht. Anschließend wenden wir unsere verbesserte Theorie der turbulenten Konvektion an, um die Entwicklung von Sternen mit geringer und mittlerer Masse zu modellieren. Wir erörtern, wie die Anwendung der turbulenten Konvektionstheorie die Größe des konvektiven Kerns und die thermische Struktur der konvektiven Überschießzone verändert. Schließlich vergleichen wir die Ergebnisse der turbulenten Konvektionstheorie mit dreidimensionalen hydrodynamischen Simulationen, um die theoretischen Annahmen und Parameterwerte zu testen.

Wir stellen fest, dass die Dissipation durch Schwerewellen ein wichtiger Mechanismus in den Überschießzone der konvektiven Kerne ist, um realistische Kerngrößen zu erhalten. Die Überschießzone ergibt sich in diesem Modell allein aus der Lösung der dynamischen Modellgleichungen, ohne dass sie von außen vorgegeben wird. Wir zeigen, dass die resultierenden konvektiven Kerngrößen in guter Übereinstimmung mit anderen parametrisierten Beschreibungen des Überschießens sind. Die thermische Struktur, die sich aus der Lösung der turbulenten Konvektionstheorie ergibt, zeigt eine Schicht mit subadiabatischer Temperaturstruktur, wie sie zuvor bei vollständigeren Modellen oder hydrodynamischen Simulationen beobachtet wurde. Der Vergleich der Theorie der turbulenten Konvektion mit hydrodynamischen Simulationen zeigt, dass das Modell die stellare Konvektion bereits mit einem akzeptablen Grad an Genauigkeit beschreibt, und weist gleichzeitig auf Mängel des Modells hin, die in zukünftigen Arbeiten behoben werden müssen. Die Anwendung einer Theorie der turbulenten Konvektion ist ein entscheidender Schritt hin zu einer realistischeren Beschreibung der Konvektion in Sternmodellen.

Abstract

The extent of convective regions in stars has a profound impact on stellar structure and evolution. The size of the convective core, directly affects age estimates, luminosities or nucleosynthetic yields of stars. The theoretical description of convection is however subject to major uncertainties due to the turbulent nature of the flows. Intrinsically, the physical processes in the stellar interior are three-dimensional in nature. However, in one-dimensional stellar models, they often get approximated by crude assumptions of the underlying physics. Observations of stars with convectively burning cores have shown that the size of these cores is substantially underestimated by the so-called mixing length theory, the most commonly used theory to describe convection in stellar models. To account for the underestimation of the extent of convective regions, ad hoc additional mixing at convective boundaries is applied, commonly referred to as overshooting. This shows the need for a physically more complete theory of stellar convection.

In this work, we apply a turbulent convection theory to stellar structure and evolution calculations. A turbulent convection theory describes the effects of turbulence on convective flows without resolving any of the details of the turbulence itself. We first discuss the importance of the dissipation of the kinetic energy and develop a new closure mechanism that takes the dissipation by buoyancy waves into account. Subsequently, we apply our improved turbulent convection theory to model the evolution of low- and intermediate-mass stars. We discuss how the application of the turbulent convection theory changes the size of the convective core and thermal structure of the convective overshooting region. Finally, we compare the results of the turbulent convection theory to three-dimensional hydrodynamic simulations to test the theoretical assumptions and parameter values.

We find that the dissipation by buoyancy waves is an important mechanism in the overshooting zones of convective cores to obtain reasonable core sizes. The overshooting zone in this model emerges purely from the solution of the dynamic model equations, without being imposed externally. We show that the resulting convective core sizes are in good agreement with other parametrised descriptions of overshooting. The thermal structure obtained as a solution from the turbulent convection theory shows a layer with subadiabatic temperature structure, as it has been observed previously from more complete models or hydrodynamic simulations. The comparison of the turbulent convection theory to hydrodynamic simulations shows that stellar convection is described already to an acceptable degree of accuracy by the model, while at the same time highlighting shortcomings of the model that need to be addressed in future work. The application of a turbulent convection theory is a crucial step towards a more realistic description of convection in stellar models.

Chapter 1

Introduction

Stars are the building blocks of the universe, the sites of chemical element production, and one of the earliest sources of observations mankind has used to probe the world beyond our own planet. The information we obtain about a star originates almost exclusively from the electromagnetic radiation leaving the stellar surface. Due to the opacity of the stellar material, the deep stellar interior and its structure are inaccessible to direct observations. One way to draw conclusions about the internal structure and evolution of stars are theoretical *stellar models*. Since the middle of the last century, the understanding of stellar structure and evolution theory has made some great advancements by computing numerical stellar models (e.g. Henyey et al. 1959; Kippenhahn et al. 1967). Current stellar models are able to reproduce a multitude of observations obtained at the stellar surface to an acceptable degree of accuracy, for example luminosities, radii, effective temperatures, surface compositions or colour-magnitude diagrams of open and globular clusters. The outcome of stellar models is widely used to make predictions about the chemical evolution of the galaxy or to characterise exoplanetary systems. However, numerical stellar models are simplified, one-dimensional (1D) representations of the actual stellar structure that can not include all the physical details involved. Therefore, it is crucial to make sure that the most relevant physical effects are still captured in the simplified descriptions and that robust assumptions are made.

Solar observations carried out over many decades have revealed that the Sun oscillates in a multitude of eigenmodes, excited by convection in the outer layers. These oscillations, observable at the solar surface, probe the stellar interior and therefore allow for studying the solar structure, a field known as *helioseismology* (e.g. Basu 2016, for a review). Due to the proximity of the Sun, it is possible to obtain vast amounts of observations with unprecedented precision. This allowed for building very accurate solar models and in conjunction with neutrino observations for demonstrating that neutrinos are able to change their original flavour. More recently, the study of global stellar oscillations, known as *asteroseismology*, has brought great advancements to the field of stellar physics (e.g. Aerts et al. 2010). Different processes in the interior are exciting stellar pulsations, making the star oscillate in its eigenmodes. As in the Sun, the stellar oscillations propagate through the stellar interior and become visible at the stellar surface through tiny variations in

stellar brightness. This allows us to pierce through the opaque surface layers and directly probe the stellar structure. Recent space-missions like CoRoT (Baglin et al. 2009), *Kepler* (Koch et al. 2010) and TESS (Ricker et al. 2015) obtained high precision photometric time series of enormous numbers of stars, allowing for accurate asteroseismic studies. This has been for example used to measure the internal sound speed (Bellinger et al. 2017), the size of convective regions (Pedersen et al. 2021), the internal rotation rates (Deheuvels et al. 2012) and the helium content of stars (Verma et al. 2019) other than the Sun. Comparing the results of asteroseismology with stellar models is a very promising way for identifying shortcomings in the stellar models.

One of the physical processes that is still poorly treated in stellar models is *convection*, the transport of energy by means of bulk fluid motion. The difficulty of including convective energy transport in stellar models is very fundamentally related to the nature of the underlying hydrodynamic flows. Due to the large length scales in stellar interiors and the low viscosity, flows in the stellar interior are highly *turbulent*. Even though the equations of hydrodynamics including molecular viscosity are known for 200 years by now (Navier 1822), a unified theory of turbulence has not been derived yet. For stars, convection plays a crucial role, as internal transport processes substantially shape their internal structure. Due to the turbulent nature of the involved flows, the transport of energy and chemical elements by convection is very efficient. In *intermediate and high mass main-sequence stars*, i.e. stars that have about more than two times the mass of the Sun, nuclear fusion on the main sequence proceeds through the so-called CNO cycle. Due to the high energy release rate by the CNO-cycle, the centres of these stars become convective. The properties of the *convective cores* have a strong impact on the lifetime and on the luminosities of the stars. Intermediate mass stars end their lives as white dwarfs, the progenitors of supernovae of type Ia which are the main source of iron in the universe. Further, nucleosynthesis in the asymptotic giant phase, preceding the white dwarf phase, is important to understand the origin of chemical elements on Earth. Therefore, it is crucial to make robust theoretical predictions about the evolution of the intermediate mass stars and the size of their convective cores. In stars with masses similar or below the mass of our Sun or stars in later evolutionary phases, the envelopes of the stars become convective. The properties of this *convective envelope* largely determine the radius of the star. Finally, in deep convective zones, convection determines the temperature gradient and dominates the chemical mixing processes due to its efficiency. This makes an accurate theoretical description of convection crucial for stellar structure and evolution modelling.

Disregarding its importance, convection remains one of the major uncertainties in stellar structure and evolution modelling. A linear instability analysis allows for obtaining an estimate of the convective boundaries. Using the dimensionless temperature gradients, $\nabla_{\rm rad}$— the gradient achieved by pure radiative energy transport— and $\nabla_{\rm ad}$— the gradient achieved by adiabatic energy transport— one finds that the temperature stratification becomes unstable for convection in case $\nabla_{\rm rad} > \nabla_{\rm ad}$ in the absence of composition gradients. This is well known as the *Schwarzschild criterion* (Schwarzschild 1906). More accurate predictions of convective properties are obtained from theoretical convection models. The most commonly used description of convection for stellar models is the so-called *mixing*

length theory (MLT) (Prandtl 1925; Biermann 1932; Böhm-Vitense 1958). In MLT, it is assumed that the mean properties of the turbulent flow can be described using macroscopic fluid elements that have about the size of the so-called *mixing length* and that travel about a mixing length until they dissolve. Despite its simplicity, MLT was used very successfully over many years to model convection in stellar interiors. With ever improving observational facilities and methods, however, more and more deficits of MLT become apparent. One of the main problems of MLT concerns the treatment of convective boundaries. When ignoring compositional effects, the acceleration drops to zero at the Schwarzschild-boundary, while the velocity generally does not. From a theoretical point, it has been shown that convective motions should pass the Schwarzschild boundary and penetrate into the stable layers (Roxburgh 1978, 1992; Zahn 1991). In stable layers, convective motions are braked and the material carried with the flow mixes with the surroundings. Most commonly, the effects of modified thermal and chemical structure beyond the Schwarzschild boundary are summarised under the general notion of *overshooting*. However, different terms are used to describe the processes at convective boundaries in the literature. Often it remains unclear which modifications of the structure are adopted and what is the reference location to determine the extent of the overshooting region. For a more detailed discussion, I refer to Sec. 2.3.2 and Ch. 4. I would like to note that the situation is further complicated by the fact that other processes than convection induce chemical mixing as well, e.g. waves, rotation, tides or atomic diffusion, that cannot easily be differentiated by observations.

In the MLT picture, the convective velocities drop to zero at the formal Schwarzschild boundary, preventing convective mixing beyond this point. In a physical configuration, however, only the acceleration of fluid elements disappears while the velocity generally remains finite. To include the effects of convective overshooting in stellar models in the MLT framework, additional descriptions have to be applied. Early attempts were proposed, for example by Saslaw and Schwarzschild (1965) and Shaviv and Salpeter (1973). For a critical review of these theories, I refer to Renzini (1987). The main effect of convective overshooting on the stellar structure can be mimicked by introducing additional mixing at convective boundaries during stellar evolution, which I will refer to as ad hoc overshooting.

The dynamic timescales of the involved flows are many orders of magnitude shorter than the nuclear timescales of stellar evolution in most evolutionary phases. This poses serious problems for numerical descriptions of convection. Full three-dimensional (3D) *hydrodynamic simulations* are computationally expensive and can cover physical time spans on the order of years only. In contrast, stellar evolution calculations usually need to be computed over at least a couple of million years. At the same time, the computational costs need to be low. Therefore, the direct inclusion of 3D hydrodynamics into stellar evolution calculations is not feasible on present day computers. This means that the effects of convection need to be included into the stellar evolution models by some other means. One way to include the results of 3D simulations into 1D stellar evolution codes is the *Reynolds-averaged-Navier-Stokes* (RANS) analysis, as for example outlined by Viallet et al. (2013) and Arnett et al. (2015). Even though the RANS equations can be written in one spatial dimension, they can not be solved self-consistently, as they still contain a number of terms that require modelling and further assumptions. These models and

assumptions are generally summarised under the term *closure relations*.

To proceed to a set of equations that can be solved self-consistently, a turbulence model needs to involved. The turbulence model provides approximate expressions and models for the unclosed terms from the RANS equations. In combination with the RANS equations, this allows to define a *turbulent convection model* (TCM). The main idea of a TCM is to construct higher order moment equations from the hydrodynamic equations using the RANS analysis and reduce the dimensionality of the problem by averaging over two spatial directions. The resulting equations of the TCM describe the dynamics of convection in an effective way. One main difference of TCM compared to MLT is the occurrence of transport terms. These terms describe the transport of physical quantities, e.g. the *turbulent kinetic energy* (TKE), by means of convective flows, and naturally lead to the emergence of phenomena like convective overshooting without any ad hoc description. As these transport terms connect different layers, they are often termed *non-local*. Furthermore, TCM provide the *convective flux* which allows computing the temperature gradient also in the overshooting region. To date, a number of TCMs have been developed for stellar astrophysics (e.g. Xiong 1978, 1986; Stellingwerf 1982; Kuhfuß 1986, 1987; Canuto 1992, 1993, 1997, 2011; Canuto and Dubovikov 1998; Li and Yang 2007). I would like to point at one specific difference between the different TCMs, that is the treatment of the dissipation rate of TKE. The viscosity of stellar matter is very low, such that the direct computation of this quantity is infeasible in the stellar context. Instead, a model or a closure relation has to be applied. From Kolmogorov's theory of turbulence a simple, local expression can be derived, involving a length scale like in MLT. This is for example applied in models by Xiong (1978); Li and Yang (2001) or Kuhfuß (1987). Problems with the parametrisation of this length scale have been noted already by Zeman and Tennekes (1977) or Moeng (1984). In the stellar TCM by Canuto (1992); Canuto and Dubovikov (1998) or in the earlier 2-equation turbulence models by Jones and Launder (1972); Hanjalić and Launder (1972) the dissipation is computed from a separate dynamical equation, that also allows for the inclusion of non-local effects. For a detailed discussion of the dissipation rate of TKE I refer to Ch. 3.

Despite the numerical challenges posed by 3D hydrodynamical simulations (see Kupka and Muthsam 2017, for a discussion), they can serve as an important tool to study stellar convection. By now a large range of numerical codes is available, e.g. `FLASH` (Fryxell et al. 2000), `PROMPI` (Meakin and Arnett 2007), `SLH` (Miczek 2013; Edelmann 2014; Edelmann et al. 2021), `MUSIC` (Viallet et al. 2016), `MAESTRO` (Almgren et al. 2006a,b, 2008; Nonaka et al. 2010), `ANTARES` (Muthsam et al. 2010) to only cite a few, that solve the hydrodynamic equations for stellar conditions. Even though these codes are designed to compute similar quantities, i.e. the 3D velocity field, there is a multitude of numerical approaches. On the one hand, there are direct numerical simulations that resolve all spatial scales down to the dissipation scale, where the TKE finally transforms into thermal energy. On the other hand there are so-called large eddy simulations, that do not resolve the smallest spatial scales, however, introduce a subgrid model to dissipate the kinetic energy. This has the advantage to reduce the spatial resolution. In the context of stellar core convection, further problems arise due to the low Mach number of the flows and from maintaining

an exact hydrostatic background state (e.g. Miczek et al. 2015; Edelmann et al. 2021). Further simplifying assumptions for 3D simulations concern the general geometry of the setup, for example only simulating a wedge instead of a full sphere, or to increase the stellar luminosity to increase the convective velocities. Due to the long stellar evolution timescale, it has not yet been possible to simulate the complete evolution of a star in 3D. Instead, always snapshots from a stellar evolution sequence are considered. This proceeds mostly through taking a hydrostatic model from a 1D stellar evolution code as an initial model for the hydrodynamic simulation (see for example Higl et al. 2021). Even though the thermal timescale is shorter than the nuclear timescale, it is still long compared to the timescale of 3D simulations. Hence, the simulation results obtained may depend more or less strongly on the chosen initial model. This short discussion shows that also 3D simulations are subject to methodological and fundamental uncertainties. As a consequence, the results of 3D simulations have to be analysed with some care, keeping in mind the shortcomings and limitations. At this point, 3D simulations could also benefit from the RANS analysis and TCM. The RANS analysis as such is analytically exact, and computing the terms for data from 3D simulations allows for a detailed analysis of the simulation results and an understanding of the behaviour of the physical processes in the simulation. Due to the chaotic behaviour of turbulent flows, also the simulation results need to be treated with statistical methods. The TCM provides predictions for the convective variables. Comparing them to the 3D simulations may help to identify problems with the simulation. A more detailed discussion on comparing 3D simulations and 1D stellar models may be found in Ch. 5.

In this thesis, I will discuss the problem of stellar convection from different points of view with the aim to improve the modelling of turbulent convection in one-dimensional stellar models. To start with I would like to give an overview of the theory of convection starting from the fundamental equations of hydrodynamics, proceed with general remarks on turbulent flows, a discussion of the RANS equations and more detailed descriptions of stellar mixing prescriptions and TCM. In this work, I have finalised the implementation of the Kuhfuß (1987) TCM into the one-dimensional *GARching STellar Evolution Code* (GARSTEC, Weiss and Schlattl 2008). In Ch. 3 I present a new closure relation for the dissipation term of TKE that takes the dissipation by buoyancy waves into account (Kupka et al. 2022). In Ch. 4 I discuss results of the (Kuhfuß 1987) TCM applied in GARSTEC and how the dissipation expression from Ch. 3 behaves (Ahlborn et al. 2022). The properties of the convection model are discussed for main-sequence stars of low and intermediate mass, i.e. between 1.5 and 8 $M_\odot$ with a focus on the emergence of overshooting zones adjacent to the convective core. I compare the results of the TCM to stellar models using MLT and an ad hoc overshooting description. I demonstrate that the results of the TCM are in good agreement with the ad hoc descriptions that have been calibrated to observations. In Ch. 5 I will compare the results of the 1D stellar models to 3D hydrodynamical simulations to test the assumptions and approximations of the Kuhfuß (1987) TCM. I show that the TCM is able to reproduce a number of important features of the hydrodynamic simulations. I will close in Ch. 6 with an outlook on future developments and conclusions.

Chapter 2

Theoretical background

Even though the general structure of stars is well described using the assumption of hydrostatic equilibrium, stars are not strictly static. Due to the nuclear burning in the centre, the stellar structure changes and the star evolves. This is well described by alternately computing the hydrostatic stellar structure for a given composition and subsequently evolving the chemical composition for the given structure. However, in the stellar interior also flows of gas can occur, which makes describing the structure of stars also a hydrodynamic problem. Flows in the stellar interior become especially important for the overall stellar structure as soon as they are involved in the energy transport or the mixing of chemical elements. In stellar interiors, energy is transported by different means: radiation, convection and conduction. Here, convection and radiation are the dominant means of energy transport under most circumstances. This makes the theory of convection an important ingredient for any stellar model. In this chapter, I will discuss the fundamental physical concepts that form the theoretical foundation of the present thesis. I will start by discussing most generally the theoretical equations governing hydrodynamics. Subsequently, I will proceed by describing turbulent flows and their modelling needed for Ch. 5. Further, I will discuss stellar convection and mixing prescriptions and close with the specific stellar convection models used in Ch. 3 and 4.

The fundamentals of modern hydrodynamics have been worked out in the first half of the 19th century by Navier (1822) and Stokes (1845) (see also Stokes 2009) who derived the dynamic equations of fluid motions including viscosity, today known to us as the *Navier-Stokes equation*. A more modern discussion may be found in Landau and Lifshitz (2007). In a general form the Navier-Stokes equation then reads

$$\rho\left(\frac{\partial \boldsymbol{u}}{\partial t}+(\boldsymbol{u}\cdot\boldsymbol{\nabla})\boldsymbol{u}\right)=-\boldsymbol{\nabla}p+\rho\boldsymbol{g}+\boldsymbol{\nabla}\cdot\boldsymbol{\sigma}\,. \tag{2.1}$$

Here $\boldsymbol{u}=\boldsymbol{u}(\boldsymbol{x},t)$ denotes the fluid velocity, p the pressure, $\boldsymbol{g}$ the gravitational acceleration, $\boldsymbol{\sigma}$ the viscous stress tensor and ρ the density. Here and in the following, I denote three-dimensional vectors and tensors with boldface. To describe the dynamics of convection, two

more conservation equations are invoked: the *conservation of mass* (continuity equation)

$$\frac{\partial \rho}{\partial t} + \boldsymbol{\nabla} \cdot (\rho \boldsymbol{u}) = 0\,, \tag{2.2}$$

and the *conservation of energy* that can be generally written as

$$\frac{\partial}{\partial t}\left(\frac{\rho \boldsymbol{u}^{\,2}}{2} + \rho e\right) = -\boldsymbol{\nabla} \cdot \underbrace{\left[\rho \boldsymbol{u}\left(\frac{\boldsymbol{u}^{\,2}}{2} + h\right) - (\boldsymbol{u}\boldsymbol{\sigma}) + \boldsymbol{q}\right]}_{\text{energy current density}} + \rho \boldsymbol{u} \cdot \boldsymbol{g} + \rho \varepsilon\,, \tag{2.3}$$

with the specific internal energy e and the specific enthalpy h. With $\boldsymbol{q}$ I denote the flux of energy due to other reasons than the fluid flow, i.e. energy flux due to conduction or radiation. Finally, ε is the specific energy generation or loss rate, e.g. through thermonuclear processes or neutrino losses. This equation reflects the change of the total fluid energy due to different processes, i.e. the transport of matter (first term, in the square brackets), viscous dissipation (second term, in the square brackets), conductivity (third term, in the square brackets), potential energy ($\rho \boldsymbol{g} \cdot \boldsymbol{u}$) (fourth term) or the release of energy due to nuclear burning ($\rho\varepsilon$) (last term).

The energy conservation equation Eq. (2.3) can be rewritten into a dynamic equation for the specific entropy s

$$\rho T\left(\frac{\partial s}{\partial t} + (\boldsymbol{u} \cdot \boldsymbol{\nabla}) s\right) = \rho\varepsilon - \boldsymbol{\nabla} \cdot \boldsymbol{q} + \sigma_{ij} \frac{\partial u_i}{\partial x_j}\,, \tag{2.4}$$

where T denotes the temperature (Landau and Lifshitz 2007). Here and in the following, summation over identical indices is implicitly assumed. This form of the energy conservation equation is more suitable for the following derivation of the dynamic convection equations. A very common approximation for the energy flux $\boldsymbol{q}$ is to follow *Fick's* first law and assume that energy flows in the opposite direction of the temperature gradient, i.e. to assume that radiation or conduction behave analogous to particles diffusing in a fluid. The energy flux $\boldsymbol{q}$ is commonly written as

$$\boldsymbol{q} = -k_{\mathrm{rad}} \boldsymbol{\nabla} T\,, \tag{2.5}$$

where k_{rad} is a diffusion coefficient that needs to be specified.

This set of equations and an equation of state in principle fully describes stellar convection. A solution of these equations is possible by means of state-of-the-art three-dimensional hydrodynamic simulations e.g. `SLH` (Edelmann et al. 2021), `MAESTRO` (Nonaka et al. 2010), `ANTARES` (Muthsam et al. 2010) for stellar conditions. However, these numerical hydrodynamic simulations are facing several methodological challenges like the dissipation of kinetic energy, the fundamental physical parameters of the involved flows and the simulation timescales and numerical costs. This makes the direct combination of hydrodynamic simulations and stellar models impossible for the near future, and implies that only the global three-dimensional effects of the hydrodynamic flows can be included

in the stellar models. This highlights the need for a thorough analysis of the theory of convection and the development of a simplified but yet physically accurate stellar convection model, i.e. incorporating *the most relevant* physical effects. This is the overarching question I want to address in this thesis.

2.1 Turbulent flows

First analytical solutions of the Navier-Stokes equations have been derived by Poiseuille, who investigated the flow profile of a *laminar* flow in pipes. Apart from laminar flows, flows can also appear as *turbulent*. This has for example first been investigated systematically by Reynolds (1883). The distinction between a laminar and a turbulent flow has been for example recognised through a change in the resistance of the fluid flow. While in a laminar flow the friction can be computed according to Stoke's law predicting that the resistance increases proportional to the velocity, in a turbulent flow the resistance increases as the velocity squared. In a pioneering experiment Reynolds (1883) has investigated the behaviour of a flow in pipes with different diameters and analysed at which flow velocity the behaviour of the flow fundamentally changes from laminar to turbulent motion. To determine whether the flow is turbulent or not, he used a colour stream injected into the flow, and hence he directly probed the turbulent mixing. His experiments led him to formulate the by now well known *Reynolds number*

$$\mathrm{Re} = \frac{U \cdot l_0}{\nu} \,,$$

where U and l_0 are typical velocity and length scales of the problem, while ν is the kinematic viscosity. This dimensionless number is used to characterise the nature of a flow. Flows with low Reynolds numbers are laminar, while for high Reynolds numbers flows become turbulent. Further, groundbreaking experiments have been carried out on convection between two plates by Strutt (1916) (more commonly known as Lord Rayleigh) or the study of a fluid between two rotating cylinders by Taylor (1923). Both experiments led to further similarity numbers termed after their discoverers the Rayleigh and Taylor number respectively. In stars, we face the situation of very large length scales and very low viscosities, which lead to very high Reynolds numbers and in turn highly turbulent flows. Estimates for stellar convective flows provide Reynolds numbers on the order of 10^{10} to 10^{14} (Kupka and Hillebrandt 2009; Kupka 2009). As a consequence, the role of turbulence for stellar structure and evolution needs to be thoroughly investigated. The above discussion shows that even though laminar and turbulent flows obey the same set of equations, their physical nature is fundamentally different.

To describe some of the fundamental concepts behind turbulence, I will follow the discussion in Pope (2000) (see also Davidson 2015). The motions of a fluid are theoretically described by the Navier-Stokes equations. Derived from classical mechanics, these equations are *deterministic* in nature. However, repeating a measurement in a turbulent flow for given initial conditions at given time and location will lead to randomly distributed

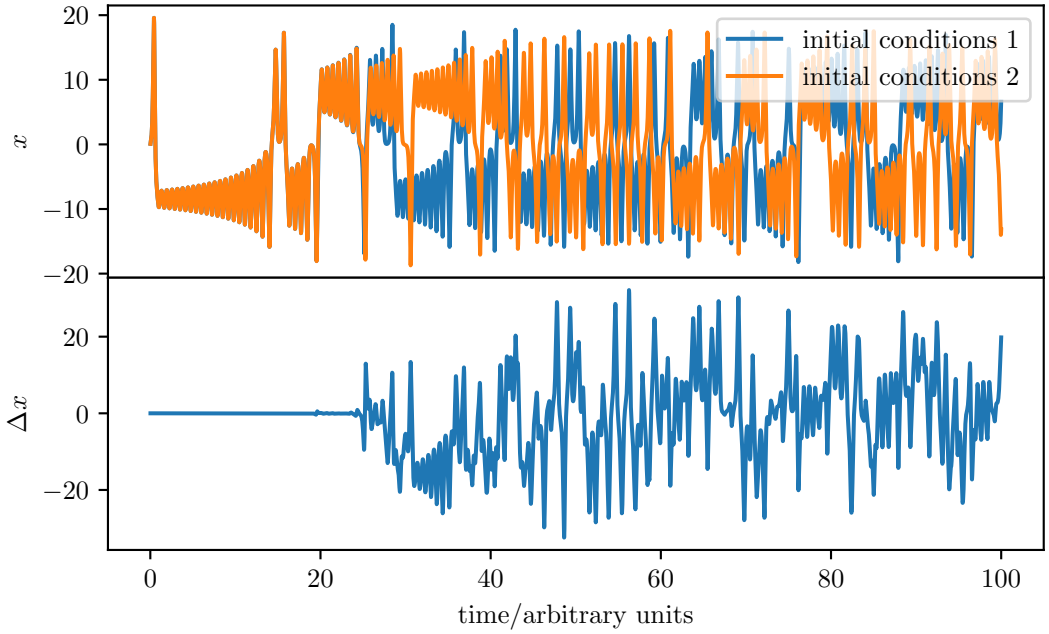

Figure 2.1: Solution for the variable x to the equations of Lorenz (1963) for parameter values $s = 10, r = 28, b = 8/3$. The upper panel shows two time series for initial conditions $\boldsymbol{x}_1 = [0, 1, 1.05]$ and $\boldsymbol{x}_2 = [10^{-5}, 1, 1.05]$. The lower panel shows the difference between the two time series. (see also Fig. 3.2 in Pope 2000)

results. This seems to be in contradiction to the deterministic nature of the underlying equations. This behaviour can be understood by drawing analogies to other deterministic systems of equations. For example, Lorenz (1963) discusses the behaviour of the solutions of a set of deterministic differential equations, describing a very simplified convection model derived by Saltzman (1962). The model describes the time-evolution of three convective variables x, y and z and contains three parameters, commonly denoted as s, r and b. Lorenz (1963) shows that the solutions are unstable with respect to small perturbations for a given set of parameters, i.e. the solutions become *chaotic*. The solution becomes unstable as soon as the model parameter related to the Rayleigh number exceeds a critical value. The behaviour of the Lorenz (1963) model is illustrated in Fig. 2.1. The upper panel shows two time series of the convective variable x for two different sets of initial conditions. The initial conditions are chosen such that only one of three values has been increased by 10^{-5}. While both time series evolve similarly in the beginning, as of $t = 35$ they start to diverge. This is even better illustrated in the lower panel, showing the difference between the two time series. The differences seem completely random after the initial phase. This means that even when knowing the solution for one set of initial conditions, the outcome for an only slightly different set of initial conditions can not be predicted. In practical applications the initial conditions can never be fully specified, e.g. due to measurement uncertainties, which makes the behaviour of this or similar sets of equations unpredictable.

The transition of the solutions into a chaotic regime, with a special focus on the transition into turbulence, has been mathematically described by Ruelle and Takens (1971) (see also Lanford 1982). However, other transitions into turbulence have been discussed as well (Landau and Lifshitz 2007).

Such a chaotic behaviour is known from even simpler non-linear deterministic equations, like the logistic equation describing the variation of a population. Today, this field of research is known as *deterministic chaos*. Due to its non-linearity, the Navier-Stokes equation is subject to the same fundamental behaviour. As soon as the Reynolds number is high enough, the solution of the Navier-Stokes equation becomes unstable for small perturbations. Considering that the initial conditions in an experiment can not be identically repeated, the solution of the hydrodynamic equations will diverge such that a repeated measurement of a variable at the same time and location appears to be random. Given two fluid particles residing next to each other, having very similar initial conditions, we can distinguish the following two cases: In a laminar flow one would expect that the paths of these two fluid particles follow each other, despite the small difference in the initial conditions. In a turbulent flow, however, the solutions to the equations are chaotic and even particles with very similar initial conditions will end up in very different locations with very different velocities. This shows very clearly why turbulence is so efficient in mixing fluids. The divergence of the initially close fluid particles happens with the flow velocity, i.e. on a dynamical timescale, which is of course much shorter than the timescale of atomic diffusion. Carrying their initial chemical composition with them, turbulent fluid particles very quickly homogenise the composition in a turbulent area.

From the above discussion, it follows that it is practically impossible to follow the details of turbulence. Neither the measurements in an experiment—subject to measurement errors— nor the results of computer simulations—subject to rounding errors—reach the required level of accuracy to exactly describe the turbulent flow. This implies that for practical purposes, quantities subject to turbulent flows are *random variables with stochastic variations*. While the details of the turbulent flow remain intractable, statistical quantities may be extracted that are of practical use. While any two repetitions of a turbulent flow will lead to different results, the average of, for example, the velocity is a well-defined quantity. Therefore, many turbulence theories aim at describing turbulence with stochastic methods e.g. evaluating mean values, variances, probability densities and correlation functions. In analogy to the moment expansion of a probability density function, the Navier-Stokes equation could be described by giving all its moments. In practical terms, it is of course equally impossible to compute an infinite number of moments or to compute an exact solution of the Navier-Stokes equation for a turbulent flow. In Sec. 2.2 I will review how the evolution equations of the statistical moments of the hydrodynamic variables can be derived analytically from the Navier-Stokes equation.

One of the first statistical theories of developed turbulence for high Reynolds numbers has been derived in the pioneering work of Kolmogorov (1941). This view of turbulence is based on the idea of the *energy or turbulent cascade*, derived earlier by Richardson (1922). In the energy cascade, it is assumed that large eddies in the flow break up into subsequently smaller eddies, transferring their kinetic energy to smaller and smaller scales. This transfer

of energy is driven by inertial forces, not by viscosity. From the *first Kolmogorov similarity hypothesis* one can deduce that, at the smallest scale, today known as the *Kolmogorov dissipation scale* η, viscous effects become important and energy is finally dissipated. It is defined as

$$\eta = \left(\frac{\nu^3}{\epsilon}\right)^{1/4} , \tag{2.6}$$

where ϵ refers to the *dissipation rate of the kinetic energy* of the flow. This can be transformed to see that the ratio of the integral length scale l_0 to the Kolmogorov dissipation scale η scales as

$$\frac{\eta}{l_0} \propto \mathrm{Re}^{-3/4} . \tag{2.7}$$

For very high Reynolds numbers, which we consider and also encounter in stellar interior flows, this shows that a huge contrast in scales is to be expected between the large flow scale l_0 and the dissipation scale η. The *second Kolmogorov similarity hypothesis* than formulates that there is a range in which $l_\mathrm{i} \gg \eta$ and the effects of viscosity are still negligible while inertial forces dominate. Therefore, this range is also called inertial subrange. In the inertial range, the statistical behaviour of the flow is hence independent of the viscosity. In the Navier Stokes equation, this means that the inertial term $(\boldsymbol{u} \cdot \boldsymbol{\nabla})\boldsymbol{u}$ dominates over the viscous term $\boldsymbol{\nabla} \cdot \boldsymbol{\sigma}$ in the inertial subrange (see also discussion in Kupka and Hillebrandt 2009).

From the first and second Kolmogorov similarity hypotheses, it follows that the energy spectrum in the inertial range has the following form (Pope 2000):

$$E(k) = C\epsilon^{2/3}k^{-5/3} , \tag{2.8}$$

where C is a constant and k denotes the wave number. An important consequence of this spectrum of turbulence will be discussed in Sec. 2.4.1. This energy spectrum describes the picture of the energy cascade and shows that the largest scales (with smallest k) are the energy carrying scales.

2.2 Reynolds Averaged Navier Stokes equations

Above, I have discussed that the details of turbulence can not be described to the required level of detail for fundamental reasons. In this section, I will discuss a statistical approach to describe turbulence in an effective way. Furthermore, one of the main assumptions of stellar models concerns the spherical symmetry, i.e. the description of the star in one spatial dimension. Therefore, I will now describe as a first step towards a stellar convection theory how the equations of hydrodynamics look like in one dimension. A first attempt of describing the effects of turbulence in a statistical sense goes back to Reynolds (1894).

Reynolds (1894) suggested splitting hydrodynamic variables into a mean part, denoted with an overbar, and a fluctuating part, denoted with a prime:

$$\boldsymbol{u} = \overline{\boldsymbol{u}} + \boldsymbol{u}', \quad \rho = \overline{\rho} + \rho', \quad \text{etc.}\,, \tag{2.9}$$

where the second part describes the turbulent contribution of the flow. This decomposition is known as the *Reynolds splitting*. We define the *Reynolds average* of a scalar $a(t, r, \theta, \phi)$ over a unit sphere S^2 as

$$\overline{a}(t, r) = \frac{1}{4\pi} \int_{S^2} a(t, r, \theta, \phi) \mathrm{d}\Omega\,,$$

where r, θ and ϕ refer to the radial distance, the polar angle and the azimuthal angle and $\mathrm{d}\Omega = \sin\theta\,\mathrm{d}\theta\,\mathrm{d}\phi$ denotes the solid angle in spherical coordinates. In the very same article, Reynolds continues to apply this splitting to the Navier-Stokes equations and derives an equation for the turbulent kinetic energy

$$E = \frac{1}{2}\rho\,\overline{\boldsymbol{u}'^2}\,, \tag{2.10}$$

which is the second order correlation function of velocity fluctuations. This is already the first step to derive a *turbulent convection model* (TCM), as we will discuss further below.

The application of the Reynolds splitting to the Navier Stokes equation is formally known as the *Reynolds Averaged Navier-Stokes* (RANS) formalism. As the example of the kinetic energy E has shown, higher order combinations of the fluctuating parts are of particular interest for stellar structure and evolution models. For example, the correlation function of velocity and entropy fluctuations is related to the *convective flux* describing the energy transport in the stellar interior. In principle, the RANS framework allows evaluating the behaviour of arbitrary correlations of hydrodynamic variables. Considering the specific TCM to which we want to compare the results we limit the discussion to the RANS equations for the following second order correlations in more detail:

$$\omega = \frac{1}{2}\overline{\boldsymbol{u}'^2} \tag{2.11}$$

$$\boldsymbol{\Pi} = \overline{s'\boldsymbol{u}'} \tag{2.12}$$

$$\Phi = \frac{1}{2}\overline{s'^2}\,. \tag{2.13}$$

In the following, I will refer to ω as the *turbulent kinetic energy* (TKE), the convective flux variable $\Pi = \boldsymbol{\Pi}_r$ (the radial component of the convective flux vector) and the entropy fluctuation variable Φ. By computing higher order correlation functions, the RANS equations describe bulk properties of the flow in a statistical way. Due to the non-linearity of the hydrodynamic equations, a series of averaged moment equations up to infinite order would be needed to describe the complete problem. The RANS formalism as such is analytically exact. Provided, all the data were available, all the terms in the RANS formalism can be evaluated. However, when turning the question around and attempting to use the RANS

equations to predict the behaviour of correlation functions relevant for stellar evolution, some terms can not be computed self-consistently within the theory. To compute these unclosed terms, approximations and models have to be applied, known as *closure relations*. Finding suitable closure relations is the task of turbulence theory, which I will describe further below in Sec. 2.4.

Using the Navier-Stokes equation Eq. (2.1) the dynamic equation for the velocity fluctuations $\boldsymbol{u}'$ can be derived by subtracting the averaged from the full equation:

$$\mathrm{d}_t \boldsymbol{u}' = -\left(\frac{1}{\rho}\boldsymbol{\nabla} p\right)' + \left(\frac{1}{\rho}\boldsymbol{\nabla}\cdot\boldsymbol{\sigma}\right)' - (\boldsymbol{u}'\cdot\boldsymbol{\nabla})\overline{\boldsymbol{u}} - ((\boldsymbol{u}'\cdot\boldsymbol{\nabla})\boldsymbol{u}')' \,.$$

The same can be done for the entropy equation Eq. (2.4) to derive a dynamic equation for the entropy fluctuations s':

$$\mathrm{d}_t s' = \left(\frac{\varepsilon}{T}\right)' - \left(\frac{\boldsymbol{\nabla}\cdot\boldsymbol{q}}{\rho T}\right)' + \left(\frac{\sigma_{ij}}{\rho T}\frac{\partial u_j}{\partial x_i}\right)' - (\boldsymbol{u}'\cdot\boldsymbol{\nabla})\overline{s} - ((\boldsymbol{u}'\cdot\boldsymbol{\nabla})s')' \,.$$

To compute the above dynamic equations, the averaged substantial derivatives have been used. They can be derived as

$$\overline{\mathrm{d}_t a} = \overline{\mathrm{D}_t a} - \overline{(\boldsymbol{u}'\cdot\boldsymbol{\nabla})a'} \tag{2.14}$$

$$(\mathrm{d}_t a)' = (\mathrm{D}_t a)' - (\boldsymbol{u}'\cdot\boldsymbol{\nabla})\overline{a} - ((\boldsymbol{u}'\cdot\boldsymbol{\nabla})a')' \,, \tag{2.15}$$

where we define the substantial derivative $\mathrm{D}_t a = \partial a/\partial t + (\boldsymbol{u}\cdot\boldsymbol{\nabla})\, a$ and the averaged substantial derivative $\mathrm{d}_t a = \partial a/\partial t + (\overline{\boldsymbol{u}}\cdot\boldsymbol{\nabla})\, a$. On the right-hand side, advective terms which contain combinations of a and $\boldsymbol{u}$ and averages or fluctuations thereof appear. I want to note that the third term on the right-hand side of Eq. (2.15) is already of second order in the perturbed quantities. In the subsequent steps of the derivation, it will become evident that this term is responsible for the occurrence of *third order moments*. Hence, the advective terms in the Navier Stokes equation, which are non-linear, give rise to the third order moments in the final equations of the stellar convection model.

Given the dynamic equations of the fluctuating quantities, the dynamic equations for the second order moments Eq. (2.11) to (2.13) are derived making use of the product rule: $\mathrm{d}_t\omega = \overline{\boldsymbol{u}'\mathrm{d}_t\boldsymbol{u}'}$ and similar for the other second order correlation functions. In the following, I give all the terms of the RANS equations and identify their physical meaning next to the

term (e.g. Kuhfuß 1987):

$$\begin{aligned}
\mathrm{d}_t\omega = &-\overline{(\boldsymbol{u}'\cdot\boldsymbol{\nabla})\frac{\boldsymbol{u}'^2}{2}} && \text{TKE flux}\\
&-\overline{u_i'u_j'\frac{\partial\overline{u}_j}{\partial x_i}} && \text{shear}\\
&-\overline{\frac{\boldsymbol{u}'}{\rho}\boldsymbol{\nabla}p} && \text{buoyancy}\\
&+\overline{\frac{1}{\rho}\boldsymbol{\nabla}\cdot(\boldsymbol{u}'\boldsymbol{\sigma})} && \text{viscous flux}\\
&-\overline{\frac{1}{\rho}\sigma_{ij}\frac{\partial u_j'}{\partial x_i}} && \text{viscous dissipation}
\end{aligned} \tag{2.16}$$

The first term on the right-hand side, referred to as TKE flux, is a third order moment in the velocity fluctuations. This term can not be computed from the second order equations alone. To compute this term, either an additional dynamic equation for the third order moment needs to be derived or a suitable closure relation may be applied. I would like to note here that when deriving the dynamic equation of the third order moments one would find terms involving *fourth order moments*, presenting one with the exact same problem as when deriving the dynamic equation of second order. In fact, the series of moment equations to be derived would have to be infinite, which is of course impossible. It is not without irony to note that by trying to circumvent the description of the details of turbulence—originating from the non-linearity of the Navier-Stokes equation—we end up with another unsolvable set of equations—due to the non-linearity of the Navier-Stokes equation. Further difficulties occur for the terms involving the molecular viscosity and the pressure correlation terms.

The evolution equation for the convective flux is given as

$$\begin{aligned}
\mathrm{d}_t\boldsymbol{\Pi} =& -\overline{(\boldsymbol{u}'\cdot\boldsymbol{\nabla})\boldsymbol{u}'s'} && \text{turbulent flux of entropy flux}\\
& -(\boldsymbol{\Pi}\cdot\boldsymbol{\nabla})\overline{\boldsymbol{u}} && \text{shear}\\
& -\overline{u_i'u_j'}\frac{\partial\overline{s}}{\partial x_j}\hat{e}_i && \text{potential}\\
& -\overline{\frac{s'}{\rho}\boldsymbol{\nabla}p} && \text{buoyancy}\\
& -\overline{\boldsymbol{u}'\frac{\boldsymbol{\nabla}\cdot\boldsymbol{q}}{\rho T}} && \text{heat flux}\\
& +\overline{\boldsymbol{u}'\frac{\varepsilon}{T}} && \text{nuclear energy}\\
& +\overline{s'\frac{\boldsymbol{\nabla}\cdot\boldsymbol{\sigma}}{\rho}} && \text{viscosity}\\
& +\overline{\boldsymbol{u}'\frac{\sigma_{ij}}{\rho T}\frac{\partial u_j}{\partial x_i}} && \text{viscosity}
\end{aligned} \tag{2.17}$$

where $\hat{e}_i$ refers to the i-th unit vector. As in the equation for the TKE the first term on the right is a third order moment of velocity and entropy fluctuations, that can not be computed within the given set of equations.

The evolution equation for the entropy fluctuations is given as

$$\begin{aligned}
\mathrm{d}_t\Phi =& -\overline{(\boldsymbol{u}'\cdot\boldsymbol{\nabla})\frac{s'^2}{2}} && \text{turbulent flux of entropy fluctuations}\\
& -\boldsymbol{\Pi}\cdot\boldsymbol{\nabla}\overline{s} && \text{potential}\\
& -\overline{s'\frac{\boldsymbol{\nabla}\cdot\boldsymbol{q}}{\rho T}} && \text{heat flux}\\
& +\overline{s'\frac{\varepsilon}{T}} && \text{nuclear energy}\\
& +\overline{s'\frac{\sigma_{ij}}{\rho T}\frac{\partial u_j}{\partial x_i}} && \text{viscosity}
\end{aligned} \tag{2.18}$$

Again third order moments of entropy and velocity fluctuations turn up.

As for the solution of the full hydrodynamic equations, the solution of the RANS equations would fully describe stellar convection in one spatial dimension, and would be in this respect suitable for a stellar evolution code. However, as pointed out above, many of the terms can not be computed self-consistently in the form presented above. This requires further approximations and assumptions to be made. In Sec. 2.4.1 and 2.5 I will describe how to finally arrive at a closed set of equations suitable for stellar evolution calculations.

2.3 Stellar convection theories

In the previous section I have discussed the equations of hydrodynamics from a general point of view with a special focus on turbulent flows. In this section I will first introduce the basics of stellar structure and evolution and subsequently describe some properties of stellar convection that need to be taken into account. I will close this section with discussing in more detail some of the approaches that are commonly used to model stellar convection.

2.3.1 Stellar structure and evolution

Comprehensive discussions of stellar structure and evolution can be found, for example, in the textbooks by Kippenhahn et al. (2012) or Weiss et al. (2004). Therefore, I will limit myself to a very brief summary of the most important aspects in this subsection. The theory of stellar structure and evolution used in this thesis is derived under a set of simplifying assumptions. Most importantly it is assumed that stars are *spherically symmetric* objects in which the theory of fluid dynamics applies and that they are dynamically stable allowing for the assumption of a *hydrostatic equilibrium*. Further, it is assumed that stars exist in *isolation*, i.e. excluding effects of planetary or stellar companions and that *no mass loss* and *no strong magnetic or electric fields* occur. Under these assumptions, the stellar structure equations can be written as

$$\begin{aligned}
\frac{\partial r}{\partial m} &= \frac{1}{4\pi r^2 \rho} \\
\frac{\partial p}{\partial m} &= -\frac{Gm}{4\pi r^4} \\
\frac{\partial l}{\partial m} &= \varepsilon_\mathrm{n} - \varepsilon_\nu + \varepsilon_\mathrm{g} \\
\frac{\partial T}{\partial m} &= -\frac{GmT}{4\pi r^4 p}\nabla \,,
\end{aligned}$$

in the Lagrangian mass coordinate m (see Kippenhahn et al. 2012, p. 89) with the independent structure variables radius r, luminosity l, pressure p and temperature T. Here, ε_n refers to the energy release by nuclear reactions per unit mass, ε_ν refers to the energy losses by neutrinos and ε_g denotes the gravothermal energy release, energy released due to expansion or contraction of the star. Finally, G refers to the gravitational constant. The first equation describes the conservation of mass, the second equation describes the hydrostatic equilibrium and the third equation describes the energy conservation. The fourth equation is usually written using the *dimensionless temperature gradient* ∇ defined as

$$\nabla = \frac{\partial \ln T}{\partial \ln p} = \frac{1}{\partial p/\partial r}\frac{p}{T}\frac{\partial T}{\partial r} \,, \tag{2.19}$$

not to be confused with the mathematical differential operator denoted as $\boldsymbol{\nabla}$. The fourth equation remains a tautological expression, where the right side can be transferred to the left side using the equation for hydrostatic equilibrium and the definition of ∇. This tautology may be resolved by providing a theory to compute ∇. In radiative regions, the temperature gradient may be set to the so-called *radiative temperature gradient* $\nabla = \nabla_{\mathrm{rad}}$ (details will be discussed further below). In convective regions, the temperature gradient is determined from the convection model, e.g. from a TCM, as will be discussed below. In very early stellar models, it has been assumed that convection zones are adiabatically stratified such that the temperature gradient equals the *adiabatic temperature gradient*, i.e. $\nabla = \nabla_{\mathrm{ad}}$. In deep convection zones, this is a valid assumption, while it fails for example close to the surface of the star where the density is low. For the discussion of convection in stars, the two dimensionless temperature gradients ∇_{rad} and ∇_{ad} play an important role.

By fusing lighter into heavier elements in its deep interior, a star evolves. The change of the chemical composition X_i of the i-th element with time due to nuclear reactions is described by the following equation

$$\frac{\partial X_i}{\partial t} = \frac{m_i}{\rho}\left(\sum_j r_{ji} - \sum_k r_{ik}\right), i = 1, I\,, \tag{2.20}$$

where m_i denotes the nucleus mass of the element i, r_{ji} denotes the reaction rate of transforming element j into i and r_{ik} indicates the reaction rate of transforming element i into k and I refers to the number of elements. Additionally, the composition of the star may change by means of mixing processes. Here, different processes can be considered, like atomic diffusion, mixing due to gas flows including convection, semiconvection, overshooting, rotation, tides or waves, or mixing due to radiative levitation. These mixing processes are mostly incorporated in stellar models through a *diffusion approximation* and Eq. (2.20) changes to

$$\frac{\partial X_i}{\partial t} = \frac{m_i}{\rho}\left(\sum_j r_{ij} - \sum_k r_{ik}\right) + \frac{1}{\rho r^2}\frac{\partial}{\partial r}\left(\rho r^2 D_{\mathrm{mix}}(r)\frac{\partial X_i}{\partial r}\right), i = 1, I\,, \tag{2.21}$$

where the different mixing processes are summarised in the diffusion coefficient D_{mix}. In convective regions, the diffusion coefficient is commonly computed as

$$D_{\mathrm{conv}} = \frac{1}{3}\Lambda u_{\mathrm{conv}}\,, \tag{2.22}$$

where Λ and u_{conv} are a typical length scale and velocity of convection (Langer et al. 1985). Due to the large convective velocities, the convective diffusion coefficient is orders of magnitude larger than the atomic diffusion coefficient, such that convection is the dominant mixing process in convective regions. In the implementation of the Kuhfuß (1987) model, we compute the convective diffusion coefficient as

$$D_{\mathrm{conv}} = \alpha_s \Lambda \sqrt{\omega}\,, \tag{2.23}$$

with an adjustable parameter α_s (see Sec. 2.5 for discussion) and $\sqrt{\omega}$ is used as a typical velocity scale. To solve the complete stellar structure and evolution problem and construct numerical stellar models, we use the one-dimensional *GARching STellar Evolution Code* (GARSTEC Weiss and Schlattl 2008) in the remainder of this thesis.

By converting the nuclei in the centre, the central composition of the star changes. Due to the low Coulomb barrier of the hydrogen nucleus (a single proton) the first nuclear burning stage consists of fusing hydrogen into helium. Due to the low stellar luminosity and the large amount of hydrogen available, this is at the same time also the longest phase of stellar evolution, known as the *main-sequence phase*. The burning and the change of the chemical composition lead to further structural changes of the star, e.g. an increase of luminosity and radius. Once the fuel in the centre is fully exhausted, the stellar structure needs to adjust even more drastically. Due to the extinction of the central energy source, the core of the starts to contract. This process proceeds until either a new energy reservoir can be tapped (fusion of another heavier element) or another mean of supporting the core against collapse starts to operate (e.g. degeneracy pressure). In cases where the chemical evolution proceeds much slower than the structural evolution one can treat the first four structural equations separate from the last chemical equation Eq. (2.21).

The most important parameter for stellar structure and evolution is the initial stellar mass. The initial stellar mass determines the lifetime of the star, the nuclear burning cycles, the structure of the star on the main sequence and its final fate once all the nuclear energy is used up. In the following, I give some typical values for important mass ranges in stellar evolution. The initial chemical composition is the second most important parameter influencing stellar evolution, and might change the given mass ranges slightly. For the sake of simplicity, this will not be discussed here. On the main sequence, the value of approximately 1.5 $M_\odot$ marks an important change in stellar structure. Below this mass, stars have a structure similar to our Sun, with a *convective envelope and radiative core*. Above 1.5 $M_\odot$ the stars develop a *convective core and a radiative envelope* on the main sequence. This change in structure is mainly due to the change of hydrogen fusion from the pp-chains to the CNO-cycle, where the latter is releasing energy at a higher rate. Another important mass range concerns stars above 8 $M_\odot$ as these stars are able to fuse all heavy elements up to the iron peak. Some high-mass stars end their lives in core collapse supernovae, even though the exact mechanism is still a matter of active research. Finally, the mass of 2 $M_\odot$ marks the upper limit of the low-mass stars, i.e. stars that develop a degenerate core before the onset of core helium burning. In low-mass stars, core helium burning sets in under an unstable thermal configuration, also known as the *helium flash*. Due to the short timescale of the helium flash, this is a situation in which the timescale of stellar evolution and convection become comparable. The evolutionary tracks in the *Hertzsprung-Russel diagram* (HRD), showing luminosity as a function of effective temperature, of three prototypical stars with masses of 1, 1.5 and 5 $M_\odot$ are shown in Fig. 2.2. Without going into the details, I would like to also point at the *red-giant phase*, a phase in which the stars develop deep convective envelopes and high luminosities, succeeding the main-sequence phase.

An important consequence of the structure of stars above 1.5 $M_\odot$ with a convective

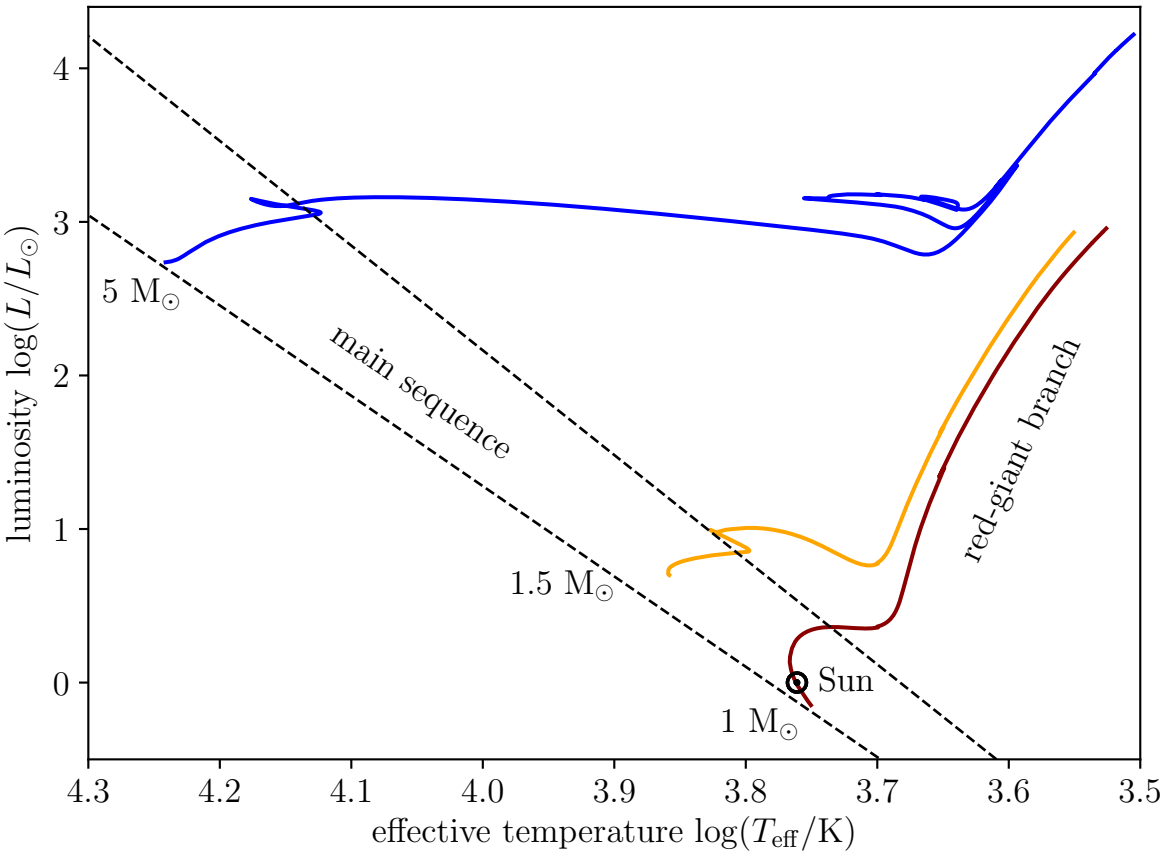

Figure 2.2: Comparison of stellar evolution tracks for different initial stellar masses of 1, 1.5 and 5 $M_\odot$ computed with GARSTEC. The main-sequence band is approximately indicated with two dashed lines. The location of the Sun is marked with the solar symbol.

core on the main sequence is the fact that convective and nuclear burning regions coincide. Following from our discussion above, convection is very efficient in mixing chemical elements, and it is therefore expected that a convective region has a more or less homogeneous composition. Further, the size of the convective region is rather uncertain due to the effects happening at the convective boundary. On the other hand, the luminosity of the star strongly depends on the composition of the burning region. Taken together, this indicates that the description of convection will have a large impact on the structure and evolution of the star. Further theoretical uncertainties are introduced by stellar winds or mass loss in general, the presence of stellar companions, magnetic fields or stellar rotation, which are however beyond the scope of this thesis.

2.3.2 Properties of stellar convection

Due to the very low viscosity of stellar matter and the large length scales—and as a result the very high Reynolds number—convective flows in stellar interiors are highly turbulent. To fully describe turbulence, very small spatial scales need to be resolved. Here, the Kolmogorov dissipation scale η given by Eq. (2.6) is the relevant length scale. Given the large Reynolds numbers of stellar flows (10^{10} to 10^{14}), Eq. (2.7) predicts a huge contrast between the integral and the dissipation scale of the flow. This is in contrast to the large radial scales of stars. From a temporal point of view, the nuclear and the dynamic timescales are competing. The nuclear evolution of a star proceeds on the nuclear timescale. For the Sun, the nuclear timescale on the main sequence is on the order of 10Gyr. For a 2 $M_\odot$, a star that possesses a convective core on the main sequence, the main-sequence lifetime is about 1 Gyr. On the other hand, the convective timescale depends on the convective velocities and the extent of the convection zone. A possible way to compute the convective timescale is

$$\tau_{\rm conv} = 2 \int_{r_{\rm up}}^{r_{\rm low}} \frac{{\rm d}r}{u_{\rm conv}(r)} \approx 200 \text{ days}\,, \tag{2.24}$$

where the convective velocity profile $u_{\rm conv}(r)$ has been computed by a stellar evolution model and $r_{\rm up}$ and $r_{\rm low}$ denote the radial location of the upper and lower convective boundary respectively (e.g. Kupka and Muthsam 2017, Eq. 15). Alternatively, it can be estimated by dividing the radial extent by a mean convective velocity. Either way, the convective timescale only provides the order of magnitude and should not be taken as a precise estimate. On the main sequence, this convective timescale is 9 orders of magnitude smaller than the nuclear timescale. This shows that stellar structure and evolution and the process of dynamic convection operate on completely different spatial and temporal scales. These large discrepancies in scales render it impossible to directly include the details of turbulent convection into stellar models for reasonable computational cost. Instead, effective models of turbulent convection need to be invoked. I would like to note that in late stellar evolutionary phases nuclear timescales become shorter and may be indeed comparable to the dynamic timescales. In these late phases, hydrodynamic simulations have been carried out successfully (e.g. Meakin and Arnett 2007; Couch et al. 2015).

Convective flows are very efficient in mixing chemical elements. Therefore, one of the most important questions to answer by a convection theory for stellar evolution concerns the size of the convective—and hence chemically mixed—region. Additionally, the thermal stratification of convective layers needs to be computed by the convection theory. A simple first estimate of the convective core size can be obtained from a linear perturbation analysis. The analysis shows that whether a fluid parcel becomes unstable against convection or not depends on the actual temperature excess. Assuming a homogeneous chemical composition, this leads to the so-called *Schwarzschild criterion* (Schwarzschild 1906)

$$\nabla_{\rm rad} > \nabla_{\rm ad}\,, \tag{2.25}$$

which implies that layers become convective as soon as the radiative gradient exceeds the adiabatic one. The Schwarzschild criterion is frequently used in stellar physics and forms

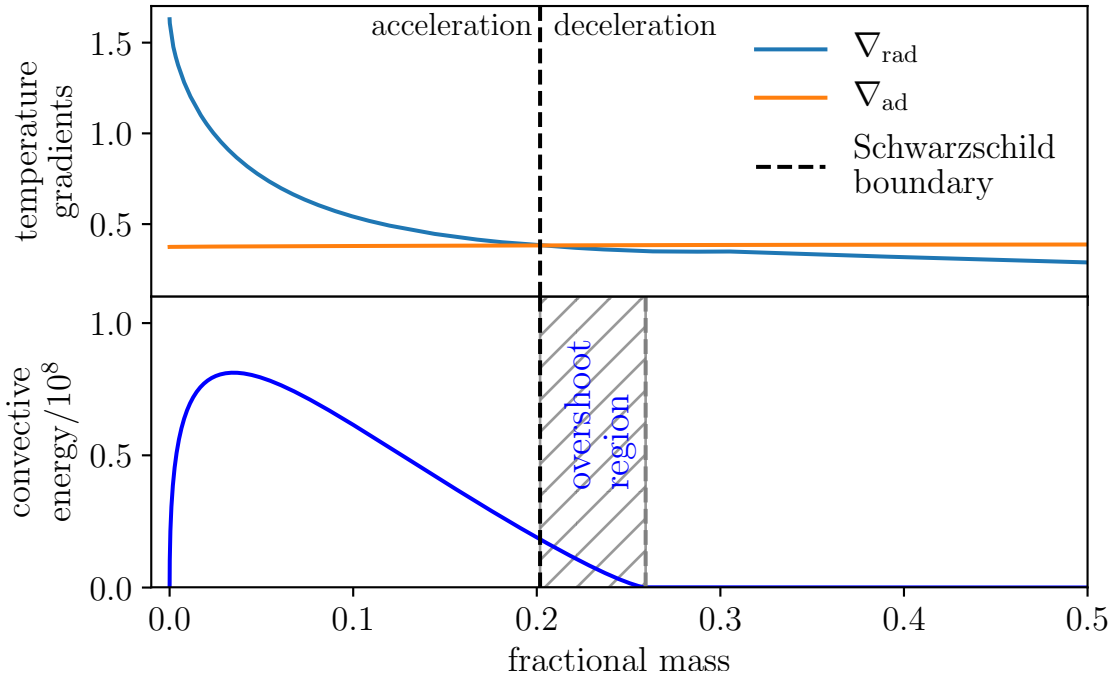

Figure 2.3: Illustration of non-local convection in a 5 $M_\odot$ main-sequence model. The upper panel shows the dimensionless temperature gradients ∇_{ad} and ∇_{rad} as a function of fractional mass with an orange and a blue line respectively. The vertical dashed line indicates the Schwarzschild boundary. The lower panel shows the TKE as a function of fractional mass. The hatched region indicates the overshooting of TKE beyond the Schwarzschild boundary.

also the basis of the most commonly used convection theory. However, I would like to lay out some simple considerations which immediately show why convective motions need to extend beyond the Schwarzschild boundary. For superadiabatic temperature gradients, fluid parcels would feel an accelerating force due to a relative underdensity compared to the surroundings. In subadiabatic regions, fluid parcels will be braked due to a relative overdensity. At the point of equality of the radiative and adiabatic gradient, the acceleration acting on a fluid parcel is zero. This situation is illustrated in the upper panel of Fig. 2.3. However, intuitively it is clear that even though the acceleration is zero at the location where $\nabla_{ad} = \nabla_{rad}$, this does not imply that the velocity becomes zero within the same instant (Kippenhahn et al. 2012; Salaris and Cassisi 2017). Due to their inertia, fluid parcels are expected to move past the formal Schwarzschild boundary (Zahn 1991) and penetrate into the stable region until the parcel has finally lost all its kinetic energy. In a region with subadiabatic temperature gradient, the motions are no longer driven by a local temperature excess, but rather from the unstable region below. These motions can be considered as a *non-local effect*. This effect moves the boundary of the turbulent convective

region further out than the actual Schwarzschild boundary. This is illustrated in the lower panel of Fig. 2.3 showing the TKE of the convective region as a function of the fractional mass, in which the TKE extends beyond the Schwarzschild boundary. The size of the turbulent convective region would be naturally provided by first principle hydrodynamic simulations. In the context of stellar models, the extent has to be provided by a stellar convection model. The computation of the exact extent of this region depends sensitively on the details of the convection model. A solution of the combined convective and stellar structure needs to be found by iteration, as in most cases the convective structure depends on the stellar structure and vice versa.

Due to the high mixing efficiency of turbulent convection, also the chemical composition beyond the Schwarzschild boundary is modified. In the context of stellar modelling, the extension of the chemically mixed region beyond the Schwarzschild boundary is often referred to as *overshooting* or *convective boundary mixing* (hatched region in Fig. 2.3). I would like to note here that in a star different physical effects may contribute to this mixing beyond the Schwarzschild boundary, e.g. convection, rotation or waves, and often all are summarised under the term overshooting. However, observations do not (yet) have the sensitivity to discriminate between different origins of the chemical extension of the convective region and do only probe the combined effect of all processes. In the remainder of this thesis, I will only discuss chemical mixing beyond the Schwarzschild boundary that originates from the turbulent convection. From an evolutionary point of view, this change of the chemical composition has a great impact. For example, in stars which have nuclear burning in convective cores the overshooting beyond the Schwarzschild boundary will increase their supply of fuel available for nuclear burning, which in turn increases the star's luminosity and extends the nuclear lifetime compared to models without the effects of overshooting. Another example of observable changes is the envelope of the Sun, where non-local convection can increase the Lithium depletion and modify the temperature gradient to better fit helioseismic observations. In addition to the size of the convective core which is important for the chemical mixing, also the modifications of the thermal structure are referred to with the notion of overshooting. Following Zahn (1991) two different cases have to be taken into account when describing non-local convection: subadiabatic penetration and overshooting. Subadiabatic *penetration* refers to thermally efficient convective penetration into stable regions such that the temperature stratification is altered and becomes nearly adiabatic. *Overshooting* instead refers to thermally inefficient convective penetration, leaving the temperature gradient unaltered, which still mixes chemical elements efficiently.

Summarising, in the stellar evolution context three radial locations are of importance, the formal Schwarzschild boundary, the boundary of adiabatic stratification and the boundary of the chemically mixed region that only in a local convection theory strictly coincide (Flaskamp 2003). As pointed out before, the extent of the chemically mixed region is most important for stellar structure and evolution. The aforementioned locations relevant for stellar convection can cause some ambiguity in determining the overshooting extent because it is not entirely clear what is used as a reference location (Angelou et al. 2020). It depends also on whether the model used takes into account a change in the temperature

stratification or only additional mixing beyond the Schwarzschild boundary. Finally, the Schwarzschild boundary itself may change when non-local effects are taken into account.

2.3.3 Mixing length theory

In Sec. 2.2, I discussed the general equations of convection averaged to one dimension. The main challenge in this respect is to provide these averaged equations in a closed form, that can be included into a 1D stellar evolution code. The challenges involved to close the set of equations are mainly related to the turbulent nature of the involved flows. This problem is of course not specific to stellar convection, but applies to any flow with high enough Reynolds number to develop turbulence. To describe the effects of turbulence, especially the exchange of momentum, Ludwig Prandtl has introduced the *mixing length* (Prandtl 1925, 1932). The main idea is to think of a turbulent fluid composed of individual turbulence elements, that have about the size of the mixing length. These elements travel in the flow keeping their initial identity, i.e. without exchanging mass with the surroundings, and dissolve after about the mixing length. The theory got further adapted to stars by Biermann (1932). In the context of stellar astrophysics, this is commonly addressed as the *mixing length theory* (MLT). The theory has been further extended by Vitense (1953) to also include the radiative losses of a fluid parcel. To date, this is still the most commonly used implementation of the MLT (Böhm-Vitense 1958). When discussing MLT, one has to consider two aspects. From the practical point of view, MLT has been shown to describe the structure and evolution of stars with acceptable accuracy. In cases where MLT itself was not able to reproduce the observations accurately, ad hoc modifications of the stellar models have been developed which account for these shortcomings. Some of the modifications will be discussed further below. From a physical point of view, it is, however, commonly accepted that MLT is describing convection not accurately, as discussed in the previous subsection. This highlights the need for a physically more accurate model of stellar convection, as it will be discussed in this thesis. In this subsection, I will discuss the mixing length theory as presented in the historical publications. More recent descriptions of MLT may be found in the textbooks by Kippenhahn et al. (2012) or Weiss et al. (2004). A brief discussion of MLT in the context of TCM may also be found in Canuto (1992). The relation to the RANS equations and other turbulence models will be discussed further below.

Without specifying the convective energy transport in detail, one can make some general statements about the energy transport in stars. The total energy flux $F_{\rm tot}$ can be split into several contributions

$$F_{\rm tot} = F_{\rm rad} + F_{\rm cond} + F_{\rm conv}\,, \tag{2.26}$$

where $F_{\rm rad}, F_{\rm cond}$ and $F_{\rm conv}$ refer to the radiative, conductive and convective energy flux respectively. The conductive energy flux is absorbed into the radiative flux by defining a conductive opacity. However, it is often small compared to the radiative or convective contribution. Using the luminosity as a function of radial coordinate $l(r)$, one can define the

radiative temperature gradient $\nabla_{\rm rad}$, the hypothetical gradient if all energy was transported by radiation

$$F_{\rm tot} = \frac{1}{4\pi r^2} l = \frac{16\sigma_{\rm B} G}{3} \frac{T^4 m}{\kappa p r^2} \nabla_{\rm rad} \tag{2.27}$$

$$\nabla_{\rm rad} = \frac{3}{64\pi\sigma_{\rm B} G} \frac{\kappa l}{m T^4} \,, \tag{2.28}$$

where κ refers to the mean opacity of the stellar matter and $\sigma_{\rm B}$ refers to the Stefan Boltzmann constant. Using this definition of the radiative temperature gradient, the sum of radiative and convective flux can be written as

$$F_{\rm rad} + F_{\rm conv} = \frac{16\sigma_{\rm B} G}{3} \frac{T^4 m}{\kappa p r^2} \nabla_{\rm rad} \,. \tag{2.29}$$

Following the diffusion approximation for the radiative energy transport Eq. (2.5), the radiative flux can be written as

$$F_{\rm rad} = \frac{16\sigma_{\rm B} G}{3} \frac{T^4 m}{\kappa p r^2} \nabla \,, \tag{2.30}$$

using the actual temperature gradient ∇ in the star, as defined by Eq. (2.19) and the diffusion coefficient

$$k_{\rm rad} = \frac{16\sigma_{\rm B} T^3}{3\kappa\rho} \,,$$

introduced in Eq. (2.5). Then Eq. (2.29) can be rewritten as

$$\nabla = \nabla_{\rm rad} - \frac{H_p}{k_{\rm rad} T} F_{\rm conv} \,, \tag{2.31}$$

with the pressure scale height H_p. To solve for the temperature gradient ∇, one needs a theory that describes $F_{\rm conv}$.

In the following, I will describe how the temperature gradient is computed using MLT. I will discuss the MLT in the version by Biermann (1932) and Böhm-Vitense (1958) in parallel to highlight interesting differences in the derivation. I review the equations and assumptions here to indicate where the model assumptions prevent a physically more accurate description of convection. After describing the TCM used in my work in Sec. 2.5, this more detailed discussion will also allow for a better comparison of the two theories. It is assumed that the turbulent elements move in pressure equilibrium with their surroundings. This is a save assumption for subsonic motions, as adjustments to achieve pressure equilibrium happen with the speed of sound. Biermann (1932) and Böhm-Vitense (1958) start by making an assumption for the convective flux. I give the Biermann (1932) expression on the left and the Böhm-Vitense (1958) expression on the right:

$$F_{\rm conv} = c_p \underbrace{\rho\, u\, l_{\rm m}}_{A} \Delta\boldsymbol{\nabla} T \qquad\qquad F_{\rm conv} = \rho\, c_p\, u D T \,, \tag{2.32}$$

where c_p refers to the specific heat capacity, u and l_m are typical convective velocity and length scales and $\Delta\boldsymbol{\nabla}T$ and DT will be defined further below. Biermann defines

$$\Delta\boldsymbol{\nabla}T = \left[\left(\frac{\partial T}{\partial z}\right) - \left(\frac{\partial T}{\partial z}\right)_\mathrm{ad}\right],$$

as the difference of the gradient of the temperature with respect to z and its adiabatic value. Here, z refers to the direction of the temperature gradient, which in most stars can be considered to be opposite to the radial direction. This expression can be easily transformed into the more familiar superadiabatic gradient $(\nabla - \nabla_\mathrm{ad})$ by introducing the pressure scale height H_p. With the symbol A, Biermann refers to "Austausch" (engl. exchange) in analogy to the dynamic viscosity $\nu \cdot \rho$. He defines this to be $A = \rho\, u\, l_\mathrm{m}$. Hence, A should be interpreted as a turbulent viscosity (e.g. Pope 2000, p. 358). In the formulation by Biermann (1932) it is evident, that Eq. (2.32) is the commonly used diffusion approximation for the convective flux similar to Eq. (2.5). On the other hand, Böhm-Vitense (1958) defines the convective flux using the excess temperature DT. With foresight, I would like to point out that knowing the value of uDT, or an appropriate average of it, would solve the problem of convective energy transport (cf. Kippenhahn et al. 2012). However, this is not the case, and we have to proceed with approximations. Following Biermann (1932) and Böhm-Vitense (1958) the excess temperature can be written as

$$\frac{\Delta\boldsymbol{\nabla}T}{T} = (\nabla - \nabla_\mathrm{ad})\, l_\mathrm{m}\, \frac{1}{H_p} \qquad\qquad \frac{DT}{T} = (\nabla - \nabla_\mathrm{e})\frac{l_\mathrm{m}}{2}\frac{1}{H_p}\,. \tag{2.33}$$

where the factor 1/2 in the Böhm-Vitense expression describes that an "average" element travelled about a distance of $l_\mathrm{m}/2$. The final expressions from Biermann (1932) and Böhm-Vitense (1958) are equivalent, except for numerical factors and the difference between ∇_e and ∇_ad. Here, Böhm-Vitense allows for the occurrence of radiative losses of the moving fluid parcels, which makes the movement non-adiabatic. Hence, one needs to introduce another temperature gradient ∇_e for the interior of the fluid parcel.

The difficulty remains to determine the convective velocity u. To determine the convective velocities, Biermann refers to the dissipation rate of TKE in the whole convection zone. He writes

$$L^3 A \left(\frac{\partial u}{\partial r}\right)^2 \approx L^3 A \frac{u^2}{l_\mathrm{m}^2} = L^3 \rho \frac{u^3}{l_\mathrm{m}}\,,$$

where L refers to the linear dimension of the convection zone. Dividing by the volume L^3, one obtains easily a local expression for the dissipation rate. To obtain the velocity he equates finally the energy released by unstable convection with the dissipated energy. Even though the final result of the derivation for the velocity is the same, the argumentation of Böhm-Vitense seems slightly different. Böhm-Vitense (1958) argues that the buoyancy force on the fluid parcel can be written as

$$k_r = -gD\rho/\rho = g\delta DT/T\,,$$

where $\delta = -(\partial \ln\rho/\partial \ln T)_{P,\mu}$ and $g = |\boldsymbol{g}|$. From the buoyancy force, the work done over a distance $l_\mathrm{m}/2$ can be computed. It is assumed that only half of this energy acts on the fluid parcel, introducing another factor of 1/2:

$$\frac{1}{2} k_r \frac{l_\mathrm{m}}{2} = g\delta(\nabla - \nabla_\mathrm{e}) \frac{l_\mathrm{m}^2}{8H_p} \,,$$

and further assuming that only half of the buoyancy energy is transformed into kinetic energy. The final expressions that need to be solved for the convective velocities from Biermann (1932) and Böhm-Vitense (1958) read

$$A \frac{g}{T} \Delta\boldsymbol{\nabla} T = \rho \frac{u^3}{l_\mathrm{m}} \qquad\qquad \frac{1}{4} k_r \frac{l_\mathrm{m}}{2} = \frac{1}{2} u^2 \,, \tag{2.34}$$

which allows solving for the velocity in terms of the super-adiabaticity. Together with the energy equation ($F_\mathrm{tot} = F_\mathrm{rad} + F_\mathrm{conv}$) this allows to solve for the temperature gradient ∇. The same result is obtained from the solution of a TCM, as I will discuss in Sec. 2.5.1

For the final equations I will focus on the expressions by Böhm-Vitense (1958) as these are more commonly used and also allow for including the additional effects of radiative losses. The expression from Biermann (1932), left side in Eq. (2.34), would lead to equivalent results except for numerical factors and the difference between ∇_ad and ∇_e. From equating the buoyancy work and the kinetic energy one can finally compute the convective velocity:

$$u^2 = g\delta(\nabla - \nabla_\mathrm{e}) \frac{l_\mathrm{m}^2}{8H_p} \,. \tag{2.35}$$

This allows to write the convective flux as

$$F_\mathrm{conv} = \rho c_p T \sqrt{g\delta} \frac{l_\mathrm{m}^2}{4\sqrt{2}} H_p^{-3/2} (\nabla - \nabla_\mathrm{e})^{3/2} \,. \tag{2.36}$$

These last two equations couple a positive convective flux and a positive convective velocity to a local comparison of the temperature gradients ∇ and ∇_e, preventing any convective motions once the temperature gradient ∇ dropped below ∇_e. Finally, we also need to describe the radiative losses of the fluid elements. To describe the energy that a turbulence element loses across its surface, again a diffusion approximation for the radiative flux is made, and another numerical factor needs to be assumed. This leads to the following relation among the dimensionless temperature gradients:

$$\frac{\nabla_\mathrm{e} - \nabla_\mathrm{ad}}{\nabla - \nabla_\mathrm{e}} = \frac{24\sigma_\mathrm{B} T^3}{\kappa\rho^2 c_p l_\mathrm{m} u} \,. \tag{2.37}$$

To close the equations, one has to finally specify the mixing length. Most commonly the mixing length is parametrised through the pressure scale height with a freely adjustable parameter α

$$l_\mathrm{m} = \alpha H_p \,. \tag{2.38}$$

This parameter is left as the only adjustable parameter of the mixing length theory. Given the mixing length, all quantities can be determined. Depending on the exact implementation of the MLT, the value of α suitable for stellar models may vary. A suitable value for α can be obtained by a so-called *solar calibration*. Given a set of input physics, a 1 $M_\odot$ model is evolved to the solar age. By adjusting the mixing length parameter and the initial helium abundance, one aims at reproducing the solar radius and luminosity. Note that also the metallicity needs to be varied in case atomic diffusion or overshooting from the bottom of the convective envelope are included. For GARSTEC a typical solar calibrated value is in the range of 1.5 to 2. It is then implicitly assumed that the same parameter value of α applies for all other applications as well. Disregarding all the physical deficits of MLT, this in itself is already a very far ranging assumption. There has been done some work to overcome the shortcomings of MLT. The calibration of the mixing length parameter has been attempted using for example observations of other stars (Joyce and Chaboyer 2018b,a; Li et al. 2018; Viani et al. 2018) or based on 3D hydrodynamic simulations (Trampedach et al. 2014; Salaris and Cassisi 2015; Magic et al. 2015; Spada et al. 2018). Further efforts have been devoted to replace the outer layers, known to be not accurately described by MLT, by results from 3D hydrodynamic simulations (Mosumgaard et al. 2018; Jørgensen et al. 2018). The latter approach is especially valuable for the computation of accurate theoretical oscillation frequencies of stars.

Even though the derivation by Biermann (1932) and Böhm-Vitense (1958) arrive at an equivalent result for the convective velocity, except for numerical factors, there seems to be a subtle difference in the argumentation. In Eq. (2.34) Biermann (1932) explicitly refers to the dissipation of the turbulence element by turbulent friction while Böhm-Vitense (1958) only considers the transformation of buoyancy work into kinetic energy, implicitly assuming that the energy is dissipated when the element dissolves after moving for a mixing length. The viscosity of stellar matter is far too small to brake the fluid parcel, and hence turbulence has to be invoked to dissipate the kinetic energy. As I will discuss in Sec. 2.5.1 this is the same argumentation as in a TCM, and the different processes which source or sink kinetic energy can be included into an evolution equation for this quantity.

One further disadvantage of MLT concerns the choice of parameters, and especially that of *hidden* parameters. At a number of points in the derivation assumptions have to be made, that enter the equations by choosing one specific numerical value. For example, it is assumed that only half the buoyancy work acts on the fluid parcel. While the fluid parcel moves, half of the kinetic energy is directly dissipated. These choices seem more or less arbitrary and similar, however yet different choices could be well justified. For the final application only a single parameter remains adjustable, the mixing length parameter α that needs to be adjusted to account for all the missing physics in the theory.

2.3.4 Overshooting

As discussed in Sec. 2.3.2 it is expected from simple arguments that the TKE extends beyond the formal Schwarzschild boundary, inducing chemical mixing in the overshooting zone. This effect has also been recognised by observations of binaries and open clusters

(Bressan et al. 1981; Maeder and Mermilliod 1981; Pietrinferni et al. 2004; Magic et al. 2010). Overshooting was further shown to play an important role for the lithium abundances in the Sun and solar-like stars (Carlos et al. 2019; Pinsonneault 1997; Dumont et al. 2021), for the determination of the base of the solar convection zone (Basu and Antia 2004; Christensen-Dalsgaard et al. 2011; Asplund et al. 2021), for the location of the RGB bump (Alongi et al. 1991; Khan et al. 2018) and for the extent of the convective cores of massive stars inferred by asteroseismology (Moravveji et al. 2015; Pedersen et al. 2021) to name a few examples. In contrast, MLT predicts the convectively mixed region only within the Schwarzschild boundary. To overcome this deficiency of MLT without invoking more complex methods, like TCM or hydrodynamic simulations, the effects of non-local convection can be included into the stellar models in a parametrised way. As the modification of the chemical composition has the greater impact on stellar evolution, these simple models parametrise only the chemical mixing and do not determine the temperature gradient. In most cases, the temperature gradient in the overshooting zone is assumed to take either the radiative or adiabatic value. In the following, I will discuss some of the recipes that are used in stellar models to mimic the effects of non-local convection. One straightforward model for overshooting is to simply extend a convectively mixed core by some distance beyond the Schwarzschild boundary. This extension is parametrised with another free parameter

$$l_{\mathrm{OV}} = \alpha_{\mathrm{OV}} H_p \,, \tag{2.39}$$

where α_{OV} takes values of about $0.1 - 0.2$. This parametrisation of convective overshooting is commonly known as *step overshooting*.

Another overshooting method relies on a description for the diffusion constant in the overshooting region:

$$D(z) = D_0 \exp\left(\frac{-2z}{f_{\mathrm{OV}} H_p}\right) . \tag{2.40}$$

The constant D_0 can be derived from MLT convective velocities slightly within the Schwarzschild boundary and f_{OV} is a free parameter as well, which takes values of about 0.02 (Kippenhahn et al. 2012, p. 352). This parametrisation has been first described by Freytag et al. (1996) and is commonly known as *exponential overshooting*. Although this approach is originally based on 2D simulations of envelopes in A-type main-sequence stars and DA-type white dwarfs which have thin convective zones subject to strong radiative losses, it is commonly applied to all convective boundaries in stellar evolution models. The parameter value of the exponential overshooting f_{OV} can be assumed to be 0.1 of α_{OV} to obtain the same mixed core size. The parameter values are not known a priori and need to be obtained from external calibration, e.g. by fitting stellar models to observations of isochrones of open clusters or binary systems. Different theoretical attempts have been made to estimate the overshooting distance, e.g. from an integral criterion (Roxburgh 1989, 1992), by assuming an adiabatic temperature gradient in the overshooting zone and computing the velocity in the MLT framework (Bressan et al. 1981) or from comparing the density contrast of ingested material to the convective temperature contrast (Spruit 2015).

Another description of convective overshooting is known as *convective entrainment*, first introduced by Turner (1986). The turbulent eddies reaching the convective boundary

always entrain portions of the material currently at rest and mix it into the turbulent convective region. This gradually increases the size of the convective core as the layers beyond the Schwarzschild boundary are entrained. The progressing of the mixed boundary is described by the entrainment velocity u_e

$$\frac{u_\mathrm{e}}{u_\mathrm{t}} = B \cdot \mathrm{Ri}_\mathrm{B}^{-n} \,,$$

where u_t is the turbulent velocity, that may be obtained from MLT and B and n are model parameters. Ri_B is the so-called bulk Richardson number defined as

$$\mathrm{Ri}_\mathrm{B} = \frac{l_\mathrm{e} \Delta b}{u_\mathrm{t}^2} \,,$$

where l_e is a typical length scale taken as a fraction of the pressure scale height. The buoyancy jump Δb is computed as

$$\Delta b = \int_{\Delta h} N^2 \mathrm{d}r \,,$$

where Δh denotes the extent of the thickness of the transition layer. Meakin and Arnett (2007) have studied this effect for an oxygen burning shell and determined the model parameters.

It has also been recognised that the efficiency of the overshooting varies with initial stellar mass (Pietrinferni et al. 2004). Lower mass stars usually need a smaller overshooting parameter than higher mass stars. The exact functional form of the overshooting parameter is still a matter of debate (Magic et al. 2010; Claret and Torres 2019; Constantino and Baraffe 2018; Higl et al. 2018; Viani and Basu 2020; Johnston 2021). I will discuss the relation between the overshooting extent and the stellar mass further in Sec. 4.4.

Applying a parametrised extension of the chemical mixing beyond the Schwarzschild boundary allows mimicking the effects of non-local convection. However, these extensions contain freely adjustable parameters, for which suitable values need to be found. The values may be found by calibrating stellar models to observations. It is however unclear whether the calibrated values will be valid in all situations in which overshooting is relevant. An example where the simple adoption of a single parameter value fails is the increase of the overshooting distance in the mass range from 1.2 to 2 $M_\odot$. Additional recipes have to be applied to incorporate this effect. Further, the present parametrisations do not make predictions about the temperature gradient in the overshooting zone. It is commonly assumed to take either the radiative or adiabatic value in the overshooting zone. Using a theoretically more realistic convection theory may ensure a more general usability of the model without the need to fine-tune parameters for each application. The temperature gradient is a natural outcome of the TCM, such that no assumptions about that need to be made.

2.3.5 Semiconvection

The situation becomes even more complicated when composition gradients are taken into account. In general, a positive *mean molecular weight gradient* ($\nabla_\mu = \partial \ln \mu / \partial \ln P > 0$)

has a stabilising effect on matter as an outward (inward) displaced element would have to penetrate into regions with lower (higher) mean molecular weight. Taking this into account, matter becomes unstable for convection if

$$\nabla_{\rm rad} > \nabla_{\rm ad} + \frac{\varphi}{\delta}\nabla_{\mu} = \nabla_{\rm L} \tag{2.41}$$

is satisfied, where $\varphi = (\partial \ln\rho/\partial \ln\mu)_{P,T}$. This criterion is known as the *Ledoux criterion*. As described above, a positive ∇_{μ} requires a larger $\nabla_{\rm rad}$ for layers to become convective, and hence has a stabilising effect.

In layers which are stable against convection according to the Ledoux criterion but unstable according to the Schwarzschild criterion, i.e. $\nabla_{\rm ad} < \nabla_{\rm rad} < \nabla_{\rm L}$, an effect termed *semiconvection* can appear. This makes the layer unstable to oscillations of turbulent elements with growing amplitude, leading to a slow mixing in these layers. The description of chemical mixing due to semiconvection is rather difficult, as any change of the chemical composition due to mixing will change the decisive gradients in the Ledoux criterion and potentially change the type of mixing. Semiconvection has important consequences for stars in different evolutionary stages and mass ranges. Firstly, in stars with masses larger than about 10 $M_{\odot}$ semiconvection becomes important on the main sequence. The receding convective core leaves behind a gradient in the hydrogen profile, such that layers at the boundary of the convective core become semiconvective. The chemical mixing in this semiconvective layer is then described by introducing a new diffusion coefficient. In GARSTEC the parametric description of Langer et al. (1983) is used, different recipes exist however, leading to different results in terms of the semiconvective mixing efficiency. Alternatively, the extent of the semiconvective region may be determined by introducing chemical mixing to achieve $\nabla_{\rm rad} = \nabla_{\rm ad}$ in semiconvective layers (Schwarzschild and Härm 1958; Kippenhahn et al. 2012; Salaris and Cassisi 2017). A thin semiconvective layer may also appear in low mass main-sequence stars with growing convective cores (1.5 $M_{\odot}$) (Silva Aguirre et al. 2011). Secondly, processes in the cores of low and intermediate mass He-burning stars are addressed as semiconvection (Castellani et al. 1971), even though the semiconvection criterion as defined above does not strictly apply. Castellani et al. (1971) already refer to this as *induced semiconvection*. Practically, the chemical mixing by semiconvection is tuned such that semiconvective layers are convectively neutral according to the Schwarzschild criterion. It is important to note that the Schwarzschild criterion needs to be satisfied on the convective side of the boundary, otherwise unphysical discontinuities would occur (Gabriel et al. 2014). In the convection model described in Sec. 2.5 and used in Ch. 3 and 4 the impact of composition on the convective properties is generally neglected. In the remainder of this thesis I will only discuss main-sequence stars in the mass range 1.5 to 8 $M_{\odot}$ with solar metallicity, hence, the effects of semiconvection are not expected to play an important role, and it is therefore neglected.

2.3.6 Time-dependent convection

When describing *time-dependent convection*, two cases need to be differentiated. More strictly, time-dependent convection refers to convection models in which the behaviour of

convective variables is described in a time-dependent way, i.e. time derivatives on the left-hand side of evolution equations are retained. By choosing an appropriate time step for the numerical integration, this in principle allows following time-dependent convective processes. As already stated above and as I will detail later, this is not the case for MLT. In a broader sense, the time-dependence of convection may be partially included by only considering time-dependent chemical mixing. This is in contrast to so-called instantaneous mixing. In time-dependent mixing, the chemical mixing is often described using a diffusion equation (see Eq. 2.21) and introducing a diffusion coefficient. The other convective variables are treated as time-independent. Normally, the timescale of stellar evolution is much longer than the timescale of convection. Hence, it is fairly safe to assume that the convective variables adjust instantaneously to changes in the stellar structure and neglect their time-dependence and that chemical mixing is instantaneous as well.

However, in some cases when stars evolve on very short timescales as for example during the Helium flash the evolutionary timescale becomes comparable to the convective timescale and an explicit time dependence of convection has to be taken into account. Using the Kuhfuß 1-equation model, this has for example been done in Flaskamp (2003). This may have an impact on the luminosity of the tip of the RGB in clusters, which may be used as a distance indicator (Serenelli et al. 2017). Recently, there has been discovered a gap in the Gaia CMD of very low mass stars (Jao et al. 2018). This has been theoretically associated with the merging of a convective core and convective envelope, and therefore got termed *convective kissing instability* (van Saders and Pinsonneault 2012; Baraffe and Chabrier 2018), in which time-dependent and non-local convection may play a role. Convection is also known to interact with pulsations and is relevant to determine the red edge of the instability strip of Cepheid and other classical variables (e.g. see work by Bono and Stellingwerf 1993, 1994). This has for example been studied in Xiong et al. (2015, 2016, 2018). For a review, see Xiong (2021). The relation between convection and non-linear pulsations using the Kuhfuß convection model have been studied by Wuchterl and Feuchtinger (1998). Feuchtinger (1999a) investigated effects of convection on pulsations of RR Lyrae stars. Finally, the effects of time-dependent and non-local convection may play a role in describing the nucleosynthesis and thermal pulses of AGB stars (see Herwig 2005, for a review).

2.4 Turbulent convection models

In the previous subsection, I have discussed different approaches that are currently used to describe convection in stellar models. None of the approaches discussed describes the effects of convection and convective boundary mixing self-consistently. In this section, I introduce the class of TCM that aim at capturing the effects of turbulence in convective regions. As already described in Sec. 2.2, the full RANS equations can not be solved self-consistently. However, a TCM provides the necessary approximations and models, that are needed to close the RANS equations. The choice of the closure relations is by no means unique, and so different TCM use different approximations, leading to different results. The set (type

and number) of variables of the TCM varies from model to model. So far, a number of TCM for stellar evolution have been developed (Canuto and Dubovikov 1998; Stellingwerf 1982; Kuhfuß 1987; Li and Yang 2007; Xiong et al. 1997). The most sophisticated models require up to 11 variables and corresponding partial differential equations (Canuto and Dubovikov 1998). An intermediate stage relies on a set of 4 variables (Xiong et al. 1997; Li and Yang 2007), and the most simple models describe turbulent convection with a single variable (Kuhfuß 1986). The models by Canuto or Xiong have been used in the past to compute the structure of convection zones in single stellar models, i.e. without stellar evolution. The model by Li and Yang (2001) has been implemented in a stellar evolution code, even though with a simplified numerical scheme compared to the present implementation. The latter authors do also not take the modifications to the dissipation rate into account that will be discussed below (Ch. 3).

Outside astrophysics, a broad range of turbulence models has been developed. Two very common applications of turbulence models are found in engineering and meteorology. Historically, the work on turbulence models originates from the simple one-equation models by Prandtl (1945) and Kolmogorov (1942). Subsequently, two-equation models like the $k-\epsilon$ (Jones and Launder 1972; Hanjalić and Launder 1972) or $k-\omega$ (Wilcox 1988) models are of interest. Note that in these models k refers to the TKE, ϵ to the dissipation rate of TKE and $\omega = \epsilon/k$ to the turbulence frequency. The original notation is given for historical reasons. A version of the $k-\omega$ model for stellar models has been developed by Li (2012). An interesting discussion of the application of turbulence models in meteorology and numerical weather predictions can be found in Mironov (2009). A further discussion about TCM in geophysical applications may be found in Mellor and Yamada (1982) or Sander (1998). In turbulence models for numerical weather predictions, it is common to distinguish a flow contribution due to unordered turbulent motions and ordered convective motions. While for the former the RANS framework and TCM are used, the latter contribution is treated using so-called mass-flux convection schemes (e.g. Tiedtke 1989).

In this thesis, I will use the turbulent convection model derived by Kuhfuß (1987). Kuhfuß (1987) uses three variables to describe turbulent convection in the stellar interior: TKE ω, turbulent convective flux Π and the squared entropy fluctuations Φ Eq. (2.11 - (2.13). We would like to point out that other TCM rather use the temperature fluctuations instead of the entropy fluctuations (Xiong et al. 1997; Canuto 1992). By using only the total TKE ω the Kuhfuß (1987) model is not able to account for a variable distribution of the kinetic energy in radial and horizontal directions. Instead, the distribution of kinetic energy in radial and horizontal directions is assumed to be isotropic at all radii, such that 1/3 goes into each spatial direction.

2.4.1 Approximations of the Kuhfuß TCM

In this subsection, I will review the most important approximations of the TCM by Kuhfuß (1987). Across all terms, we will neglect shear terms resulting from mean flows, i.e. $\overline{\boldsymbol{u}} = 0$. Following the approximation of isotropically distributed TKE we define an isotropic, radial velocity as: $u_{\rm iso} = \sqrt{2/3\omega}$. I will refer to alternative approximations for some of the terms

when appropriate.

Buoyant driving

Most importantly, the RANS equations for ω and Π, Eq. (2.16) and Eq. (2.17), contain buoyancy terms that need to be rewritten. These terms are rewritten in the approximation by Boussinesq (1903) (see e.g. Canuto 1993; Sander 1998; Kupka and Muthsam 2017, for a discussion). I will discuss the buoyancy term of Eq. (2.16) as an example. In a first step, the buoyancy term is split into a contribution due to the mean and the fluctuating pressure:

$$-\overline{\frac{\boldsymbol{u}'}{\rho}\boldsymbol{\nabla}p} = -\boldsymbol{\nabla}\overline{p}\cdot\overline{\frac{\boldsymbol{u}'}{\rho}} - \overline{\frac{\boldsymbol{u}'}{\rho}\boldsymbol{\nabla}p'}\,.$$

The second term describing effects due to pressure fluctuations is neglected in the Kuhfuß (1987) model. There is extensive literature on modelling this term to retain it in the model. The return-to-isotropy model by Rotta (1951) is a well known example. A more recent discussion on the modelling of these terms may be found in Canuto (1992) or Sander (1998). Subsequently, the first term is expanded to first order in terms of density fluctuations. Following the Boussinesq approximation, the density fluctuations are then expanded in terms of the entropy and composition fluctuations:

$$\begin{aligned}
-\overline{\frac{\boldsymbol{u}'}{\rho}\boldsymbol{\nabla}p} &\approx \frac{\boldsymbol{\nabla}\overline{p}}{\overline{\rho}^2}\,\overline{\boldsymbol{u}'\rho'} \\
&\approx \frac{\boldsymbol{\nabla}\overline{p}}{\overline{\rho}^2}\left\{\overline{\left(\frac{\partial\rho}{\partial s}\right)}_{p,c}\boldsymbol{\Pi} + \frac{1}{\overline{\rho}}\sum_i \overline{\left(\frac{\partial\rho}{\partial c_i}\right)}_{p,s}\boldsymbol{j}_i\right\} \\
&\approx \frac{\nabla_{\mathrm{ad}}T}{H_p}\Pi\,,
\end{aligned} \tag{2.42}$$

where the scalar quantity Π refers to the radial component of $\boldsymbol{\Pi}$. An analogous derivation is done for the buoyancy term of Eq. (2.17) to find

$$-\overline{\frac{s'}{\rho}\boldsymbol{\nabla}p} \approx \frac{2\nabla_{\mathrm{ad}}T}{H_p}\Phi\,. \tag{2.43}$$

Viscous dissipation

In Ch. 3 and 4 I will discuss a new closure for the dissipation rate of the TKE. With foresight, I will discuss the modelling of this term here in a bit more detail. One important aspect of convection models is the viscous dissipation of the TKE. Fluid motions are finally braked on the smallest length scale by interactions of the smallest particles. To capture these small-scale effects in direct numerical simulations, a very high spatial resolution is necessary. Kolmogorov (1941) has shown that in turbulent fluids, kinetic energy is dissipated on a turbulent cascade, on which energy is propagated from the large flow scales

down to the Kolmogorov dissipation scale. Although the dissipation happens only at the smallest scales, the dissipation rate is determined by the largest scales at which the energy is fed into the cascade and is independent of the actual viscosity. This is explained by the fact that by decreasing (increasing) the viscosity only the scale at which energy is dissipated is decreased (increased) without changing anything else in the energy cascade (see Eq. 2.6).

One approach to compute the dissipation rate ϵ in a local model is to use the Kolmogorov spectrum of turbulence Eq. (2.8). Assuming that there is an energy cut-off for the largest length scales, i.e. $E(k) = 0$ for $k < k_0$, we can integrate Eq. (2.8):

$$\begin{aligned}\omega &= \int_{k_0}^{\infty} E(k)\mathrm{d}k \\ &= \int_{k_0}^{\infty} Ck^{-5/3}\epsilon^{2/3} \\ &= \left[-\frac{3}{2}C\epsilon^{2/3}k^{-2/3}\right]_{k_0}^{\infty} \\ &= \frac{3C}{2}\frac{\epsilon}{k_0}^{2/3},\end{aligned}$$

(see e.g. Canuto and Dubovikov 1998; Kupka et al. 2022). The wave number can be rewritten in a length scale $k_0 = \pi/l_0$ such that we can rewrite the above equation to

$$\epsilon = \underbrace{\pi\left(\frac{2}{3C}\right)^{3/2}}_{c_\epsilon}\frac{\omega^{3/2}}{l_0}, \tag{2.44}$$

where I define the dissipation constant c_ϵ (Spalding 1991; Kolmogorov 1942, 1968, 1962; Canuto and Dubovikov 1998).[1] This can be compared to the MLT expression of Biermann in Eq. (2.34) when identifying $u \propto \sqrt{\omega}$. In Eq. (2.44) the length scale l_0 refers to the largest scale of the turbulent cascade. This expression is also employed in TCM to model the dissipation rate of TKE (e.g. Xiong 1978; Li and Yang 2001, 2007). This transforms the challenge of computing ϵ into a challenge of computing l_0. Concerning stellar TCM, only the descriptions by Canuto (1992, 1993) and Canuto and Dubovikov (1998) compute the dissipation with a fifth dynamic equation or the 2-equation model by Li (2012) that encompasses the dissipation rate in an equation for the turbulence frequency $f = \omega/\epsilon$ (note that in the original notation $f = \omega$ and $\omega = k$). In these models the length scale is calculated consistently within the model or rather the usage of a length scale is circumvented after all.

In the Kuhfuß model, most terms containing the molecular viscosity are neglected because they are of minor importance compared to competing terms. Only the viscous dissipation term for the kinetic energy is considered to be non-negligible. Kuhfuß (1987)

[1] Note there is a typo in Canuto and Dubovikov (1998) in Eq. (5c) which should have the constant C in the denominator.

models the dissipation of the kinetic energy with a Kolmogorov cascade as described above:

$$\epsilon = C_{\mathrm{D}} \frac{\omega^{3/2}}{\Lambda}, \tag{2.45}$$

where C_{D} denotes the dissipation parameter. Kuhfuß (1987) suggests a value of $C_{\mathrm{D}} = 8/3 \cdot \sqrt{2/3}$ to be compatible with MLT in the local limit of his model (see Sec. 2.5.1 for the calibration of the parameter). For historic reasons, I refer to the largest length scale at which energy is fed into the turbulent cascade with Λ, denoted as l_0 in Eq. (2.44).

A first local approximation for the length scale and hence the dissipation rate may be obtained by adopting the MLT approximation for the length scale. It is parameterised using the pressure scale height H_p and an adjustable parameter α: $\Lambda = \alpha H_p$. The assumption of a local flow does not apply however in overshooting layers, as these flows are driven by non-local fluxes of TKE from the convection zone below. The problems of this parametrisation in stably stratified layers have been for example already acknowledged in Zeman and Tennekes (1977) and Moeng (1984). More intuitively, this parametrisation may be also questioned from a geometric point of view, recalling that Λ refers to the largest scale of the turbulent cascade. Well inside a stellar convection zone, the boundary may be more than a pressure scale height away. When getting closer and closer to the boundary, this distance shrinks well below that. This makes the assumption of a constant length scale also in boundary regions questionable. In Ch. 3 we will discuss a non-local equation for the dissipation rate and subsequently derive a parametrisation also suitable for stably stratified regions.

Radiative dissipation

Convective elements lose energy through radiation. This is considered in the energy conservation equation by including radiative fluxes as sink terms. In the RANS equations for Π and Φ (2.17 and 2.18) they show up as second order moments. In the Kuhfuß equations the radiative losses finally appear as dissipation terms:

$$\epsilon_{\mathrm{rad},\Pi} = \frac{1}{\tau_{\mathrm{rad}}} \Pi \,, \quad \epsilon_{\mathrm{rad},\Phi} = \frac{2}{\tau_{\mathrm{rad}}} \Phi \,, \tag{2.46}$$

where Kuhfuß (1987) models radiative dissipation by introducing the radiative timescale τ_{rad}, which he defines as

$$\tau_{\mathrm{rad}} = \frac{c_p \kappa \rho^2 \Lambda^2}{4 \sigma_{\mathrm{B}} T^3 \gamma_R^2} \,.$$

Here, γ_R is a parameter which Kuhfuß (1987) sets to $2\sqrt{3}$, again to recover the MLT model in the local limit. Note that the models by Canuto (1992, 1993) or Canuto and Dubovikov (1998) keep the full derivatives in the radiative loss terms without approximating them through a dissipation timescale.

Higher order moments

The Navier-Stokes equation contains non-linear advection terms. As discussed in Sec. 2.2 when constructing the equations for the second order moments, these advection terms give rise to third order moments (TOMs). These higher order moments are the source of the non-local behaviour of the convection model. Using the anelastic approximation $\boldsymbol{\nabla} \cdot (\overline{\rho} \boldsymbol{u}') = 0$ (Spiegel and Veronis 1960), they can be cast into the form

$$\mathcal{F}_a = \frac{1}{\overline{\rho}} \boldsymbol{\nabla} \cdot \boldsymbol{j}_a \quad \text{with} \quad \boldsymbol{j}_a = \overline{\rho}\, \overline{\boldsymbol{u}' a}\,,$$

where a is a second order quantity. The closure of these TOMs is one of the main challenges of any TCM. Kuhfuß (1987) closes the system of equations at second order and describes each TOM using the so-called *downgradient approximation* (Daly and Harlow 1970; Launder et al. 1975; Xiong 1978; Li and Yang 2007). In the downgradient approximation the fluxes $\boldsymbol{j}_a$ are modelled following Fick's law similar to the radiative flux in Eq. (2.5):

$$\boldsymbol{j}_a = -D_a \boldsymbol{\nabla} \overline{a}\,, \tag{2.47}$$

$$D_a = \alpha_a \overline{\rho} \Lambda \sqrt{\omega}\,. \tag{2.48}$$

I would like to point out that the diffusion coefficient D_a is very similar to the "Austausch" A defined by Biermann (1932) (see Sec. 2.3.3). Kuhfuß (1987) has also suggested a local closure for the TOMs of Π and Φ by approximating the flux by $j_a = \sqrt{\omega}\, a$ for $a = \Pi, \Phi$ and replacing the divergence of the flux by dividing by the length scale Λ. Throughout this thesis I apply the non-local approximation for the TOMs appearing in the equations for ω, Π, and Φ with $a = \boldsymbol{u}'^2/2$, $\boldsymbol{u}' s'$, or $s'^2/2$ as this appears to be more realistic than its local counterpart (see for example the discussion in Sec. 4.3). The parameters α_a control the impact of the non-local terms. Kuhfuß (1987) suggests a default value of $\alpha_\omega \approx 0.25$. The values for the parameters $\alpha_{\Pi,\Phi}$ are calibrated to MLT in a local version of the Kuhfuß theory. However, no values for the non-local case are provided.

Alternatively, one could compute the TOMs by deriving dynamic equations for the TOMs in the same way as for the second order moments. This has been shown in Canuto (1992, 1993), Canuto and Dubovikov (1998), or Xiong et al. (1997), for example, and introduces fourth order moments which again have to be closed. Further, models of the TOMs involve the skewness of the turbulent flow (e.g. Canuto and Dubovikov 1998). A combination of the skewness and downgradient type closures for the TOMs could for example allow for the characterisation of small-scale, unordered and large-scale, ordered motions at the same time (Mironov 2009). Ultimately, closure relations for the TOMs could be supplied by 3D simulations (Chan and Sofia 1989, 1996; Kupka 1999b; Kupka and Muthsam 2007a,b,c; Kupka 2007; Kupka and Muthsam 2008; Viallet et al. 2013; Arnett et al. 2015).

2.5 The Kuhfuß turbulent convection model

In this section, I review the final model equations as derived in Kuhfuß (1987). I will refer to the specific closures from Sec. 2.4.1 that are applied when appropriate. The Kuhfuß (1987)

model has been partially implemented into GARSTEC originally by Flaskamp (2003) and finalised in the current work. The dynamic equations of the TCM are solved together with the stellar structure equations in the implicit Henyey-scheme such that the implementation solves for up to seven equations simultaneously. The second order spatial derivatives are computed over three grid points. This creates a consistent solution of the stellar and convective structure in every iteration. For the details of the implementation, I refer to Flaskamp (2003).

2.5.1 The 1-equation model

The most important equation to describe turbulent convection is the equation for the TKE. I will therefore start by discussing how to arrive at an equation for the TKE following Kuhfuß (1986) and Kuhfuß (1987). The general assumptions of the Kuhfuß model allow us to remove the terms including the mean velocity and the viscous flux and write the first RANS equation Eq. (2.16) as

$$\frac{\partial \omega}{\partial t} = -\overline{(\boldsymbol{u}' \cdot \boldsymbol{\nabla})\frac{\boldsymbol{u}'^2}{2}} - \overline{\frac{\boldsymbol{u}'}{\rho}\boldsymbol{\nabla} p} - \overline{\frac{1}{\rho}\sigma_{ij}\frac{\partial u_j'}{\partial x_i}}\,. \tag{2.49}$$

As discussed above, the buoyant driving term is rewritten using the Boussinesq approximation involving the convective flux variable Π. As a first step, Π is modelled using a diffusion approximation as done in MLT (see Eq. 2.32) instead of involving another dynamic equation to solve for Π (see also Kuhfuß 1986):

$$\Pi = \overline{u_r' s'} \approx -D_s \boldsymbol{\nabla}_r \overline{s}\,, \tag{2.50}$$

involving a diffusion coefficient D_s. The entropy gradient can be further rewritten to

$$\boldsymbol{\nabla}_r \overline{s} = -\frac{c_p}{H_p}(\nabla - \nabla_{\mathrm{ad}})\,, \tag{2.51}$$

using basic thermodynamic relations and the definitions of the gradients $\nabla, \nabla_{\mathrm{ad}}$ and the pressure scale height H_p. The diffusion coefficient D_s is defined as $D_s = \alpha_s \Lambda \sqrt{\omega}$ following for example Prandtl (1945) or Kolmogorov (1942) (see also Pope 2000, p. 369) and similar to the diffusion coefficient of the TOMs. Note that this can be directly compared to the choice of $A = \rho u l_{\mathrm{m}}$ from Biermann (1932) except for an additional factor of ρ. Here, the parameter α_s is a closure parameter which determines the efficiency of the diffusive transport of entropy. The choice of a parameter value will be discussed further below. The convective flux is then computed as $F_{\mathrm{conv}} = \rho T \Pi$

$$F_{\mathrm{conv}} = \alpha_s \rho \sqrt{\omega} \Lambda c_p \frac{T}{H_p}(\nabla - \nabla_{\mathrm{ad}})\,, \tag{2.52}$$

which is equivalent to the MLT expressions Eq. (2.36) when identifying $\sqrt{\omega} = u$ and $\Lambda = l_{\mathrm{m}}$.

Including the approximations Eq. (2.50) and (2.51) for Π as well as the approximations for the viscous dissipation Eq. (2.45) and the TOM Eq. (2.47) and (2.48) into the equation for the convective energy Eq. (2.49) yields

$$\frac{\partial \omega}{\partial t} = \frac{\nabla_{\mathrm{ad}} T \Lambda \alpha_s c_p}{H_p^2} \sqrt{\omega} (\nabla - \nabla_{\mathrm{ad}}) - \frac{C_{\mathrm{D}}}{\Lambda} \omega^{3/2} - \mathcal{F}_\omega \,. \tag{2.53}$$

By approximating the convective flux variable Π, it does no longer appear in the TKE equation such that it is only necessary to solve for the single convective variable ω. We will refer to this model as the *1-equation model*. When applying the 1-equation model, the length scale for the dissipation of the convective energy will be defined as $\Lambda = \alpha H_p$ – with a freely adjustable parameter α – throughout the rest of the thesis, equivalent to the usual mixing length. Additionally, we apply the reduction of the mixing length towards the centre following Wuchterl (1995) to counter-act the divergence of the pressure scale height in this region. For a value of order unity for α results are indeed comparable to MLT results. Given an expression for the convective flux, the temperature gradient ∇ is computed by invoking Eq. (2.31). Solving for ∇ yields

$$\nabla - \nabla_{\mathrm{ad}} = \frac{\nabla_{\mathrm{rad}} - \nabla_{\mathrm{ad}}}{1 + \frac{\rho c_p \alpha_s \Lambda \sqrt{\omega}}{k_{\mathrm{rad}}}} \,, \tag{2.54}$$

depending only on known quantities. Hence, the system is closed and can be implemented into a stellar evolution code. In summary, the 1-equation model has five parameters $\alpha_\omega, C_{\mathrm{D}}, \alpha_s, \alpha$ denoting the non-local, dissipation, entropy flux and mixing length parameter, and β appearing in the Wuchterl (1995) model. The choice of α_s and C_{D} will be discussed further below in this section. For α_ω Kuhfuß (1987) suggests a default value of 0.25, and we will see in Ch. 4 that this indeed results in reasonable convective core sizes. A more in depth discussion of parameter choices can be found in Sec. 5.5.1.

Interestingly, a very similar equation to Eq. (2.53) has been derived by Prandtl (1945) and independently by Kolmogorov (1942) (see also Pope 2000, p. 369). Instead of the buoyancy, for which Kuhfuß assumed a diffusion approximation like in MLT, Prandtl however considered shear as the source of the turbulence. The dissipation term he chooses has the same form as in the Kuhfuß model and the earlier mixing length descriptions from Prandtl (1932) and Biermann (1932).

One immediate consequence of the mixing length approximation for the convective flux is the coupling of the convective flux to the superadiabatic gradient (see Eq. 2.52). Due to this coupling, the convective flux changes its sign at the same location as the superadiabatic gradient. This prohibits the emergence of layers with a stable, subadiabatic stratification and a positive convective flux. These layers are also known as Deardorff or counter-gradient layers (Deardorff 1966). However, these layers are known to exist in physical systems and therefore a model of convection in stars should at least in principle allow for the existence of such layers. Examples of Deardorff layers are found in simulations of stellar convection (Chan and Gigas 1992; Muthsam et al. 1995, 1999; Tremblay et al. 2015; Käpylä et al. 2017; Kupka et al. 2018) or in other Reynolds stress models (Kupka 1999a; Xiong and

Deng 2001; Kupka and Montgomery 2002; Montgomery and Kupka 2004; Zhang and Li 2012). This is also an indication that the approximation of the convective flux variable Π Eq. (2.50) needs to be lifted to compute a more realistic model of stellar convection. For a further discussion, I refer to Ch. 4 and Ch. 5.

Relation to MLT

The comparison of MLT and the 1-equation model has been already discussed in the original work by Kuhfuß (1987). To explicitly show the relation to MLT, I consider it worthwhile to repeat the derivation here. We start from the RANS equations described above in the reduced form given by Eq. (2.49) and further neglect time-dependent terms, i.e. the time-derivative on the left-hand side and also the non-local terms. Then the RANS equation for the TKE reads

$$0 = -\overline{\frac{\boldsymbol{u}'}{\rho}\boldsymbol{\nabla} p} - \overline{\frac{1}{\rho}\sigma_{ij}\frac{\partial u_j'}{\partial x_i}}\,, \tag{2.55}$$

which is stating that the production of TKE by buoyancy equals the dissipation due to viscosity. This leaves us with two terms, that have to be modelled. To obtain a closed solution of the equations, we need to again employ a certain turbulence model. For simplicity, we will use the model by Kuhfuß (1987) as discussed above. Then the equation for the TKE reads

$$0 = \frac{\nabla_{\mathrm{ad}} T \Lambda \alpha_s c_p}{H_p^2}\sqrt{\omega}(\nabla - \nabla_{\mathrm{ad}}) - \frac{C_{\mathrm{D}}}{\Lambda}\omega^{3/2}\,. \tag{2.56}$$

However, one could also consider choosing different closure relations to model the impact of turbulence and arrive at a different local and time-independent convection model. Rearranging, we find the following equation for ω:

$$\omega = \frac{\Lambda}{C_{\mathrm{D}}}\frac{\nabla_{\mathrm{ad}} T \Lambda \alpha_s c_p}{H_p^2}(\nabla - \nabla_{\mathrm{ad}})\,.$$

As discussed above, the Kuhfuß model assumes fully isotropic turbulence. We can further rewrite the adiabatic temperature gradient as $\nabla_{\mathrm{ad}} = P\delta/(\rho c_p T)$ and $H_p = p/\rho/\delta$. Putting this together, we find the following equation for the isotropic convective velocity:

$$u_{\mathrm{iso}}^2 = \frac{2}{3}\frac{\alpha_s}{C_{\mathrm{D}}} g\delta \frac{\Lambda^2}{H_p}(\nabla - \nabla_{\mathrm{ad}})\,.$$

Together with the equation for the convective flux Eq. (2.52) one finds

$$F_{\mathrm{conv}} = \rho c_p T \sqrt{g\delta}\sqrt{\frac{\alpha_s^3}{C_{\mathrm{D}}}}\Lambda^2 H_p^{-3/2}(\nabla - \nabla_{\mathrm{ad}})^{3/2}\,.$$

Comparing these expressions with the respective MLT expressions Eq. (2.36) and (2.35) the parameter values α_s and C_{D} can be chosen such that both theories are equivalent

except for the difference in ∇_e and ∇_{ad}. For the parameters, values of $\alpha_s = 1/2\sqrt{2/3}$ and $C_D = 8/3\sqrt{2/3}$ need to be chosen to achieve equivalence. This detailed comparison shows that, in fact, MLT can be derived as the local and time-independent limit of a TCM with the additional diffusive approximation for the convective flux. This relation was already indicated in the work of Biermann discussed above in which he equates the buoyancy work with the dissipation rate, for which he has chosen the same expression as in the Kuhfuß model (compare Eq. (2.45) and Eq. (2.34)). It is worth noting that, in the absence of radiative losses, MLT would need at least two adjustable parameters, i.e. C_D to control the dissipation and α_s to control the relation between the temperature gradient and the convective flux. Other combinations of two parameters out of α, α_s and C_D may be used equivalently.

Starting from the RANS equation for ω Eq. (2.16) different convection models may be derived by choosing different approximations. The above derivation shows that MLT is the result of a particular set of assumptions (diffusive convective flux, local, time-independent, no pressure-correlations, no mean flow, Kolmogorov dissipation). As I will discuss in Ch. 5, the non-local term is not negligible and needs to be taken into account. In the framework of TCM, it is possible to thoroughly discuss the importance of individual terms and adjust their parameters and functional form based on physical arguments or 3D hydrodynamic simulations. For the development of more realistic stellar convection models, I consider it therefore necessary to start from the full RANS equations and carefully consider which terms should be modelled and considered and which terms could be safely neglected.

2.5.2 The 3-equation model

In the 1-equation model discussed in the previous subsection, the convective flux variable Π got approximated by a diffusion approximation, as in MLT (see Eq. (2.50)). In the complete version of his convection model, Kuhfuß (1987) has derived an additional dynamic equation for this variable. When deriving the dynamic equation for Π, i.e. Eq. (2.17), and approximating the unclosed terms, a second variable needs to be introduced. This becomes apparent when looking at the buoyancy term of Eq. (2.17), approximated in Eq. (2.43), where the second order entropy fluctuation variable denoted as Φ emerges. To solve for Φ, a third dynamic equation needs to be derived and solved. The final model equations can be compiled by including the approximations discussed in Sec. 2.4.1 into the full equations Eqs. (2.16), (2.17) and (2.18). The viscous dissipation is modelled according to Eq. (2.45) and the TOM are described by Eq. (2.47) and (2.48), the buoyancy term is written in the Boussinesq approximation according to Eq. (2.42) and Eq. (2.43). The potential terms do not need to be approximated and can be written using Eq. (2.51). The radiative dissipation terms are approximated using the radiative timescale, as in Eq. (2.46). Following the previous considerations, one arrives finally at the following three equations for the turbulent variables ω, Π and Φ in the original version (Kuhfuß 1987; Flaskamp

2003):

$$\frac{\partial \omega}{\partial t} = \frac{\nabla_{\rm ad} T}{H_p}\Pi - \frac{C_{\rm D}}{\Lambda}\omega^{3/2} - \mathcal{F}_\omega \tag{2.57}$$

$$\frac{\partial \Pi}{\partial t} = \frac{2\nabla_{\rm ad} T}{H_p}\Phi + \frac{2c_p}{3H_p}(\nabla - \nabla_{\rm ad})\omega - \mathcal{F}_\Pi - \frac{1}{\tau_{\rm rad}}\Pi \tag{2.58}$$

$$\frac{\partial \Phi}{\partial t} = \frac{c_p}{H_p}(\nabla - \nabla_{\rm ad})\Pi - \mathcal{F}_\Phi - \frac{2}{\tau_{\rm rad}}\Phi\,. \tag{2.59}$$

Using the convective flux from the convection model one can compute the temperature gradient of the stellar model self-consistently from Eq. (2.31):

$$\nabla = \nabla_{\rm rad} - \frac{H_p \rho}{k_{\rm rad}}\Pi\,. \tag{2.60}$$

Owing to the increased model complexity of the 3-equation model, the model parameters α_Π and α_Φ describing the non-local terms of the convective flux and entropy fluctuation equation and $\gamma_{\rm R}$ needed to be introduced. The parameter α_s that parametrises the entropy transport in the 1-equation model became however dispensable, as Π is no longer approximated. A detailed discussion of the model parameter in the 3-equation model may be found in Sec. 5.5.2.

This closes again the set of equations, such that they can be solved self-consistently and implemented into a stellar evolution code. The stellar structure is coupled directly to the convection model through the temperature gradient and indirectly through the predicted convective chemical mixing. The self-consistent computation of the temperature gradient through Eq. (2.60) allows predicting its behaviour in the overshooting region. This is in contrast to ad hoc descriptions of overshooting in which the temperature gradient is set manually. By decoupling the convective flux from the superadiabatic temperature gradient, the 3-equation model allows at least in principle for a layer in which both quantities have a different sign and a Deardorff layer emerges. This shows that at least three equations are necessary to achieve this. For a further discussion of the Deardorff layer, I refer to Sec. 4.3 and 5.3. I would like to note that Eq. (2.60) may be extended to include further means of energy transport, e.g. the transport of TKE by the convective flow. However, the TKE flux is small compared to the convective flux described through Π, and its contribution to the temperature gradient is therefore neglected in the following.

The description of the 3-equation model closes my discussion of the theoretical background of stellar convection. In the subsequent chapters I will discuss the derivation of a new closure relation for the dissipation of TKE, the application of the 3-equation model to intermediate mass main-sequence stars and the comparison of the Kuhfuß (1987) TCM to 3D hydrodynamic simulations.

Chapter 3

Dissipation by buoyancy waves

Parts of this chapter are submitted for publication in Astronomy and Astrophysics (Kupka et al. 2022). The work has been done in collaboration with Friedrich Kupka and Achim Weiss. I have contributed to the derivation of the new expression and implemented it into the Kuhfuß (1987) TCM in GARSTEC. Further, I computed the stellar models to test the TCM including the new expression. The text has been written by Friedrich Kupka and me, I have contributed most of the figures.

3.1 Introduction

In this chapter we will discuss the role of the dissipation rate of TKE for TCM with a special focus on the dissipation of TKE due to *buoyancy waves*, waves for which the restoring force is buoyancy. These waves are also known as *gravity waves*, and the terms are used interchangeably. As discussed previously, numerous TCM have been developed (Xiong et al. 1997; Canuto 1992, 1993; Canuto and Dubovikov 1998; Li and Yang 2001, 2007; Kuhfuß 1986, 1987) which differ in the set of variables used and the set of approximations and assumptions made (see Canuto 1993 and Kupka and Muthsam 2017 for comparisons and a review). Among other physical effects, the dissipation of TKE requires a careful discussion in the context of TCM. Acting as a sink term for TKE in overshooting layers, the dissipation rate has a direct impact on the extent of convectively mixed regions. Assuming a Kolmogorov spectrum of turbulence Eq. (2.8), the dissipation rate of TKE can conveniently be computed by a local expression involving a dissipation length scale with a single constant parameter. This expression is, however, inapplicable in non-local situations, encountered in layers adjacent to convectively unstable zones. To treat the dissipation of TKE in non-local convection models, a physically more complete description of the dissipation rate is required (Zeman and Tennekes 1977; Canuto and Dubovikov 1998).

The derivation of a new expression for the TKE dissipation rate takes the discussion of the local dissipation expression in Sec. 2.1 and 2.4.1 as a starting point. From the dissipation rate equation in non-local convection theories, we derive a model to account for the dissipation of TKE by buoyancy waves in overshooting layers in Sect. 3.3. In

Sect. 3.4 we then discuss implications of the improved dissipation model when applied to stellar models. For the computation of the stellar models we use the TCM derived by Kuhfuß (1987) described in Sec. 2.5 and implemented into GARSTEC. The key assumptions and approximations of the Kuhfuß (1987) model are reviewed in Sec. 2.4. Using the local expression for the dissipation rate of the TKE we find an excessive overshooting extent beyond convective cores. When including the dissipation by buoyancy waves, this overshooting is limited to a physically more reasonable range. This allows us to predict the convective core sizes and temperature structures of stars with different masses. We present our conclusions in Sect. 3.5. A detailed discussion of the results obtained from the improved TCM can be found in Ch. 4 (see also Ahlborn et al. 2022). The derivation of the new dissipation mechanism in this chapter is based on the TCM by Canuto (1992, 1993); Canuto et al. (1994) and Canuto and Dubovikov (1998). We will hence to a large degree stick to the notation in the original papers. For the sake of simplicity, I point at some of the most important differences here. Most importantly, the convective variables of the Canuto models are referred to as K, J and $\overline{\theta^2}$, where K is the TKE, identical to ω (Eq. 2.11) and $J = \overline{w\theta}$ is the convective flux variable, equivalent though not identical to Π (Eq. 2.12), where w and θ refer to the vertical velocity and temperature fluctuations. We further occasionally use $\overline{q^2} = 2K$. Finally, the squared temperature fluctuations $\overline{\theta^2}$ are equivalent to Φ (Eq. 2.13). The derivation of the Canuto model is carried out in Cartesian coordinates in which z locally points in the radial direction such that frequently partial derivatives with respect to z appear. Note that this convention is opposite to the one used in the original derivation of the MLT discussed in Sec. 2.3.3. Then we define the superadiabatic temperature gradient as

$$\beta = -\left[\left(\frac{\partial T}{\partial z}\right) - \left(\frac{\partial T}{\partial z}\right)_{\mathrm{ad}}\right],$$

in agreement with the notation in the Canuto model.

3.2 Computation of the dissipation rate in non-local models

The dissipation rate of TKE due to viscosity, commonly denoted as ϵ, requires a very high spatial resolution to be computed directly. This is generally not affordable for stellar evolution models, and also problematic for 3D hydrodynamics simulations. To close Eq. (2.49) it is hence necessary to model the dissipation rate of the TKE. In Sec. 2.4.1 we have already discussed a local model for ϵ that is based on Kolmogorov's similarity hypotheses. This expression is one key assumption of MLT (see Eq. 2.34) and the Kuhfuß 1- and 3-equation models in their original form. This expression for ϵ is however strictly local, while we aim at modelling the non-local effects of convection. This motivates the usage of a non-local description also of the dissipation rate ϵ. This can be for example done by providing a dynamic evolution equation of ϵ. The exact evolution equation for ϵ was first derived by

Davidov (1961). In their Sect. 3, Hanjalić and Launder (1972) emphasised[1] why it is difficult to close this equation. But in the same paper, they also point out how to proceed to derive a new equation which models the transport of ϵ. One term (diffusional transport due to pressure fluctuations) is argued to be small on general grounds compared to other contributions, while others are modelled such that the ensuing closure constants can be determined in the case of simple flows directly from experiments: decaying turbulence behind a grid and a constant-stress layer adjacent to a wall. Their model equation for ϵ reads (see Hanjalić and Launder 1972, Eq. 3.5)

$$\frac{\partial \epsilon}{\partial t} + D_{\mathrm{f}}(\epsilon) = c_1 \frac{\epsilon P}{K} - c_2 \frac{\epsilon^2}{K} + \frac{\partial}{\partial z}\left(\nu \frac{\partial \epsilon}{\partial z}\right), \tag{3.1}$$

where P means production of dissipation (due to shear or buoyancy or both) and c_1 and c_2 are model parameters. The term $\partial/\partial z(\nu \partial \epsilon/\partial z)$ is only relevant at moderate or low Reynolds numbers and can always be neglected for small Prandtl numbers, as is the case for stars. The term $D_{\mathrm{f}}(\epsilon)$, describing the non-local transport of ϵ equivalent to $\mathcal{F}_a$ defined in Sec. 2.4.1, was suggested to be parametrised as

$$D_{\mathrm{f}}(\epsilon) \equiv \frac{\partial \overline{\epsilon w}}{\partial z} \approx -\frac{1}{2}\frac{\partial}{\partial z}\left(\nu_{\mathrm{t}} \frac{\partial \epsilon}{\partial z}\right). \tag{3.2}$$

where ν_t requires a model for turbulent viscosity such as[2] $\nu_t = C_\mu K^2/\epsilon$ with a closure constant C_μ. Given the MLT description of ϵ the turbulent viscosity is again equivalent to the "Austausch" defined by Biermann (1932) discussed in Sec. 2.3.3. Although this term is mainly relevant for moderate to low Reynolds numbers, it must be kept and modelled, since this is just what we also encounter in the case of overshooting zones. This is in contrast to terms only relevant for moderate to large Prandtl numbers (i.e., only in a non-stellar case) or which are small independently of the parameter space considered: those we can safely neglect for our applications. We emphasise that contrary to Eq. (2.49) all contributions to Eq. (3.1) contain closure approximations. Hence, Eq. (3.1) is essentially a model for $\partial\epsilon/\partial t$ and not an exact evolution equation.

Equation (3.1) was reconsidered by Canuto et al. (1994) and Canuto and Dubovikov (1998), who also suggested the additional contribution to Eq. (3.1) introduced in Zeman and Tennekes (1977):

$$\begin{aligned} \frac{\partial \epsilon}{\partial t} + D_{\mathrm{f}}(\epsilon) &= c_1 \frac{\epsilon g \alpha_{\mathrm{v}} \overline{w\theta}}{K} - c_2 \frac{\epsilon^2}{K} + c_3 \epsilon \tilde{N} + \frac{\partial}{\partial z}\left(\nu \frac{\partial \epsilon}{\partial z}\right), \\ \tilde{N} &\equiv \sqrt{g \alpha_{\mathrm{v}} |\beta|}, \end{aligned} \tag{3.3}$$

where g refers to the gravitational acceleration, α_{v} to the volume expansion coefficient, $\tilde{N}$ denotes the buoyancy or Brunt-Väisälä frequency in the absence of composition gradients

[1] In the literature the model discussed here is known as $K-\epsilon$ model or "Imperial College model" since there the model had been developed by Hanjalić and Launder (1972).

[2] Note that this definition is different from Canuto and Dubovikov (1998), Eq. (24c), which appears to have a typo.

and c_3 is a model parameter. Here, the production of dissipation has been assumed to be exclusively due to buoyancy $P = P_\mathrm{b} = g\alpha_\mathrm{v}\overline{w\theta}$. In addition to $c_1 = 1.44$ and $c_2 = 1.92$, which is close to the middle of the typical range of values in earlier work (Tennekes and Lumley 1972; Hanjalić and Launder 1976), Canuto and Dubovikov (1998) suggested $C_\mu = 0.08$ from their turbulence model (Canuto and Dubovikov 1996), which they obtained using the Kolmogorov spectrum Eq. (2.8).

Before quantifying the new term $c_3\,\epsilon\,\tilde{N}$ more closely, the physical origin of the contributions to Eq. (3.3) requires some explanation. The first term on the right-hand side provides a closure for the production of dissipation by buoyancy (Hanjalić and Launder 1972). The second term was discussed already in detail by Hanjalić and Launder (1972) and represents a closure for the combined effects of the exact terms describing the generation of vorticity fluctuations through self-stretching in turbulent flows and the decay of turbulence due to viscosity. For the exact term of diffusion of ϵ by velocity fluctuations, $D_\mathrm{f}(\epsilon)$, both a downgradient closure (Hanjalić and Launder 1972) and a direct closure based on the flux of turbulent kinetic energy (Canuto 1992) have been proposed. The viscous diffusion term $\partial/\partial z(\nu\partial\epsilon/\partial z)$ is also part of the exact expression for diffusional transport and is suggested to be kept when modelling flows in the regime of low to moderately high Reynolds numbers, especially in the case of moderate to high Prandtl numbers (see Hanjalić and Launder 1976).

For buoyancy driven flows, Eq. (3.1) requires several changes in comparison with Hanjalić and Launder (1972, 1976). We refer the reader to the work by Zeman and Lumley (1976) and Zeman and Tennekes (1977) which eventually allowed the derivation of Eq. (3.3). What follows from their and similar considerations is, that, irrespectively of the detailed physical nature of increased local dissipation in the overshooting zone, a separately parametrised loss term that involves the superadiabatic temperature gradient β, or actually, the Brunt-Väisälä frequency, $\tilde{N}$, is needed. With hindsight, gravity waves are expected to play the most important role as a source of ϵ. As argued by Zeman and Tennekes (1977), this involves a characteristic length scale, which can be computed from the ratio of flow velocity w^2 and $\tilde{N}$. It can also be viewed as the distance which eddies of a certain size that penetrate into the stable layer with a certain lapse rate can travel until their potential energy is fully converted into kinetic energy. It turns out that this yields the same expression as the parametrisation of dissipation by internal gravity waves: their contributions may differ in magnitude, but their functional form remains the same.

Hence, Canuto et al. (1994) suggested that this term should indeed be added to the standard form of Eq. (3.1). As they pointed out, this contribution also allows maintaining stationarity in homogeneous, stratified turbulence, as confirmed by data from direct numerical simulations of shear turbulence by Holt et al. (1992). Thus, Canuto et al. (1994) suggested $c_3 = 0.3$ for stably stratified layers and $c_3 = 0$ elsewhere to complete Eq. (3.3). Canuto and Dubovikov (1998) followed that proposal.

Clearly though, among all the parametrisations which appear in Eq. (3.3), $c_3\,\epsilon\,\tilde{N}$ remains the most uncertain one, but yet it is also crucial. Its choice requires to be tested carefully. Otherwise, the width of convective overshooting may turn out to be sensitive to the detailed calibration of its parameters.

3.3 A new model for the dissipation rate in non-local convection models in GARSTEC

Based on the discussion of the dynamic equations of the dissipation rate ϵ in the previous section, we will now derive a new expression for this quantity to close Eq. (2.49). We start by discussing problems with the local expression for the dissipation rate Eq. (2.44) when used in stellar evolution calculations including the 3-equation model, continue by comparing to a fully non-local Reynolds stress model to get an intuition for the behaviour of ϵ and finally derive a new expression for ϵ that can be included in the 3-equation model.

3.3.1 The problem: overshooting zones of convective cores growing unlimitedly during main-sequence stellar evolution

The equations of the 3-equation model Eq. (2.57), (2.58) and (2.59) are essentially equivalent to the dynamical equations for the TKE K, the squared fluctuations of temperature $\overline{\theta^2}$, and for the cross correlation between velocity and temperature fluctuations, denoted here by $J = \overline{w\theta}$. The latter can be derived from the physically more complete model of Canuto and Dubovikov (1998) by assuming (i) an isotropic velocity distribution, (ii) a local prescription to compute the distribution of the dissipation rate ϵ, (iii) the diffusion approximation for the non-local fluxes, and (iv) some minor simplifications in the closures used in the dynamical equations. As a variant, the 3-equation model may be used with local limit expressions for the non-local transport terms for $\overline{\theta^2}$ as well as J. As a theoretical analysis shows (see Kupka 2020 and references therein) only a full 3-equation model can feature a countergradient or "Deardorff" layer where J is positive, while the superadiabatic gradient β is negative. Only in such a model, both quantities can change their sign independently (the key to a positive convective flux in a countergradient stratification is the non-local transport of $\overline{\theta^2}$, as originally shown by Deardorff 1961 and Deardorff 1966). However, in both the fully non-local and the local limit of the 3-equation model variant as described above, overshooting gradually mixes the entire star in a stellar evolution calculation for a 5 $M_\odot$ (B-type) main-sequence star. In Fig. 3.1 we show the profile of the TKE as a function of fractional mass in this calculation. It can be seen that the energy extends substantially beyond the Schwarzschild boundary, reaching very close to the surface of the star. Due to the high efficiency of convective mixing the whole star would become essentially homogeneous which is unrealistic, because the star would evolve from the hydrogen to the helium main sequence, i.e. to the left in the colour-magnitude diagram, contrary to all observations (see Kippenhahn et al. 2012, Ch. 23.1). This problem was originally identified in the PhD thesis of Flaskamp (2003).

To solve this problem, Flaskamp (2003) suggested giving up the assumption of isotropy of TKE of the model of Kuhfuß (1987) in the overshooting zone and let the ratio of vertical to horizontal kinetic energy tend to zero. This limits the mixing efficiency in the outer layers of the overshooting zone, located above the stellar convective core, and avoids its unphysical growth throughout main-sequence evolution. If this simulation were plausible,

also a more realistic model for the anisotropy of the convective velocity field, derived, for instance, from the stationary limit of Eq. (19d) of Canuto and Dubovikov (1998), should solve this problem. Both variants of this approach are discussed below in Sect. 3.4.1.

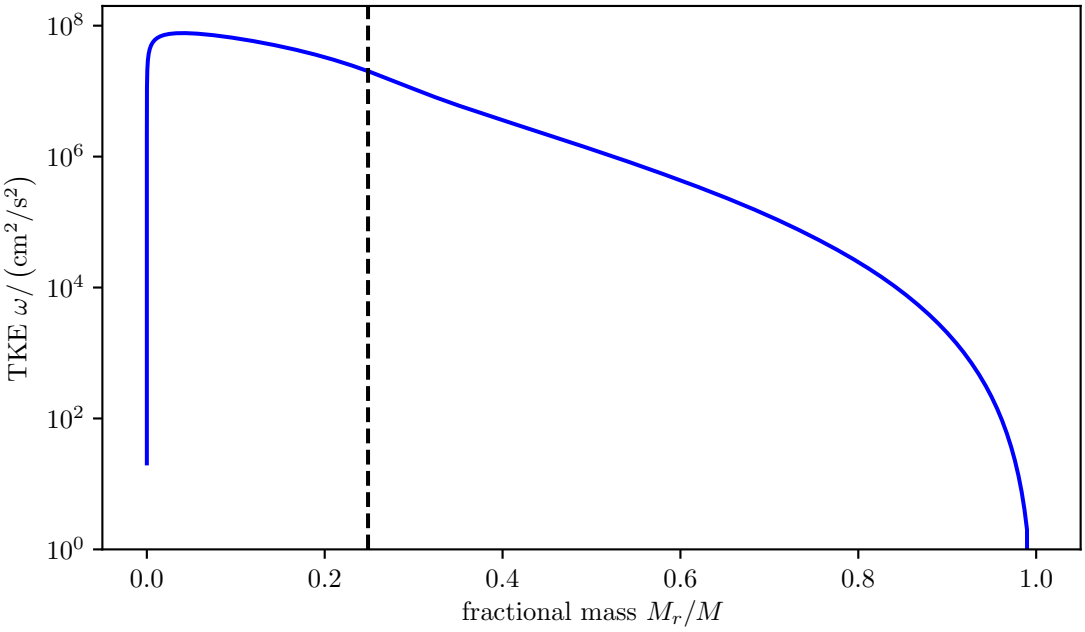

Figure 3.1: TKE as a function of the fractional mass for the original Kuhfuß 3-equation model. The formal Schwarzschild boundary, defined by $\nabla_{\mathrm{rad}} = \nabla_{\mathrm{ad}}$, is indicated by a dashed black line.

3.3.2 A comparison with a fully non-local Reynolds stress model

A progressive growth of the overshooting zone with time is not observed in 3D radiation hydrodynamical simulations of overshooting in DA white dwarfs (Kupka et al. 2018) either. Since the extension of the different zones in that case (Schwarzschild unstable convective zone with $J > 0$ and $\beta > 0$, countergradient region with $J > 0$ and $\beta < 0$, plume dominated region with $J < 0$ and $\beta < 0$, and wave dominated region with $J \approx 0$ and $\beta < 0$) compare quite well with results from the non-local Reynolds stress model of Canuto and Dubovikov (1998) solved in Montgomery and Kupka (2004) for the same type of stars, the latter can provide a guideline for the behaviour of variables such as ϵ as a function of depth. The overall structure of the overshooting zones and the behaviour of the convection related variables described in Montgomery and Kupka (2004) is very similar to that one which had already been found for A-type main-sequence stars in Kupka and Montgomery (2002), which in turn had been compared to earlier 2D radiation hydrodynamic (RHD) simulations of Freytag et al. (1996).

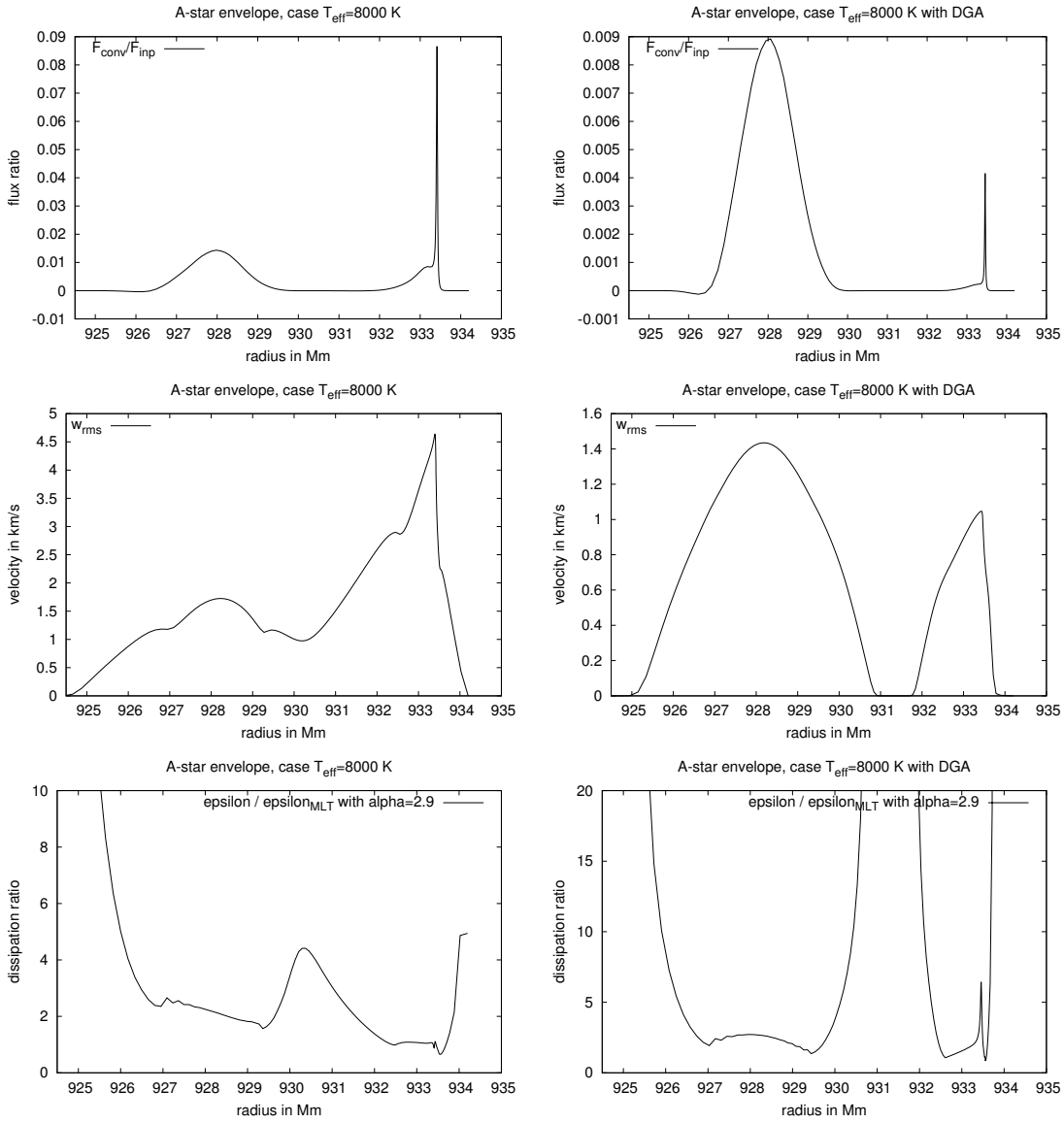

Figure 3.2: *Left panels*: convective flux in units of total flux, root mean square vertical velocity in units of km/s, and dissipation rate ϵ from Eq. (3.3) relative to a value computed from Eq. (2.44) and (2.38) with α as given in the figure legend as a function of radius. *Right panels*: same quantities as left panels, however, the downgradient approximation is used to compute third order moments instead of the full model used in Kupka and Montgomery (2002). The results are for one of the A-star envelope models discussed in Kupka and Montgomery (2002) (courtesy of F. Kupka).

We hence use the Reynolds stress convection model calculations of Kupka and Montgomery (2002) in Fig. 3.2 to illustrate the convective flux, the root mean square vertical velocity, and the dissipation rate as a function of depth. The left panels show results for

the full third order moment model, while the right panels shows results computed using the downgradient approximation. For an effective temperature of $T_{\rm eff} = 8000\,{\rm K}$ and $\log g$ slightly below the main sequence (see Kupka and Montgomery 2002 for further details) there are two convective zones, an upper one due to ionisation of neutral hydrogen and a lower one caused by double-ionisation of helium. They are connected by an overshooting region at a radius of ~ 931 Mm, and there is another overshooting region underneath the lower convective zone at ~ 926.5 Mm. For this setting, we compare the computation of dissipation rates from the full equation of Canuto and Dubovikov (1998) Eq. (3.3) with the standard mixing length prescription Eq. (2.44) for a range of bulk convective and overshooting layers. Clearly, the dissipation rate ϵ becomes much larger than the value computed from the MLT prescription as soon as the plume region of the overshooting zones (with $J < 0$ and $\beta < 0$) is reached, and which can be determined from the behaviour of the convective flux. At the bottom of the lower overshooting zone, ϵ becomes even order(s) of magnitudes larger than the oversimplified MLT prescription would predict. Note that if the downgradient (diffusion) approximation is used to compute third order moments, such as $\overline{q^2 w}$ in the model of Canuto and Dubovikov (1998) (the non-local fluxes of K, J, $\overline{\theta^2}$, and $\overline{w^2}$), a smaller overshooting is obtained in comparison with the complete third order moment model used in Kupka and Montgomery (2002). Hence, the two convection zones become separated at $T_{\rm eff} = 8000\,{\rm K}$, which allows observing this behaviour of ϵ even between the two convective zones. At lower $T_{\rm eff}$, for example at 7500 K, convection and overshooting are stronger also for the downgradient approximation of third order moments and the same behaviour is recovered as for the physically more complete third order moment model already for $T_{\rm eff} = 8000\,{\rm K}$. For that latter model the two convective zones become more tightly coupled and the increase of ϵ compared to the MLT prescription is eventually restricted to the lower overshooting zone only, for instance, for models with $T_{\rm eff} = 7200\,{\rm K}$.

We hence can draw the following conclusions from solutions of the Reynolds stress model of Canuto and Dubovikov (1998) for convective envelopes of A-type stars: irrespective of the various situations described above, deep inside the plume-dominated region characterised by $J < 0$ and $\beta < 0$ the MLT prescription to compute ϵ begins to fail by entirely missing out the drastic increase in dissipation in that region. However, the proper computation of ϵ is essential to determine the extent of the mixed region, since it drains kinetic energy from the overshooting flow. From Eq. (2.44) one can immediately conclude that underestimating ϵ in the MLT framework can be easily caused by overestimating the mixing length Λ or ℓ_0.

3.3.3 Reducing the mixing length in the overshooting zone

There is also a physical argument why the mixing length must be limited and even gradually shrink in the overshooting zone on top of a stellar convective core. Taking Λ to be about a pressure scale height at the convective core boundary results in a very large length scale. This is essentially the size of the convective core itself. The claim that such a large structure penetrates into the radiative zone makes no sense, both from the viewpoint of available

potential energy and from the viewpoint of the typical size of a convective structure. We note here that existing numerical simulations of convective cores are actually for extremely different physical parameter regimes, featuring mostly $\mathrm{Pr} \gtrsim 1$ or even $\mathrm{Pr} \gg 1$ (see, for instance, Rogers et al. 2013, Rogers 2015, Edelmann et al. 2019). They are unable to reproduce the very small levels of superadiabaticity ($\beta > 0$, but $|\beta/(\partial T/\partial r)_{\mathrm{ad}}| \ll 1$) at realistic stellar luminosities. This inevitably leads to excessive numerical heat diffusion and unrealistically small effective Peclet numbers (see Kupka and Muthsam 2017 for a discussion). Numerical simulations of convective cores are hence likely also subject to the convective conundrum problem reported for the Sun (cf. Gizon and Birch 2012, Hanasoge et al. 2016). Probably, they are not as reliable for guiding us as numerical simulations are in the case of convective overshooting near stellar surfaces (cf. Freytag et al. 1996, Tremblay et al. 2015, Kupka et al. 2018, and many others). In the following, we thus use a different chain of arguments to derive an improved estimate of Λ.

As a very first step, one could let Λ decay to zero within the overshooting zone, either linearly or exponentially, from the value it has at the Schwarzschild boundary. This ad hoc "fix" has been implemented into GARSTEC. The exponential decay model was chosen, and indeed this easily stops the growth of the overshooting zone as a function of stellar evolution time. The so enhanced dissipation rate, introduced by the decrease of the dissipation length, can be seen in Fig. 3.3 at the outer edge of the convective region. The model including the exponential decay has a central hydrogen abundance of 0.6. The stellar model computed with the original Kuhfuß 3-equation model was chosen to have the same maximum TKE in the convection zone to make the dissipation rates comparable.

Physically plausible extensions of the overshooting zone can be obtained from a "reduction factor", which forces an e-folding extent of the "decay" of the mixing length of 2% to 6% of the mass of the Schwarzschild-unstable region. In a 5 $\mathrm{M}_\odot$ main-sequence star, this limits the overshooting zone to contain about 12% to 29% in terms of the Schwarzschild core mass. The relative extent of the overshooting region in terms of the Schwarzschild core mass remains mostly constant along the main sequence. For an e-folding extent of 4% the overshooting region contains about 5% of the stellar mass at the beginning of the main sequence while it is shrinking to about 2% of the total mass at the end of the main sequence. The procedure introduces a free parameter, but it is sufficient as a proof of concept: a physically more complete model of ϵ constrains the overshooting contrary to earlier, alternative explanations that require unphysical parameter values to do so (such as $\overline{w^2}/K \to 0$ which is at variance with Kupka et al. 2018, see Sect. 3.4.1 below).

3.3.4 Some input from the dissipation rate equation

Can we carry over some of the physics contained in Eq. (3.1) or Eq. (3.3) into a local model for ϵ, which avoids the solution of an additional differential equation? If we model the non-local transport of TKE in Eq. (2.49) by a downgradient approximation, the closure $\overline{w\epsilon} \propto \tau^{-1}\,\overline{q^2 w}$ (see Canuto 1992, Eq. 37f) relates $\overline{w\epsilon}$ to $\partial\overline{w^2}/\partial z$ in Eq. (3.3) where τ refers to the dissipation rate timescale. The same behaviour is found for a direct downgradient closure for $\overline{w\epsilon}$ (i.e., computing it from $\partial\epsilon/\partial z$) as for example in Eq. (3.2). Let us hence assume

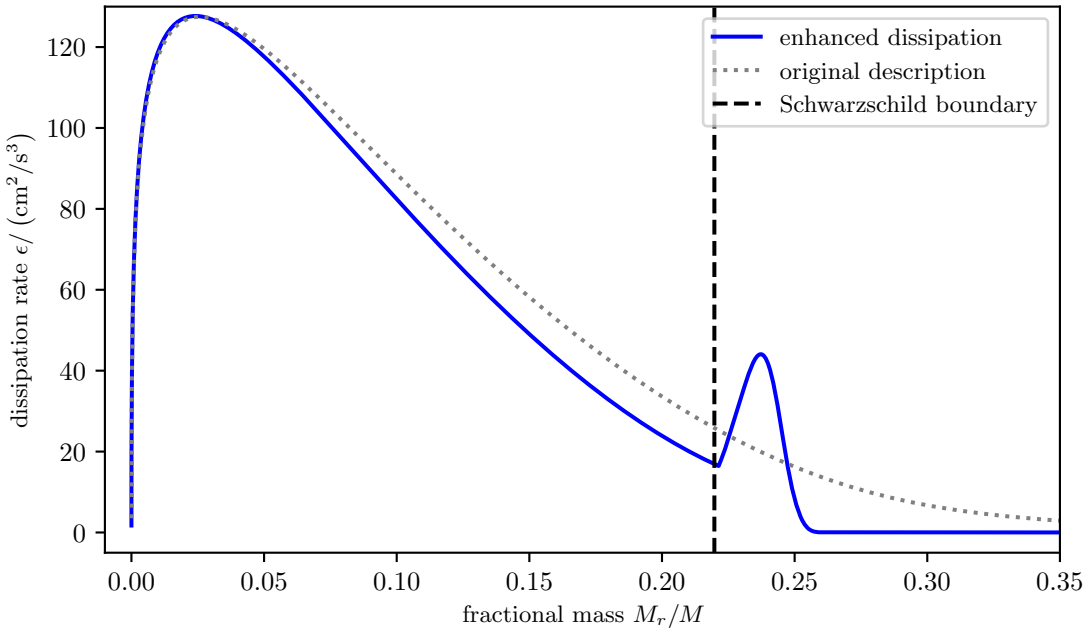

Figure 3.3: Dissipation rate as a function of fractional mass for the original Kuhfuß model and the Kuhfuß model including an ad hoc exponential decay of the dissipation length, shown with a grey dotted and a blue continuous line, respectively. The ad hoc exponential decay of the dissipation length leads to an increased dissipation rate at the beginning of the overshooting zone, indicated by the local maximum beyond the Schwarzschild boundary, followed by a sharp drop due to the rapid decay of TKE. The models have been chosen to have the same maximum TKE.

a local approximation for $D_\mathrm{f}(\epsilon)$, the non-local flux of ϵ, which replaces the derivatives of the outer divergence operator and the gradient operator in Eq. (3.3) by a product of reciprocal length scales. Inspecting Eq. (3.3), for the sake of simplicity, it appears desirable to model as many contributions as possible by expressions of type $\epsilon^2/K \propto \epsilon/\tau$. Instead of a length scale, we hence use the dissipation rate timescale $\tau = 2K/\epsilon$ to approximate $D_\mathrm{f}(\epsilon) \propto -\alpha_\epsilon \epsilon/\tau$ with a parameter α_ϵ. The same can be done also in the case of Eq. (3.1). If we furthermore assume the local limit of Eq. (2.49), $P = P_\mathrm{b} = \epsilon$, i.e. production of TKE by buoyancy equals its dissipation (Eq. 2.55), and if we also assume $c_3 = 0$, we obtain the following approximation for both Eq. (3.1) and Eq. (3.3):

$$-\frac{\alpha_\epsilon \epsilon}{\tau} = 2\,c_1 \frac{g\alpha_\mathrm{v} J}{\tau} - 2\,c_2 \frac{\epsilon}{\tau}\,. \tag{3.4}$$

To remain consistent with $g\alpha_\mathrm{v} J = \epsilon$ we have to require that $\alpha_\epsilon = 2c_2 - 2c_1$ if ϵ itself is computed from Eq. (2.44) and (2.38). In this case, we obtain a completely local model for the computation of ϵ.

We now use Eq. (3.4) to understand some implications from the different physical contri-

butions, that would be instead accounted for by its physically more complete counterpart, Eq. (3.1). To this end, let us relax the requirement $P_\mathrm{b} = \epsilon$ in Eq. (2.49) somewhat. In this case, whether the 1-equation or the 3-equation version of the Kuhfuß (1987) model is used, due to the non-locality of the flux of kinetic energy in Eq. (2.49), $\partial(\overline{q^2 w}/2)/\partial z \neq 0$, there is always a point where $J = 0$ (cf. Chap. 5 in Kupka 2020). At such a point, $\alpha_\epsilon = 2c_2$ is required from Eq. (3.4) for a non-vanishing dissipation rate ϵ. Right next to such a point, where $\epsilon > 0$ with $J < 0$, a value of $\alpha_\epsilon > 2c_2$ would be required whereas $\alpha_\epsilon < 2c_2$ where $J > 0$. So α_ϵ would have to be a function that has to be fine-tuned to obtain consistent results from Eq. (3.4) in the vicinity of $J = 0$. Moreover, because of the downgradient closure for $\overline{w\epsilon}$ also constraints on $\overline{w^2}/K$ would be imposed.

Such constraints appear unphysical: Eq. (3.4) does not provide a good starting point for a local model capable to capture at least the main gist of either Eq. (3.1) or Eq. (3.3). To proceed we need a physically more complete model for ϵ, i.e., we either have to abandon the mixing length prescription altogether or we need a more complete model equation than Eq. (3.1) to start from. Let us hence first have a look at Eq. (3.3), i.e., we no longer impose $c_3 = 0$ everywhere. The sibling of Eq. (3.4) which accounts for the production of dissipation by gravity waves in a stably stratified fluid then reads

$$-\frac{\alpha_\epsilon \epsilon}{\tau} = 2\,c_1 \frac{g\alpha_\mathrm{v} J}{\tau} - 2\,c_2 \frac{\epsilon}{\tau} + c_3 \epsilon \tilde{N}\,. \tag{3.5}$$

If we were to combine this equation with the 1-equation model of Kuhfuß (1986), β and J change sign at the same point so the perfect balancing constraint between $D_\mathrm{f}(\epsilon)$ and $-2\,c_2\epsilon/\tau$ reappears. In the region where $J < 0$, more freedom of how $D_\mathrm{f}(\epsilon)$ behaves is permitted. This changes once we switch to the 3-equation model of Kuhfuß (1987): since β and J then change sign at different locations, α_ϵ is no longer forced by c_2 at any point. In the end, the $c_3\epsilon\tilde{N}$ contribution decouples both $D_\mathrm{f}(\epsilon)$ and $\overline{w^2}/K$ from peculiar constraints required to be fulfilled at where $\beta = 0$ or where $J = 0$.

On the other hand, now there is an efficient local source for ϵ also where $\beta < 0$. This is particularly important for the 3-equation model which through its countergradient layer permits much larger enthalpy (and hence also TKE) fluxes in this region: considering that property it is understandable that the 3-equation model can be prone to large overshooting, unless the latter is limited by efficient dissipation. And this is just what gravity waves can provide.

3.3.5 Deriving a local model for ϵ with enhanced dissipation

For the sake of physical completeness, it would be preferable to switch to Eq. (3.3) and give up the local model Eq. (2.44) and (2.38) altogether. However, as a first step into that direction we can aim at modifying the computation of Λ for the stably stratified layers by guiding the necessary physical input through Eq. (3.3) and in particular through its local approximation, Eq. (3.5). In a local framework, we cannot accurately account for $D_\mathrm{f}(\epsilon)$.

Hence, we first express τ in terms of Λ in the local limit,

$$\epsilon = \frac{2K}{\tau} = c_\epsilon \frac{K^{3/2}}{\Lambda}\,, \tag{3.6}$$

from which we obtain that

$$\tau = \frac{2}{c_\epsilon}\frac{\Lambda}{K^{1/2}}\,. \tag{3.7}$$

To proceed we can now rewrite $c_3\epsilon\tilde{N}$ as follows:

$$c_3\epsilon\tilde{N} = c_3\frac{\epsilon}{\tau_\mathrm{b}} = 2\,c_3\frac{K}{\tau\,\tau_\mathrm{b}}\,, \tag{3.8}$$

where τ_b denotes the buoyancy timescale. Following the analysis in the previous subsection we now compare Eq. (3.8) with

$$-c_2\frac{\epsilon^2}{K} = -2\,c_2\frac{\epsilon}{\tau}\,. \tag{3.9}$$

In the stationary, local limit and assuming that we can absorb the contribution from $\alpha_\epsilon\epsilon/\tau + 2\,c_1 g\alpha_\mathrm{v} J/\tau$ into $-2\,c_2\epsilon/\tau$ for sufficiently small J and $\overline{w\epsilon}$ we obtain from Eqs. (3.5), (3.8), and (3.9) that

$$\frac{c_3/\tau_\mathrm{b}}{2\,c_2/\tau} = \frac{c_3}{2\,c_2}\frac{\tau}{\tau_\mathrm{b}} \approx 0.078125\frac{\tau}{\tau_\mathrm{b}} = \frac{25}{320}\frac{\tau}{\tau_\mathrm{b}} \approx 1\,, \tag{3.10}$$

where the numerical value is obtained from setting $c_2 = 1.92$ and $c_3 = 0.3$. Contributions absorbed into the $-2\,c_2\epsilon/\tau$ term could be accounted for by a small change of c_2. As inspection of the full Reynolds stress models solved in Kupka and Montgomery (2002) demonstrates, this is well justified since the two terms compared in Eq. (3.10) completely dominate where $J < 0$.

This motivates the idea to also scale Λ, which according to Eq. (3.7) is proportional to τ, by a contribution $\propto \frac{25}{320}\frac{\tau}{\tau_\mathrm{b}}$. In GARSTEC the mixing length required for the turbulent convection model of Kuhfuß (1987) is computed following the prescription of Wuchterl (1995),

$$\frac{1}{\Lambda} = \frac{1}{\alpha\,H_p} + \frac{1}{\beta_\mathrm{s}\,r}\,, \tag{3.11}$$

where β_s is a factor chosen to be 1 in convectively unstable layers, where $\beta > 0$ and thus $\nabla - \nabla_\mathrm{ad} > 0$, and β_s is possibly less than 1 elsewhere. We now account for the effect of enhanced dissipation by gravity waves through reducing β_s to values less than 1. To this end, we can interpolate between the two asymptotic cases $\tilde{N} \to 0$ and $\tilde{N} = \tau_\mathrm{b}^{-1} \gg \tau^{-1}$ through

$$\beta_\mathrm{s} = (1 + \lambda_\mathrm{s}\,\tilde{N})^{-1} \quad \text{for} \quad M_r > M_\mathrm{schw}\,, \tag{3.12}$$

where $M_{\rm schw}$ is the mass of the convectively unstable core and thus identifies the mass shell for which $\nabla = \nabla_{\rm ad}$ and λ_s is a model parameter. Comparisons with solutions of the non-local Reynolds stress model of Canuto and Dubovikov (1998) for A-type stars (Kupka and Montgomery 2002) show that $\tau_{\rm b} \approx 0.1\,\tau$ where the convective flux reaches its negative minimum. This range of values for $\tau_{\rm b}$ is what we also expect from Eq. (3.10) for a moderate variation of c_2.

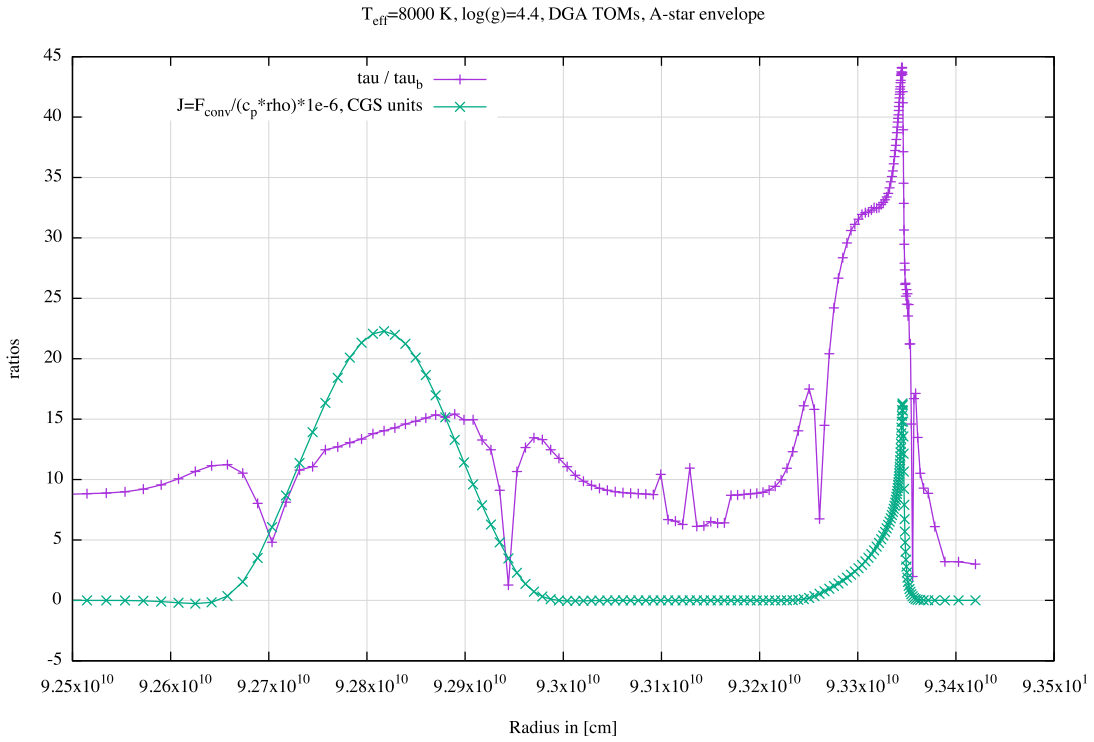

Figure 3.4: Ratio of $\tau/\tau_{\rm b}$ as a function of radius from a solution of the non-local Reynolds stress model as presented in Kupka and Montgomery (2002) assuming the downgradient approximation for third order moments. The timescale $\tau_{\rm b}$ is computed from $\tilde{N}^{-1}$ where the absolute value of β is taken. Sign changes are hence indicated by spikes. Both the overshooting zones below and above the lower and the upper convectively unstable zone show the same increase of $\tau/\tau_{\rm b}$ from 0 to more than 10 (the finite grid resolution prevents $\tau/\tau_{\rm b}$ from becoming actually zero) (courtesy of F. Kupka).

The results of Kupka and Montgomery (2002) can hence provide a rough guideline for the choice of $\lambda_{\rm s}$ and imply that Λ is rapidly reduced by an order of magnitude already within the countergradient region from the value it has at the Schwarzschild stability boundary (see Fig. 3.4 showing the ratio $\tau/\tau_{\rm b}$ with the purple line). This value is then maintained throughout the remainder of the countergradient region and the entire region with negative convective flux, in agreement with the $\tau\,\tilde{N} = O(1)$ suggested by Canuto (2011) in his Eq. (5h). The preceding arguments and the analysis in the previous subsection show how

this relation is connected with the full Eq. (3.3) and how this result can be implemented into a physically motivated reduction factor for the mixing length through Eq. (3.11) and (3.12). Since the rough constancy of τ/τ_b (or the "dominance" of the term $c_3\epsilon\tilde{N}$ in Eq. 3.3) also causes the linear decay of the root mean square velocity as a function of distance in the results of Kupka and Montgomery (2002) and Montgomery and Kupka (2004), and because the latter has also been recovered from 3D RHD (Kupka et al. 2018) for just those layers, the entire procedure is at least indirectly supported by this physically much more complete modelling. Similar results are not yet available for convective cores, however.

In spite of its simplicity, the disadvantage of Eq. (3.12) is the fact that λ_s is a dimensional parameter. It hence has to be determined separately for each stellar evolution model by numerical experiments, which yield the value it has to have for a sufficient reduction of Λ by an order of magnitude. For stars of different mass this may have to be changed, and for later stages of stellar evolution it will be even less convenient. What we need here is an estimate for τ. Without solving Eq. (3.3) this is akin to a hen and egg problem, since in the end this would require just the quantity Λ we are up to compute: $\lambda_\mathrm{s} = (25/320)\,\tau$ with τ computed from Eq. (3.7). We could simplify this by setting $\tau = (2/c_\epsilon)(\alpha H_p K^{-1/2})$ or $\tau = (2/c_\epsilon)(rK^{-1/2})$, as this formula is to be used only for $r > 0$ and $H_p < \infty$ anyway. However, this has the disadvantage that near the outer edge of the overshooting zone, where $K \to 0$ one obtains $\tau \to \infty$. From standard calculus applied to Eq. (3.11) we then obtain that $\Lambda \approx \alpha H_p$ right there, which is exactly not what we want. But we can rewrite Eq. (3.12) into

$$\beta_\mathrm{s} = (1 + c_4\Lambda K^{-1/2}\tilde{N})^{-1} \quad \text{for} \quad M_r > M_\mathrm{schw} \tag{3.13}$$

with

$$c_4 = \frac{c_3}{2\,c_2}\frac{2}{c_\epsilon} \approx \frac{25}{320}\frac{2}{c_\epsilon} \approx \frac{5}{32c_\epsilon} = 0.19659 \approx 0.2\,, \tag{3.14}$$

for which we have used $c_\epsilon = \pi(2/(3\,\mathrm{Ko}))^{3/2} \approx 0.7948 \approx 0.8$ with $\mathrm{Ko} = 5/3$ from Canuto and Dubovikov (1998)[3]. This is achieved by realising that

$$\begin{aligned}\lambda_\mathrm{s}\,\tilde{N} &= c_4\Lambda K^{-1/2}\,\tilde{N}\\ &= \frac{c_3}{2c_2}\cdot\frac{\tau}{\tau_\mathrm{b}}\,,\end{aligned}$$

which is just Eq. (3.10) and where we have used Eq. (3.7) and the definition of the parameter c_4. Equation (3.13) is equivalent to Eq. (3.12) and also interpolates between the two asymptotic cases, the transition between locally stable to unstable stratification ($\tilde{N} \to 0$) as well as the overshooting region far away from the convective zone, where flow motions are dominated by waves ($\tilde{N} = \tau_\mathrm{b}^{-1} \gg \tau^{-1}$). Equation (3.11) combined with Eq. (3.13)–(3.14) can be rewritten into a quadratic equation for Λ for which the positive branch can be taken or which can be solved implicitly, for instance, by an iterative scheme (the

[3]If we used the value of $c_\epsilon \approx 2.18$ suggested in Kuhfuß (1987) we would instead obtain that $c_4 \approx 0.07$. However, in the product $c_\epsilon K^{3/2}/\Lambda$ the constant c_ϵ to some extent cancels out, hence, the overshooting distance is only weakly depending on this parameter. We discuss this further in Sec. 4.3.1

former will be done in Ch. 4). In principle, the parameter c_4 could be adjusted to achieve the goal of $\tau_\mathrm{b} \approx 0.1\,\tau$ or rather $\Lambda(\min(F_\mathrm{conv})) \approx 0.1\Lambda(M_r = M_\mathrm{schw})$ which mimics the result discussed in Fig. 3.4 and in the previous paragraphs. However, we prefer to assume sufficient generality of Eq. (3.3) and its parameters and therefore use them without further adjustments. Some numerical experiments on the effects of varying c_4 can be found in Sec. 4.3.1. In the next section we show that this procedure also leads to a finite overshooting layer which does not (notably) grow during stellar evolution.

3.4 Discussion: Kuhfuß 3-equation model with enhanced dissipation

3.4.1 Flow anisotropy instead of enhanced dissipation

A very important difference between the Kuhfuß (1987) and the Canuto and Dubovikov (1998) model is the set of convective variables considered. In addition to the total TKE Canuto and Dubovikov (1998) also solve for the vertical component $\overline{w^2}$ of the TKE. This means that the ratio of $\overline{w^2}/K$ is not fixed a priori, but is an outcome of the theory. Kuhfuß (1987) on the other hand, assumes full isotropy in the whole convection zone which translates to a fixed ratio of $\overline{w^2}/K = 2/3$. Furthermore, the Kuhfuß model uses an isotropic estimate of the radial velocity $u_\mathrm{iso} = \sqrt{2/3\omega}$ in the non-local terms. Hence, these terms are potentially overestimated in the overshooting zone by overestimating the ratio of vertical to total kinetic energy. This could result in an unreasonably large overshooting zone. The treatment of the flow anisotropy is especially problematic at convective boundaries where the flow turns over. In the convective boundary layers, the motions change from being predominantly radial to becoming predominantly horizontal. This means that the ratio of vertical to total kinetic energy should drop from the isotropic value to smaller values. To study the impact of anisotropy, we mimic the change of the flow pattern by introducing an artificial anisotropy factor $\xi^2 = \overline{w^2}/K$. This anisotropy factor is set to a value of $\xi = \sqrt{2/3}$ in the bulk of the convection zone and then linearly decreases to a value of zero from the Schwarzschild boundary outwards. This is most probably not a very physical behaviour, but just meant for illustrative purposes. The profile of this artificial anisotropy factor is shown in the left panel of Fig. 3.5. The profile of the TKE computed with this anisotropy factor is shown in the right panel of the same figure. The black dashed line indicates the Schwarzschild boundary. It can be seen that an overshooting zone beyond the Schwarzschild boundary emerges, which has, however, a clearly limited extent. As intended, a limitation of the anisotropy could solve the problems observed with the original version of the 3-equation model. The description requires another free parameter which is the slope of the linear function. The slope parameter directly controls the overshooting distance, which is very similar to other ad hoc descriptions of convective overshooting. Also, the functional form of ξ has not been determined by physical arguments but has been chosen arbitrarily.

This unfavourable situation should be avoided by a physically motivated estimate for

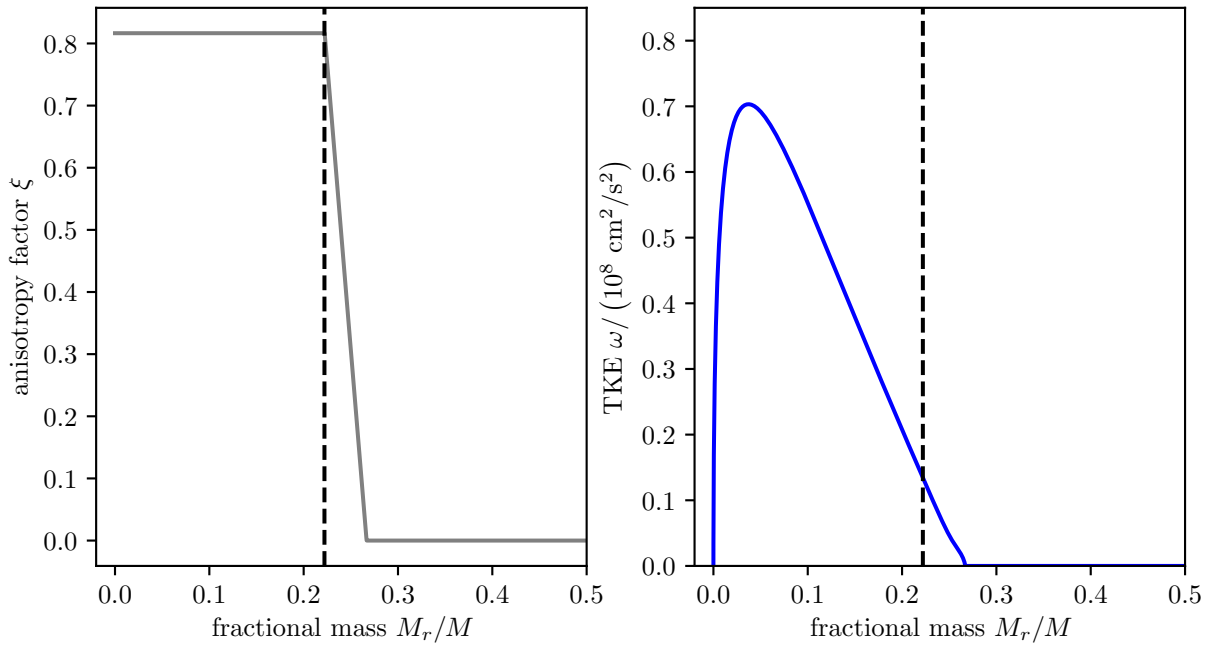

Figure 3.5: Artificial anisotropy factor ξ and TKE as a function of fractional mass in the left and right panel, respectively. The black dashed line indicates the Schwarzschild boundary.

the anisotropy factor. This requires to compute the vertical TKE. To obtain an estimate of the distribution of the TKE in the Kuhfuß (1987) model, we start from the fourth equation of the Canuto and Dubovikov (1998) model:

$$\frac{\partial}{\partial t}\frac{1}{2}\overline{w^2} + D_\mathrm{f}\left(\frac{1}{2}\overline{w^2}\right) = -\frac{1}{\tau_{pv}}\left(\overline{w^2} - \frac{2}{3}K\right) + \frac{1}{3}(1+2\beta_5)g\alpha_\mathrm{v}J - \frac{1}{3}\epsilon\,, \tag{3.15}$$

which solves for the vertical turbulent kinetic energy $\overline{w^2}$. Here, τ_{pv} refers to the dynamic timescale of pressure velocity correlations and β_5 is a parameter assumed to be 1/2. Not solving the dynamic equation for $\overline{w^2}$ implies that also $D_\mathrm{f}\left(\frac{1}{2}\overline{w^2}\right)$ is unknown. A reasonable way to compute this quantity from the Kuhfuß (1987) model is again to assume an isotropic distribution of the fluxes: $D_\mathrm{f}\left(\frac{1}{2}\overline{w^2}\right) = \frac{1}{3}D_\mathrm{f}(K)$. By rearranging and neglecting the time-dependence in Eq. (3.15) we can define an anisotropy factor:

$$\frac{\overline{w^2}}{K} = \frac{2}{3} - \frac{\tau_{pv}}{K}\left(\frac{1}{3}D_\mathrm{f}(K) - \frac{1}{3}(1+2\beta_5)g\alpha_\mathrm{v}J + \frac{1}{3}\epsilon\right)\,. \tag{3.16}$$

All quantities in Eq. (3.16) can be computed within the Kuhfuß 3-equation model.

We have computed the anisotropy factor according to Eq. (3.16) for a stellar model which used the original version of the Kuhfuß 3-equation model. The result is shown in

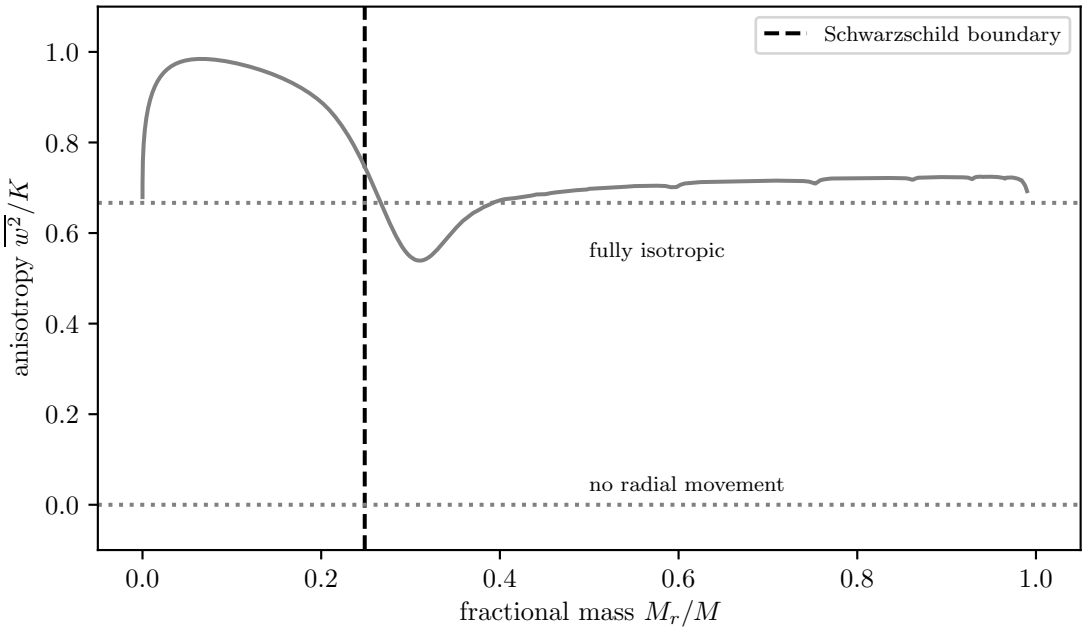

Figure 3.6: Estimate of the anisotropy factor according to Eq. (3.16) for a 3-equation model without limited dissipation length scale Λ. The profile of the turbulent kinetic energy of this model is shown in Fig. 3.1.

Fig. 3.6. In the bulk of the convection zone within the Schwarzschild boundary, the estimated anisotropy points towards a radially dominated flow. Directly beyond the Schwarzschild boundary, the estimated anisotropy factor drops below the isotropic value of 2/3. This can be attributed to the negative convective flux in the overshooting zone, which according to Eq. (3.16) reduces the ratio of vertical to total kinetic energy. Further out in mass coordinate, the estimated anisotropy increases again slightly above a value of 2/3 and remains to a good approximation constant over the region in which positive kinetic energy is observed (see Fig. 3.1).

Introducing this anisotropy factor into the Kuhfuß 3-equation model would not substantially reduce the estimate of the radial velocity. On the contrary, over large parts of the model the value of the radial velocity would be even larger than the current estimate, as we find an anisotropy factor above the isotropic value of 2/3. To finally settle the question of the flow anisotropy in Reynolds stress models, one also has to solve the respective equation for the vertical kinetic energy (Eq. 3.15 shown here, as taken from the Canuto and Dubovikov 1998 model) self-consistently coupled to the non-local convection model. However, since such a more realistic anisotropy factor cannot resolve the problem of excessive mixing found in the original Kuhfuß 3-equation model and because its implementation as an additional differential equation increases the complexity of the model, we first perform a thorough analysis of the improved 3-equation model in Ch. 4 and postpone the extension of this new model to future work.

3.4.2 Dissipation in the Kuhfuß 1- and 3-equation model

We have implemented the enhanced dissipation mechanism, developed in Sect. 3.3.5, into GARSTEC. For the details of the implementation, we here refer to Ch. 4. With this implementation, we solve the stellar structure equations and the convective equations (2.57) - (2.59) self-consistently. We note that for consistency and to simplify the comparison between the 1-equation and the 3-equation model, we set $c_\epsilon = C_\mathrm{D}$, whence it follows that $c_4 \approx 0.072$ in those calculations. As an example, we show here the TKE in a 5 $\mathrm{M}_\odot$ main-sequence star in Fig. 3.7. The Schwarzschild boundary is indicated with a black dashed line. In this model, the TKE extends slightly beyond the Schwarzschild boundary, which means that an overshooting zone emerges consistently from the solution of the model equations. However, in contrast to Fig. 3.1 the energy does no longer extend throughout the whole star but has a clearly limited extent as one would expect for this kind of star in this evolutionary phase. This shows already that the enhanced dissipation mechanism proposed above is able to solve the problems observed in the original version of the 3-equation Kuhfuß convection model. The detailed structure and the behaviour of stellar models with different initial masses will be discussed in Ch. 4.

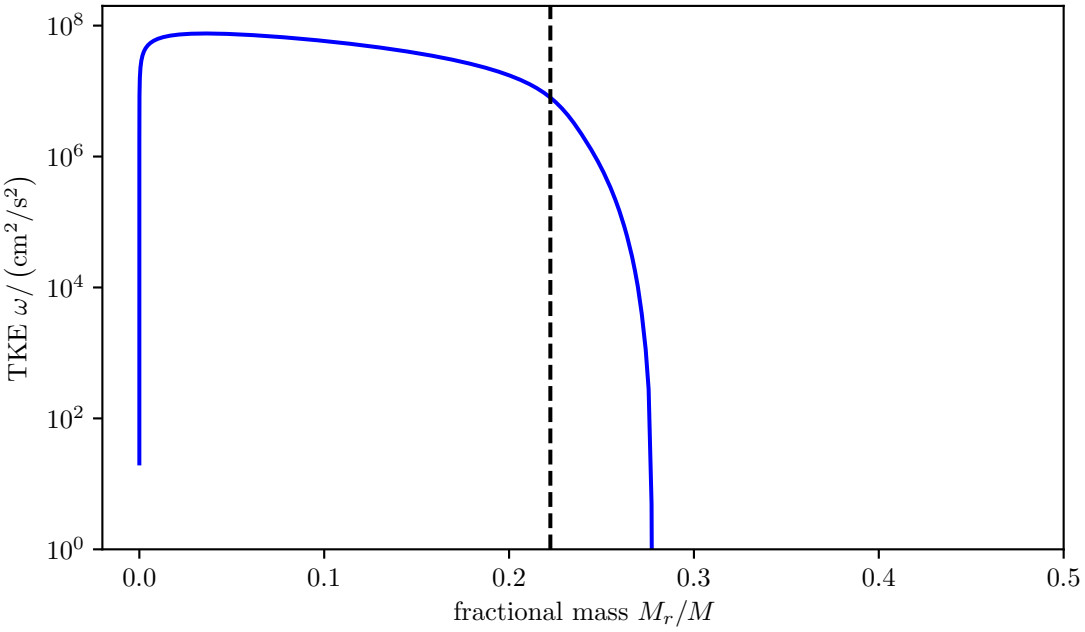

Figure 3.7: TKE as a function of the fractional mass for the Kuhfuß 3-equation model, including the improved dissipation mechanism. The Schwarzschild boundary is indicated by a dashed black line.

The results obtained from the different versions of the Kuhfuß model can be interpreted by studying the individual terms of the TKE equation (Eq. 2.57) in more detail. In Fig. 3.8 we show the three terms of the TKE equation—buoyant driving, dissipation and non-local

term—with a corresponding red, black, and blue line respectively for the 1-equation model (panel a), the original 3-equation model (panel b) and the improved 3-equation model (panel c). Stellar models applying the non-local 1-equation theory posses a clearly bounded convective region with a reasonable extent. However, this is achieved by suppressing the countergradient layer and artificially coupling the sign of the convective flux to that one of the superadiabatic gradient.

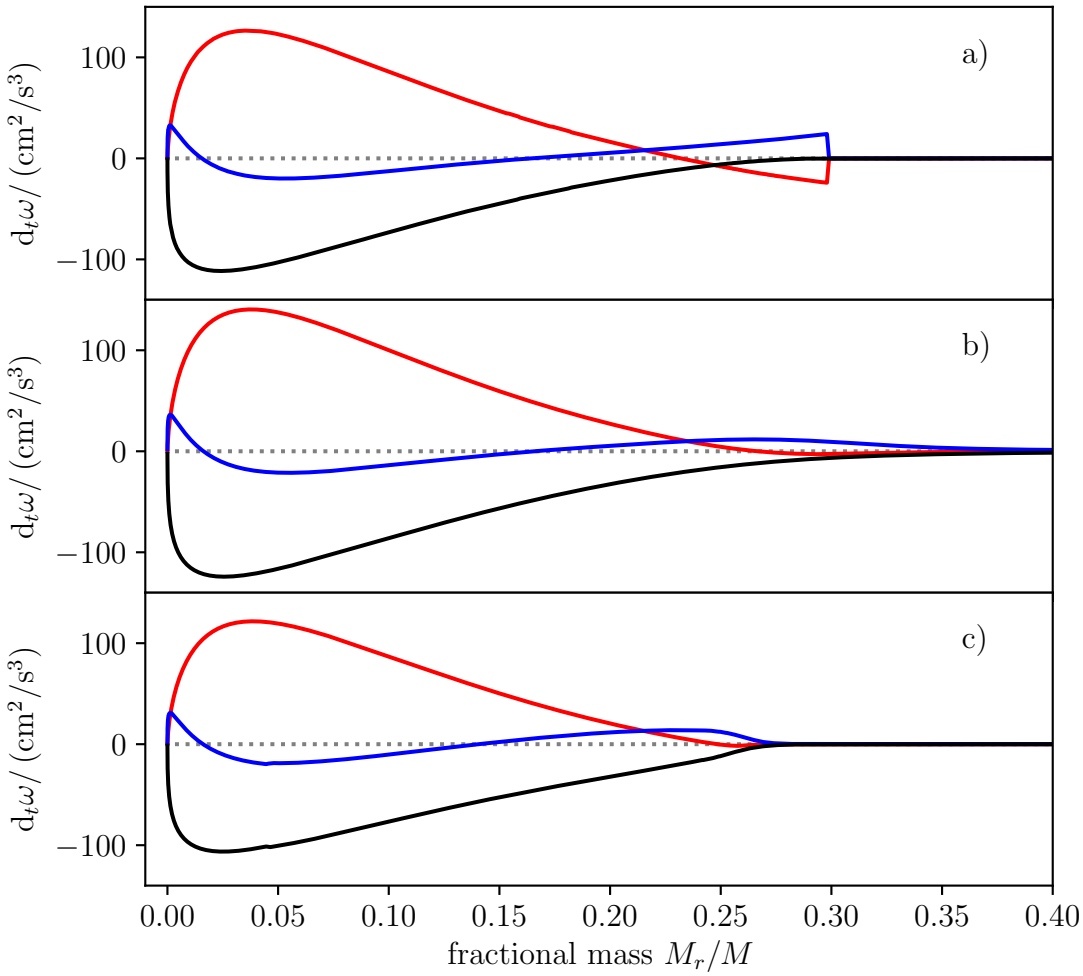

Figure 3.8: Comparison of the different terms in the TKE equation (Eq. 2.57) in the Kuhfuß 1-equation (panel a), original 3-equation (panel b) and improved 3-equation (panel c) model. The buoyant driving term, the dissipation term and the non-local flux term are shown with a red, black, and blue line here.

When using the 3-equation model in its original version, this welcome property vanishes and the stellar models become fully convective. As discussed in Sec. 2.5 the 3-equation model does not approximate the convective flux by a local model, but rather solves an

additional differential equation for it. This reduces the coupling of the different convective variables. Intuitively, one would expect this model to be physically more complete than the 1-equation model and to yield physically improved stellar models (see the discussion in Sect. 5 of Kupka 2020). However, the stellar models computed with the 3-equation model look physically unreasonable, as the existence of fully convective B-stars with 5 $M_\odot$ is excluded from the lack of stars hotter than the hydrogen main sequence.

This raises the question of why a seemingly physically more complete model leads to worse results. It can be illustrated by comparing the TKE terms in the 1- and original 3-equation models shown in panels a) and b) in Fig. 3.8. In the 1-equation model, the buoyant driving term which is proportional to the convective flux shows negative values in the overshooting zone, which is expected due to the buoyant braking in the stable layers. The buoyant term even exceeds the actual dissipation term in magnitude. This means that in the 1-equation model it is not the dissipation term but rather the buoyant driving term which acts as the main sink term in the overshooting zone. When applying the 3-equation model, the buoyant term is still negative in the overshooting zone. The values are, however, much smaller in magnitude compared to the 1-equation model. The dissipation and non-local flux term have about the same magnitude in the overshooting zone as obtained with the 1-equation model, because their functional form did not change. Considering that it was the buoyant driving term which was acting as the main sink term, the 3-equation model in its original form is lacking a sink term in the overshooting zone. This naturally explains the excessive overshooting distance found for this model.

To understand how the dissipation by buoyancy waves can mitigate this problem, it is worth to recall the approximation for the convective flux in the 1-equation model. Kuhfuß (1987) has approximated this to be $\Pi \propto (\nabla - \nabla_{\rm ad})$ as shown in Eq. (2.50) and (2.51). As the convective flux is the major sink term in the overshooting zone in the 1-equation model, one possibility is to introduce a dissipation term which has the same dependence, $\epsilon \propto (\nabla - \nabla_{\rm ad})$. A process with this dependence would be, for example, the dissipation by buoyancy waves as proposed above. We have demonstrated that the enhanced dissipation by buoyancy waves reduces the overshooting distance again to a more reasonable extent for the TKE (see Fig. 3.7). The related terms of the TKE equation are shown in Fig. 3.8 in panel c). In the overshooting zone, the magnitude of the dissipation term is now substantially larger than the negative buoyancy term, such that it acts as the dominant sink term. Also, the shape of the dissipation profile has changed compared to the original 3-equation case. The transition from finite to zero values looks smoother for the improved 3-equation model because the temperature gradient which has readjusted differs in comparison with the 1-equation model.

This comparison shows why the original version of the 3-equation model results in fully convective stars. The fact that a sink term is missing points again at the importance of a dissipation term, which is proportional to $(\nabla - \nabla_{\rm ad})$. At a first glance, a negative convective flux with larger magnitude in the overshooting zone could also increase the sink term in the TKE equation. But the following line of arguments shows that this hypothesis leads to implausibly large non-local fluxes.

Here, we consider Eq. (2.57)–(2.59).[4] Let us assume that J, or, equivalently, Π in Eq. (2.57)–(2.59) becomes larger in magnitude in the region where it is negative. Then, the buoyant driving term shown in panel b of Fig. 3.8 changes towards more negative values. This permits the source, the divergence of the flux of kinetic energy, to become smaller. However, in that case, the driving term (containing Π) also becomes larger in the entropy fluctuation equation Eq. (2.59). Since the vertical velocities have to become smaller, when the non-local flux of kinetic energy becomes smaller (and we assume a constant anisotropy in this thought experiment), the squared fluctuations of entropy, Φ, or of temperature, $\overline{\theta^2}$, have to become larger instead. But for $\Pi < 0$ in the region we consider here, both $-\Pi/\tau_{\rm rad}$ and $(2\nabla_{\rm ad}T/H_p)\Phi$ act as sources, which are boosted in the convective flux equation Eq. (2.58). Unless we would consider a large rate of change in the non-local transport of convective flux and entropy fluctuations, the only way to obtain an equilibrium solution in this model is to increase velocities and thus also the flux of kinetic energy. This is exactly the solution observed in panel b of Fig. 3.8 with its excessively extended overshooting. The closure used in Canuto (1993) and Canuto and Dubovikov (1998), which also accounts for buoyancy contributions to the correlation between fluctuations of temperature and the pressure gradient (the $-\Pi/\tau_{\rm rad}$ term in Eq. 2.58) does not change this argument. But a scenario that builds up large fluctuations of entropy in the overshooting region, where radiative cooling should efficiently smooth them while it has to suppress high velocities, appears unphysical. Thus, this alternative can be excluded.

Since extensive overshooting, which eventually mixes the entire B-star, is ruled out by observations, we are left with flow anisotropy or enhanced dissipation due to the generation of waves as physical mechanisms to limit overshooting in the 3-equation framework. Because extreme levels of flow anisotropy are neither found in solar observations nor in numerical simulations of overshooting in white dwarfs (Kupka et al. 2018), nor in solutions of the model of Canuto and Dubovikov (1998) for A-stars (Kupka and Montgomery 2002) or white dwarfs (Montgomery and Kupka 2004), there is hardly evidence for this idea. On the contrary, the enhanced energy dissipation rate is contained in the full model of Canuto and Dubovikov (1998), which yields at least some qualitative agreement with numerical simulations of several scenarios of stellar overshooting (see Kupka and Montgomery 2002 and Montgomery and Kupka 2004 and compare with Kupka et al. 2018 for the latter). This makes the improved computation of the dissipation rate of kinetic energy the most plausible improvement of the 3-equation model to remove the deficiency the model has had in its original version, proposed by Kuhfuß (1987).

[4] We point out that exactly the same sequence of arguments applies to the equivalent three equations for the turbulent kinetic energy $K = \overline{q^2}/2$, the squared fluctuation of the difference between local temperature and its Reynolds average, $\overline{\theta^2}$, and the cross correlation between velocity and temperature fluctuations, $J = \overline{w\theta}$, as they appear in the model of Canuto and Dubovikov (1998) and discussed in Kupka (2020).

3.5 Conclusions

The original model by Kuhfuß (1987) was shown by Flaskamp (2003) to lead to convective overshooting zones on top of convective cores that fully mix the entire object on a fraction of its main sequence lifetime. We verified that the ad hoc cure to reduce the ratio of vertical to total TKE to zero no longer works once realistic models for that quantity are used. From a physical point of view, the ad hoc cure is hence ruled out as an explanation for this deficiency of the model by Kuhfuß (1987). In this chapter, a physically motivated modification of the mixing length has hence been suggested, which takes into account that the dissipation rate of TKE has been underestimated by the original 3-equation model of Kuhfuß (1987). In Ch. 4 we present more detailed tests of the improved 3-equation model proposed in this chapter based on stellar evolution tracks for A- and B-type main sequence stars of different masses.

One conclusion from these analyses appears to be that the minimum physics to obtain realistic models of overshooting layers require accounting for non-locality of the fluxes of kinetic energy and potential temperature (as intended by Kuhfuß 1987) and in addition to account for the variation of the anisotropy of turbulent kinetic energy as a function of local stability and non-local transport. If the latter is done in a realistic way, it becomes also clear that a physically more complete model of the dissipation rate of TKE is needed. All these features are already provided by the model of Canuto and Dubovikov (1998), which in its most simple form accounts for non-locality with the downgradient approximation (as in the model of Kuhfuß 1987). However, such a complex convection model has not yet been implemented in a stellar structure and evolution code. The present simplification is an attempt to carry over the most important features of the more complete model by Canuto and Dubovikov (1998) into the Kuhfuß (1987) model, which we have implemented in the stellar structure and evolution code GARSTEC.

Switching to more complex non-local convection models in a stellar evolution code is not an easy task. This requires that the model and its implementation also account for the following:

1. Realistic, mathematically self-consistent boundary conditions. This is taken care of in the current implementation of the Kuhfuß (1987) model in GARSTEC.

2. A fully implicit, relaxation based numerical solver for the resulting set of equations. This is fulfilled by GARSTEC as well. Adding further differential equations always means some non-trivial work on this side.

3. A stable, monotonic interpolation scheme for the equation of state. Again this is fulfilled in GARSTEC (Weiss and Schlattl 2008). If this is not fulfilled, β cannot be computed correctly and any closure depending on its sign becomes uncertain, since oscillations may be fed into its computation.

4. A robust formulation of the dynamical equations which avoids cancellation errors introduced through a nearly perfectly adiabatic stratification. This is realised in

the implementation of the Kuhfuß (1987) model in GARSTEC indicated by the smoothness of the equation terms in Fig. 3.8. This can be attributed to the fact that the implementation uses Eq. (2.60) to compute the temperature gradient instead of numerical derivatives.

If the modified mixing length Eq. (3.11) and (3.12) and even more so Eq. (3.11) with Eq. (3.13)–(3.14) turns out to produce stable, physically meaningfully evolving overshooting zones with GARSTEC, further tests of this approach are highly warranting. These may also motivate the implementation of fully non-local Reynolds stress models at the complexity level of Canuto and Dubovikov (1998) which completely avoid the introduction of a mixing length with all its shortcomings in future work (see discussion in Ch. 6). In the remainder of the thesis, the 3-equation model including the new dissipation mechanism will be applied.

Chapter 4

Overshooting in intermediate-mass main-sequence stars

Parts of this chapter have been submitted to Astronomy and Astrophysics (Ahlborn et al. 2022) in collaboration with Friedrich Kupka, Achim Weiss and Martin Flaskamp. The manuscript is currently undergoing revision for resubmission. The work in this chapter has been carried out by me. The text has been written mainly by me, with contributions from the other authors. The original introduction to Ahlborn et al. (2022) has been used for Ch. 1.

4.1 Introduction

We have discussed in Sec. 2.3.2 that the extent of convective regions is substantially underestimated when using MLT (e.g. Bressan et al. 1981; Maeder and Mermilliod 1981; Pietrinferni et al. 2004; Pedersen et al. 2021). To account for the underestimation and increase the extent of convective regions, ad hoc overshoot mixing at convective boundaries has been introduced, some of which have been discussed in Sec. 2.3.4. Overshooting has profound effects on the luminosity, lifetime and age of stars possessing a convectively burning core. As we have pointed out, most of the ad hoc descriptions do not constrain the size or thermal structure of the overshooting region self-consistently. Both deficiencies can be overcome by the class of TCM described in 2.4. In this chapter, we describe the application of the Kuhfuß (1987) TCM as described in Sec. 2.5 including the dissipation mechanism described in Ch. 3 implemented into GARSTEC to compute the evolution of low and intermediate mass main-sequence stars. We show that an overshooting zone emerges naturally as a solution of the TCM equations. To characterise the thermal structure of the overshooting zone resulting from the TCM, we refer to Zahn (1991) who differentiates between thermally efficient and inefficient convection. Thermally efficient convection is able to modify the model temperature gradient and is therefore referred to as subadiabatic penetration. Thermally inefficient convection leaves the temperature gradient unchanged while still mixing chemical elements. Zahn (1991) refers to this as overshoot mixing. The stellar

models computed including the Kuhfuß (1987) TCM will be compared to stellar models using parametrised overshooting descriptions as described in Sec. 2.3.4. To account for the required mixing at convective boundaries, we use the exponential overshooting described by Freytag et al. (1996). For the overshooting zone, the radiative temperature gradient is assumed in the models with parametrised overshooting.

This chapter is structured as follows. In Sec. 4.2 we describe the implementation of the newly derived dissipation mechanism into the Kuhfuß (1987) TCM. In Sec. 4.3 we describe the detailed structure of the core of a 5 $M_\odot$ main-sequence star and show that the newly derived dissipation mechanism leads to physically reasonable properties of convection in the framework of the Kuhfuß convection model. In Sec. 4.4 we compute stellar models on the main sequence in a mass range of 1.5 to 8 $M_\odot$. The results are discussed in Sec. 4.5 and we conclude in Sec. 4.6.

4.2 Implementation of the Kuhfuß (1987) model

We have implemented the Kuhfuß (1987) convection model as described in Sec. 2.5 into GARSTEC. This includes the three partial differential equations for the turbulent kinetic energy (TKE) ω, the convective flux Π, and the entropy fluctuations Φ, as well as the increased dissipation rate in the overshooting zones. We will refer to this model as the 3-equation model.

4.2.1 Convection equations

As most modern stellar evolution codes, GARSTEC makes use of the implicit Henyey scheme to solve the four stellar structure equations (Henyey et al. 1964, 1965; Kippenhahn et al. 1967). The equations describing convection by MLT are solved algebraically outside the four stellar structure equations. To incorporate the three equations of the convection model, Flaskamp (2003) has extended the Henyey-scheme of GARSTEC to solve for in total seven variables (four stellar structure variables + three convection variables). A solution for both the stellar structure and the convective variables is found by iterating over all variables simultaneously. The coefficients of the convection model depend on the stellar structure variables, such that the behaviour of the convection model is strongly coupled to the stellar structure. On the other hand, the stellar structure is coupled to the convective variables through the temperature gradient and the chemical composition. As described in Sec. 2.5.2 the temperature gradient of the stellar model is computed self-consistently from the convective flux in each iteration (see Eq. 2.60). The chemical mixing in convective zones is computed in the framework of a diffusion equation alongside the composition changes due to nuclear burning after the structure equations have been solved. The diffusion constant is computed from the TKE determined by the convection model. Following Langer et al. (1985) the diffusion coefficient is computed as

$$D_{\mathrm{conv}} = \alpha_s \Lambda \sqrt{\omega}\,, \tag{4.1}$$

where we have chosen the same parameter α_s as for the diffusion coefficient D_s of entropy in Eq. (2.50) (see also the discussion in Sec. 2.3.1).

The equations can also describe time-dependent effects. This was demonstrated for example by Flaskamp (2003), when computing models through the core helium flash at the tip of the red-giant branch, by Wuchterl and Feuchtinger (1998) in an application to protostars and non-linear pulsations, and by Feuchtinger (1999b) for RR Lyrae stars. In this work, however, we focus on main-sequence stars which evolve on the nuclear timescale of hydrogen burning. This means that structural changes are sufficiently slow to neglect time-dependent terms and immediately solve for the stationary solution of the convection equations (left-hand sides of the TCM equations Eq. (2.57) to (2.59) are set to zero). By iterating for the stationary solution, the code searches for the converged stellar structure and convection variables for a given chemical composition. When non-local effects are included in the convection model, the stationary solution describes the overshooting zone self-consistently. Its extent and temperature gradient are only constrained by the convection model, without any external descriptions.

As described in Sec. 2.5.2, the Kuhfuß (1987) convection model contains a number of parameters. The values for these parameters need to be set. As described above, C_D and γ_R are obtained by calibrating a local model to MLT. The parameter values for the non-local terms $\alpha_\omega, \alpha_\Pi$ and α_Φ cannot be calibrated to MLT as they describe intrinsically non-local effects. Kuhfuß (1987) suggests a default value of $\alpha_\omega = 0.25$ by comparing kinetic energy and dissipation in a ballistic picture. No default values have been given for the parameters α_Π and α_Φ in the non-local case. Although both the 1- and 3-equation models still contain a number of parameters, they are advantageous compared to for example MLT because the parameters describe physically more fundamental properties of the theory. For example, the parameter α_ω describes the impact of the non-local flux of the TKE, which is responsible for the extent of the overshooting region. However, compared to exponential overshooting or step overshooting α_ω does not set the actual length scale of the overshooting. The extent of the overshooting is determined self-consistently from the solution of the TCM equations. We will investigate the impact of these other parameters further below.

4.2.2 Dissipation rate

In Ch. 3 we showed that the original description of the dissipation rate proposed by Kuhfuß (1987) leads to an excessively large overshooting region. Therefore, in Ch. 3 the dissipation rate was increased by taking into account buoyancy waves as a sink for the TKE. The increase of the dissipation rate is realised through a modification of its associated dissipation length scale. The dissipation rate is inversely proportional to this length scale, $\epsilon = c_\epsilon \omega^{3/2}/\Lambda$, such that a decrease of the latter leads to an increase of the dissipation rate. For the sake of convenience, we will repeat the most important equations here. The modification of the TKE dissipation length scale was implemented through a harmonic

sum (Eq. 3.11):

$$\frac{1}{\Lambda} = \frac{1}{\alpha H_p} + \frac{1}{\beta_s r}\,, \tag{4.2}$$

where the newly introduced parameter β_s is defined as (Eq. 3.12)

$$\beta_s = (1 + \lambda_s \tilde{N})^{-1}$$

and (Eq. 3.13)

$$\lambda_s = c_4 \Lambda \omega^{-1/2}\,, \tag{4.3}$$

where $c_4 = c_3/(c_2 c_\epsilon)$ (see Eq. 3.14). The parameters $c_2 = 1.92$ and $c_3 = 0.3$ are model parameters from Canuto and Dubovikov (1998) and c_ϵ is the dissipation parameter of the convection model. The buoyancy frequency $\tilde{N}$ is computed according to

$$\tilde{N}^2 = \frac{g^2 \rho}{p} \left(\nabla_{\rm ad} - \nabla + \nabla_\mu\right)\,,$$

assuming an ideal gas law. Here, ∇_μ indicates the dimensionless mean molecular weight gradient and g refers to the gravitational acceleration. Close to the stellar centre the pressure scale height and in turn the dissipation length scale Λ, if defined through the pressure scale height, diverge. To avoid this divergence, Flaskamp (2003) introduced the modification by Wuchterl (1995) in the Kuhfuß model. This extension of the model we also implemented equivalently to Eq. (4.2), but with a constant parameter $\beta_s = 1$. In unstably stratified regions, the new correction factor is not applied and $c_4 = 0$ as c_3 drops to 0 (Canuto and Dubovikov 1998). Hence, the harmonic sum Eq. (4.2) recovers the Wuchterl (1995) expression automatically. We note that at this point where $\nabla - \nabla_{\rm ad} \to 0$, also $\tilde{N} \to 0$ and β_s smoothly transitions to 1, such that setting $c_3 = 0$ does not introduce any discontinuity. The harmonic sum Eq. (4.2) can be converted into an equation for the dissipation length Λ. Rewriting Eq (4.2) yields

$$\Lambda = \underbrace{\frac{r}{r + \alpha H_p \frac{1}{\beta_s}}}_{<1} \alpha H_p\,, \tag{4.4}$$

which immediately shows that the derived expression is in essence a reduction factor for the dissipation length Λ. Plugging in the definitions for β_s and λ_s one finds the following expression:

$$\Lambda = \frac{r}{r + \alpha H_p \left(1 + c_4 \Lambda \omega^{-1/2} \tilde{N}\right)} \alpha H_p\,.$$

This is a quadratic equation in Λ which can be solved to obtain the reduced length scale. Here, we have expressed the dissipation rate timescale $\tau = 2\omega/\epsilon$ in terms of ω and Λ through

noting that $\epsilon = c_\epsilon \omega^{3/2}/\Lambda$ and $\tau = 2\Lambda/(c_\epsilon \omega^{1/2})$ which allowed rewriting an expression proportional to the ratio of turbulent kinetic energy to buoyancy timescales, τ/τ_b, into one proportional to $\Lambda\omega^{-1/2}\tilde{N}$ (see Ch. 3 for details). The final model of Λ in the convection zone reads

$$\Lambda(r) = -\frac{r+\alpha H_p}{2c_4\tilde{N}\omega^{-1/2}\alpha H_p} + \sqrt{\left[\frac{r+\alpha H_p}{2c_4\tilde{N}\omega^{-1/2}\alpha H_p}\right]^2 + \frac{r}{c_4\tilde{N}\omega^{-1/2}}} \tag{4.5}$$

for $\nabla < \nabla_\mathrm{ad}$, and

$$\Lambda(r) = \left(\frac{1}{\alpha H_p} + \frac{1}{\beta_\mathrm{c} r}\right)^{-1}, \tag{4.6}$$

for $\nabla > \nabla_\mathrm{ad}$, where $\beta_\mathrm{c} = 1$. To obtain a physically reasonable, positive dissipation length scale Λ, the plus sign in front of the square root in the solution of the quadratic equation has to be chosen.

We note that the parameter c_ϵ takes different values in the Canuto and Kuhfuß convection models. Here, we take $c_\epsilon = C_\mathrm{D}$, which is the dissipation parameter in the Kuhfuß model. In unstably stratified regions with $c_4 = 0$, Eq. (4.2) solves explicitly for Λ. In stably stratified regions, the parameter takes a value of $c_4 \approx 0.072$ using the parameters c_2 and c_3 from Canuto and Dubovikov (1998) and $c_\epsilon = C_\mathrm{D}$. As mentioned already in Sec. 3.3.5, the effect of changing c_ϵ on changing c_4 to some extent cancels out. We discuss this further in Sec. 4.3.1.

4.3 Stellar models

We have used GARSTEC to compute stellar models in a mass range of 1.5-8 $\mathrm{M}_\odot$ in the core hydrogen burning phase. We have used the OPAL equation of state, OPAL opacities (Iglesias and Rogers 1996), extended by low temperature opacities by J. Ferguson (private communication and Ferguson et al. 2005), both for the Grevesse and Noels (1993, GN93) mixture of heavy elements. For the initial mass fractions we have chosen $X = 0.7$ and $Z = 0.02$ for all models. Convective chemical mixing is described in a diffusive way according to Eq. (2.21). We use MLT plus exponential overshooting as described by Freytag et al. (1996) to evolve the models through an initial equilibration to the beginning of the main-sequence phase. Then we first switch to the 1- and subsequently to the 3-equation model to generate a starting model for the computation with the 3-equation model. As we are interested in the effects of overshoot mixing, all models shown in the following are computed, including the non-local terms in the 1- and 3-equation version of the Kuhfußtheory.

For the exponential overshooting, we have used the default GARSTEC parameter value of $f_\mathrm{OV} = 0.02$, which has been calibrated by fitting GARSTEC-isochrones to the colour-magnitude diagrams of open clusters (Magic et al. 2010). The diffusion coefficient is computed according to Eq. (2.40). For small convective cores, excessively large overshooting zones can occur when applying the ad hoc overshooting schemes due to the diverging

pressure scale height in the centre. To avoid such unfavourable conditions a reduced overshooting parameter value is determined in GARSTEC, by applying a geometrical cut-off depending on the comparison between the radial extent of the convective region and the scale height at its border. For a brief discussion of different geometric cut-off descriptions, we refer to Sec. 4.4. For the results in this section, the "tanh"-cut-off according to Eq. (4.9) has been used. For the parameter α_ω we have chosen a value of 0.3 as this value results in a similar convective core size as the ad hoc overshooting models for $f_{\rm OV} = 0.02$ in the 5 $M_\odot$ model, which is in the middle of our mass range. For the parameters α_Π and α_Φ we have chosen the same value assuming that the non-local transport behaves similar for all convective variables. We point out that α_ω is an adjustable parameter and an external calibration will be necessary. This will be discussed further below.

4.3.1 The 3-equation model

As a representative example, we will first discuss the evolution and the internal structure of a 5 $M_\odot$ model applying the 3-equation, non-local convection theory. Figure 4.1 shows the profiles of the TKE variable ω (panel a), the convective flux variable Π (panel b), the superadiabatic gradient $\nabla - \nabla_{\rm ad}$ (panel c), where ∇ is the temperature gradient resulting from the convection model, and the diffusion coefficient according to Eq. (4.1) on a logarithmic scale (panel d). The TKE clearly extends beyond the Schwarzschild boundary, which we compute as usual as the point where $\nabla_{\rm ad} = \nabla_{\rm rad}$. Such a behaviour cannot be observed in MLT models, as it is a direct result of the non-local terms in the Kuhfuß convection model. The associated diffusion coefficient shows a rather high value beyond the Schwarzschild boundary and throughout the overshooting zone. This will increase the size of the mixed convective core and therefore naturally create an overshooting zone. Given the profile of the diffusion coefficient, the chemical mixing will resemble the step overshooting rather than the exponential overshooting scheme. The convective flux variable shows a region of negative flux beyond the Schwarzschild boundary. In the right panel of Fig. 4.8 the region of negative convective flux is shown enlarged in the inset (likewise for the convective flux variable Π in the third panel of Fig. 4.1). This is due to the braking of the convective motions in the stable, radiative stratification. The extent and magnitude of the negative convective flux are very comparable to early results from Xiong (1986), who found that the convective flux penetrates less deeply into the stable layers than for example the kinetic energy and has a nearly negligible magnitude compared to the total flux.

Finally, panel c) shows the superadiabatic temperature gradient of this stellar model (notice the vertical scale). In the inner part of the convection zone the model shows a very small superadiabatic gradient as it is expected for regions with convective driving. At a fractional mass of about 0.05 the temperature gradient drops below the adiabatic value. In contrast to local models this point does not coincide with the formal Schwarzschild boundary, however, the sign change happens substantially before the formal boundary. At the formal Schwarzschild boundary, the temperature gradient has dropped to about $\mathcal{O}(10^{-3})$ below the adiabatic value. The comparison of panels b) and c) shows that there exists an

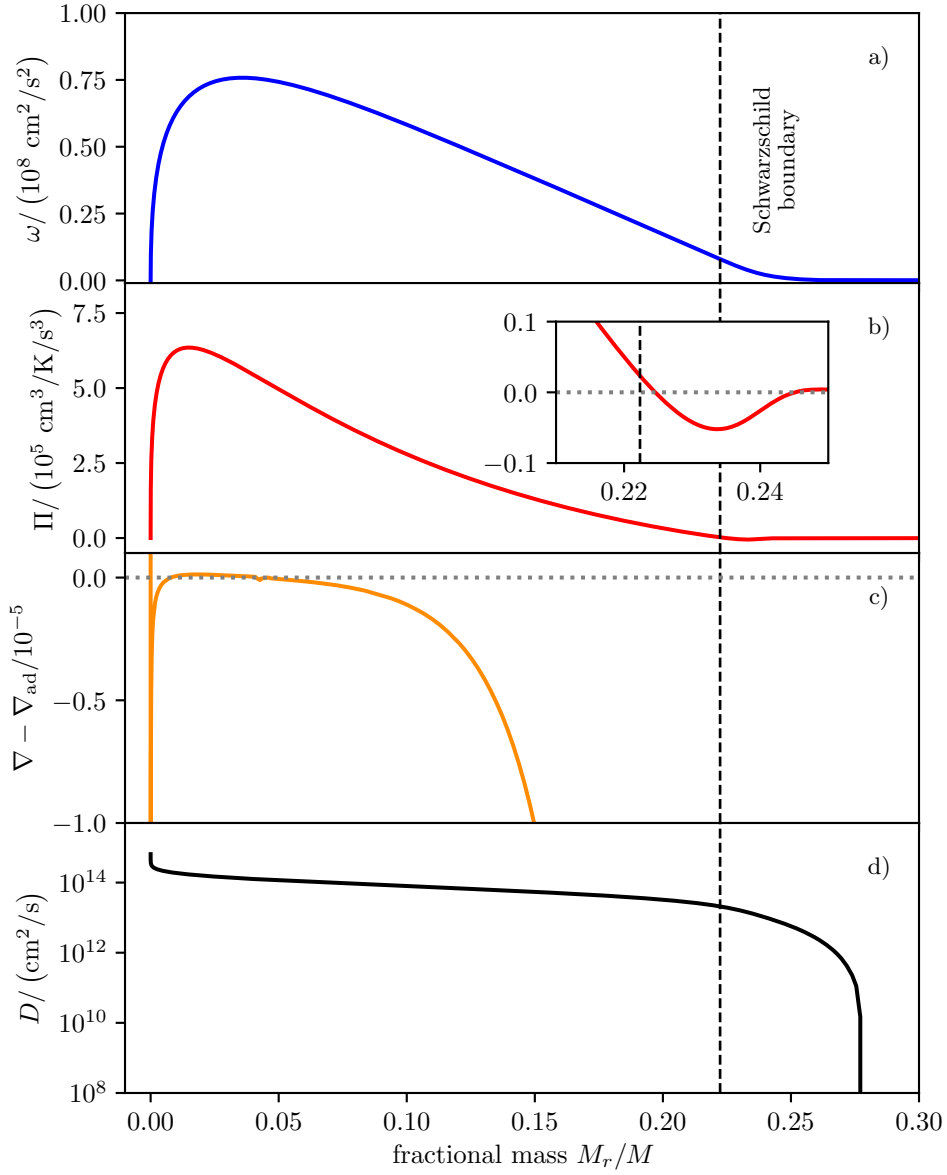

Figure 4.1: Summary of the interior structure of the convective core of a 5 $M_\odot$ main-sequence model, calculated with the 3-equation model. The black dashed line indicates the Schwarzschild boundary. The different panels show a) TKE b) convective flux variable c) super adiabatic temperature gradient and d) the diffusion coefficient according to Eq. (4.1). The selected stellar model has a central hydrogen abundance of $X_c = 0.6$. The inset in panel b) shows the region of negative convective flux just beyond the Schwarzschild boundary.

extended region in the model in which the convective flux is positive while the temperature gradient is already subadiabatic. This region is also known as a Deardorff layer (Deardorff 1966) and has been observed in simulations of stellar convection (Chan and Gigas 1992; Muthsam et al. 1995, 1999; Tremblay et al. 2015; Käpylä et al. 2017; Kupka et al. 2018) or other Reynolds stress models (Kupka 1999a; Xiong and Deng 2001; Kupka and Montgomery 2002; Montgomery and Kupka 2004; Zhang and Li 2012). Such a layer cannot exist in convection models, which do not have enough degrees of freedom. In MLT and the Kuhfuß 1-equation model, the convective flux is directly coupled to the superadiabatic gradient and the convective velocities (see Eq. 2.50 for the 1-equation model). This of course inhibits any region in which the convective flux and the superadiabatic gradient have a different sign like in the Deardorff layer and forces the convective flux and the TKE to have the same penetration depth. The 3-equation model lifts the strong coupling of convective flux and superadiabatic gradient by directly solving for two more variables (Π and Φ) and therefore allows for the existence of such a layer. Deardorff (1966), in the case of atmospheric conditions, argued that it is mainly the non-local term in the equation for Φ which supports the positive heat flux for subadiabatic temperature gradients (see also Sec. 13 of Canuto 1992, and references therein). The diffusion term $\mathcal{F}_\Phi$ in the equation for the entropy fluctuations Eq. (2.59) acts as a source of entropy fluctuations even though no local source (a superadiabatic temperature gradient) is present. This allows for the outward directed transport of entropy fluctuations, i.e. a positive convective flux even in subadiabatic layers. This has little impact on the stellar structure and evolution, as the temperature gradient remains nearly adiabatic, and the whole convection zone is chemically well mixed. The existence of such a layer is therefore expected, and confirms the physical relevance of the 3-equation Kuhfuß model. The extent of this layer is difficult to determine from a priori arguments, and asteroseismic analyses might provide observational constraints in the future.

In Fig. 4.2 we show the temperature gradients in the overshooting zone of the same 5 $M_\odot$ main-sequence model as in Fig. 4.1. At the formal Schwarzschild boundary the model temperature gradient has already a slightly subadiabatic value as discussed previously. Beyond the Schwarzschild boundary, the model temperature gradient does not drop to the radiative gradient immediately. Instead, it gradually transitions from slightly subadiabatic to radiative values in a rather narrow mass range. As a consequence, the model temperature gradient takes slightly super-radiative values in this transition region. However, the temperature gradient reaches a radiative value well before the boundary of the mixed region, indicated with the black dotted line in Fig. 4.2. Considering the small extent of the super-radiative region and the small deviation from the radiative temperature gradient, the overshooting zone in the 3-equation non-local model is mostly radiative. We point out that the shape of the temperature gradient is not subject to assumptions about the thermal stratification (e.g. adiabatic, radiative or any gradual transition between both) in the overshooting zone but instead is a result of the convection model. In the transition region, the convective flux is negative due to the buoyancy braking, which effectively means that energy transport by convection is directed inwards instead of outwards. This effect is counter-balanced by increasing the energy transport by radiation, through an increased

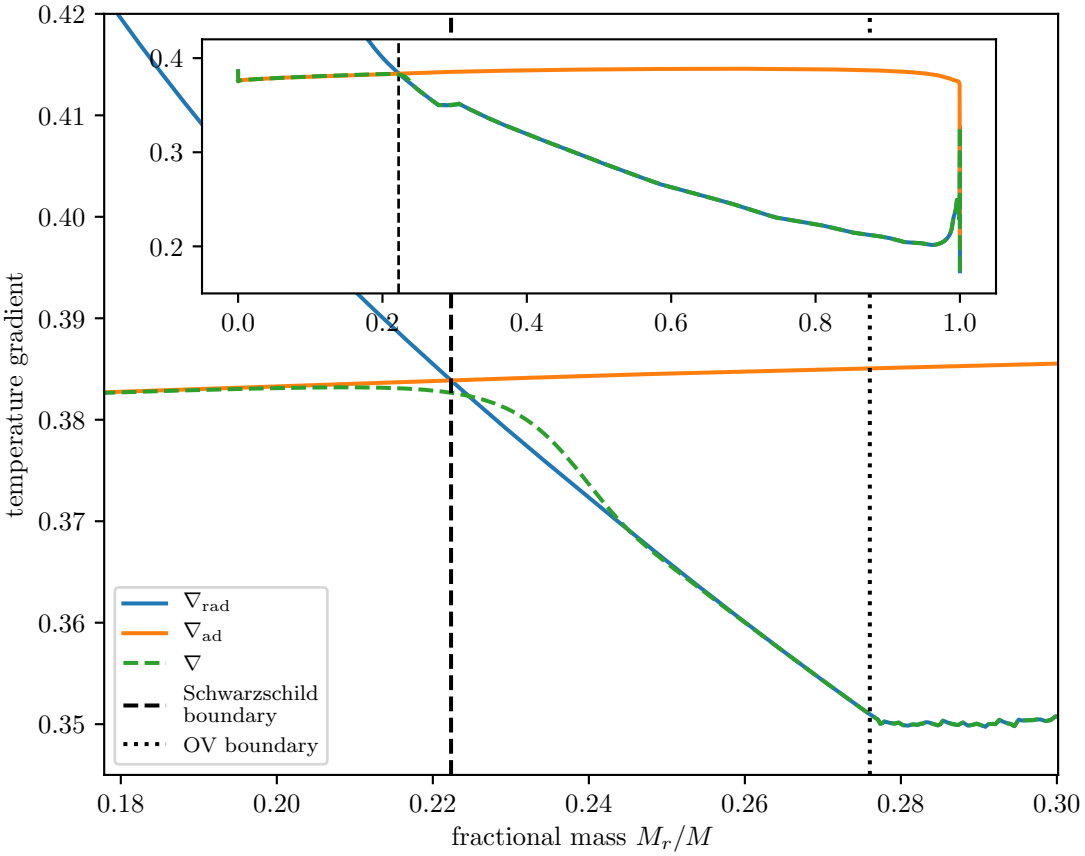

Figure 4.2: Temperature gradients in the overshooting zone of the same 5 $M_\odot$ main-sequence model as in Fig. 4.1. The blue and orange lines indicate the radiative ($\nabla_{\rm rad}$) and adiabatic ($\nabla_{\rm ad}$) temperature gradients, respectively. The green dashed line indicates the model temperature gradient ∇ obtained from the 3-equation non-local convection model. The black dashed line indicates the Schwarzschild boundary, while the black dotted line indicates the boundary of the well mixed overshooting region. The selected stellar model has a central hydrogen abundance of $X_{\rm c} = 0.6$. The inset shows the three temperature gradients from the centre to the surface of the stellar model.

model temperature gradient (e.g. Chan and Sofia 1996).

The temperature gradient of the 3-equation model is comparable to results of different TCM approaches (Xiong and Deng 2001; Li and Yang 2007) for the base of the solar convective envelope. Both Zhang and Li (2012) (their Figs. 6 and 7) and Xiong and Deng (2001) (their Fig. 8) find a temperature gradient that transitions gradually from the adiabatic to the radiative value. They also find a Deardorff layer with a degree of subadiabaticity at the formal Schwarzschild boundary comparable to our findings. From the convective flux as presented in Xiong (1986) one also would expect a similar temperature gradient in the overshooting zone. Furthermore, the shape of the model temperature gradient is

also in qualitative agreement with the discussion in Viallet et al. (2015). They argue that under the physical conditions in convective cores, efficient chemical mixing and a gradually transitioning temperature gradient are expected in overshooting regions. In the 3-equation non-local model, the extent of the nearly adiabatic overshooting zone is controlled by the shape of the negative convective flux in the overshooting zone. For smaller (more negative) values of the convective flux (i.e. more efficient buoyancy braking) the temperature gradient is expected to be closer to the adiabatic value, while for larger (less negative) values it will be closer to the radiative temperature gradient. In Eq. (2.57) the negative convective flux and the dissipation term act as sink terms in the overshooting zone. Hence, the behaviour of the dissipation term will impact also on the convective flux and in turn on the value of the temperature gradient in the overshooting zone. In computations with the 1-equation non-local version of the theory, the negative convective flux is the dominant sink term for the TKE and the actual dissipation term is negligible (see Fig. 3.8). This leads to more negative values of the convective flux and thus to a mostly adiabatic temperature gradient in the overshooting zone. We will discuss this in more detail in Sec. 4.5.1 (see also Fig. 4.15).

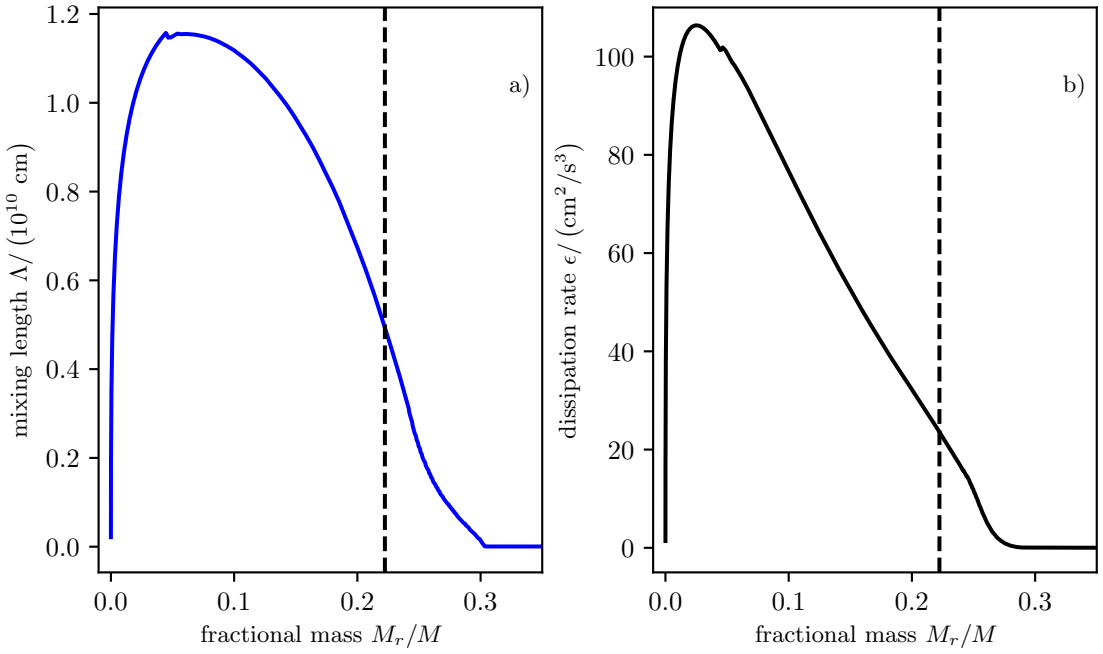

Figure 4.3: Dissipation length scale Λ (*left panel*) and dissipation rate (*right panel*) in a 5 $M_\odot$ main-sequence model. Same stellar model as in Fig. 4.1. The vertical dashed line indicates the Schwarzschild boundary of the model.

As discussed above and in Ch. 3 we have implemented the increase of the dissipation rate in the overshooting zone through a decrease of the dissipation length scale Λ. In the original version, Kuhfuß (1987) models the dissipation of the TKE by a Kolmogorov-type term (Eq. 2.44, $\epsilon = C_\mathrm{D}\omega^{3/2}/\Lambda$ with $\Lambda(r)$ as in Eq. 4.6). The dissipation length scale Λ

describes the scale over which the kinetic energy is dissipated such that in the Kolmogorov model, at fixed TKE, a shorter length scale results in an increased dissipation rate. In Fig. 4.3 we show the length scale Λ (panel a) and the dissipation rate (panel b) computed in the same stellar model as in Fig. 4.1. At a fractional mass of about 0.05 the profile of the dissipation length scale shows a slight kink in this model, where the transition starts. At about 0.28 in fractional mass, the dissipation length scale Λ drops to zero, which means that convective motions stop at that point. This coincides with the dying of the TKE beyond the Schwarzschild boundary, as seen in Fig. 4.1, panel a). The onset of the decrease of the dissipation length scale Λ also coincides with the sign change of the superadiabatic gradient (see Fig. 4.1, panel c). Towards the centre of the model, the dissipation length scale Λ drops to zero as well. This is a result of the Wuchterl (1995) correction, also used in our implementation (cf. Ch. 3). We have also investigated the prescription of Roxburgh and Kupka (2007) as an alternative to that one of Wuchterl (1995) but found little difference with respect to the overshooting region.

Parameter dependence

We explore some of the parameter dependencies in the following. The model for the modification of the dissipation length scale comes with a number of parameters (c_2, c_3, c_ϵ). These parameters are not necessarily free, but have been calibrated in the framework of the convection models developed by Canuto (1992). These parameters enter the equation of the reduction factor as a single parameter which was previously defined as c_4. Given the dissipation parameter of the 3-equation model, we find $c_4 \approx 0.072$ while for the dissipation parameter of the Canuto and Dubovikov (1998) model $c_4 \approx 0.2$ as described in Ch. 3. As mentioned already in Sect. 3.3.5, the effect of changing c_ϵ on changing c_4 to some extent cancels out in the calculation of Λ, as c_ϵ appears in the denominator of $c_4 = c_3/(c_2 c_\epsilon)$ and in the numerator of $\Lambda = c_\epsilon \omega^{3/2}/\epsilon$. Hence, if c_4 is adjusted according to $c_4 = c_3/(c_2 c_\epsilon)$, a change of c_ϵ first of all influences the TKE dissipation rate ϵ throughout the whole model and is not specifically changing ϵ only within the overshooting zone. We studied the impact of the new parameter c_4, appearing in Eq. (4.3) (see also Eq. 3.13) on the structure of the convective core by varying its value. As the parameters c_2, c_3 and c_ϵ enter the equations as one parameter we only varied this effective parameter value c_4 by $\pm 60\%$. All other parameters take their default values. A comparison of TKE profiles for different values of c_4 is shown in Fig. 4.4. It can be seen that the variation of the parameter c_4 leads to some noticeable variation in the TKE profile. However, within these ranges, the models keep their property of a limited overshooting range. The direction of the variation can be explained by the theory as well. An increase of the parameter will lead to a decrease of the dissipation length scale Λ. A decreased length scale leads in turn to an increased dissipation. This reduces the overshooting which can be observed for the dark red line. For the case with a decreased parameter value, the same argument applies in the opposite direction. The expected behaviour can be similarly observed for the yellow line.

Apart from the new parameters for the reduction of the dissipation length scale Λ, the model still contains the original parameters of the Kuhfuß model. The parameter

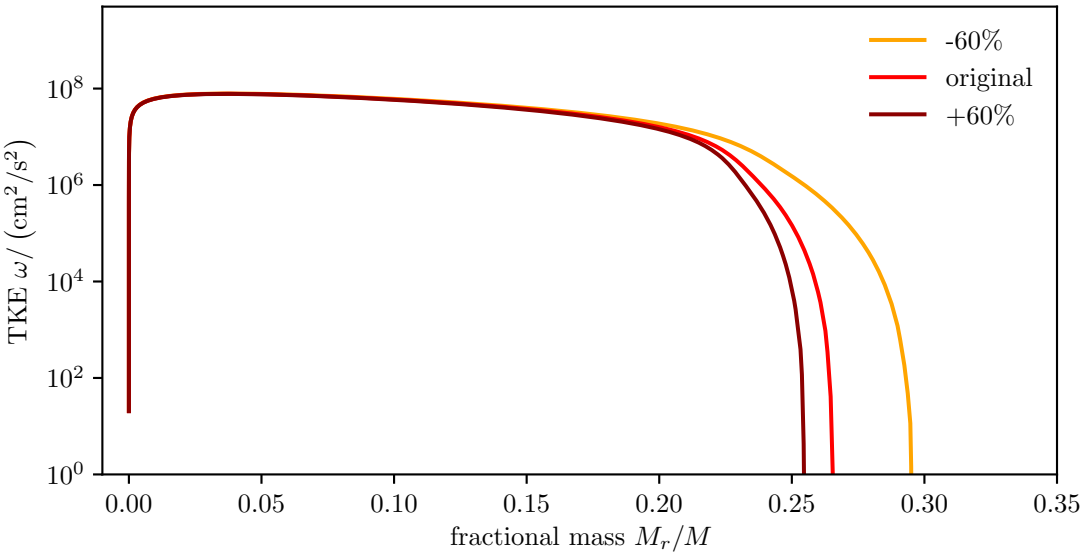

Figure 4.4: Comparison of the TKE as a function of fractional mass on a logarithmic scale for different values for the parameter c_4 in a 3-equation non-local 5 $M_\odot$ main-sequence model with limited dissipation length scale Λ.

α_ω, appearing in Eq. (2.57), controls the non-local flux of the turbulent kinetic energy. Because this flux is mainly responsible for the extension of the kinetic energy beyond the Schwarzschild boundary, one expects that this parameter impacts on the overshooting distance. Kuhfuß suggested a default value of $\alpha_\omega = 0.25$. In Fig. 4.5 we show three different hydrogen profiles for the 5 $M_\odot$ model at the same age. The parameter α_ω takes values of 0.1, 0.3 and 0.5. It can be clearly seen that the original property of this parameter of controlling the overshooting extent is still given. For a higher value of the parameter, the size of the convective core is larger throughout the evolution of the model. Smaller parameter values reduce the convective core size. Although Kuhfuß (1987) provides a default value for α_ω, this value is not known a priori from the theory. Hence, a calibration will be necessary, e.g. from observations or 3D hydrodynamic simulations.

Another parameter that enters the TKE equation is the dissipation parameter C_D. In Fig. 4.6 we show hydrogen profiles of a 5 $M_\odot$ star at the end of the main sequence for different values of the dissipation parameter $C_\mathrm{D} = 0.79, 1, 2.18$ and 3. We always assume $C_\mathrm{D} \equiv c_\epsilon$, as both parameters have the same role in the Canuto and Dubovikov (1998) and in the Kuhfuß model. Here, the value of 0.79 refers to the default dissipation parameter from the Canuto and Dubovikov (1998) model while 2.18 is the numerical default value in the Kuhfuß model (see Sec. 2.5.1). The extent of the hydrogen profile is largest for the model computed with the smallest dissipation parameter and smallest for the largest parameter. This behaviour is expected, as a decreased dissipation allows the TKE flux to extend further out. Compared to the parameter of the TKE flux α_ω, the impact of the dissipation parameter on the overshooting extent is rather limited, as the variation is much

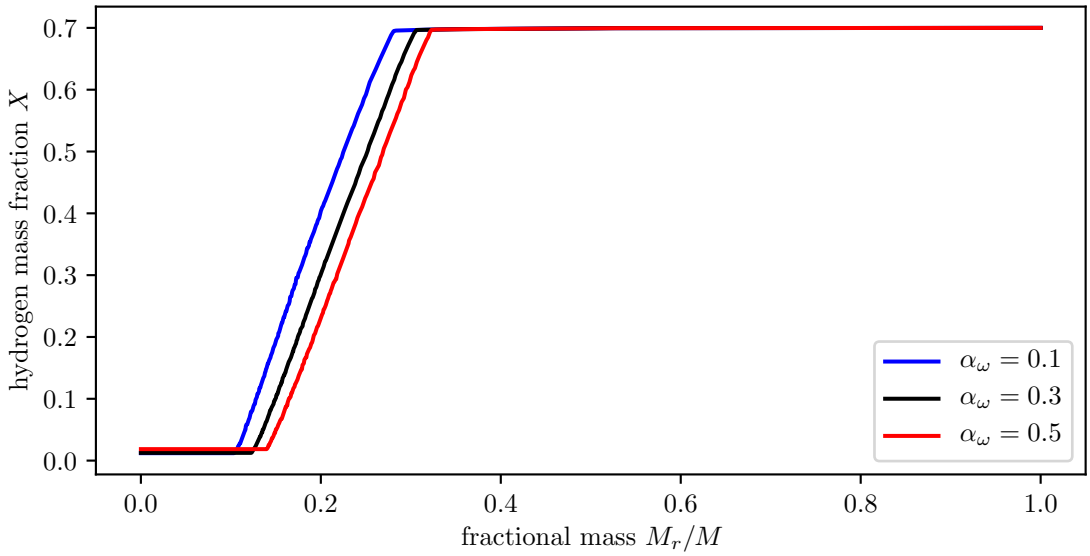

Figure 4.5: Comparison of the hydrogen profiles as a function of fractional mass for different values for the parameter α_ω in a 3-equation non-local 5 $M_\odot$ main-sequence model with limited dissipation length scale Λ.

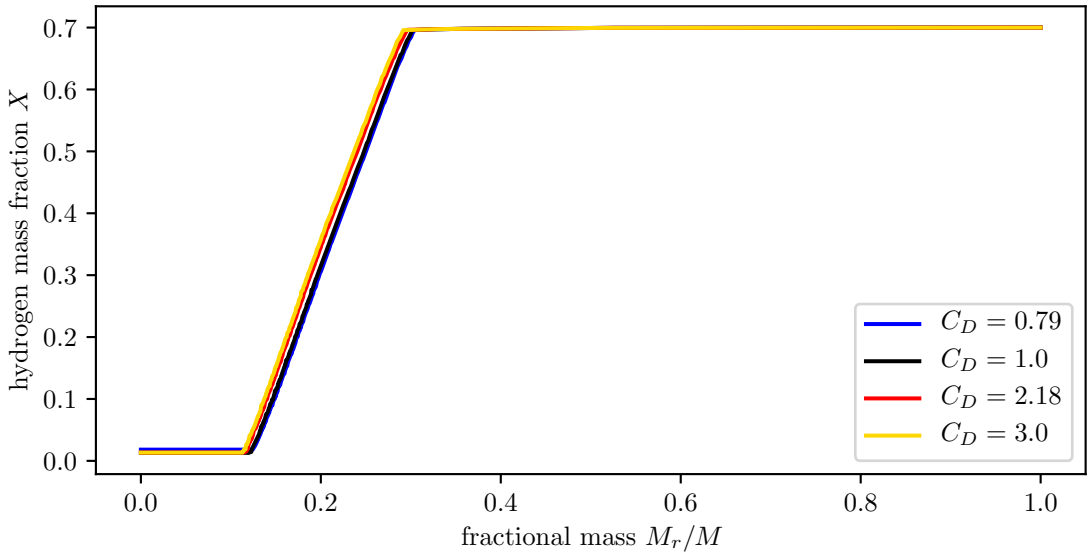

Figure 4.6: Comparison of the hydrogen profiles as a function of fractional mass for different values for the parameter C_D in a 3-equation non-local 5 $M_\odot$ main-sequence model with limited dissipation length scale Λ.

smaller when compared to the results shown in Fig. 4.5. The variation of the overshooting

extent is also smaller, as one could have expected from the comparison shown in Fig. 4.4. This is because by changing C_{D} also c_4 will change, while in Fig. 4.4 only c_4 is changed. The effects of changing c_4 and C_{D} partially compensate each other, resulting in a smaller net effect. Finally, one could find combinations of parameters α_ω and C_{D} which allow obtaining models with equal convective core sizes. We note, however, that the dissipation parameter also changes the magnitude of the TKE that may be constrained from the 3D hydrodynamic simulations (see Sec. 5.5.1).

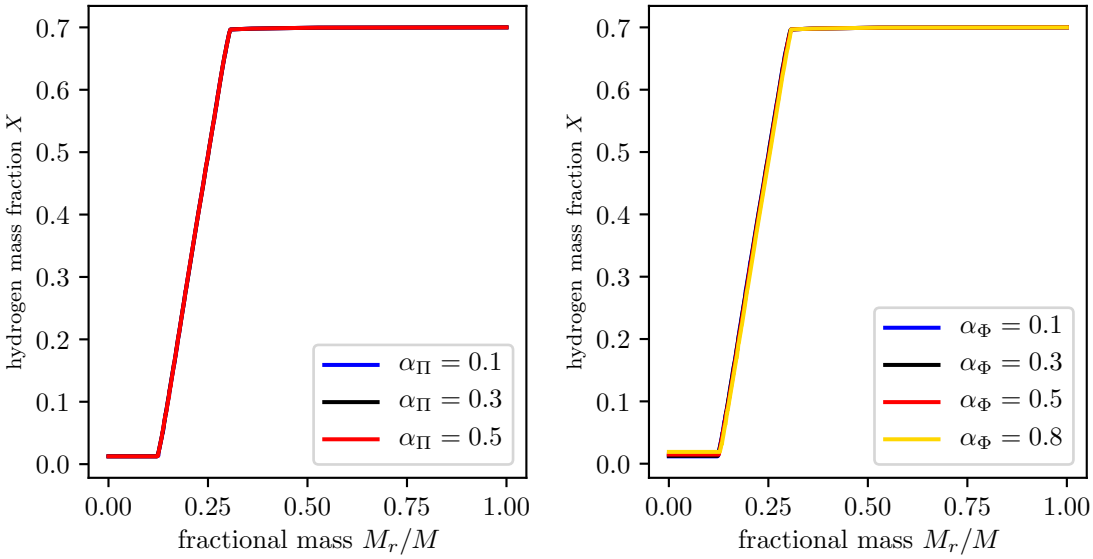

Figure 4.7: Comparison of the hydrogen profiles as a function of fractional mass for different values for the parameters α_Π (*left panel*) and α_Φ (*right panel*) in a 3-equation non-local 5 $\mathrm{M}_\odot$ main-sequence model with limited dissipation length scale Λ.

In Fig. 4.7 we show the impact of the parameters of the non-local terms in the Π and Φ equations α_Π and α_Φ, appearing in Eq. (2.58) and (2.59), in the left and right panel, respectively. We see that these parameters have a negligible impact on the overshooting extent, which is yet smaller than the impact of the dissipation parameter C_{D}. Instead, they have a larger impact on the temperature gradient as the variables Π and Φ are more closely related to the temperature structure. By increasing the parameter α_Π the magnitude of the superadiabatic gradient increases, while the extent of this region stays the same. Decreasing the value of the parameter α_Φ is increasing the size of the superadiabatic region, therefore reducing the size of the Deardorff layer, while the magnitude stays the same. This is expected because the non-local term in the Φ equation is the one which is driving convection in the Deardorff-layer. This indicates again that the parameter α_ω which determines the importance of the TKE flux has the largest impact on the overshooting distance (note that Fig. 4.4 has a different scale for the fractional mass axis). The impact of α_Π and α_Φ will be further discussed in Sec. 5.5.2.

4.3.2 Comparison to MLT

The MLT is still the most commonly used theory to describe convection in stars. Therefore, we will now compare the results of the 3-equation model with results obtained from standard MLT, i.e. without and with an additional treatment of overshooting. A comparison to the 1-equation model will be discussed in the next subsection. The fractional hydrogen abundances early on and at the end of the main sequence computed with the 3-equation model and an MLT model without overshooting are shown in the left panel of Fig. 4.8. At the same central hydrogen abundance, the fully mixed region of the 3-equation model always extends past that of the MLT model. This is comparable to models which include ad hoc overshooting beyond the formal Schwarzschild boundary. In contrast to the ad hoc overshooting models, the overshooting in the 3-equation model results from the solution of the model equations. The right panel of Fig. 4.8 shows a comparison of the convective fluxes in the 3-equation model and an MLT model. Both models have been selected to have the same central hydrogen abundance. Ad hoc overshooting has been included in this MLT model, and tuned in such a way as to obtain a model with the same core size as obtained from the 3-equation model. In the bulk of the convection zone, both fluxes show very close agreement. Beyond the Schwarzschild boundary, the narrow region with negative convective flux in the non-local model can be identified. This region is shown enlarged in the inset.

Finally, in Fig. 4.9 we compare the evolutionary tracks of the 3-equation model, indicated by the solid blue line, with an MLT model without ad hoc overshooting (yellow line) and an MLT model including ad hoc overshooting (black line). The black dot indicates the position of the stellar model with $X_c = 0.6$ discussed in subsection 4.3.1 in Figs. 4.1 to 4.8. The computation of the 3-equation model starts at the beginning of the main sequence from an MLT model including exponential overshooting as described above and then evolves through core hydrogen burning up until core hydrogen exhaustion. Compared to the MLT model the non-local model shows a higher luminosity throughout the main sequence, as expected for the larger convectively mixed core.

4.3.3 Comparison to the 1-equation non-local models

In addition to the 3-equation non-local models, we have also computed stellar models, in which convection is described by the 1-equation model (see Sec. 2.5.1). As before, we included the non-local terms. The upper panel of Fig. 4.10 shows a comparison of the TKE profiles for the 1- and 3-equation, non-local models on a logarithmic scale. The TKE on a linear scale can be found in the lower panel of Fig. 4.10. The models have been selected at the same central hydrogen abundance to ensure that they are in the same evolutionary stage. This comparison shows that the overshooting extent in the 1-equation non-local model is very comparable to the 3-equation non-local model for the same choice of the parameter α_ω. The overall behaviour of the 1-equation non-local model and the 3-equation non-local model including the new dissipation mechanism looks very similar.

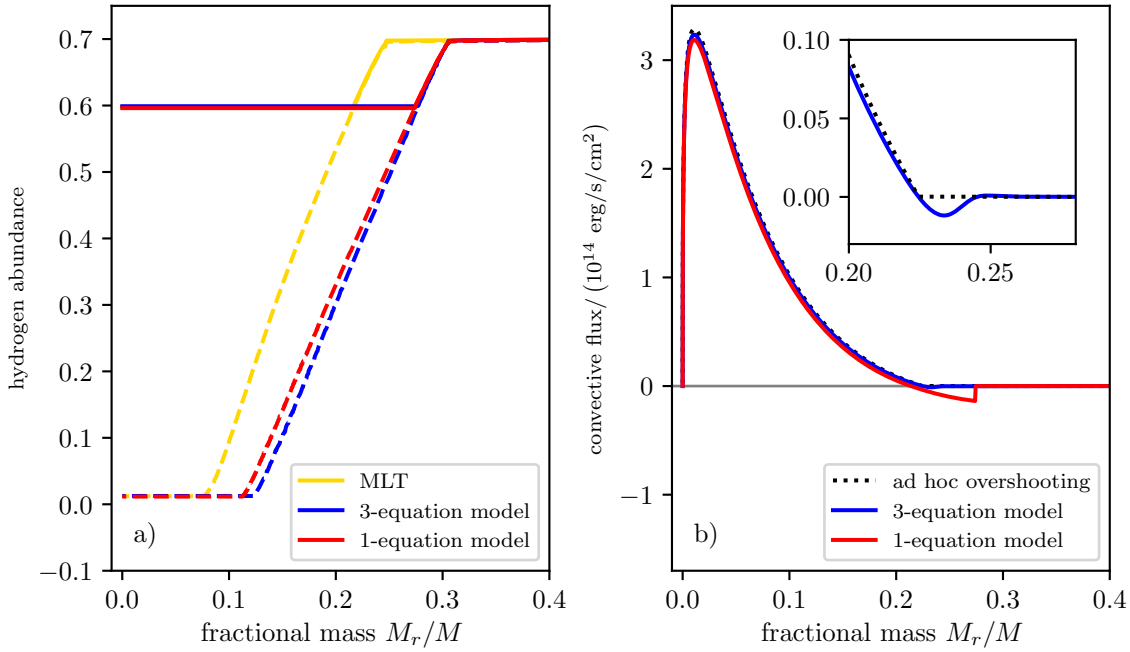

Figure 4.8: *Left panel:* Comparison of models using MLT without overshooting (yellow lines) to those computed with the 3-equation theory (blue lines) and the 1-equation model (red lines). The hydrogen profiles at an early stage on the main sequence, when $X_c = 0.6$ (solid lines), and at the end of it ($X_c \approx 0$; dashed lines) are shown. *Right panel:* Convective fluxes of an MLT model with exponential overshooting (dotted black line), a 3-equation model (solid blue line) and a 1-equation model (solid red line) as a function of fractional mass. These models have been selected to have the same central hydrogen abundance of $X_c = 0.6$ and the same chemically homogeneous core size.

The overshooting extent is clearly limited, and there is a steep drop in the TKE at the overshooting boundary. Also the absolute values of the TKE look comparable in the bulk of the convection zone (lower panel, Fig. 4.10). We will analyse the absolute value of the TKE in more detail below. We note that this result is obtained without tuning the parameters of the models. For the parameters which both models have in common, the same values were chosen. In the overshooting zone, the 3-equation model has much smaller TKE than the 1-equation model. Nevertheless, the energies are still high enough to fully mix the overshooting region in the 3-equation model.

In the left panel of Fig. 4.8 we compare the hydrogen profiles of the 1-equation model with the results from the 3-equation model and an MLT model at the beginning and at the end of the main sequence. As expected from the similar TKE profiles shown in Fig. 4.10 the hydrogen profile of the 1-equation model extends past the local MLT model and looks very similar to the 3-equation model. Towards the end of the main sequence, the 1-equation model has a smaller core than the 3-equation model, leading to a slightly different slope in the hydrogen profiles. Likewise, the evolutionary track of the 1-equation

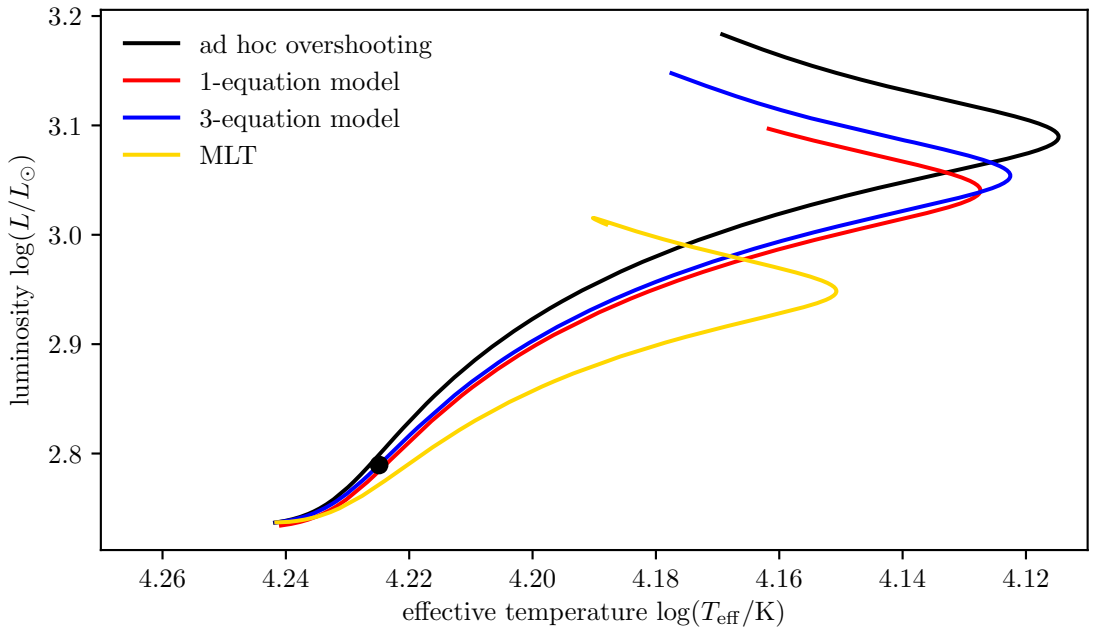

Figure 4.9: Evolutionary tracks in the Hertzsprung-Russell diagram of a 5 $M_\odot$ model computed with MLT, shown with a yellow line, ad hoc overshooting, shown with a black line, the 1-equation shown with a red line and the 3-equation, non-local model, shown with a blue line. The black dot marks the model selected at a central hydrogen abundance of $X_{\rm c} = 0.6$.

model shown in Fig. 4.9 looks very similar to the 3-equation model. Towards the end of the main sequence, the luminosity is slightly lower owing to the smaller convective core. In the right panel of Fig. 4.8 we compare the convective flux of the 1-equation model to the 3-equation model and an MLT model including ad hoc overshooting. As for the 3-equation model, the convective flux shows close agreement with the other two models in the bulk of the convection zone. Only in the overshooting zone, where the convective flux becomes negative, discrepancies become apparent. Compared to the 3-equation model, the zone of negative convective flux is more extended and the absolute value is larger, i.e. the convective flux is more negative. This can be attributed to the parametrisation of the convective flux in the 1-equation model Eq. (2.50). As discussed in Sec. 3.4 (see also Fig. 3.8) the buoyancy term, proportional to the convective flux, acts as the main sink term in the overshooting zone, requiring larger absolute values in the overshooting zone. We note that this strongly negative convective flux in the overshooting zone will also cause the 1-equation model to have a nearly adiabatic overshooting zone, as compared to the nearly radiative overshooting zone in the 3-equation model.

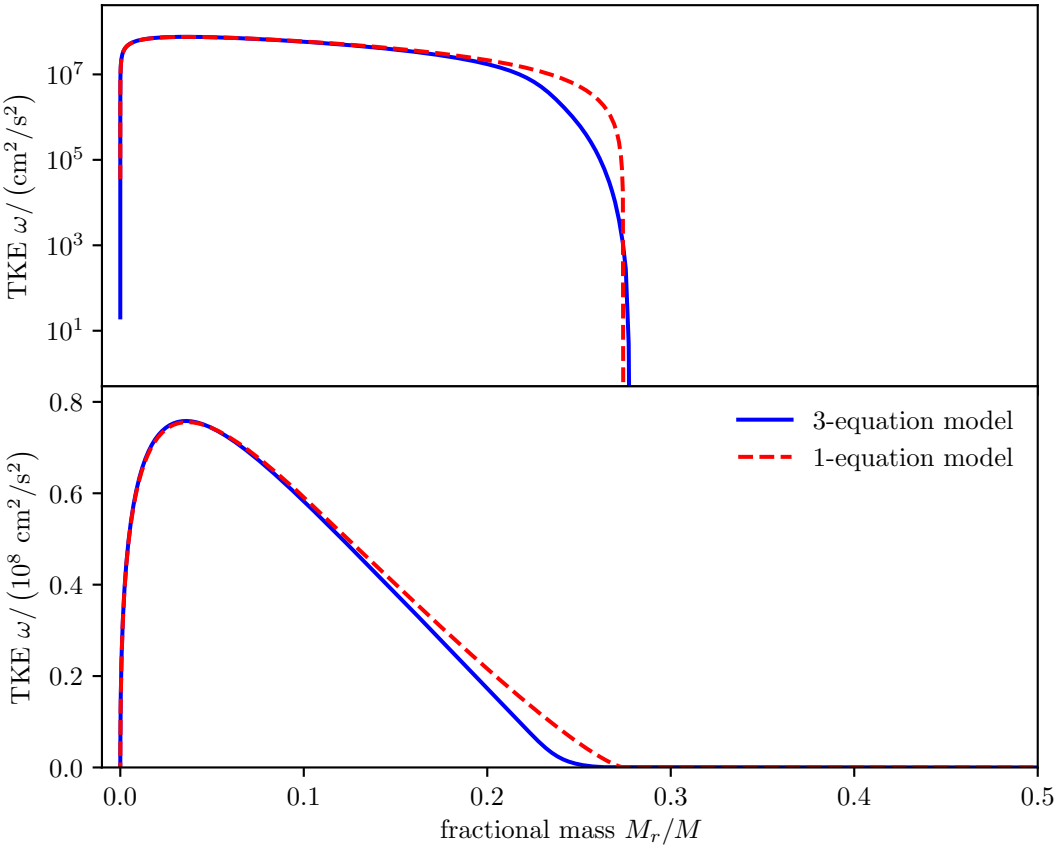

Figure 4.10: Comparison of the TKE in the 1-equation non-local model and the 3-equation non-local model with enhanced dissipation rate of TKE in a 5 $M_\odot$ main-sequence model on a logarithmic scale (*upper panel*) and on a linear scale (*lower panel*). The models have been selected to have the same central hydrogen abundance as the model in Fig. 4.1. The 1-equation model computes Λ according to Eq. (4.6).

4.4 Non-local convection for varying initial masses

We computed stellar models in a mass range of 1.5-8 $M_\odot$, using the 3-equation non-local model. The models have been constructed in the same way and using the same parameters as for the 5 $M_\odot$ model presented so far. For comparison, we have computed three other sets of stellar models with different convection descriptions: (i) with the Kuhfuß 1-equation model to compare the results of the 3-equation model to a simpler TCM; (ii) with MLT plus exponential overshooting as described by Freytag et al. (1996) to compare to one of the standard ad hoc descriptions of convective overshooting with the same parameter value $f_{\rm OV} = 0.02$ as discussed above. Finally, (iii), we computed MLT models without overshooting to compare the results to a local convection theory. At least in terms of core size and temperature structure, models using the local Kuhfuß theories would be equivalent

to MLT models (see Sec. 2.5.1). For the Kuhfuß theory, we used the same value of 0.3 for the parameter α_ω, as before. To allow for a comparison across the mass range and the different convection descriptions, the models are selected at the same central hydrogen abundance of $X_c = 0.6$.

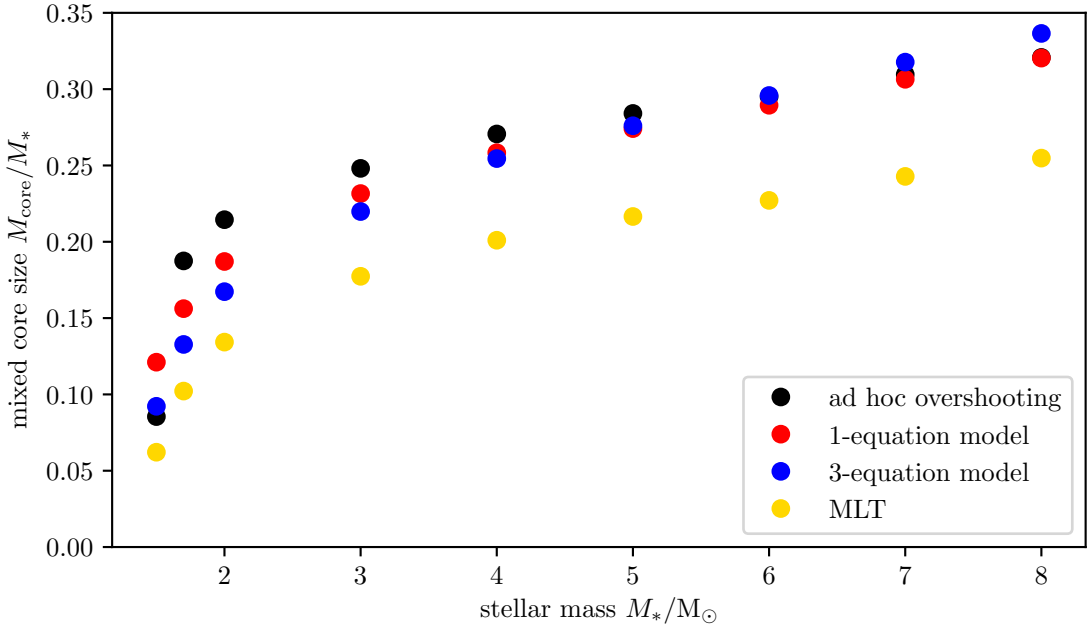

Figure 4.11: Comparison of chemically mixed core sizes of stellar models in units of the stellar mass M_* over a range of initial stellar masses computed with different convection models. The models with ad hoc overshoot include a geometric cut-off to limit the size of small convective cores in lower mass stars. The models have been selected at a central hydrogen abundance of $X_c = 0.6$. The MLT models are computed without overshooting.

Figure 4.11 shows the chemically mixed cores sizes in models computed with these four descriptions of convection and convective overshooting over a range of initial masses. For all masses under consideration, the mixed core from the 3-equation model is larger than the convective core from an MLT model, as expected. This shows that when applying the 3-equation model, an overshooting zone emerges across the whole mass range investigated. Comparing the 3-equation model to the 1-equation model and the ad hoc overshoot model, the mixed core sizes show good qualitative agreement. We repeat that this is achieved without fine-tuning any of the involved parameters. The relative size of the mixed cores decreases with decreasing stellar mass for all four descriptions, but differences in the details between the different convection descriptions are evident. For higher masses, the derived values for the mixed core sizes are almost identical among the ad hoc overshooting and the 1- and 3-equation Kuhfuß models. For low stellar masses, the results show larger discrepancies. Stellar models applying the 3-equation non-local model have the smallest cores, and the core size decreases faster with decreasing stellar mass than in

the 1-equation models and the ad hoc overshoot models. As the ad hoc overshoot model has been calibrated to observations, this allows at least for an indirect comparison of the 1- and 3-equation model with observations.

In addition to the core sizes, we have also analysed the absolute values of the convective velocities. The Kuhfuß model does not solve for the convective velocity itself, but rather for the TKE ω. We approximate the mean convective velocity from the TKE by assuming full isotropy:

$$u_{\mathrm{iso}} = \sqrt{\frac{2}{3}\omega}\,. \tag{4.7}$$

When using MLT, the convective velocities are computed from Eq. (2.35) (e.g. Kippenhahn et al. 2012, Ch. 7). The computation of convective velocities is the same in MLT models with and without exponential overshoot, as the inclusion of ad hoc overshooting does not impact on the description of convection. To compare MLT and the Kuhfußtheories, we evaluate the maximum convective velocity in the convection zone. The maximum is reached well within the Schwarzschild boundaries for all models, and therefore allows for a consistent comparison.

We show this comparison of the maximum convective velocities in the core as a function of stellar luminosity in Fig. 4.12. The convection descriptions are the same as in Fig. 4.11. For all cases, the scaling relation of the convective velocities has the same slope. A linear fit (dotted lines) to the data results in a slope value of ~ 0.3 for all of them. However, the absolute values from the Kuhfuß and MLT models differ by a constant factor of about two, indicated by the offset between the two pairs of lines. This difference in the absolute value is the result of two different effects. The change of the mixing length has the largest impact on the velocity. A reduced mixing length will lead to an increased dissipation rate and smaller velocities as a consequence. In the Kuhfuß models we use a smaller value of $\alpha = 1$ as obtained by a solar calibration instead of $\alpha = 1.6$ for the MLT models. In addition, the mixing length is reduced towards the centre according to the Wuchterl (1995) formulation. The convective velocity is reduced further compared to the local MLT models by taking the non-local terms into account, which act as a sink term in the bulk of the convection zone (see Fig. 3.8). The slope of 0.3 is very close to the $u_{\mathrm{conv}} \propto L^{1/3}$ scaling relation expected from MLT, where L denotes the stellar luminosity. This comparison also demonstrates that the absolute values of the TKE are very similar between the 1- and the 3-equation Kuhfuß theories over the full mass range. For the 5 $\mathrm{M}_\odot$ model, this was already apparent when comparing the TKE profiles in Fig. 4.10. We will discuss the absolute value of the convective velocities again in Sec. 5.3 and 5.5.1 from a slightly different perspective.

Ad hoc overshooting for small convective cores

Parametrised descriptions of overshooting like the exponential or step overshooting use the pressure scale height at the Schwarzschild boundary to define the overshooting distance. The pressure scale height is, however, diverging towards the stellar centre. Hence, the

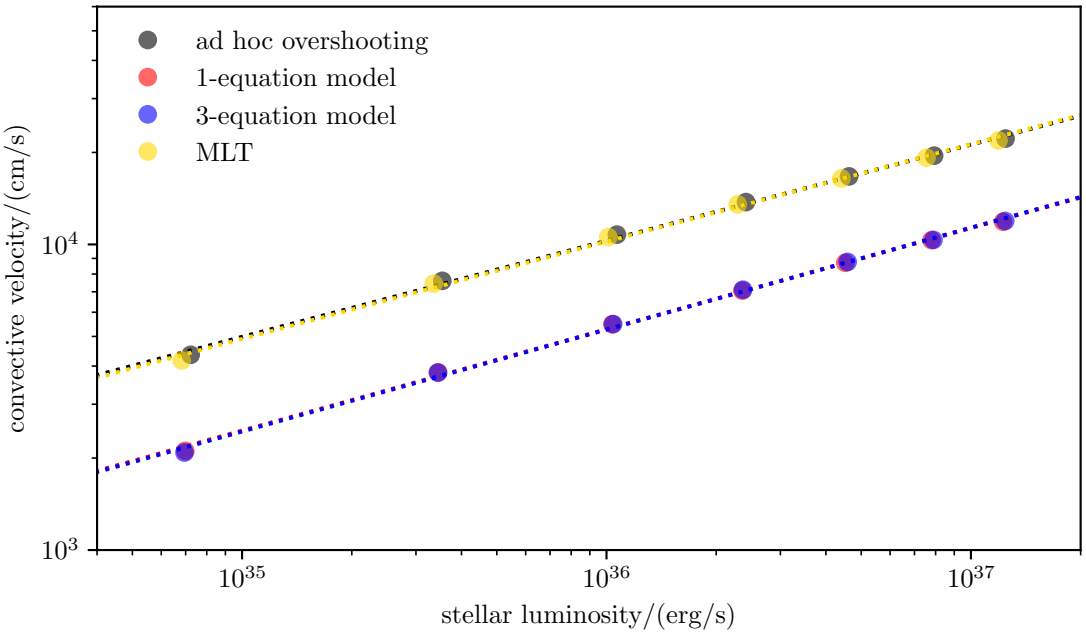

Figure 4.12: Comparison of the maximum convective velocities for different convection models as a function of stellar luminosity for stellar masses of 2-8 $M_\odot$. For the Kuhfuß model, the isotropic convective velocity u_{iso} is plotted. The dotted lines indicate a linear fit to the logarithmic data. Please note that the data of the 1- and 3-equation Kuhfuß-models (red and blue points respectively) are largely overlapping, as well as the black and yellow dots.

inferred overshooting distance for a fixed overshooting parameter will increase for a decreasing convective core size as well as the size of the mixed region. The resulting mixed core sizes for a fixed parameter value have been shown to be too large when comparing to observations (Pietrinferni et al. 2004; Magic et al. 2010). To avoid the unphysical growth of the overshooting region, the overshooting parameter needs to be artificially restricted. In GARSTEC the unphysical growth of the overshooting zone in the parametrised models is prevented by comparing the size of the Schwarzschild core to the pressure scale height and use the smaller one as the relevant length scale. As usual, there are different ways to implement this. Originally, Magic et al. (2010) suggested the following expression:

$$\widetilde{H_p} = H_p \cdot \min\left(1, \left(\frac{r_{\mathrm{CZ}}}{H_p}\right)^2\right) ,$$

where r_{CZ} is the radius of the Schwarzschild boundary. A correction factor of the same type was also used in Higl et al. (2021) when comparing GARSTEC results to 2D simulations,

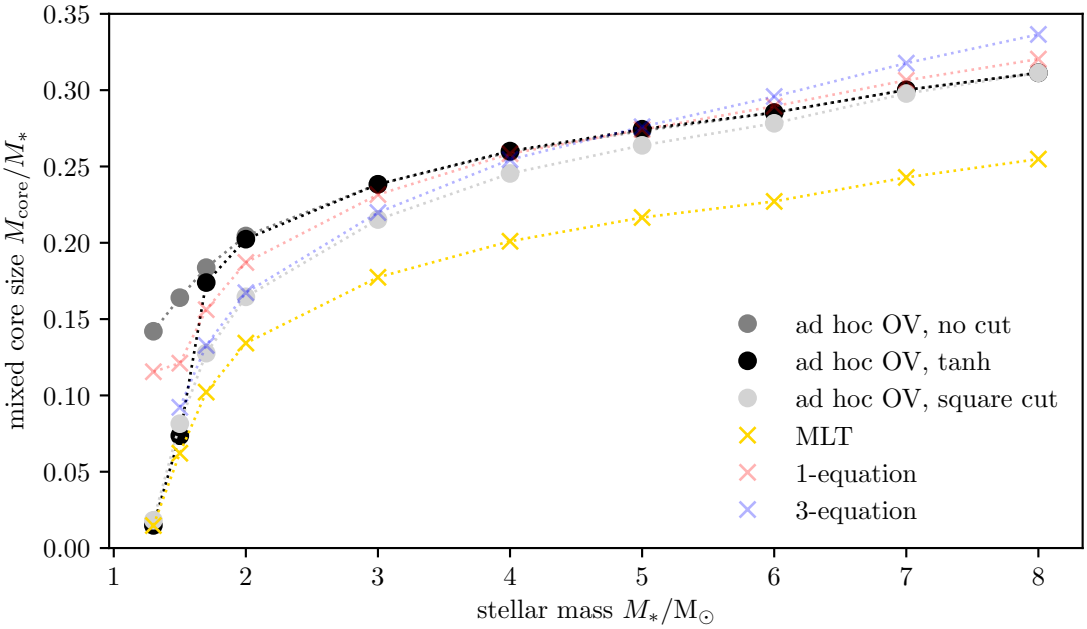

Figure 4.13: Comparison of chemically mixed core sizes obtained with different descriptions of convection and different geometric cut-off functions to limit the overshooting for small cores in the ad hoc overshooting model.

while introducing a factor of 2 in the denominator:

$$\widetilde{H_p} = H_p \cdot \min\left(1, \left(\frac{r_{\rm CZ}}{2H_p}\right)^2\right) . \tag{4.8}$$

As the size of the convective core is now compared to a length scale twice as large as the original expression the size of the overshooting region is limited more strongly by the latter expression. The comparison to 2D simulations (Higl et al. 2021) as well as the study of the eclipsing binary TZ For (Higl et al. 2018) revealed, however, that this expression is finally limiting the size of the convective core too strongly. This led to the introduction of a different functional form of the limitation:

$$\widetilde{H_p} = H_p \cdot \min\left(1, \frac{1}{2}\left[\tanh\left(5\left(\frac{r_{\rm CZ}}{H_p} - 1\right)\right) + 1\right]\right) , \tag{4.9}$$

which is limiting the core sizes less strongly at 2 $M_\odot$ but is very quickly limiting the size of the mixed cores for smaller masses.

In Fig. 4.13 we show a comparison of the mixed core sizes obtained without any cut, with the square cut according to Eq. (4.8) and with the tanh cut according to Eq. (4.9). For reference, results obtained with MLT and the 1- and 3-equation models are shown in the same figure. As discussed above, the square cut is more restrictive than the tanh cut at

masses around and above 2 $M_\odot$. Only at a mass of 8 $M_\odot$ the square cut does not restrict the convective core size any more. In contrast, the tanh cut restricts the core size only marginally already at 2 $M_\odot$. For lower masses below about 4 $M_\odot$, the results of the square cut are in good agreement with the 3-equation model.

4.5 Discussion

4.5.1 Relation between 1- and 3-equation model

As discussed in Sec. 2.5.1 the 1-equation model is a simplification of the 3-equation model, for which Kuhfuß (1987) assumes that the convective flux is proportional to the superadiabatic temperature gradient and the square-root of the TKE (Eq. 2.50 and 2.51). This allows removing two of the three equations, namely for the entropy fluctuations Φ and the velocity entropy correlations Π. The equation for the TKE ω remains unchanged. The approximation for the convective flux allows expressing the temperature gradient as a function of the TKE. This couples the thermal structure and the TKE very closely. In the 3-equation model, the convective flux is evolved with an additional equation which reduces the coupling of the thermal structure and the TKE. Despite the increased model complexity, the behaviour of the TKE in the 1- and 3-equation model is quite similar, as seen in Fig. 4.10.

In the bulk of the convection zone, both models result in the same absolute value of the TKE. This can be also seen in Fig. 4.12 by the agreement between red and blue points for a wider mass range. It can be attributed to the similarity of the equations. The additional dissipation is not or only weakly operating in the bulk of the convection zone. Hence, both the dissipation and the non-local term have the same functional form. The convective flux is adjusted such that a nearly adiabatic stratification is achieved in both models; therefore, the buoyancy term is also very comparable in the 1- and 3-equation models. As soon as the temperature gradient becomes subadiabatic, which happens already well within the Schwarzschild boundary in the 3-equation model, the dissipation by buoyancy waves is taken into account. This means that the functional form of the dissipation term changes. Due to the difference in the thermal structure in this region also the convective flux looks different. This will lead to a different solution for the TKE in the overshooting zone, as is evident from Fig. 4.10 towards the edge of the convection zone.

The main difference between the 1- and 3-equation model is probably the temperature stratification which results from the solution of the model equations. Due to the coupling of the convective flux to the superadiabatic gradient and the convective velocities in the 1-equation model, the convective flux is forced to have the same penetration depth into the stable layers as the TKE and at the same time to have the same sign as the superadiabatic gradient (see Eq. 2.50 and 2.51). As seen in our models and pointed out by Xiong and Deng (2001) this strong coupling leads to a nearly adiabatic temperature gradient in the overshooting zone and prevents the existence of a Deardorff layer (see also Ch. 3). Also with respect to other models of convection (e.g. MLT) the existence of a large subadiabatic

zone in the convective region for the case of the 3-equation model is striking. To better understand the behaviour of the temperature gradient in the overshooting zone, we will analyse it in terms of the Peclet number. The Peclet number is the ratio of the timescales of radiative and advective transport and can be interpreted as an indicator for convective efficiency. A common definition of the Peclet number is

$$\mathrm{Pe} = \frac{U \cdot l_0}{\chi} \,,$$

where U and l_0 are a typical velocity and length scale of the convective flow. The radiative diffusivity is defined as

$$\chi = \frac{16\sigma_\mathrm{B} T^3}{3\kappa\rho^2 c_p} \,.$$

As a typical convective velocity we use again the isotropic velocity, Eq. (4.7). Due to the usage of typical scales for velocities and length scales which are not rigorously defined, the interpretation of absolute values of the Peclet number remains difficult. Hence, we will only look at ratios of the Peclet number to compare different models. We will also assume that the length scale and the radiative diffusivity are the same, when comparing different models. Under these assumptions, it is easy to see that

$$\frac{\mathrm{Pe}_1}{\mathrm{Pe}_3} \propto \sqrt{\frac{\omega_1}{\omega_3}} \,.$$

The ratio of the Peclet numbers obtained for the 1- and 3-equation models for a 5 $\mathrm{M}_\odot$ main-sequence model is shown in Fig 4.14. In the bulk of the convection zone, the 1- and 3-equation models have very similar Peclet numbers, which means the transport of energy by convection behaves very comparable. In the overshooting zone, however, the 1-equation model has a Peclet number which is up to 7 times higher than that of the 3-equation model. This indicates that convection as described by the 1-equation model is much more efficient in the overshooting zone than when described by the 3-equation model.

This change in efficiency will also impact the temperature gradient. Following the approximation of the convective flux in the 1-equation model, the convective flux scales as $\Pi \propto \sqrt{\omega}$. Using the ratio of the Peclet numbers, one can therefore write a Peclet-scaled convective flux

$$\Pi_{3,\mathrm{Pe}} = \Pi_1 \cdot \frac{\mathrm{Pe}_3}{\mathrm{Pe}_1} \,, \tag{4.10}$$

to mimic the convective flux in the 3-equation model. The resulting convective flux is shown with a blue dashed line in the left panel of Fig. 4.15. Using this scaled convective flux, a scaled temperature gradient can be computed, as illustrated by the green dashed line in the right panel of Fig. 4.15. For comparison, the model temperature gradients of the 1- and 3-equation model are visualised by a green dotted and solid line, respectively.

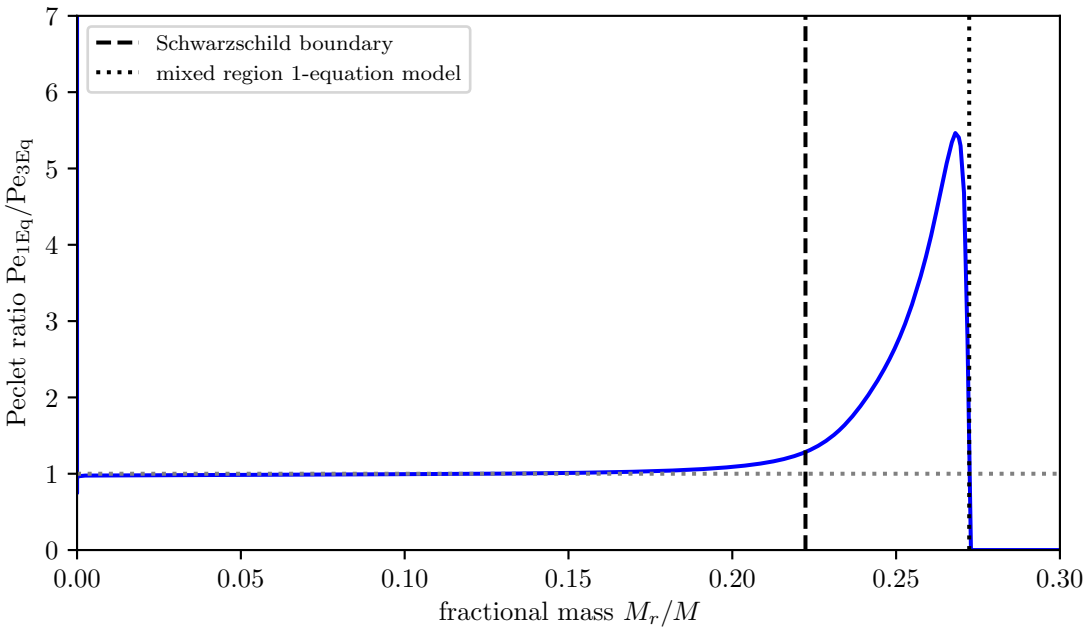

Figure 4.14: Ratio of the Peclet numbers for the 1- and 3-equation models for a 5 $M_\odot$ main-sequence model.

This comparison confirms that the reduced convective efficiency obtained from the Peclet numbers is sufficient to change the behaviour of the temperature gradient from nearly adiabatic to more radiative in the overshooting zone, and implies that the behaviour of the temperature gradient in the overshooting zone can at least qualitatively be predicted from the TKE alone without invoking the other convective equations for Π and Φ. The fact that the region of negative values in the scaled convective flux is more extended compared to the actual convective flux from the 3-equation model is due to the different penetration depths of TKE and convective flux in the 3-equation model. We conclude that this is an important indication for internal consistency of the model. It furthermore shows that the mostly radiative temperature gradient in the overshooting zone is in fact a result of reduced convective efficiency in the overshooting zone in the 3-equation model. Following the terminology proposed by Zahn (1991), in the 1-equation model the overshooting zone is best described by subadiabatic penetration while the more inefficient convection in the 3-equation model concerns overshooting of chemical element distributions only.

Considering the chemical mixing, both models will result in a more step-like chemical mixing profile. The extent of the mixed region is mainly dependent on the choice of the parameter α_ω as discussed in Sec. 4.3.1. This parameter cannot be determined from first principles. As for the ad hoc descriptions of convective core overshooting, a calibration of this parameter is required, which will be discussed below. Furthermore, the resulting convective flux is also very similar in the bulk of the convection zone and differences become only obvious in the overshooting zone. Given the relative freedom in choosing α_ω and the

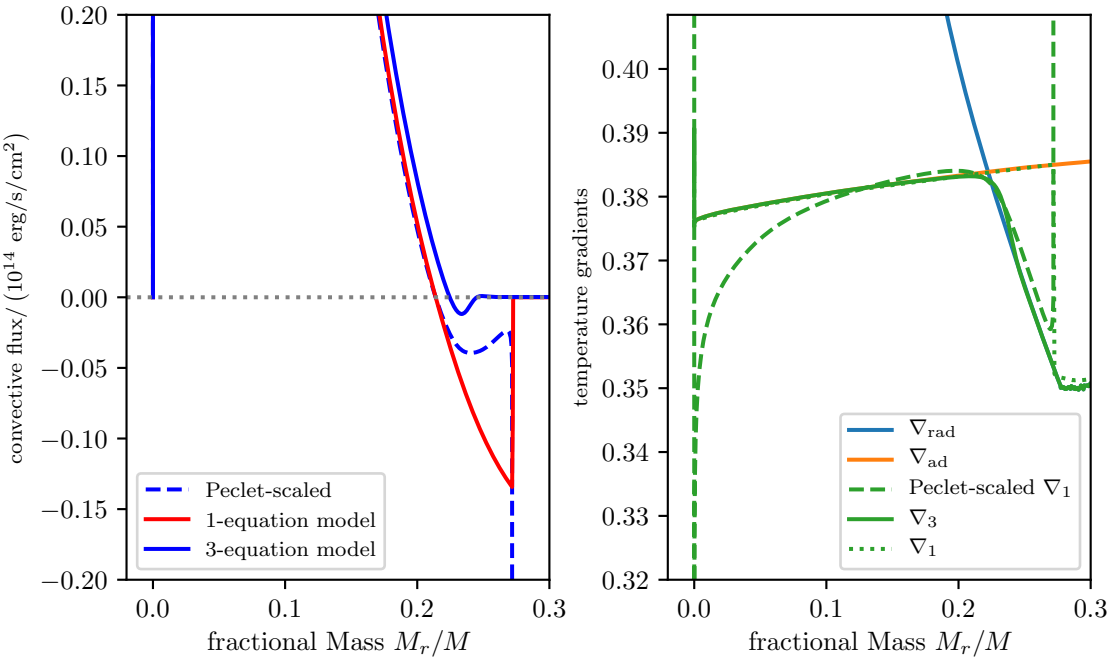

Figure 4.15: *Left panel:* Convective flux as a function of fractional mass. The red and the blue lines show the results obtained from the 1- and 3-equation model, respectively. The blue dashed line indicates the convective flux scaled with the Peclet number according to Eq. (4.10). *Right panel:* Temperature gradients as a function of fractional mass. The blue and orange lines indicate the radiative and adiabatic temperature gradient, respectively. The green dotted and solid lines indicate the temperature gradient as obtained by the 1- and 3-equation models. The green dashed line shows the temperature gradient of the 1-equation model computed from the scaled convective flux shown in the left panel.

similarity in the mixing properties of both models, resulting stellar models are basically indistinguishable when comparing the chemical structure. Once the observations become sensitive enough to the thermal structure in the overshooting zone as, for example, with the help of asteroseismology (Michielsen et al. 2019), it will become possible to detect differences between both models. In view of the general agreement between 1- and 3-equation model, the application of the 1-equation model seems to be sufficient to obtain the chemical structure from a non-local convection model. The parameter α_ω can be tuned to obtain the correct size of the convective core. However, the stratification obtained from the 1-equation model is less realistic.

4.5.2 Other constraints on core overshooting

To date, a range of different approaches to determine the extent of convective cores has been followed. In this subsection, we discuss a few examples of convective core size determinations. The need for a larger mixed core has been recognised already in the '80s of the

last century (see, for example, Bressan et al. 1981 in relation to the Hertzsprung-Russell-diagram of massive stars, or Maeder and Mermilliod 1981 concerning that of open clusters). In the latter case, isochrones derived from stellar models which include core overshooting match the morphology of the turn-off region better than models without overshooting (Pietrinferni et al. 2004; Magic et al. 2010). The comparison to observations showed further that the overshooting distance in terms of pressure scale heights needs to increase with mass in the range between 1.2 and ~ 2 $M_\odot$. This mass dependence can be included explicitly in the computations by expressing the overshooting parameter as a function of the total stellar mass. Alternatively, this mass dependence can also be introduced in the stellar models by limiting the radial extent of the overshooting zone geometrically. In both cases, the parameter of the overshooting scheme effectively needs to increase with stellar mass. For the TCM, however, this is a natural outcome without imposing it.

Eclipsing binary systems offer an excellent opportunity to put constraints on stellar physics. Claret and Torres (2019) used a large sample of eclipsing binaries to determine the overshooting parameter as a function of mass. They find a clear increase of the overshooting parameter (extent) with mass, even though the statistical significance of this result has been debated (Constantino and Baraffe 2018). In a detailed analysis, Higl et al. (2018) addressed the evolution of the binary system TZ Fornacis with an evolved red giant primary and a main-sequence secondary star, both with masses of ~ 2 $M_\odot$. They found that a basically unrestricted overshooting extent, using the standard value for the free parameter is required to explain the evolution of this system. This puts further constraints on the mass dependence of the overshooting parameter.

The high precision photometric data obtained from space telescopes like *Kepler* or CoRoT allowed setting further constraints on the stellar evolution models. Using asteroseismology of g-mode pulsators, the convective core masses of intermediate mass stars has been determined for larger samples of stars (e.g. Pedersen et al. 2021; Mombarg et al. 2019). Similarly, the seismology of p-mode pulsators allows determining the required overshooting efficiency in lower mass stars (e.g. Deheuvels et al. 2016; Angelou et al. 2020). In agreement with the previously mentioned studies, they find that the relative mass of the mixed core needs to increase with stellar mass. A more detailed comparison of the TCM models discussed in this work with asteroseismic observations needs to be addressed in future work. Finally, asteroseismology allows probing the temperature gradient in the overshooting zone. Michielsen et al. (2021) inferred a predominantly radiative overshooting zone in a ~ 3.5 $M_\odot$ main-sequence star, which is in agreement with the temperature gradient obtained from the 3-equation model but disagrees with the 1-equation model. However, they point out that this result is only obtained for this single B-type star and might not be generalisable for all B-type stars.

With the increase of computational resources in recent years, more and more multi-dimensional hydrodynamic simulations of stellar core convection have been carried out (e.g. Meakin and Arnett 2007; Gilet et al. 2013; Edelmann et al. 2019; Higl et al. 2021). These simulations confirmed, for example, the scaling of the stellar luminosity with the third power of the convective velocities (e.g. Edelmann et al. 2019; Higl et al. 2021, and references therein). In Higl et al. (2021) the authors calibrate the overshooting parameter

$f_{\rm OV}$ in GARSTEC to 2D simulations of core convection in low and intermediate mass stars. By matching the size of the mixed convective core in the 1D GARSTEC models to the size of the mixed region in the 2D simulations, they find that the effective parameter of $f_{\rm OV}$ needs to decrease with stellar mass. To limit the size of the convective cores for small stellar mass in the 1D models, they use the geometric "square" cut-off according to Eq. (4.8). As they use the same stellar evolution code as we do, this allows for a direct comparison of the results. Higl et al. (2021) find that the size of the convective cores resulting from the 2D simulations need to be larger than the GARSTEC models computed including the square cut-off (Eq. 4.8) at a constant overshooting parameter. This indicates that the geometric square cut-off is too restrictive. As the 3-equation model predicts mixed core masses similar to the GARSTEC models including this geometric cut-off (see Fig. 4.13) this indicates that our 3-equation model might be too restrictive as well at this lower mass range.

Finally, other TCMs have been used to compute stellar models, including the effects of non-local convection. Xiong (1986) has computed stellar models in the mass range of 7 to 60 $M_\odot$. He finds that by solving the convection equations, the TKE extends beyond the formal Schwarzschild boundary and that this also increases the size of the mixed region. The size of the well mixed region increases with increasing stellar mass. Both results are in agreement with our findings employing the 3-equation model. Xiong (1986) also finds that the convective flux penetrates much less deeply into the stable layers than the TKE. The magnitude of the convective flux in this region is negligible, which causes the temperature gradient to be mostly radiative in the overshooting region. This is in good agreement with the decoupling of the thermal and the chemical structure we discussed in detail in Sect. 4.3 and Ch. 3. Zhang (2016) applied the TCM by Li and Yang (2007) in a similar mass range as in this work. They develop a simplified model comparable to the 1-equation model and find very good agreement between the full model and the simplified version. Li (2017) applies the simplified TCM by Li (2012) to compute stellar models of a 5 $M_\odot$ star and find an overshooting distance of about $0.2H_p$, which is comparable to the overshooting distance obtained with our 3-equation model.

4.6 Conclusions

In this chapter, we have presented results of stellar structure and evolution calculations using the TCM proposed by Kuhfuß (1987). We have implemented the Kuhfuß model into GARSTEC which solves the four stellar structure equations and the three equations of the convection model simultaneously with the implicit Henyey method. We have computed main-sequence models of low- and intermediate-mass main-sequence stars between 1.5 and 8 $M_\odot$ which consistently compute the structure and evolution of the TKE, convective flux, and entropy fluctuations. This naturally includes the effects of convective overshooting for the thermal and chemical structure. In Ch. 3 we have demonstrated that the original 3-equation model with standard MLT prescription for the dissipation length of TKE leads to convection zones which essentially extend throughout the entire stellar interior. We have

therefore implemented the dissipation by gravity waves as discussed in Ch. 3 in addition to the original Kuhfuß model. We showed that the Kuhfuß 3-equation model with an increased dissipation rate results in models with physically reasonable overshooting distances. This indicates that the dissipation was actually underestimated by the original description, and that dissipation by gravity waves is a relevant effect in core overshooting zones.

In Fig. 4.1 we have shown a summary of the TKE, convective flux and the superadiabatic temperature gradient for a convective core of a 5 $M_\odot$ main-sequence model. We find that the TKE extends beyond the formal Schwarzschild boundary of convective neutrality. This is the result of the non-local terms in the Kuhfuß model. The convective flux shows a region of negative values beyond the Schwarzschild boundary, which is, however, penetrating less deeply into the stable layers than the TKE. As the convective motions are very efficient in mixing chemical elements, the extended convective core will have essentially the same composition as the convective core. This can be seen in Fig. 4.8, left panel, in which the hydrogen profiles at the end of the main sequence of an MLT and a Kuhfuß 1- and 3-equation model are compared. In the Kuhfuß model, this extension beyond the Schwarzschild boundary is the outcome of the solution of the model equations and not due to the inclusion of any sort of ad hoc overshooting. We also compared the results of the full 3-equation model to the simplified 1-equation model and find qualitative and quantitative agreement of the TKE throughout a large part of the convection zone. This is a result of the similarity of the model equations and the chosen parameters, which are the same for both models. In addition to the convective velocity and the associated mixing also the temperature gradient is part of the model solution. This is another important difference compared to ad hoc descriptions of convective overshooting, in which the temperature gradient needs to be assumed separately and independently.

The analysis of the temperature gradient has shown the existence of a Deardorff-layer in the 3-equation model (Deardorff 1966), in which the temperature gradient is subadiabatic and the convective flux is still positive. The existence of the Deardorff-layer has been confirmed in different numerical simulations of stellar convection (Chan and Gigas 1992; Muthsam et al. 1995, 1999; Tremblay et al. 2015; Käpylä et al. 2017) and other Reynolds stress models (Kupka 1999a; Xiong and Deng 2001; Kupka and Montgomery 2002; Montgomery and Kupka 2004; Zhang and Li 2012). Beyond the Deardorff-layer, the convective flux becomes negative as the result of the stable stratification (cf. also Muthsam et al. 1995 and references in Canuto 1992). In the overshooting region, the model temperature gradient gradually transitions from a slightly subadiabatic to a radiative value, exhibiting a small region with a super-radiative temperature gradient (see Fig. 4.2). However, this transition region is rather narrow, such that the overshooting zone has a mostly radiative temperature gradient. This is in agreement with very recent results from asteroseismology (Michielsen et al. 2021). In contrast to the 3-equation model, the overshooting zone of the 1-equation model shows a mostly adiabatic temperature gradient. As pointed out by Xiong and Deng (2001) this can be attributed to the assumption of a full correlation between the convective flux and the convective velocities, as it is done in the 1-equation model (see Eq. 2.50). The approximation Eq. (2.50) does not allow for a Deardorff layer, as the convective flux is proportional to the superadiabatic gradient. From a theoretical

point of view, the existence of a Deardorff-layer can be attributed to the non-local term of the Φ-equation Eq. (2.59) (Deardorff 1966). This shows that an independent equation for the convective flux is required (see also Kupka et al. 2022) and highlights the necessity to consider more complex turbulence models like the 3-equation model to capture the temperature structure in the overshooting zone more accurately. The comparison of the Peclet numbers of the 1- and 3-equation models shows further that the mostly radiative temperature gradient in the overshooting zone of the 3-equation model can be explained by the reduced TKE/velocities compared to the 1-equation model. The narrow range of the transition region from an adiabatic to a radiative temperature gradient can be attributed to the shallower penetration of the convective flux into the stable layers compared to the 1-equation model.

A comparison with stellar models using MLT shows qualitative agreement of the TKE and the convective flux in the part of the convection zone unstable according to the Schwarzschild criterion ($\nabla_{\rm ad} = \nabla_{\rm rad}$). For the convective flux, we even find a very good quantitative agreement between the Kuhfuß model and MLT in that region (see Fig. 4.8, right panel). The convective velocities found in the Kuhfuß model are smaller than in MLT by a factor of two. This qualitative agreement indicates that the stellar structure has the largest impact on the convective properties in the bulk of the convection zone, irrespectively of the convection model in use. The nuclear energy released in the centre determines the convective flux — about 80% of the local flux in the centre — and the coefficients of the convection model determine the absolute values of the other convective variables. Differences appear in the overshooting zone, which is sensitive to more subtle changes in the convection model. In the overshooting zone the stellar flux is mainly transported by radiation, such that the convective structure of this region is less constrained by the stellar structure but a result of the convection model.

The results of the 1- and 3-equation models over a broader mass range show qualitative agreement with other overshoot descriptions. For given values of α_ω and $f_{\rm OV}$ this is achieved without fine-tuning any of the model parameters, as we have used the closure parameters suggested by the authors of the turbulence model (see Canuto and Dubovikov 1998, and references therein). Tests of those parameters — for different physical scenarios — are published in the literature (Kuhfuß 1986, 1987; Wuchterl 1995; Canuto 1992; Canuto and Dubovikov 1998; Kupka and Muthsam 2007c). In Fig. 4.11 we have shown a comparison of chemically mixed hydrogen core sizes computed with exponential overshooting, the 1-equation and the 3-equation model, and MLT. The comparison shows that the exact extent of the convective core depends on the details of the model. For the same parameter choice of the parameter α_ω at lower masses, the 3-equation model shows a reduced amount of overshooting compared to the 1-equation model, while the 3-equation models have larger cores at higher masses. The newly introduced parameters which control the reduction of the dissipation length scale Λ were shown to have a moderate impact on the overshooting extent. For its default overshoot parameter the exponential mixing model produces yet larger mixed core sizes. Towards the lower end of the mass range, both Kuhfuß models show a decrease of the mixed core size, as implemented by other methods to match observations from open clusters and binaries (Claret and Torres 2019; Pietrinferni et al. 2004; Magic

et al. 2010). Higl et al. (2018) found that the overshooting parameter needs to increase steeper with mass than predicted by GARSTEC including the geometric square cut-off from the analysis of the TZ For binary system. In agreement with the conclusion from the 2D simulations (Higl et al. 2021), this indicates that the convective core size predicted by the 1- and 3-equation model increases too shallowly with stellar mass for a constant parameter α_ω. To match the observations and the results from the 2D simulations, this would require to modify the parameter α_ω as a function of mass. Further constraints on the parameter α_ω can be obtained by comparing the Kuhfuß model to results from asteroseismology of intermediate mass stars.

However, such tuning of α_ω seems non-advisable: the physical incompleteness of the ad hoc model of convective overshooting, as an example, is well demonstrated by the shrinking of the convective core size with mass for stars with $M < 2\ \mathrm{M}_\odot$ not only requiring an extra cut-off function (Eq. 4.8) to limit the convective core size to values compatible with observations, but even demanding a more fine-tuned function (Eq. 4.9) to pass such a stringent test. While applying a similar procedure to α_ω as for f_{OV} appears to be a convenient ad hoc solution to match exactly the observational data, it provides no new insights and requires redoing similar procedures in related, but different scenarios. Finding the physical reason for the remaining, now already much smaller discrepancies with the data, on the other hand, might allow for a model not requiring such measures in other applications either (cf. also the discussion on such requirements in Kupka and Muthsam 2017).

Our study of stellar models applying the 3-equation model from Kuhfuß (1987) has shown that the resulting stellar structure depends sensitively on the details of the convection model. Although the original 1- and 3-equation theories are very closely related, their application results in very different structures of the convection zone (see Ch. 3). We demonstrated that modifying the dissipation term of the TKE can remedy this discrepancy. The improved 3-equation model compares very well with the 1-equation model, both in terms of the TKE and the mixing properties. For applications in which the temperature structure of the overshooting zone is not important, the 1-equation model describes the convective core similarly well as the 3-equation model. The parameter α_ω allows obtaining the required convective core size to match with the observations. Only when the thermal structure of the overshooting zone is of major interest, a more complex convection model like the 3-equation model needs to be used. A self-consistent prediction of the detailed convective core structure appears to require a physically more complete (and thus more complex model). As discussed above, at least three equations are required to allow for more complex phenomena like, for example, a Deardorff layer. In Canuto and Dubovikov (1998) further partial differential equations for the dissipation rate and the vertical component of the TKE are discussed. This potentially allows removing some of the simplifications still present in the 3-equation model. However, increasing the number of equations comes at the price of gaining numerical complexity. Including these equations into stellar structure and evolution models has to remain the task of future work. Finally, a comparison with more and more realistic 3D hydrodynamic simulations of convective cores will be useful to put further constraints on our TCM model, in particular to restrict closure conditions.

This will be discussed in the next chapter. In any case, turbulent convection models offer a convincing and feasible improvement of the treatment of convection in 1D stellar models beyond the standard mixing-length theory.

Chapter 5

Comparing turbulent convection models and hydrodynamic simulations

The work for this chapter has been carried out in collaboration with Johann Higl at the Heidelberg Institute for Theoretical Studies (HITS). Johann Higl has carried out the 3D simulations and computed the numerical averages for the analysis. I have provided starting models for the 3D simulations, worked out the equations and terms that need to be considered and carried out the analysis of the numerical averages provided by Johann Higl. The text of this chapter is written by me.

5.1 Introduction

In the previous chapter, we have discussed how the TCM compares to different descriptions of convection in stellar models and also to observations. In this chapter, we now turn to comparing the TCM to hydrodynamic simulations. Hydrodynamic thee-dimensional (3D) simulations numerically solve the fundamental hydrodynamic equations Eq. (2.1), (2.2) and (2.3). In astrophysical applications, the molecular viscosity is most often negligibly small, such that it is sufficient to solve the inviscid Euler equations instead of the Navier-Stokes equations. As a result, the simulations provide us with a time series of hydrodynamic variables like velocities, densities or temperatures in three spatial dimensions. Compared to other theoretical descriptions of hydrodynamics, 3D simulations apply a limited set of assumptions and approximations. Therefore, their results are considered as a rather accurate representation of the physical reality. As described above, stellar models are constructed under a number of assumptions and approximation, among which the most important one is probably the assumption of spherical symmetry. Hence, also the hydrodynamics need to be described in one spatial dimension. To compute accurate stellar models, it is crucial to make sure that the one-dimensional (1D) models capture the most relevant aspects of the hydrodynamic flows. In this chapter, we compare results from 1D stellar models includ-

ing the Kuhfuß convection theory to the 3D simulations by constructing the convective variables as well as the individual equation terms from the 3D data using the Reynolds Averaged Navier Stokes analysis (RANS) as described in Sec. 2.2.

We will compare the Kuhfuß model in different ways to the hydrodynamic simulations. The first and simplest comparison is to directly compare the convective variables, the TKE ω, the convective flux variable Π and the squared entropy fluctuations Φ, defined in Eq. (2.11) - (2.13), obtained from the stellar model and extracted from the hydrodynamic simulation. With this approach, we aim at testing how well the stellar models represent the results obtained from the hydrodynamic simulations. As discussed a couple of times before, the most relevant question for stellar structure and evolution concerns the size of the convective core and hence the convectively mixed region. Furthermore, the temperature gradient in the convective region is computed according to Eq. (2.60) and we will use the convective flux from the 3D simulations to draw conclusions about the thermal stratification in the convection and overshooting zone. However, such a comparison will only show global discrepancies, without indicating their physical origin. In Sec. 2.2 we have described the derivation of the dynamic equations of the convective variables Eq. (2.16) to (2.18). We showed how the terms on the right-hand-side of the dynamic equations can be related to different physical processes, for example buoyancy or turbulent transport of quantities. To go more into the details and study the reason for potential discrepancies of the convective variables in the 1D and 3D data, we will compare the individual terms computed in the simulations and stellar models. These terms can be either directly compared to their 1D counterparts, computed as described in Sec. 2.4.1, which again allows us to assess the overall physical accuracy of the TCM used. Alternatively, they can be compared to their approximations fed with 3D data, which allows assessing the accuracy of the individual physical approximations (e.g. Snellman et al. 2015). In this chapter, we will only follow the former approach. Finally, the RANS analysis of 3D simulation data is essential to interpret the behaviour of the simulation at a deeper physical level. This has been already discussed in Viallet et al. (2013) for convection in a red-giant envelope and oxygen shell burning, in Arnett et al. (2015) and Mocák et al. (2018) to study turbulent mixing and burning in massive stars and in Horst et al. (2021) to study a He-burning shell in a massive star. Comparing the results of hydrodynamic simulations with the TCM in a stellar model is therefore a powerful way to identify shortcomings of the convection model and understand turbulent convection in stars in general (Grossman 1996; Cai 2020; Arnett et al. 2015; Kupka and Muthsam 2007a,b,c).

With this comparison, we aim at answering whether the Kuhfuß model is an acceptable model to describe convection in stars and whether it does describe the overshooting zone correctly. In Sec. 5.2 we describe the simulation code used and the numerical setup of the simulations. In Sec. 5.3 we start by comparing the convective variables to their representations computed from the 3D simulations. Subsequently, we compute the terms of the relevant equations as described in Sec. 2.2 and compare them to their counterparts computed in the Kuhfuß 1- and 3-equation model. Given the individual terms of the Kuhfuß model computed from the hydrodynamic simulations, we discuss how varying the model parameters may improve the agreement between the model and the simulations in Sec. 5.5.

Considering the theoretical and numerical uncertainties of the hydrodynamic simulations, this analysis can be only carried out in the theoretical limits of the simulations used (see Secs. 5.2 and 5.6).

5.2 Three-dimensional hydrodynamic simulations of stellar core convection

In this section we describe the numerical code used, to compute the 3D simulations as well as the specific setup of our simulations. Furthermore, we describe how the spherical averages are computed from the 3D data.

5.2.1 Simulation setup and numerics

For our 3D simulations of stellar core convection, we use the Seven Leagues Hydro code (SLH, Miczek 2013; Edelmann 2014). The original numerical solver has been described in Miczek et al. (2015). As discussed above, the stellar matter has very low viscosity. Therefore, viscous effects are neglected in the numerical simulations and the inviscid Euler equations are solved (see Edelmann et al. 2021, for details). We use the Helmholtz equation of state by Timmes and Swesty (2000) to close the set of hydrodynamic equations. The hydrodynamic equations are discretised using a finite volume scheme. The discretised equations are evolved in time using an explicit ordinary differential equation solver, e.g. a Runge-Kutta solver, or using an implicit time integration. Across the cell interfaces, a Riemann problem occurs. To compute the approximate fluxes of the Riemann problem, the SLH code applies the AUSM$^+$-up scheme (Advective Upstream Splitting Method, Liou and Steffen 1993; Liou 1996, 2006). The choice of these numerical flux functions is crucial for the computation of low Mach number flows, as many conventional flux approximations lead to very high numerical dissipation, rendering the computation of slow flows impossible (see for example the discussion in Miczek et al. 2015; Edelmann et al. 2021). Another important requirement for hydrodynamic flows in the stellar interior concerns the state of hydrostatic equilibrium. Deviations from the hydrostatic equilibrium, due to the numerical scheme or the initial model, may cause spurious flow velocities. These numerical deviations occur in case of an imperfect balance of pressure and gravity terms. To avoid this, the numerical scheme needs to preserve the state of hydrostatic equilibrium over longer times. In Edelmann et al. (2021) several schemes for this well-balancing that are implemented in SLH are discussed. In the solution of the Euler equations, no explicit viscosity is considered. This means that there is no explicit source of dissipation. Dissipation nevertheless occurs as a result of the numerical viscosity when computing the numerical fluxes of the Riemann problems.

The code SLH has been used for several applications in stellar astrophysics, e.g. convective He-shell burning (Horst et al. 2021), the study of internal gravity waves (IGW) (Horst et al. 2020), shear instability (Edelmann et al. 2017) and silicon burning (Röpke

et al. 2018). Recently, Andrassy et al. (2022) carried out a code comparison project including SLH among other codes and demonstrated that all codes are in good agreement with each other for a convection setup of astrophysical relevance. This is an indication of the robustness of the numerical methods used.

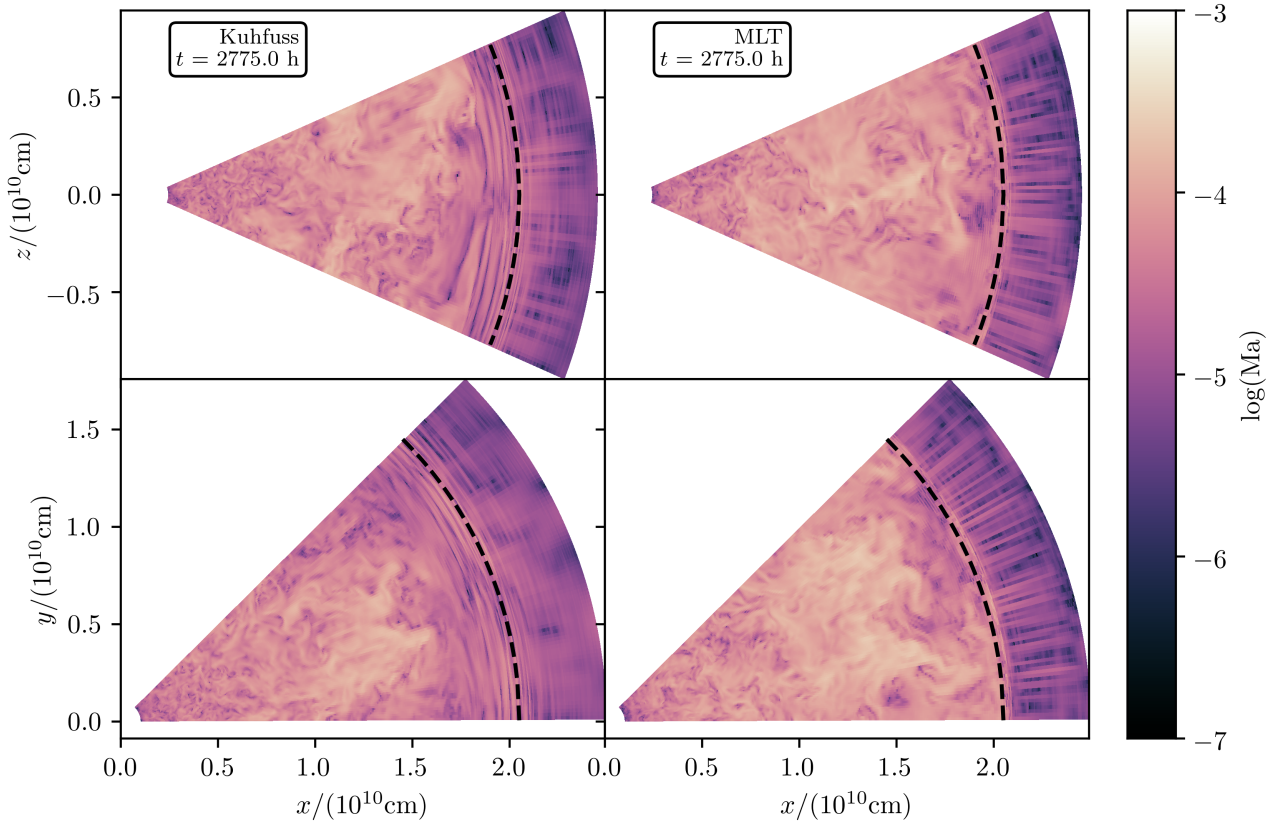

Figure 5.1: Visualisation of the convective flow from the 3D simulations in the $x-z$ and the $x-y$ plane using the Mach number of the flow in the upper and lower panel respectively. The results from simulation 1 are shown in the left column and the results from simulation 2 are shown in the right column. The Mach number is indicated with the logarithmic colour-scale. The Schwarzschild boundary of the initial stellar models is indicated with a black dashed line in each panel.

We have set up the simulation in a wedge geometry with an extent of 45° in the θ direction and 45° in the φ direction. Each angular direction is discretised in 96 cells. In the radial direction, the wedge comprises $\sim 2.5 \cdot 10^{10}$ cm discretised using 384 grid cells. In the core, a region of $0.1 \cdot 10^{10}$ cm has been cut out to avoid the coordinate singularity in the centre. This is about 4% of the whole simulation domain. The impact of this inner boundary is considered to be negligible. In the θ and φ direction, periodic boundaries have been applied. In the radial direction, wall boundaries have been used, i.e. the velocity component perpendicular to the boundary is set to zero such that the flow

turns sideways. To set up the hydrodynamic simulation, we use results from 1D stellar structure models. These models are mapped as a background into the 3D simulation following Edelmann et al. (2017). The model is first interpolated from the Lagrangian grid onto the Eulerian grid, which causes deviations from the initially perfect hydrostatic equilibrium. Subsequently, the density of the interpolated model is changed to reinstate a perfect hydrostatic equilibrium. In this process, the temperature stratification is forced to match the temperature stratification of the initial 1D stellar model. This last step is mainly necessary due to small differences of the EOS between GARSTEC and SLH. The energy generated by nuclear fusion in the stars is supplied to the hydrodynamic simulation by a constant heating rate. The radial distribution of the heating rate is taken from the initial stellar model. We use two different 1D stellar models of a 3 $M_\odot$ main-sequence star computed with GARSTEC to initiate two 3D simulations. The first model is computed, employing the Kuhfuß 3-equation theory as described in Sec. 2.5. The second simulation is initialised with a starting model computed using MLT and ad hoc overshooting, as described in Sec. 4.3. In the following, we will refer to these simulations as simulation 1 and simulation 2, respectively. Due to the local nature of MLT, this model will have a different temperature stratification than the 3-equation Kuhfuß model and therefore serve as a valuable reference simulation. The stellar models were evolved to a central hydrogen abundance of $X_c = 0.6975$, which means that the star has reduced its initial hydrogen abundance by less than 1%. This reduces the impact of chemical gradients in the 3D simulation. The Kuhfuß and MLT simulations have been evolved over $1.17 \cdot 10^7$ s physical time, corresponding to about 1 convective turnover. The convective flow is seeded by introducing sinusoidal velocity perturbations with a relative amplitude of 10^{-7}. An initial transient phase, lasting for $8.1 \cdot 10^6$ s, in which the convective flow develops is excluded from our analysis, such that our averaging interval consists of 1000 h elapsed time in the simulation.

In Fig. 5.1 we show a representation of the convective flow in slices through the computational domain. The results of simulation 1 and 2 are shown in the left and right column, respectively. The upper panels show a slice in the $x - z$ plane rotated by $\pi/8$ around the vertical axis, and the lower panels show a slice in the $x - y$ plane. The Mach number is colour coded on a logarithmic scale. As discussed above, the Mach number of flows in the stellar interior is low and indeed does not exceed approximately $3 \cdot 10^{-4}$ in the present simulations. In SLH, this is dealt with the numerical flux functions with low numerical viscosity described above. Alternatively, the luminosity of the star could be boosted by a large factor to increase the convective velocities and in turn the Mach number. It is visible that convection has set in, and a turbulent flow has developed at the time the snapshot has been taken in both simulations. We note that in simulation 1 the turbulent convective motions seem to cease at a radius of about $1.9 \cdot 10^{10}$ cm. Beyond this point the motions seem to be more ordered, probably related to waves. Beyond $2.05 \cdot 10^{10}$ cm motions substantially decrease related to the formal Schwarzschild boundary of the initial models which we have indicated with a dashed line in each panel. In simulation 2 the turbulent convective motions extend until the Schwarzschild boundary, whereafter an abrupt drop of motions is visible. At the edge of the turbulent convective region, beyond the formal Schwarzschild

boundary, some spurious velocity features are visible due to unresolved waves. The extent of the turbulent convective region will be discussed in more detail below. No data are available below $x = 0.1 \cdot 10^{10}$ cm, as this is beyond the lower edge of the computational domain.

5.2.2 Computation of averages

The hydrodynamic simulations provide us with time series of hydrodynamic variables in three spatial dimensions. To compute the RANS equations described in Sec 2.2 and compare the 3D data with the stellar convection models, we need to compute suitable averages. In addition to the spatial average, we also compute a temporal average following Mocák et al. (2018). The resulting average then reads

$$\overline{a}(r) = \frac{1}{\tau \Delta\Omega} \int_{\tau_0}^{\tau_0+\tau} \int_{\Delta\Omega} a(t, r, \theta, \phi) \mathrm{d}\Omega \mathrm{d}t \,,$$

where $\mathrm{d}\Omega = \sin\theta \, \mathrm{d}\theta \, \mathrm{d}\phi$ denotes the solid angle in spherical coordinates, τ and $\Delta\Omega$ refer to the time interval and the solid angle that are averaged over, respectively. The initial time-interval needed for convection to fully establish is denoted as τ_0. This interval is excluded from the averaging to avoid spurious results by this transient phase. The final average $\overline{a}(r)$ is then time-independent, as we integrate over the remaining simulation time. In principle, a time-dependence could be reinstated by shortening the time interval τ. However, we assume the simulation to be stationary after the initial transient, such that the time-dependence may be neglected. Furthermore, the averages become more reliable for longer averaging times. We note that both convection models we want to compare to are time-independent. The MLT is time-independent by construction, and for the Kuhfuß equations we have chosen to neglect the time-derivatives. Therefore, the time-dependence in the simulations is not of interest for us at the moment.

For the computation of the averages required for the RANS analysis, it is useful to quote a number of identities. Many terms contain averages of at least two fluctuating quantities. These can be conveniently rewritten as

$$\begin{aligned} \overline{a'b'} &= \overline{(a - \overline{a})(b - \overline{b})} \\ &= \overline{ab - \overline{a}b - a\overline{b} + \overline{a}\overline{b}} \\ &= \overline{ab} - \overline{a}\overline{b} \,, \end{aligned} \tag{5.1}$$

where we used $\overline{\overline{a}} = \overline{a}$. In this way, we avoid computing fluctuations locally to average them subsequently. Instead, we compute averages of the full hydrodynamic variables and reconstruct the correlation functions subsequently. The same procedure may be applied to third order combinations of fluctuating quantities to obtain

$$\overline{a'b'c'} = \overline{abc} - \overline{a} \cdot \overline{bc} - \overline{c} \cdot \overline{ab} - \overline{b} \cdot \overline{ca} + 2\overline{a} \cdot \overline{b} \cdot \overline{c} \,.$$

For a few terms it turned out that reconstructing the correlation functions from averages of the individual contributions results in very noisy and hence unreliable results. For these,

we resort to computing the fluctuations locally and average over them. We will indicate in the text for which terms this was done.

Finally, it is worth noting that taking the average and taking a derivative commute:

$$\overline{\frac{\partial a}{\partial t}} = \frac{\partial \overline{a}}{\partial t}$$
$$\overline{\boldsymbol{\nabla} a} = \boldsymbol{\nabla} \overline{a}$$

(see e.g. Pope 2000, Sec. 3.7). As the averaged quantities only depend on the radius by definition, the second identity has the convenient consequence that applications of the $\boldsymbol{\nabla}$ operator[1] reduce to a radial derivative.

5.3 Convective variables

In this section, we compare the convective variables, i.e. ω, Π and Φ, obtained from the 3D simulations described in the previous section to the 3-equation model and the MLT model including ad hoc overshooting that we have used as initial models for the simulations as well as to a 1-equation model (see Sec. 2.5 and 4.3 for a description of the models). The 1-equation model is a simplification of the full Kuhfuß 3-equation model. Instead of solving another dynamic equation for the convective flux, it is approximated by Eq. (2.50) and (2.51). Despite its simplicity, the 1-equation model allows for the emergence of an overshooting zone and the modification of the model temperature gradient (see Fig. 4.10 and 4.15). Therefore, we consider it worth to also compare the 3D simulation data to the 1-equation model. The stellar models are all selected to have the same central hydrogen abundance of $X_\mathrm{c} = 0.6975$. As the MLT model itself does not compute the TKE, we compute an isotropic estimate of the TKE using the convective velocities computed by MLT as $\omega_\mathrm{MLT} \approx 3/2 u_\mathrm{conv}^2$. The parameter α_ω of the 1-equation Kuhfuß model has been tuned to achieve the same extent of the TKE as in the 3-equation model. As seen in Fig. 4.13 a different core size is obtained for the default parameter value for a stellar mass of 3 $\mathrm{M}_\odot$. Therefore a value of $\alpha_\omega = 0.15$ has been chosen for the 1-equation model. The TKE ω as well as the convective flux variable Π are expected to have the largest impact on the stellar structure and evolution, as they define the convectively induced mixing through Eq. (2.22) and the temperature gradient in the convection and overshooting zone through Eq. (2.60). While a more detailed comparison between the simulations and the 1D stellar models will be necessary to understand the differences in the physics, this comparison might disclose already some discrepancies. The comparison of the individual equation terms will be presented in the subsequent section.

In Fig. 5.2 we show the total TKE ω as a function of radius on a logarithmic scale. The results of simulation 1 and 2 are shown in the upper and lower panel, respectively. For comparison, we show the TKE obtained from the 1- and 3-equation Kuhfuß models

[1] Note that $\boldsymbol{\nabla}$ refers to the gradient operator while ∇ refers to the dimensionless temperature gradient Eq. (2.19).

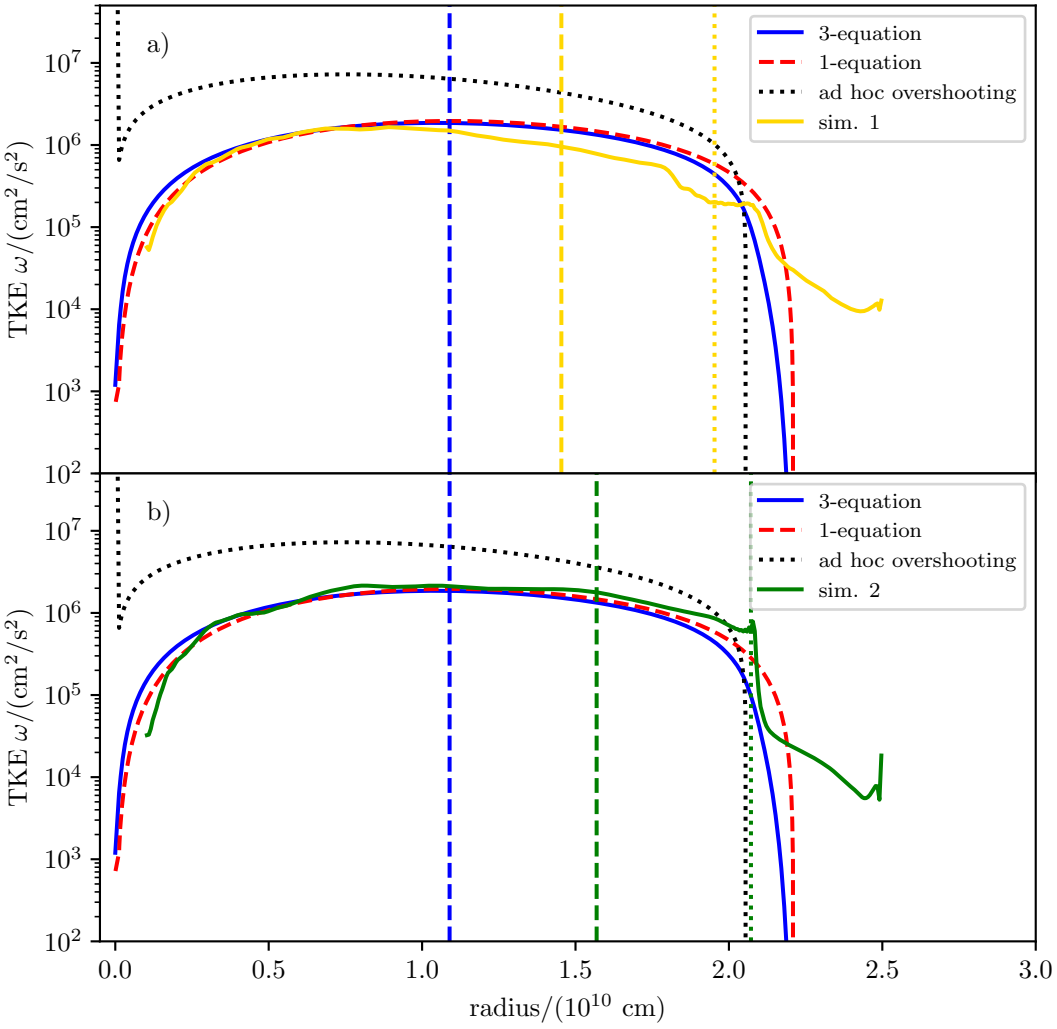

Figure 5.2: Comparison of the TKE ω as a function of radius on a logarithmic scale. The results obtained from the 1- and 3-equation model as well as from an MLT model are shown with a blue, red and black line respectively. The associated RANS correlations extracted from simulation 1 and 2 are shown in the upper panel and lower panel, respectively. The vertical dashed lines indicate the boundary of the superadiabatic region of the respective simulation. The vertical dotted line indicates the boundary of the turbulent convective core. (See text for definitions).

and from the MLT model including ad hoc overshooting. We indicate the edge of the turbulent convective region obtained from the 3D simulations by a dotted vertical line in the respective colour. This provides a useful reference location for the comparison of the different quantities of interest. We describe how we determine this location in more

detail further below (see discussion of Fig. 5.3). Another important radial location is the extent of the superadiabatic region. Following Eq. (2.51) we compute the boundaries of the superadiabatic region in the 3D simulations from the sign change of the gradient of the mean entropy (see discussion of Fig. 5.5 further below). The boundaries of the superadiabatic region from simulation 1 and 2 and the 3-equation model are indicated in the upper and lower panel of Fig. 5.2 with vertical dashed lines in the respective colour. We find that the absolute value of the TKE of the Kuhfuß models is generally in good agreement with simulation 1 and 2 in the bulk of the convection zone. Both simulations better reproduce the TKE of the 1- and 3-equation models towards the centre. Towards the outer boundary, simulation 1 underestimates the TKE of the 1- and 3-equation model, while simulation 2 overestimates it. As discussed in Sec. 4.3 the 1- and 3-equation models result in very similar absolute values of the TKE. The TKE estimate from MLT is larger than the Kuhfuß models by a factor of 4 as expected from the discussion in Sec. 4.4 (see Fig. 4.12) and larger by the same factor compared to the simulations. We conclude that the TKE obtained from MLT is not a good representation of the TKE in our simulations and even simulation 2, initialised with the MLT model, more closely reproduces the Kuhfuß models in that respect. At the convective boundary, the TKE of simulation 2 initialised from the MLT model, is more extended than the TKE of simulation 1, initialised from the Kuhfuß 3-equation model, as one would have expected from the Mach numbers shown in Fig. 5.1. We argue that this is a result of the difference in the temperature structure of the initial stellar models. Due to the smaller superadiabatic region in simulation 1 there is a smaller region in which the convective motions are driven by the superadiabaticity and as a result the TKE is less extended. It also shows that the 3D simulations are still sensitive to their initial state. We discuss this further in Sec. 5.6. Overall, the shape of the TKE profiles from the 3D simulations and the Kuhfuß models is comparable, which is indicating that the Kuhfuß model captures the main behaviour of the TKE in a convective stellar core. However, the smaller extent of the TKE in simulation 1 would create a smaller mixed region compared to the 1D model. In conventional 1D stellar models this would translate to a smaller overshooting distance and in turn lower luminosities and shorter main-sequence lifetimes. Beyond the vertical dotted lines, some residual TKE remains present. This can be attributed to the travelling of unresolved waves, as it can be also seen in the visualisation of the turbulent flow in Fig. 5.1.

Given the velocity field obtained from the 3D simulation, we determine the spatial distribution of the total TKE. To compute an anisotropy factor, we split the TKE into a vertical part, considering only motions in radial direction, and a horizontal part, considering motions in θ and ϕ direction. We denote the vertical part of the TKE by $\overline{w^2}$ to agree with definition Eq. (3.16) in Sec. 3.4.1. We compute an anisotropy factor as the ratio of the vertical to the total TKE $\xi^2 = \overline{w^2}/\omega$. A value of 2/3 indicates an equal distribution among the vertical and horizontal directions, while larger values indicate a more vertically dominated flow and smaller values indicate a more horizontally dominated flow. The resulting anisotropy profiles for simulation 1 and 2 are shown in Fig. 5.3. In the bulk of the convection zone, the anisotropy factor takes values greater than 2/3 and tends towards 1. This means that the flow is radially dominated, as has been for example observed in

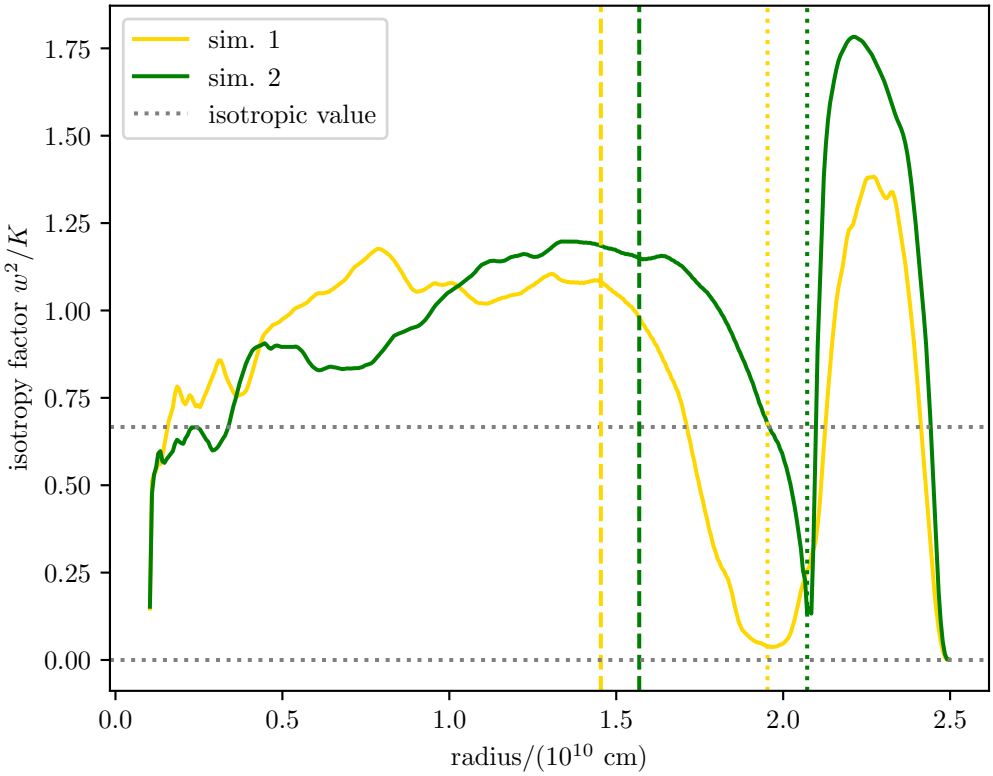

Figure 5.3: Flow anisotropy as a function of radius computed from the RANS data obtained from simulation 1 and 2 shown in yellow and green, respectively. We indicate the boundary of the superadiabatic regions with dashed lines and the TKE boundary with the dotted lines in the respective colour.

simulations by Andrassy et al. (2022) or Viallet et al. (2013). Towards the upper boundary, the anisotropy factor drops from the maximum value and reaches values close to zero at the boundary of the turbulent convective region. Beyond this initial drop of the isotropy factor, we observe a steep increase of this quantity, again indicating a radially dominated flow. As the temperature structure is radiative in this region and the total TKE dropped already considerably, we associate this radially dominated flow with the appearance of unresolved waves in the simulation and not with another convective region. This is confirmed by the comparatively small values of the total TKE in this region shown in Fig. 5.2. The initial drop of the flow anisotropy is expected towards convective boundaries as the flow has to turn over and return into the bulk of the convection zone. We use this behaviour to determine the boundary of the turbulent convective region. A value close to zero indicates that the convective flow turned over and the edge of the convective region is reached. This is indicated with the vertical dotted lines in Fig. 5.2 and 5.3. The TKE profiles show a

drop at the determined locations as well. We refer to this boundary as the TKE boundary. The residual TKE present beyond this radius can be attributed to the waves, which are especially pronounced in simulation 1 (see Fig. 5.1). The extents of the TKE in the different simulations and stellar models are summarised in the fourth column of Tab. 5.1 in terms of radius, and in the fifth column in terms of fractional mass. For the MLT model, the TKE boundary coincided with the formal Schwarzschild boundary given in the third column, due to the local nature of the model. Therefore, the values quoted in the fourth and fifth column refer to the chemically mixed core size in this case. By construction, the TKE of the 1- and 3-equation model have the same radial extent. We note that there are different ways to determine the boundary of the convective core, as for example discussed in Higl (2019) or Higl et al. (2021).

The anisotropy profiles obtained from the 3D simulations are clearly at odds with the assumption of fully isotropic convection, reflected by the usage of a single variable for the total TKE, as done in the model of Kuhfuß (1987). Note that this assumption fails both in the bulk and at the boundary of the convection zone. At the convective boundary the assumptions about flow anisotropy are expected to have a larger impact on the outcome of the convection model as they strongly change the behaviour of the non-local terms as discussed in Ch. 3 and 4 (see also Kupka et al. 2022; Ahlborn et al. 2022). To also describe the effects of anisotropic flows in the TCM, the vertical part of the TKE needs to be taken into account as well. In Sec. 3.4.1 we have discussed the theoretical difficulties of constructing a realistic artificial anisotropy factor that could be included into a 3-equation model. Given the profiles observed in Fig. 5.3 this seems also difficult to achieve from the side of hydrodynamic simulations. Considering that this anisotropy profile would externally determine the overshooting distance, this approach does not seem desirable. We conclude that a realistic treatment of the vertical component of the TKE requires a more complex TCM with at least four equations. This approach is for example followed by Xiong et al. (1997) or Canuto (1992).

model	$\nabla = \nabla_{\mathrm{ad}}/(10^{10}\ \mathrm{cm})$	$\nabla_{\mathrm{rad}} = \nabla_{\mathrm{ad}}/(10^{10}\ \mathrm{cm})$	$r_{\mathrm{core}}/(10^{10}\ \mathrm{cm})$	M_r/M	OV/H_P
1-eq.	2.03	2.03	2.21	0.24	0.12
3-eq.	1.09	2.05	2.21	0.24	0.12
MLT	2.06	2.06	2.28	0.26	0.18
sim. 1	1.45	2.05	1.95	0.18	n.a.
sim. 2	1.57	2.06	2.07	0.21	n.a.

Table 5.1: Comparison of different radial locations in the stellar models and simulations. The first column indicates the model, the second column contains the boundary of the superadiabatic region, the third column the Schwarzschild boundary, the fourth column gives the radius of the TKE boundary r_{core}, the fifth column gives fractional convective core mass and the last column contains the overshooting distance measured from the Schwarzschild boundary in terms of the pressure-scale height. Note that the quantities for the MLT model have a slightly different meaning than for the other models and simulations (see text for details).

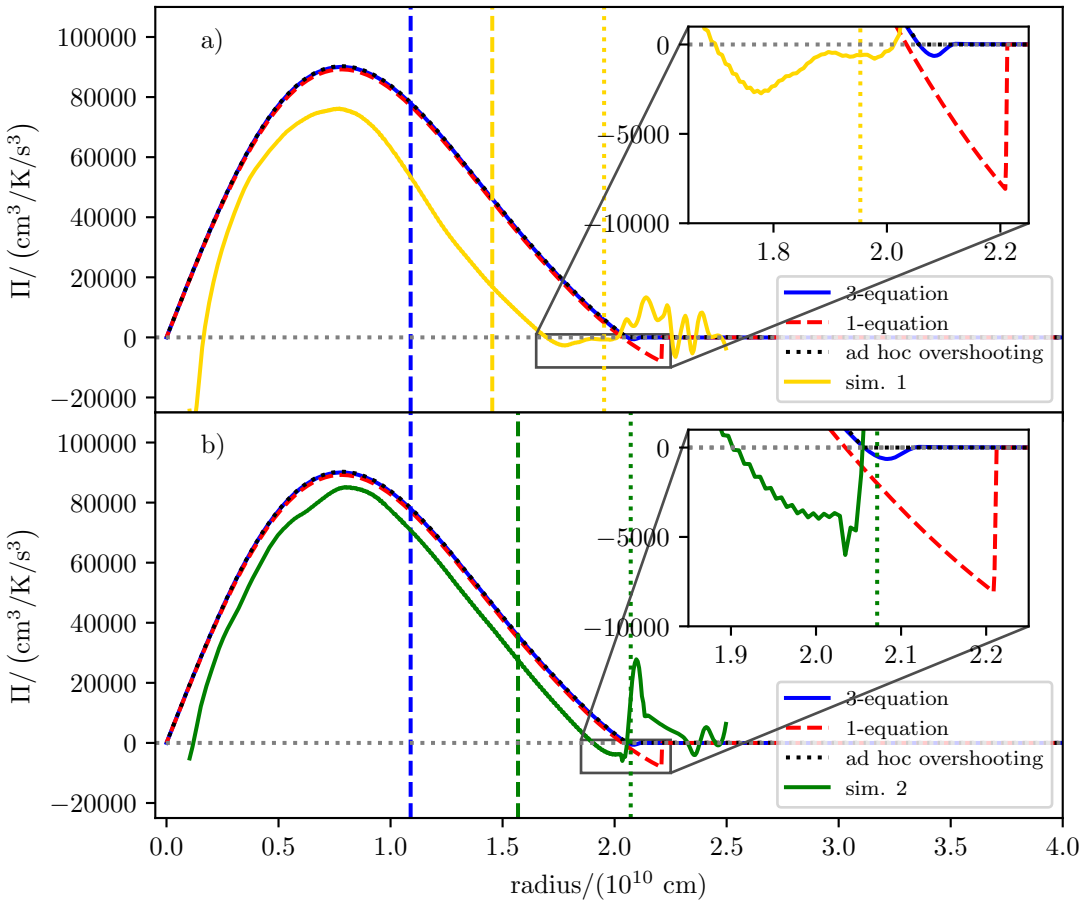

Figure 5.4: Comparison of the convective flux variable Π as a function of radius. The results obtained from the 1- and 3-equation model as well as from an MLT model are shown with a blue, red and black line respectively. The associated RANS correlations extracted from simulation 1 and 2 are shown in the upper panel and lower panel, respectively. The vertical dashed lines indicate the boundary of the superadiabatic region of the respective simulation. The vertical dotted line indicates the boundary of the turbulent convective core.

In Fig. 5.4 we show the convective flux variable Π as a function of radius obtained from simulation 1 and 2 in the upper and lower panel, respectively. For comparison, we again show results obtained from the 1- and 3-equation models as well as MLT including ad hoc overshooting. As already discussed in Sec. 4.3 the three 1D models show very close agreement in the bulk of the convection zone (see Fig. 4.8, right panel). Reproducing the observations from the TKE in Fig. 5.2, we find again that the convective flux of simulation 1 is less extended than the 1D models, while simulation 2 is reproducing the radial profile of the stellar models more closely. Overall, the 1D stellar models reproduce the simulations with a similar level of accuracy as in the case of the TKE. We now point at some important

features that the simulations and the stellar models have in common.

Close to the TKE boundary of the convective core, the convective flux variable obtained from both simulations shows a region of negative values. This region is found in both the 1- and 3-equation model as well, and it can be attributed to the braking of fluid motions in the stable stratification. We note that this region does not emerge in the MLT model, due to the local nature of the theory. However, in the simulations, we find different amplitudes of the negative convective flux of this region compared to the 1- and 3-equation models. The depth of the negative convective flux mainly determines whether the overshooting zone has a more radiative or adiabatic temperature stratification. To quantify the behaviour of the negative buoyancy region, we compute the ratio of the minimum to the maximum convective flux. The results are shown in Tab. 5.2. While the maximum convective fluxes of the 1D models agree very well, some differences in the overshooting zone become apparent. For the MLT model, the ratio is zero for obvious reasons. For the 1-equation model, we find that the absolute value of the ratio is about one order of magnitude larger than for the 3-equation model. The depth of the negative convective flux of simulation 1 and 2 are in between the results for the 1- and 3-equation models, while simulation 1 is closer to the 3-equation model and simulation 2 is closer to the 1-equation model. As a consequence, for longer simulation timescales, the temperature gradient in the simulations should adjust to a value in between the nearly adiabatic and nearly radiative temperature gradient obtained in the 1- and 3-equation models, respectively. The maximum convective fluxes from simulation 1 and 2 are slightly smaller than the 1D stellar models. Here, simulation 2 is closer to the stellar models as found for the TKE.

model	max/(10^4 cm^3/K/s^3)	min/(10^4 cm^3/K/s^3)	ratio
1-equation	8.921	−0.808	−0.091
3-equation	9.004	−0.064	−0.007
MLT	9.028	0	0
sim. 1	7.622	−0.273	−0.036
sim. 2	8.519	−0.601	−0.071

Table 5.2: Comparison of the negative convective flux region in the models and simulations. The second and third column show the maximum and minimum value of Π for the different models given in column one. The last column gives the ratio of column three and two.

Furthermore, the radial extent of the negative flux region differs between the simulations and the 1- and 3-equation models. To compare the different models and simulations, we compute the full-width at half maximum of the negative excursion of the convective flux. The results are given in Tab. 5.3. The radial extent of the negative convective flux is clearly larger in the 1-equation model than in the 3-equation model. This was already expected from a visual inspection of the inset in Fig. 5.4. The radial extent as obtained from both simulations is very comparable to the results from the 1-equation model. Given a larger radial extent of the region with negative convective flux in the 3D simulations, one would expect a larger transition region of the temperature gradient from nearly adiabatic

in the convection zone, to radiative beyond the overshooting zone than predicted from the 3-equation model (see Fig. 4.2). Towards the central region of the convection zone, the simulations show a region of negative values before the stellar centre is reached. This behaviour is clearly unphysical. We relate this to the presence of the inner boundary.

model	$r_{\max}/(10^{10}$ cm)	$r_{\min}/(10^{10}$ cm)	$\Delta r/(10^{10}$ cm)
1-equation	2.115	2.210	0.095
3-equation	2.066	2.099	0.033
MLT	n.a.	n.a.	n.a.
sim. 1	1.728	1.847	0.119
sim. 2	1.966	2.047	0.081

Table 5.3: Radial extent of the negative convective flux excursion for the models and simulations given in the first column. The second and third column give the minimum and maximum radius of the half maximum, respectively. The last column gives the full width at half maximum.

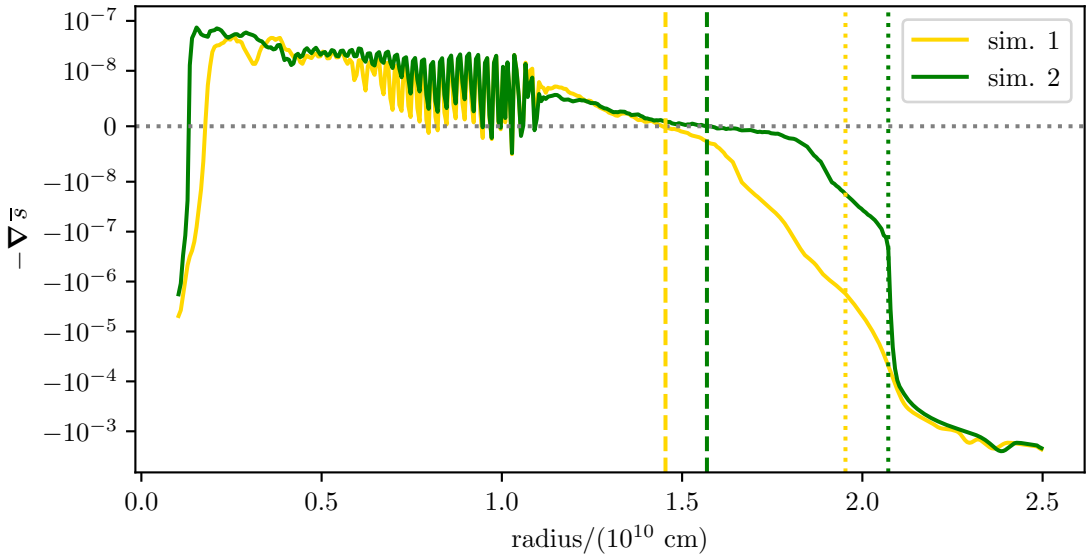

Figure 5.5: Negative gradient of the mean entropy as a function of radius on a symmetric logarithmic scale. The boundary of the superadiabatic region is indicated with a vertical dashed line in the respective colour. The boundary of the TKE is indicated with a vertical dotted line in the respective colour.

In Sec. 4.3 we have already discussed the emergence of the Deardorff layer in the Kuhfuß 3-equation model. Using the 3D simulation data, we now investigate whether a Deardorff layer emerges in these as well. As mentioned before, we compute the boundaries of the superadiabatic region from the gradient of the mean entropy. In Fig. 5.5 we show the

negative gradients of the mean entropy as a function of radius. In both simulations, the sign change happens well before the boundary of the TKE and the Schwarzschild boundary are reached. We note, that the entropy gradient of simulation 1 transitions more gradually from the nearly isentropic to the value beyond the TKE boundary, while in simulation 2 this transition happens more abruptly. We summarise the boundaries of the superadiabatic region from the stellar models and simulation 1 and 2 in the second column of Tab. 5.1. The boundaries of the superadiabatic region are indicated in the upper and lower panel of Fig. 5.4 from simulation 1 and simulation 2 with dashed lines in the respective colour. The boundary of the superadiabatic region from the 3-equation model is indicated with the dashed blue line. In both simulations exists a region with a positive entropy gradient (subadiabatic temperature gradient) that has a positive convective flux, i.e. energy flowing against the entropy gradient. As defined previously, this is a Deardorff- or counter-gradient layer. This confirms results from earlier simulations of stellar convection and also the result from the Kuhfuß 3-equation model (Chan and Gigas 1992; Muthsam et al. 1995, 1999; Tremblay et al. 2015; Käpylä et al. 2017; Kupka et al. 2018; Kupka 1999a; Xiong and Deng 2001; Kupka and Montgomery 2002; Montgomery and Kupka 2004; Zhang and Li 2012). Compared to the initial models of the simulations, the boundary of the superadiabatic region moved outwards in simulation 1 and inwards in simulation 2. As the initial MLT model of simulation 2, did not have a Deardorff layer by construction, it emerged as a result of the hydrodynamic simulation. The outward shift in simulation 1 may be an indication that the Deardorff layer of the 3-equation model is too extended. As discussed earlier, the existence of the Deardorff-layer necessitates a TCM with a high enough degree of physical complexity. In the 1-equation model in which the convective flux variable has been coupled to the superadiabatic gradient, no Deardorff layer exists and only when solving the dynamic equation for Π, as in the 3-equation model, it emerges. This indicates the physical relevance of the 3-equation model.

Finally, Fig. 5.6 shows the auto-correlation of the entropy fluctuations. We found that the results are very noisy when computing Φ according to Eq. (5.1). The behaviour of this average could be related to the fact that two very large numbers are subtracted to obtain a comparatively very small difference. Therefore, we construct the convective variable Φ as follows: we first compute the field of entropy fluctuations locally by subtracting a time average of the entropy and subsequently average over the squared entropy fluctuations. The same is done for all the terms of the entropy fluctuation equation, as well as the buoyancy term of the convective flux equation. We find that the resulting entropy fluctuations shown in Fig. 5.6 look very smooth and strictly positive, as expected. The resulting profiles reflect the behaviour of the mean entropy gradient shown in Fig. 5.5. In the superadiabatic region, the entropy fluctuations seem to be positively correlated with the negative mean entropy gradient, while they seem to be anti-correlated with it in the subadiabatic regions. In this way simulation 1 produces the peak in the 3-equation model better than simulation 2 as the thermal structure of simulation 1 is still close to the thermal structure of the 3-equation model. In simulation 2 the change from the superadiabatic to the radiative gradient is more abrupt which creates a steeper increase in the entropy fluctuations. As we shall discuss further below, the magnitude of the superadiabatic gradient is substantially

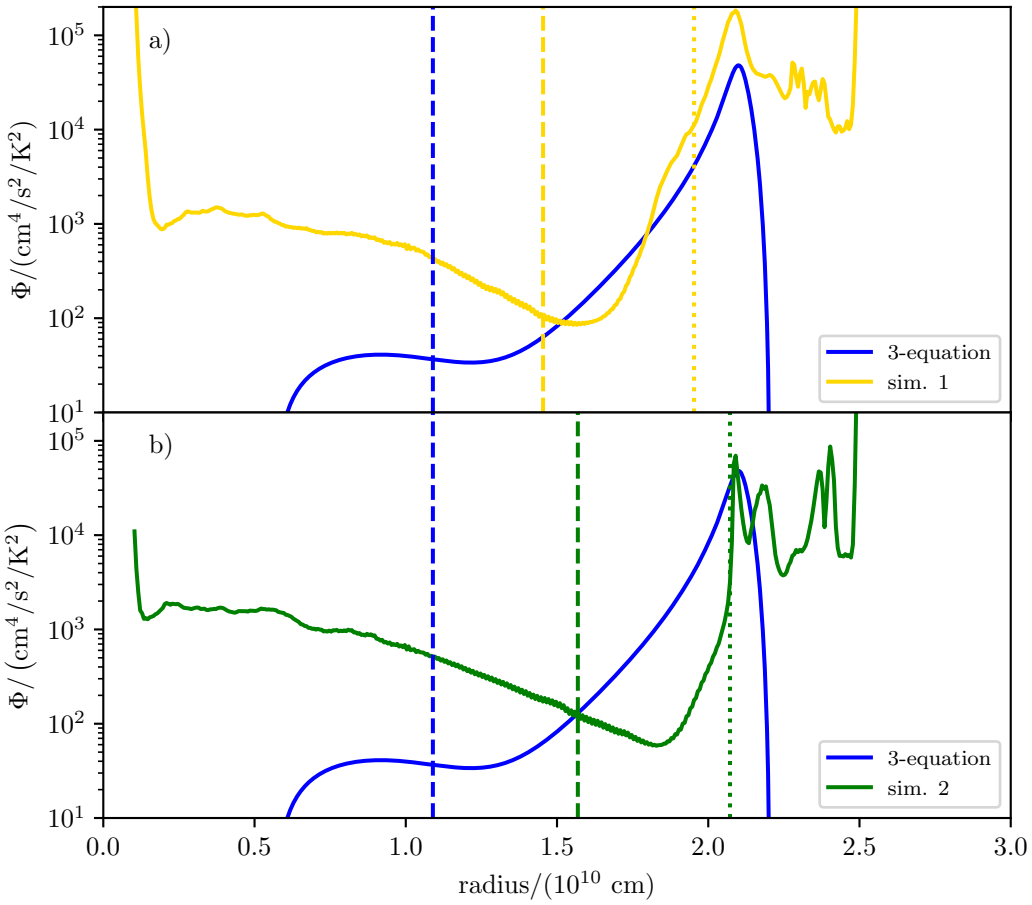

Figure 5.6: Comparison of the squared entropy fluctuations Φ as a function of radius. The results from the 3-equation model are shown with a blue line. The associated RANS correlations extracted from simulation 1 and 2 are shown in the upper panel and lower panel, respectively. The vertical dashed lines indicate the boundary of the superadiabatic region of the respective simulation. The vertical dotted line indicates the boundary of the turbulent convective core.

larger in the 3D simulations than in the stellar models, which probably also causes the difference in magnitude of the entropy fluctuations.

5.4 Analysis of individual terms

In Sec. 5.3 we have compared the general behaviour of the convective variables of the Kuhfuß model with the results of the hydrodynamic simulations. Even though these variables have the greatest impact on the resulting stellar structure and evolution, a more in-depth

analysis of the individual equation terms is necessary to understand the global behaviour of convective variables. Due to the comparatively short simulation time, the results obtained from the 3D simulations still show significant statistical variations. This needs to be taken into account when discussing the results. Especially for terms involving derivatives, it is necessary to smooth the data before computing the derivative to reduce the statistical fluctuations. In the following, we discuss the results for each equation (2.16) to (2.18) in a separate subsection. The difference in the radial extent of the TKE in simulation 1 and 2 also has a large impact on the comparison of the individual terms.

5.4.1 TKE equation

The TKE equation of the Kuhfuß model as used in Ch. 3 and 4 has three terms that are not neglected. We start with discussing the non-local and the buoyancy term of this equation. Subsequently, we discuss the terms that are neglected. Finally, we study the dissipation term of the TKE equation.

In Fig. 5.7 we show the non-local term of the TKE equation as a function of radius. The non-local term of Eq. (2.16), computed from simulation 1 and 2 in the anelastic approximation, is shown in the upper and lower panel, respectively. For comparison, we show the non-local terms of the 1- and 3-equation models in each panel, computed using the downgradient approximation Eq. (2.57). The radial extent of the non-local term obtained from simulation 1 is generally smaller compared to the 1D models. For simulation 2 the radial extent is in good agreement with the 3-equation model, while being slightly smaller than in the 1-equation model. Both conclusions could be already expected from the TKE profiles shown in Fig. 5.2. Within the convection zone, the non-local terms from the 3D simulations show two regions with predominantly positive values towards the centre and the TKE boundary and a region with negative values in the middle of the convection zone. The sign changes are similarly located as in the 1D models. Furthermore, the order of magnitude of the non-local terms in the simulations and the 1D stellar models is comparable. For simulation 1 the magnitude is essentially the same as in the 1D models, while for simulation 2 it is larger by a factor of about two. The difference in magnitude between simulations 1 and 2 can be explained by the different magnitude of the TKE in both simulations. In the overshooting region, the shape of the non-local terms obtained from the 3D simulations is in better agreement with the 3-equation model. We conclude that the functional form assumed for the non-local term of the Kuhfuß models can be confirmed by the hydrodynamic simulations. The correct order of magnitude may be achieved by tuning the model parameters. The agreement of the non-local terms obtained from the simulations and the 1D stellar models is an important indication that the Kuhfuß solution for the TKE is a rather accurate solution.

We have discussed previously that the non-local term of the TKE equation is the most relevant one to determine the extent of the TKE (e.g. Sec. 4.3.1). Due to the high mixing efficiency of convection, the extent of the TKE has a major impact on the extent of the mixed region. Hence, given an accurate solution of the TKE equation alone, the resulting stellar model will have the correct convective core size, stellar luminosity and lifetime.

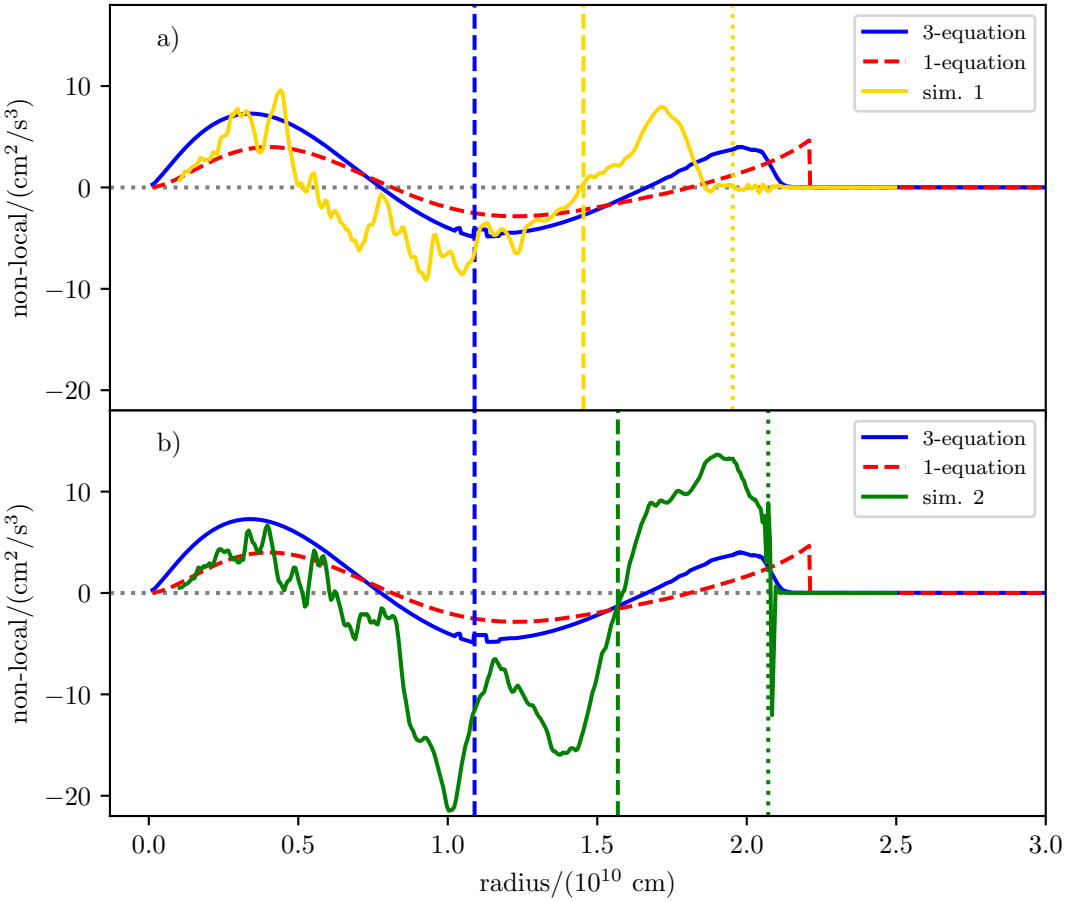

Figure 5.7: Comparison of the non-local terms of the TKE equation. The results obtained from the 1- and 3-equation model are shown with a blue and red line, respectively. The associated RANS correlations extracted from simulation 1 and 2 are shown in the upper panel and lower panel, respectively. The vertical dashed lines indicate the boundary of the superadiabatic region of the respective simulation. The vertical dotted line indicates the boundary of the TKE.

However, the Kuhfuß model consists of three coupled differential equations and hence also the behaviour of the other two equations needs to be considered to reach a conclusion about the model accuracy.

Convection in the stellar core is driven by the buoyancy of the fluid. As discussed in Sec. 2.4.1 the buoyancy term of Eq. (2.16) can be split into a part containing the mean pressure and a part containing the pressure fluctuations. As the pressure fluctuations are neglected in the Kuhfuß model we first discuss the contribution due to the mean pressure and discuss the pressure fluctuation term further below. In the Kuhfuß models, the buoyancy term is related to the convective flux variable Π through the Boussinesq

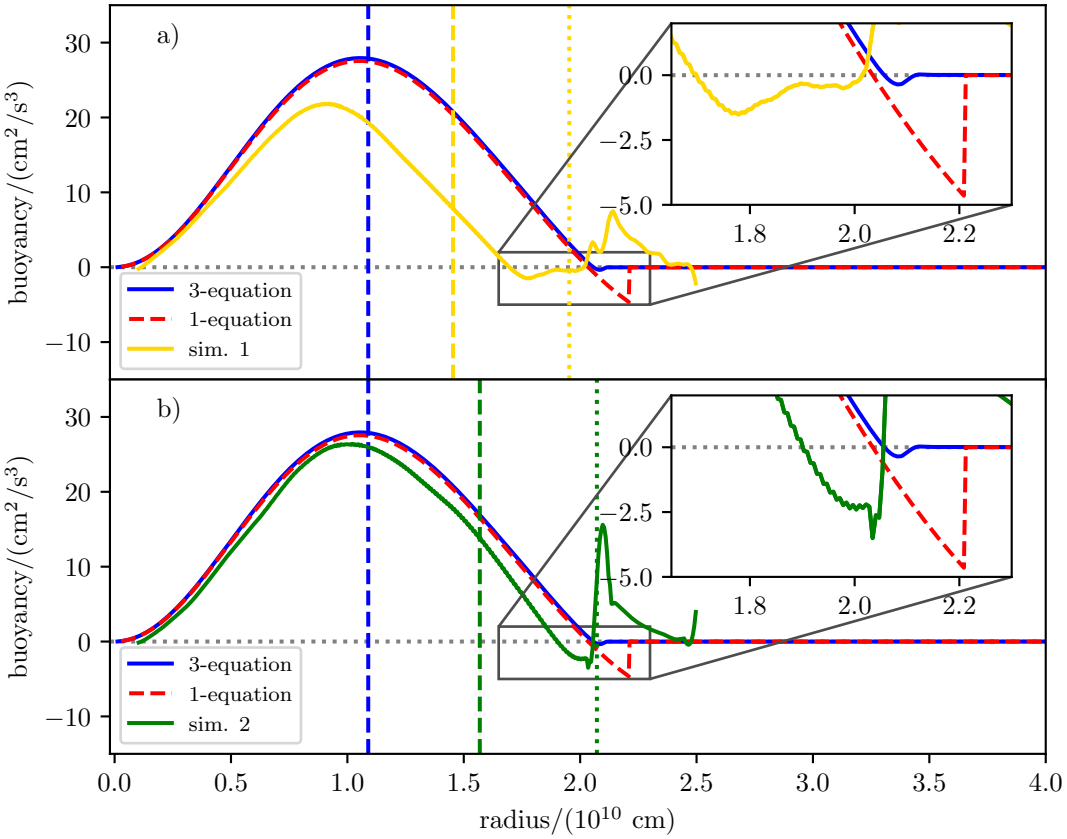

Figure 5.8: Comparison of the buoyancy term as a function of radius. The results obtained from the 1- and 3-equation model are shown with a blue and red line, respectively. The associated RANS correlations extracted from simulation 1 and 2 are shown in the upper panel and lower panel, respectively. The vertical dashed lines indicate the boundary of the superadiabatic region of the respective simulation. The vertical dotted line indicates the boundary of the TKE. The insets show the region of negative convective flux.

approximation. The buoyancy terms

$$\text{buoyancy} = -\boldsymbol{\nabla}\bar{p}\frac{\overline{\boldsymbol{u}'}}{\rho} \tag{5.2}$$

as obtained from simulation 1 and 2 are shown in Fig. 5.8 in the upper and lower panel, respectively. We find that the buoyancy terms of simulation 1 and 2 closely resemble the convective flux variables shown in Fig. 5.4. In SLH, the full Euler equations without the Boussinesq approximation are solved such that the agreement between the simulations and the TCM confirms the Boussinesq approximation in the Kuhfuß models. Therefore, the discussion of the buoyancy term is completely analogous to the discussion of the convective flux variable shown in Fig. 5.4, and we will not repeat it here. Overall, this comparison

shows that there is a general agreement between the buoyancy terms obtained from the 3D simulations and the 1D stellar models. As this term is responsible for the driving of the convection in the Kuhfuß model this is another important confirmation of the TKE equation.

As described in Sec. 2.5 some terms have been neglected in the Kuhfuß model, as they are argued to be small on general grounds. Given the simulation data, we can compute these terms and compare their magnitude with the other terms of the TKE equation. A time derivative computed from the 3D simulations would be an artefact of the adjustment of the simulation to a stationary state as the background state of the simulation is fixed. In a real star, the structure of the convection zone changes due to the stellar evolution, a situation that is not reproduced by our 3D simulations. Therefore, we do not discuss the time-derivative obtained from the simulations here. Another term that is neglected in the Kuhfuß model is the shear term in the TKE equation. The shear term is shown in the upper panel of Fig. 5.9. Compared to the non-local and the buoyancy term, the shear term is small in the bulk of the convection zone. Its maximum remains below about 1% of the maximum buoyancy term value. This comparison shows that the shear term is in fact very small compared to competing terms and can be safely neglected in the Kuhfuß model. The lower panel of Fig. 5.9 shows the pressure fluctuation terms. In both simulations, we find it to have a magnitude comparable to the non-local and buoyancy terms. Physically, pressure fluctuations are expected to scale as Ma^2 (e.g. Miczek et al. 2015; Guillard and Viozat 1999). As discussed in Sec. 5.2 the Mach numbers are generally small in stellar core convection, and in our simulations in particular (see Fig. 5.1). Furthermore, Viallet et al. (2013) argued that pressure fluctuations should be small in cases with a shallow density stratification, which is the case for the core of the 3 $\mathrm{M}_\odot$ model. Hence, the relatively large pressure fluctuation terms are more likely an artefact of the 3D simulations.

As discussed above, the molecular viscosity is not included in the 3D simulations. The dissipation happens only for numerical reasons. Therefore, it is not possible to compute the dissipation rate of the TKE explicitly from the 3D data. To obtain an estimate for the dissipation we compute the residuals of the left side of Eq. (2.16), i.e. the time derivative, and all known terms on the right side. The residuals for simulation 1 and 2 as a function of radius are shown in Fig. 5.10 in the upper and lower panel, respectively. For comparison, we show the dissipation terms computed from the 1- and 3-equation models, according to Eq. (2.45) with a suitable description for the dissipation length Λ as described in Sec. 4.2. As expected from the TKE profiles of the 1- and 3-equation models, their dissipation terms look very similar (compare also to Fig. 3.8). Towards the convective boundary, the 3-equation model shows a somewhat increased dissipation, which can be attributed to the dissipation by buoyancy waves introduced in Ch. 3. Both simulations show negative residual values throughout the whole simulation domain, indicating that TKE is indeed dissipated as expected. The magnitude of the dissipation term is smaller than obtained from the 1- and 3-equation model. The agreement between the stellar models and the simulations should improve, for smaller pressure fluctuation terms. Both simulations show some spurious residuals at about the TKE boundary in simulation 2. This is potentially again a signature of the unresolved waves beyond the formal Schwarzschild

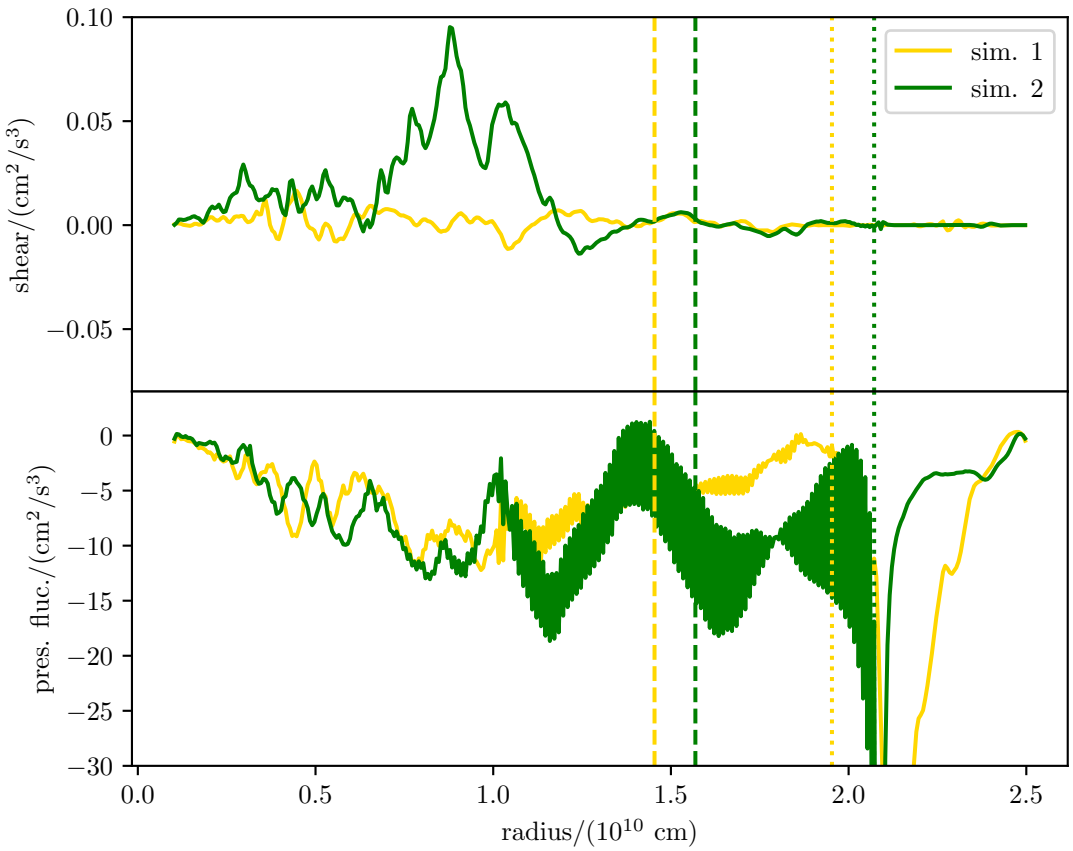

Figure 5.9: Comparison of terms neglected in the TKE equation of the Kuhfuß model as a function of radius. The upper panel shows the shear term and the lower panel shows the pressure fluctuation terms. The results of simulation 1 and 2 are shown with yellow and green lines, respectively. We indicate the boundary of the superadiabatic region and the TKE boundary of the simulations with dashed and dotted lines in the respective colour.

boundary ($\nabla_{\mathrm{rad}} = \nabla_{\mathrm{ad}}$).

5.4.2 Convective flux equation

After discussing the TKE equation in some detail, we will now proceed to discuss the terms of the convective flux equation, Eq. (2.17). We note, that this equation has no analogue in the 1-equation model or MLT and hence, the simulation data will be only compared to the 3-equation model.

The comparison of the non-local terms as a function of radius is shown in Fig. 5.11. The results for simulation 1 and 2 are shown in the upper and lower panel, respectively. The result of the 3-equation model is shown with a blue line. As for the non-local term of the TKE equation, the results are rather noisy, preventing a more detailed comparison

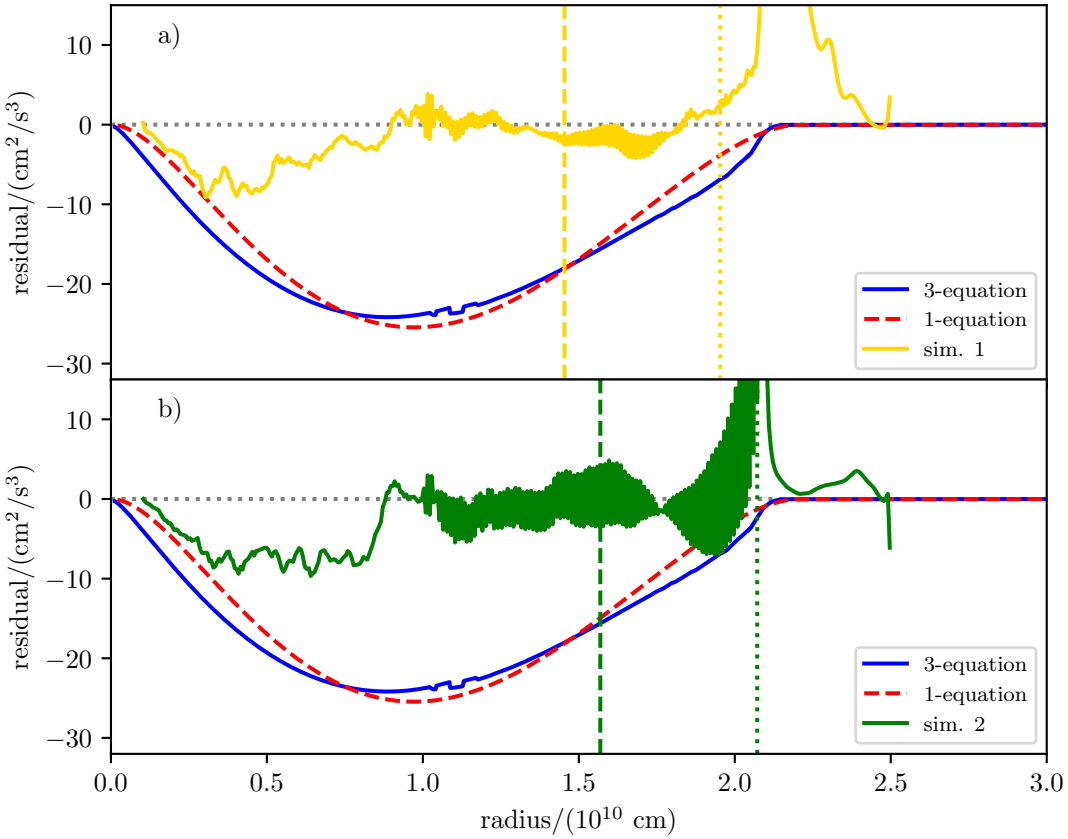

Figure 5.10: Residual of the 3D simulations as a function of radius. The results of simulation 1 and 2 are shown in the upper and lower panel, respectively. For comparison, we show the dissipation term from the 1- and 3-equation model with a red and blue line, respectively. We indicate the boundary of the superadiabatic region and the TKE boundary of the simulations with dashed and dotted lines in the respective colour.

at this stage. We note that the non-local term from the 3-equation model does also show numerical noise, occurring at the transition from a superadiabatic to a subadiabatic stratification. However, we find some features in agreement between the 3-equation model and the simulations. For both simulations, the non-local term of the Π equation shows two regions of predominantly positive values, towards the centre and the TKE boundary, and a region of predominantly negative values in the middle of the convection zone. The sign changes are located similarly in the simulations and the 3-equation model. The order of magnitude of the non-local term from the simulations is comparable with the 3-equation model, while the magnitude of this term in simulation 1 reproduces the 3-equation model more closely. The non-local term of simulation 2 has a slightly larger magnitude than the 3-equation model, analogous to the non-local term of the TKE equation in Fig. 5.7. Towards the edge of the turbulent convective region, the non-local term of the 3-equation

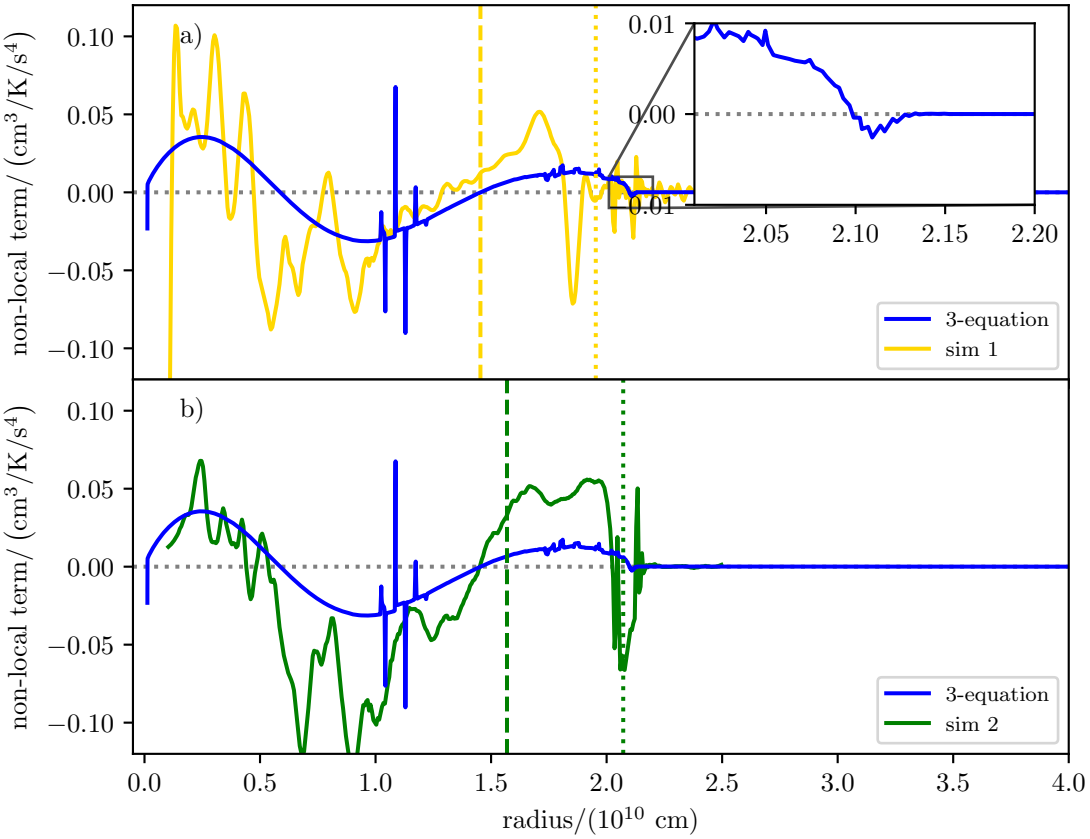

Figure 5.11: Comparison of the non-local term of the convective flux equation Eq. (2.17) as a function of radius. The results for simulation 1 and 2 are shown in the upper and lower panel, respectively. The results of the 3-equation model are shown with the blue line. We indicate the boundary of the superadiabatic region and the TKE boundary of the simulations with dashed and dotted lines in the respective colour.

model shows a small and shallow region of negative values again, shown enlarged in the inset of Fig. 5.11. This can be attributed to the negative convective flux excursion discussed in Fig. 5.4. A similar feature is visible in the non-local terms obtained from simulation 1 and 2 close to the TKE boundary. As for the non-local term of the TKE equation, we conclude that the functional form of the non-local term of the convective flux equation is correct. The order of magnitude may be adjusted by varying the model parameters, as we will discuss below.

The comparison of the potential terms as a function of radius is shown in Fig. 5.12. The results for simulation 1 and 2 are shown in the upper and lower panel, respectively. The result of the 3-equation model is shown with a blue line. Note that the sign change of the potential term coincides with the boundary of the superadiabatic region in the respective simulation, as the potential term is proportional to the gradient of the mean entropy. As

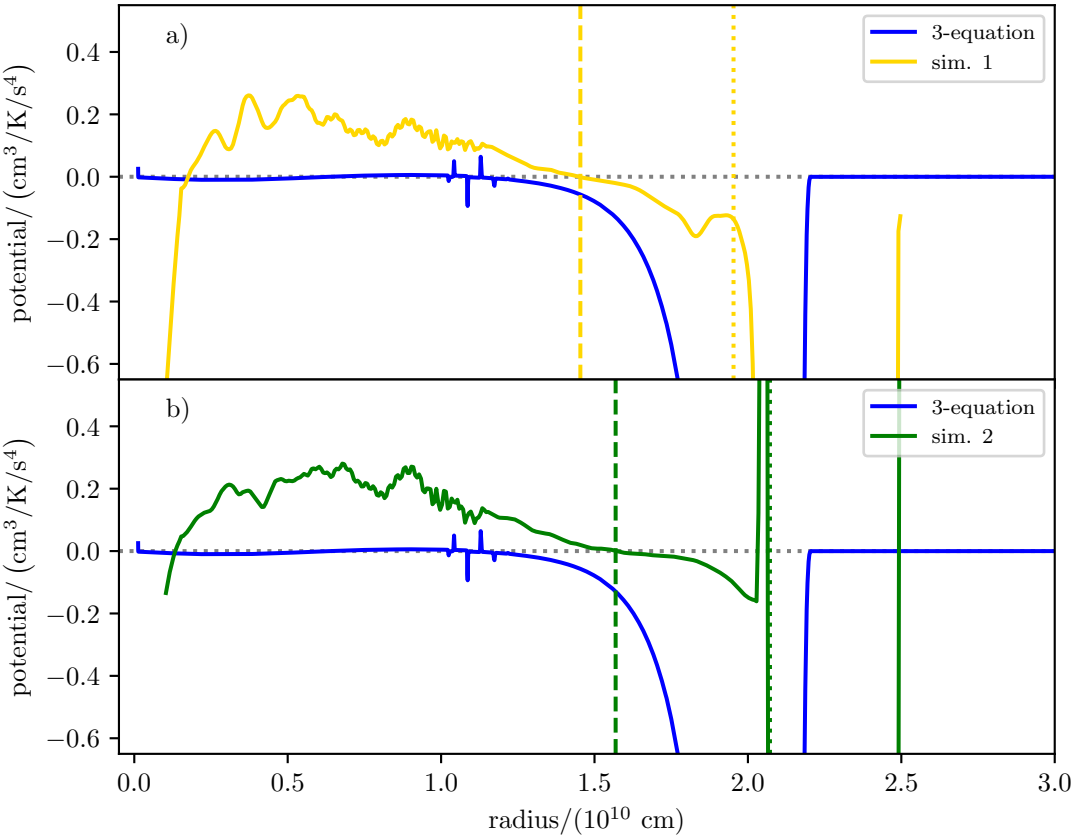

Figure 5.12: As Fig. 5.11 for the potential term of Eq. (2.17).

already noted previously, the boundary of the superadiabatic region of simulation 1 and 2 towards the overshooting region is located further out than in the 3-equation model. This is reflected in the potential term as well. The sign change towards the centre is located further inside than in the 3-equation model. The different locations of the sign changes in the stellar model and the simulations are again hinting at a discrepant temperature structure between the simulations and the 3-equation model. We note that the sign change towards the centre might be affected by the inner boundary as well. Furthermore, the magnitude of the potential term is larger in the simulations. As the convective velocities are very similar in the simulations and the 3-equation model, this discrepancy may be caused by a too small superadiabatic gradient in the stellar model. We will discuss further below the ability of the 3-equation model to change the magnitude of the superadiabatic gradient.

The comparison of the buoyancy terms as a function of radius is shown in Fig. 5.13. The results for simulation 1 and 2 are shown in the upper and lower panel, respectively. Note that this term has been computed by determining the fluctuations locally and averaging them subsequently. The result of the 3-equation model is shown with a blue line. As for the buoyancy term of the TKE equation, we first discuss the buoyancy due to the mean

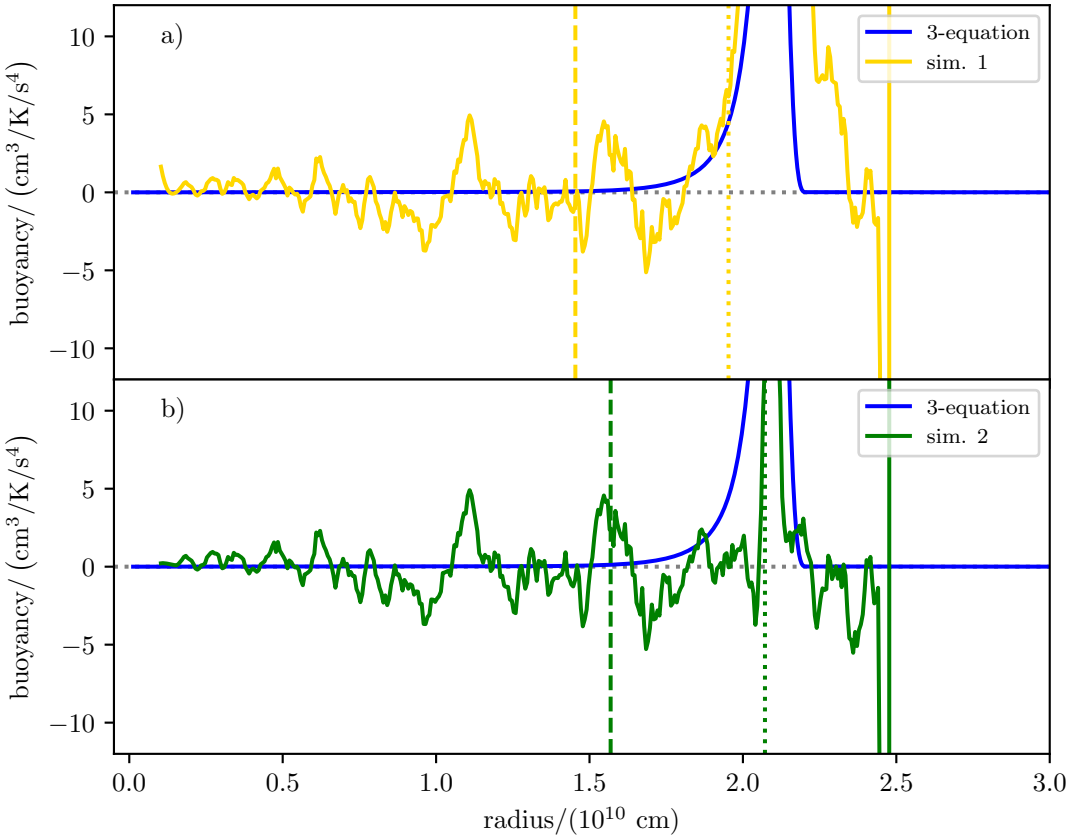

Figure 5.13: As Fig. 5.11 for the buoyancy term of Eq. (2.17).

pressure:

$$\text{buoyancy} = -\boldsymbol{\nabla}\overline{p}\frac{\overline{s'}}{\rho} \tag{5.3}$$

and describe the pressure fluctuation terms of the Π equation further below. The noise present in the RANS data makes the comparison of the terms increasingly difficult. From the 3-equation model we expect a positive buoyancy term throughout the whole convective core as it is related to the squared entropy fluctuations, which are strictly positive. The buoyancy term of the Π equation obtained from simulation 1 and 2 show several regions of negative values. There is an indication of increasing values towards the TKE boundary, especially in simulation 1. Comparing the buoyancy term of the convective flux equation to the entropy fluctuations shown in Fig. 5.6 we find that the buoyancy term shows large statistical fluctuations that are not seen in the squared entropy fluctuations. As density and pressure show rather smooth profiles, these statistical fluctuations are most likely related to the entropy fluctuations in the buoyancy term. We expect the statistical fluctuations to reduce for longer simulations times.

The radiative dissipation term is found in the simulations to be about four orders of magnitudes larger than in the 3-equation model, where it is included through a radiative dissipation timescale. Also the functional form adopted in the 3-equation model seems discrepant with the 3D simulations. However, in terms of absolute numbers the radiative losses are small such that they could be safely neglected even when adopting the values from the simulations. Instead of the simple dissipation timescales, one could refer to the radiative dissipation terms by Canuto (1992) who keeps the complete second order derivatives in the terms for a physically more complete radiative dissipation term. Furthermore, Canuto and Dubovikov (1998) suggest additional dissipation terms for the convective flux equation. As in the TKE equation a number of terms have been neglected in the final equation for the convective flux Π in the 3-equation model. Using the RANS analysis of simulation 1 and 2 we assessed the order of magnitude of these neglected terms compared to the other terms in the model. We find the pressure fluctuation term of the convective flux to amount to about 10% of the buoyancy term, as in the TKE equation. This is again not a small quantity and is probably an artefact of the 3D simulation. The terms related to mean radial velocities are again very small and can be safely neglected. Finally, terms related to the release of nuclear energy are very small and may be safely neglected as well.

5.4.3 Entropy fluctuation equation

Finally, we analyse the terms of the entropy fluctuation equation Eq. (2.18). As for the convective flux equation, there is no analogue in the 1-equation model or MLT, and comparisons will be only carried out with the 3-equation model.

The comparison of the non-local terms as a function of radius is shown in Fig. 5.14. The results for simulation 1 and 2 are shown in the upper and lower panel, respectively. The result of the 3-equation model is shown with a blue line. While the non-local terms of the TKE and Π equation computed from the 3D simulations reproduce the sign changes and the magnitude of the non-local terms from the 3-euqation model, we observe larger discrepancies for the non-local term of the Φ equation. The structure occurring at or beyond the TKE boundary is again most likely due to the unresolved waves and not considered here. Even though the noise in this non-local term is somewhat increased compared to the other two equations, we see an indication of a similar structure with two regions of positive values and a region of negative values in between. Such a structure is not reproduced by the non-local term obtained from the 3-equation model. This might be an indication of an incorrect parametrisation of this term.

The potential term of the entropy fluctuation equation looks very similar to the potential term shown in Fig. 5.12 and the discussion is analogous. The radiative dissipation term of the entropy fluctuation equation modelled through the dissipation timescale is several orders of magnitude too small compared to the simulation data, as it was observed for the convective flux equation. They are however still small enough to be neglected. Similarly, the functional form of the radiative dissipation term of the 3-equation model does not agree with the 3D simulations. Finally, the terms related to the release of nuclear energy are small and can be safely neglected.

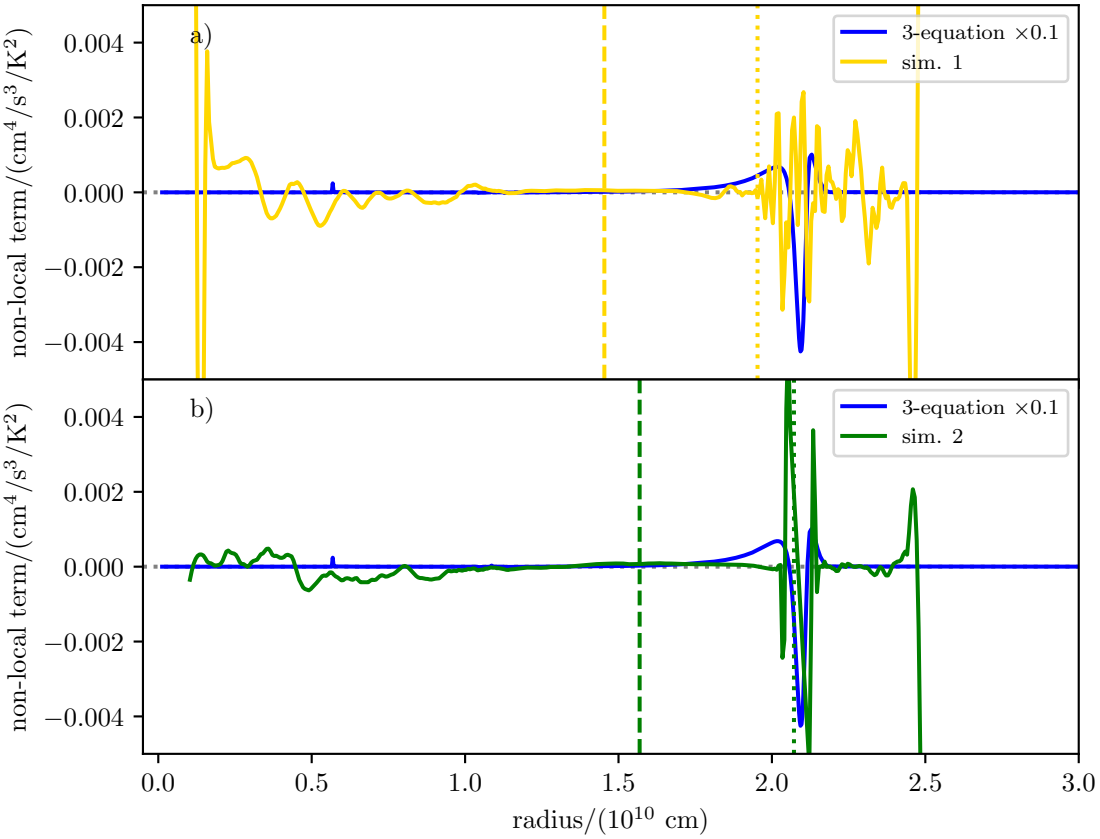

Figure 5.14: As Fig. 5.11 for the non-local term of Eq. (2.18).

5.5 Parameter estimation

The Kuhfuß models as well as MLT contain a number of model parameters. To obtain physically accurate results and ensure that the convection model is able to accurately predict the structure of convective regions, a set of sensible parameter values has to be found. In Sec. 2.3.3 we have discussed the derivation of MLT and at which points values of numerical constants need to be assumed. Most commonly, only the single adjustable mixing length parameter α is adjusted. In Sec. 2.5 we have discussed the Kuhfuß 1- and 3-equation models and how some of the involved parameters may be calibrated from MLT such that the Kuhfuß theory collapses to MLT in the local and time-independent limiting case. One of the main differences of the Kuhfuß TCM compared to MLT, apart from the inclusion of more physical effects, is to keep the parameters introduced for different assumptions explicitly. This allows adjusting each parameter and varying the impact of the parametrised physical effect individually when constructing stellar models. In principle the same could be done for the hidden parameters of MLT, however, this is not foreseen in the default implementations of MLT. In this section, we will discuss how different terms

of the Kuhfuß 1-equation model and subsequently the 3-equation model react to changing the different model parameters. Finally, we will attempt to calibrate them from external sources, i.e. the RANS data discussed above. In ad hoc overshooting models only the final size of the convective core can be calibrated, disregarding the physical details that lead to this size. This is a major advantage of TCM, like the Kuhfuß model, in which the impact of individual effects can be calibrated. As discussed in Sec. 5.3 the extent of the TKE is substantially smaller in simulation 1 than in the simulation 2 and compared to results obtained from the Kuhfuß 1- and 3-equation model. This discrepancy could be only resolved by assuming unreasonably small values for the non-local parameter α_ω. Therefore, we will not attempt to calibrate the convective core size of the Kuhfuß models, even though the size of the convectively mixed core is the most relevant quantity for stellar models. Instead, we focus on comparing the absolute magnitudes of quantities and the functional form obtained from the simulations. Considering that both simulations result in different extents of the TKE even though they only differ in the initial model, makes calibrating the parameters to the size of either one of them questionable anyway.

5.5.1 The 1-equation model

The 1-equation model itself contains four parameters: $\alpha_\omega, C_\mathrm{D}, \alpha_s$ and α denoting the non-local, dissipation, entropy flux and mixing length parameter respectively. A value for the mixing-length parameter α may be obtained by a solar calibration. We find that both for a local and a non-local model, a value of $\alpha \approx 1$ reproduces the radius, luminosity and surface metal abundance of the present Sun. In agreement with Flaskamp (2003) we note that the Wuchterl (1995) correction is necessary to ensure that the present Sun does not possess a convective core when using the 1-equation non-local model. The Wuchterl (1995) correction, introduced to limit the dissipation length in the centre, contains another parameter which we have left unchanged so far at a value of $\beta_s = 1$. For a fixed value of β_s effectively, only three of the other four parameters are independent, as the mixing length parameter α always occurs in combination with another parameter. The effect of changing the fourth parameter, e.g. the mixing length, could be equivalently obtained by rescaling the three independent parameters accordingly. Therefore, it is sufficient to only vary three of the four parameters to explore the parameter space of the 1-equation model. In the following we explore the behaviour of varying α_ω between 0.15 and 0.3, C_D between 1.0 and 4.0 and α_s between 0.1 and 2.0.

A comparison of the TKE for varying the non-local and dissipation parameters α_ω and C_D is shown in Fig. 5.15. We focus mainly on the radial extent and the magnitude of the TKE in this comparison. For comparison, we show the TKE obtained from simulation 1 and 2 as well as the TKE from the 3-equation model in each panel. In each panel of Fig. 5.15 one of the two parameters is varied, while the others are kept fixed. The red dashed line indicates the default choice of parameter values in each panel. The impact of the non-local parameter α_ω is shown in the upper panel. As discussed previously in Sec. 4.3.1 varying this parameter mainly changes the extent of the TKE and hence the size of the convective core (see Fig. 4.5). Furthermore, increasing α_ω slightly decreases the TKE in the bulk of

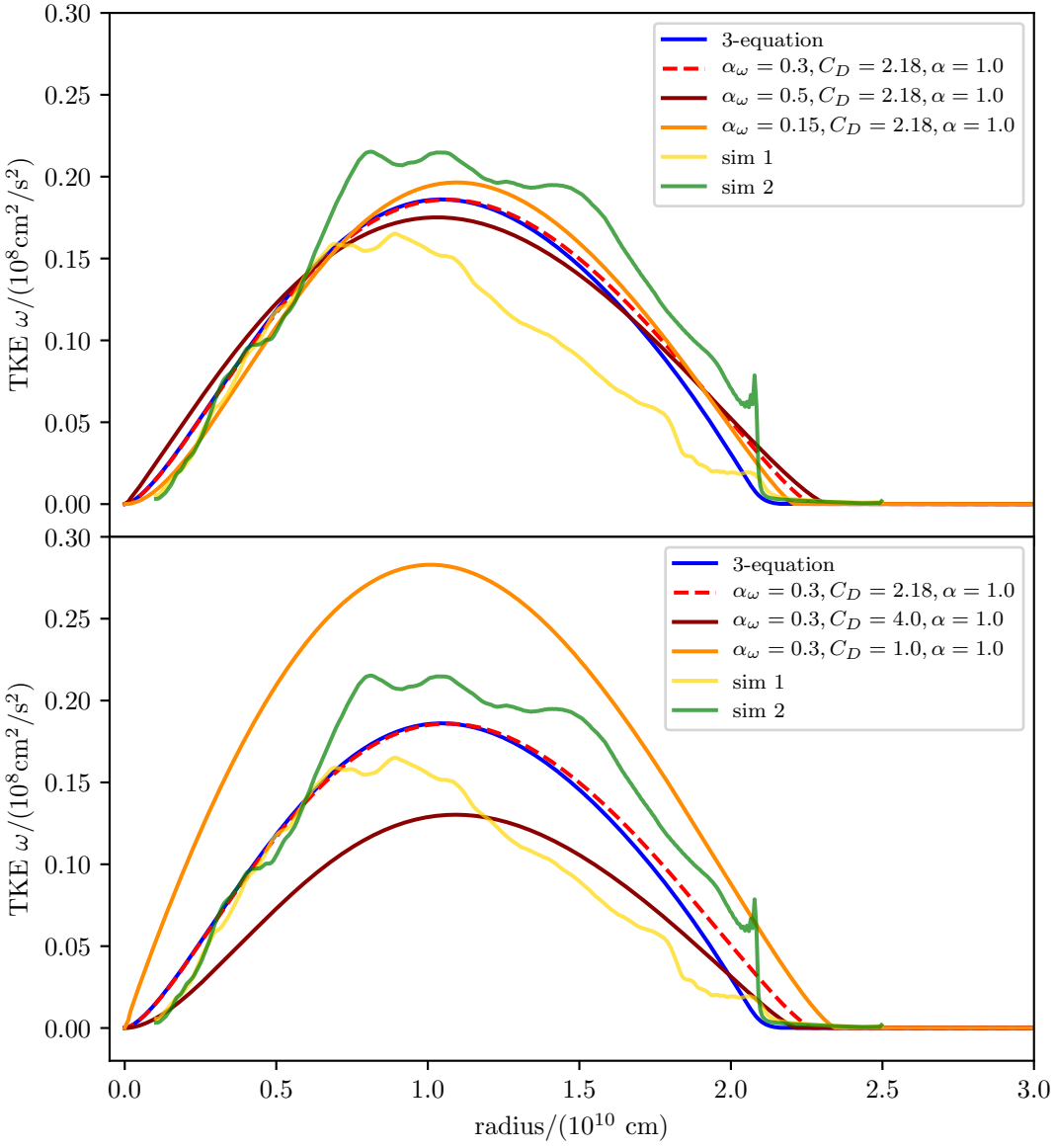

Figure 5.15: Comparison of TKE as a function of radius. We show the results of the 3-equation model with a blue, simulation 1 with a yellow and simulation 2 with a green line respectively. The results of the 1-equation model are shown with the remaining coloured lines (see legend for details). The parameters α_ω and C_D are varied in the upper and lower panel respectively. The red dashed line refers to the default parameters.

the convection zone, as the non-local term is acting as a sink in this region (see Fig. 5.7). The lower panel shows the reaction of the TKE to changing the dissipation parameter

C_{D}. The behaviour can be easily interpreted as follows: by decreasing the dissipation of the TKE, parametrised through C_{D}, the solution TKE extends further out in radius and takes higher values throughout the convection zone. The comparison of the TKE profiles to simulation 1 and 2 shows that an increased dissipation parameter value is required to match the magnitude of the TKE in simulation 1 while a slightly smaller parameter will improve the agreement with simulation 2. Finally, we also explored the behaviour of the TKE when varying α_s. Even when varying α_s by a factor of 20—from 0.1 to 2.0—we do not observe notable changes of the TKE profile. Hence, we conclude that the default value calibrated to MLT may be chosen for this parameter, as the effect on the resulting TKE is negligible. The origin of this insensitivity will be discussed further below.

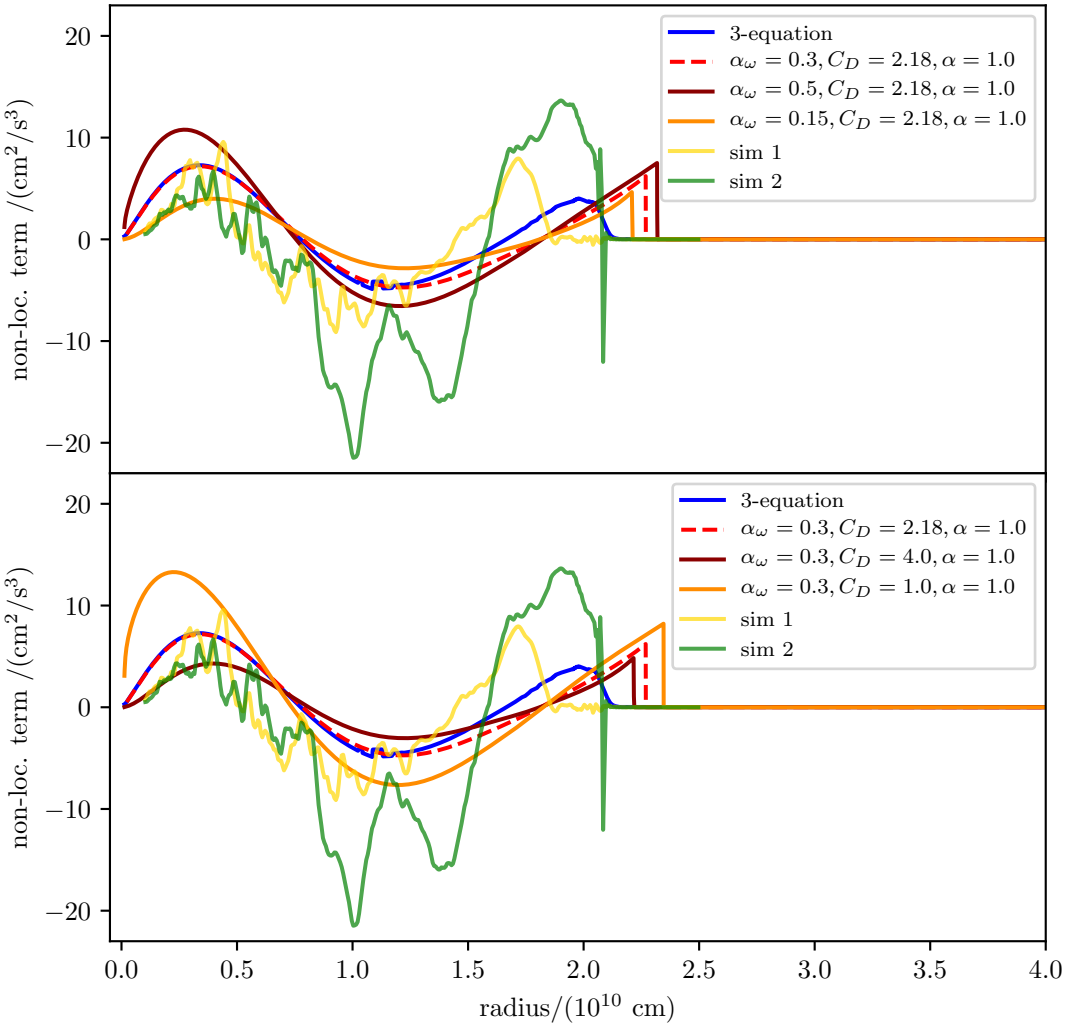

Figure 5.16: As Fig. 5.15, but for the non-local term of the 1-equation model.

In Fig. 5.16 we show a comparison of the non-local term of the 1-equation. The data are the same as in Fig. 5.15. The results for varying the non-local parameter α_ω are shown in the upper panel. As the non-local term is proportional to the non-local parameter, a change of this parameter mainly changes the magnitude of this term. In addition, the radial extent is changing following the extent of the TKE discussed previously. In the lower panel again the parameter C_D is varied. As for the TKE, a clear change of the non-local term is visible when varying the dissipation parameter. The lower the dissipation, the higher the magnitude of this term. At the same time, the radial extent increases following the TKE. Finally, we explore the behaviour of this term to changing α_s. As expected from the behaviour of the TKE when varying α_s, the non-local term is hardly affected by varying this parameter, and we do not observe a notable change.

We also analysed the behaviour of the convective flux variable Π, that determines the behaviour of the buoyancy term in the 1-equation model. We find that Π is mostly insensitive to changes of the model parameters and for any set of parameters the resulting Π closely resembles the one shown in Fig. 5.4. As we have already argued in Sec. 4.6, the stellar structure determines the convective flux that is required to transport the energy released by nuclear fusion in the centre. The model parameters of the convection model determine the behaviour of the convective variables and the temperature gradient. Only in the overshooting zone, the convective flux looks different for different parameter values. There, the behaviour of Π mainly depends on the extent of the TKE. The further out the TKE extends, the further and deeper extends the negative convective flux variable into the stable layers. The insensitivity to a change of the model parameters may be easily understood for α_s: decreasing this parameter means entropy transport is less efficient (see Eq. 2.50 and 2.51 for definitions), as a consequence the temperature gradient will be slightly increased to achieve the same convective flux. This can also be understood from the governing equations. While the temperature gradient described by (2.54) changes approximately inversely proportional to α_s the superadiabatic gradient is multiplied with α_s to compute the convective flux in Eq. (2.52) such that the dependence on this parameter actually cancels out. As the convective flux, appearing in the first term of the TKE equation, does not change notably, also the other variables remain unaffected by changing α_s.

As already described in Sec. 5.3 and 5.4 we find general agreement between the 1-equation model and the simulation results. To reproduce simulation 1 a higher dissipation parameter is needed which simultaneously would reduce the radial extent of the TKE. As discussed previously, the TKE as obtained from the 1-equation model is in excellent agreement with simulation 2 for the default parameters. Considering the insensitivity of Π to changes of the model parameters, it is not possible to reduce the discrepancy observed in Fig. 5.4. The non-local term is in slight disagreement with both simulations. For simulation 1 it is mainly again the radial extent of the TKE that causes this disagreement. For simulation 2 we find that in the bulk and towards the TKE boundary the magnitude of the non-local term needs to increase by about a factor of two, and remain approximately the same towards the centre. The magnitude of the non-local term may be increased by decreasing the dissipation parameter C_D. As this will lead to a larger radial extent of

the TKE, one needs to decrease the non-local parameter at the same time to keep the extent of the TKE in agreement. Changing the overall shape of the non-local term may be achieved by varying the mixing length or alternatively the Wuchterl (1995) parameter, as the reduction of the mixing length towards the centre impacts on the shape of the TKE profile. The asymmetric shape of the non-local term observed in the simulations could however also be a result of the inner boundary, which is not placed exactly in the centre. Finally, the shape of the non-local term towards the outer boundary seems to be more in agreement with the 3-equation model than with the 1-equation model. However, we are not able to reproduce the magnitude of the TKE and the non-local term at the same time by varying the model parameters, pointing at a more fundamental shortcoming. The assumption of a fully isotropic distribution of turbulence could be the reason for this discrepancy. According to the distribution of the TKE shown in Fig. 5.3, the magnitude of the non-local term would increase in the middle of the convection zone, where the flow is radially dominated, and decrease towards the outer boundary, where the flow becomes horizontally dominated.

We conclude that the magnitude of the TKE can be easily adjusted by varying the dissipation parameter C_{D}, even though a value close to the default results in the closest agreement. Decreasing the dissipation parameter to better reproduce simulation 2 also modifies the magnitude of the non-local term and reduces the discrepancy. Changing the non-local parameter has about the same effect on the non-local term as changing the dissipation parameter, but with opposite sign. For the TKE the effect of varying α_ω is the same as varying C_{D} but with a smaller magnitude. The remaining discrepancy between the 1D models and the simulations might be related to the anisotropic distribution of the TKE not considered by the Kuhfuß model. Finally, it has to be kept in mind that the radial extent is the most decisive quantity for stellar evolution, such that parameters need to be chosen to reproduce observed convective core sizes.

5.5.2 The 3-equation model

Following the 1-equation model, we will now analyse how the terms of the 3-equation model behave when changing the model parameters. Owing to the increased model complexity, the 3-equation model encompasses more parameters than the 1-equation model. Each additional closure relation introduces another free parameter. In the 3-equation model there are α_ω and C_{D} for the non-local and dissipation term of the TKE equation. Additionally, there are two parameters α_Π and α_Φ for the non-local terms of the convective flux and entropy fluctuation equation, γ_{R} to parametrise radiative losses and c_4 introduced in the new dissipation closure in Ch. 3. Finally, there is the original mixing length parameter α and the parameter of the Wuchterl (1995) correction β that we keep fixed, however. Hence, there are eight parameters in total. As we have discussed in Sec. 5.3 the radiative dissipation term of the 3-equation model as well as from the hydrodynamic simulations is negligibly small. Therefore, we do not expect changes to the results unless the parameter is increased by many orders of magnitude and leave γ_{R} fixed for the following discussion.

We have pointed out previously that the convective flux is mainly determined by the

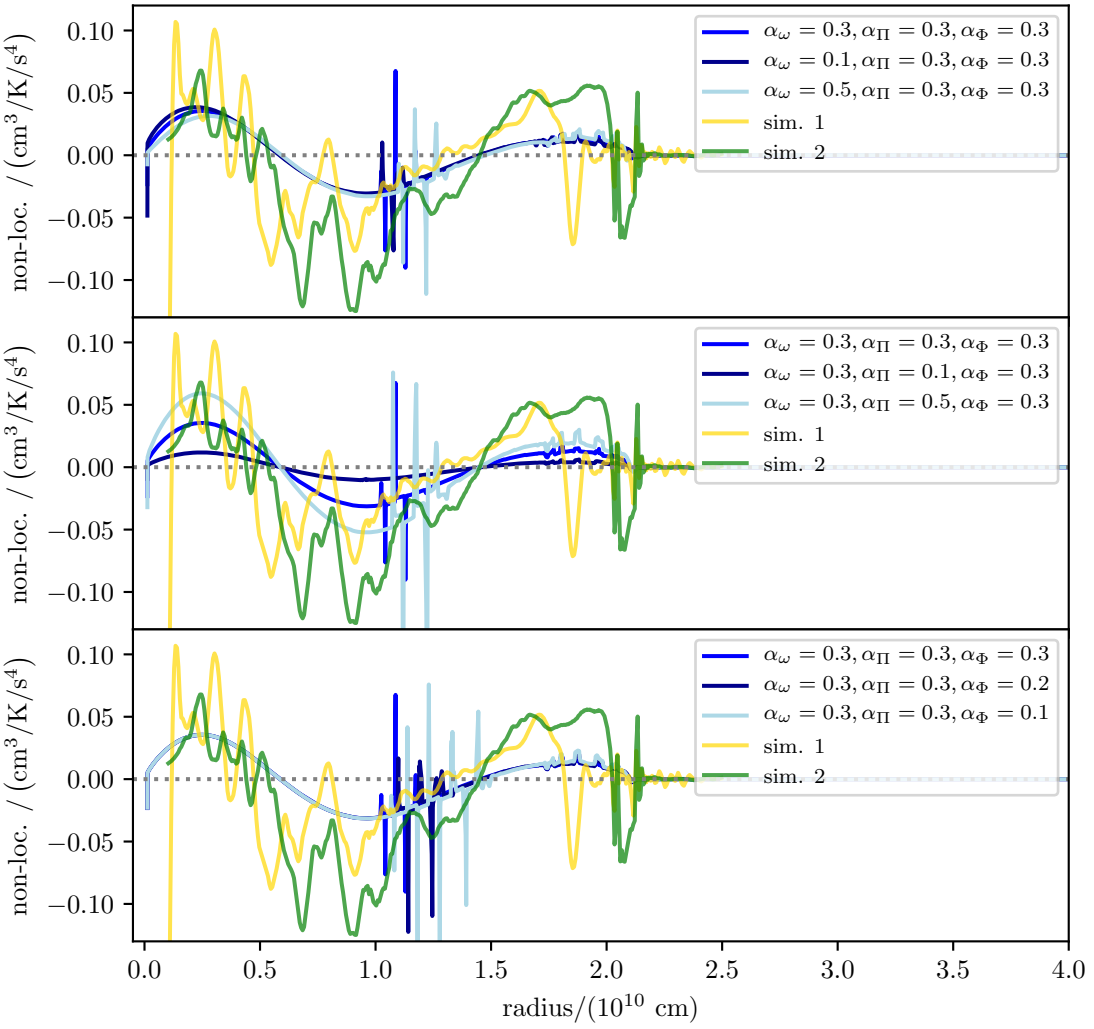

Figure 5.17: Comparison of non-local terms of the convective flux equation of the 3-equation model as a function of radius. The results of simulation 1 and 2 are shown with a yellow and green line, respectively. The non-local terms of the convective flux equation obtained from the 3-equation model are shown with the remaining coloured lines (see legend for details). The parameters $\alpha_\omega, \alpha_\Pi$ and α_Φ are varied in the upper, middle and lower panel respectively. The mid-blue line indicates the default parameter values.

stellar structure. This conclusion does not change for the 3-equation model. Unless the stellar model changes drastically, the convective flux will look the same for most parameter values. Only in the overshooting zone, variations will be visible. Due to this similarity of the convective flux variable, we find that the behaviour of the TKE is very similar when changing the parameters α_ω and C_D as in the 1-equation model. As discussed in Sec. 4.3.1

the effect of changing $C_{\rm D}$ is partially cancelled out in the 3-equation model by the new dissipation mechanism. As discussed already in Sec. 4.3.1 the parameters α_Π and α_Φ have very little impact on the overshooting distance, and we will hence not discuss how the results of the TKE equation depend on these two parameters. Changing the parameter c_4 changes the strength of the newly introduced dissipation mechanism. We have discussed in Sec. 4.3.1 that this changes the extent of the TKE and leaves its absolute value in the bulk of the convection zone unchanged. We therefore keep c_4 fixed in the following discussion as well.

We now discuss how the terms of the convective flux equation vary when changing the non-local parameters $\alpha_\omega, \alpha_\Pi$ and α_Φ. A similar discussion for the terms of the entropy fluctuation equation could be carried out. Due to the increasing noise in the simulations, there is limited use of a comparison to the 3-equation model. In Fig. 5.17 we show the non-local term of the convective flux equation as a function of radius for different values of the non-local parameters of the 3-equation model. For comparison, we show the results of simulation 1 and 2 in each panel. As the 1-equation model has no counterpart for this term, we cannot compare to this model. The results for varying α_ω are shown in the upper panel of Fig. 5.17. As could be expected, the non-local term of the convective flux equation shows only minor variations when this parameter is changed. The radial extent increases slightly following the increase of the TKE when increasing α_ω. The largest variation of this term is observed when varying α_Π, which is parametrising the behaviour of this term (middle panel of Fig. 5.17). For increasing parameter values, the magnitude of this term increases, improving the agreement of the 3-equation model and the results of simulation 2 both in the centre and towards the boundaries of the convection zone. This behaviour is also reflected in the middle panel of Fig. 5.18 in which increasing α_Π leads to an increase of the superadiabaticity to counteract the decrease of the non-local term in this region. Finally, the lower panel shows the reaction of the non-local term to changing α_Φ. This parameter has again a negligible impact on the non-local term of the convective flux equation. We note that for increasing the parameters α_Π and α_Φ the non-local term of the convective flux equation becomes increasingly noisy. This happens at the location where the temperature gradient becomes subadiabatic and the newly derived dissipation mechanism becomes relevant. The parameters α_Π and α_Φ impact the behaviour of the temperature gradient and hence the dissipation mechanism. This coupling causes apparently some numerical difficulties.

In Fig. 5.18 we show the potential term of the convective flux equation as a function of radius. The data are the same as in Fig. 5.17. As described previously, this term mainly reflects the temperature stratification in the convective core. The variation of the potential term when changing α_ω is shown in the upper panel. Increasing this parameter leads to a more extended close to adiabatic region and a flatter profile of the potential term without changing its magnitude notably. An appropriate value of α_ω is however mostly determined by the extent of convective core, such that it cannot be tuned to obtain the correct thermal structure and potential term. As expected, increasing α_Π leads to a larger magnitude of the potential term. However, in the ranges investigated here, the magnitude of the potential term from both simulations cannot be reached. Increasing the parameter

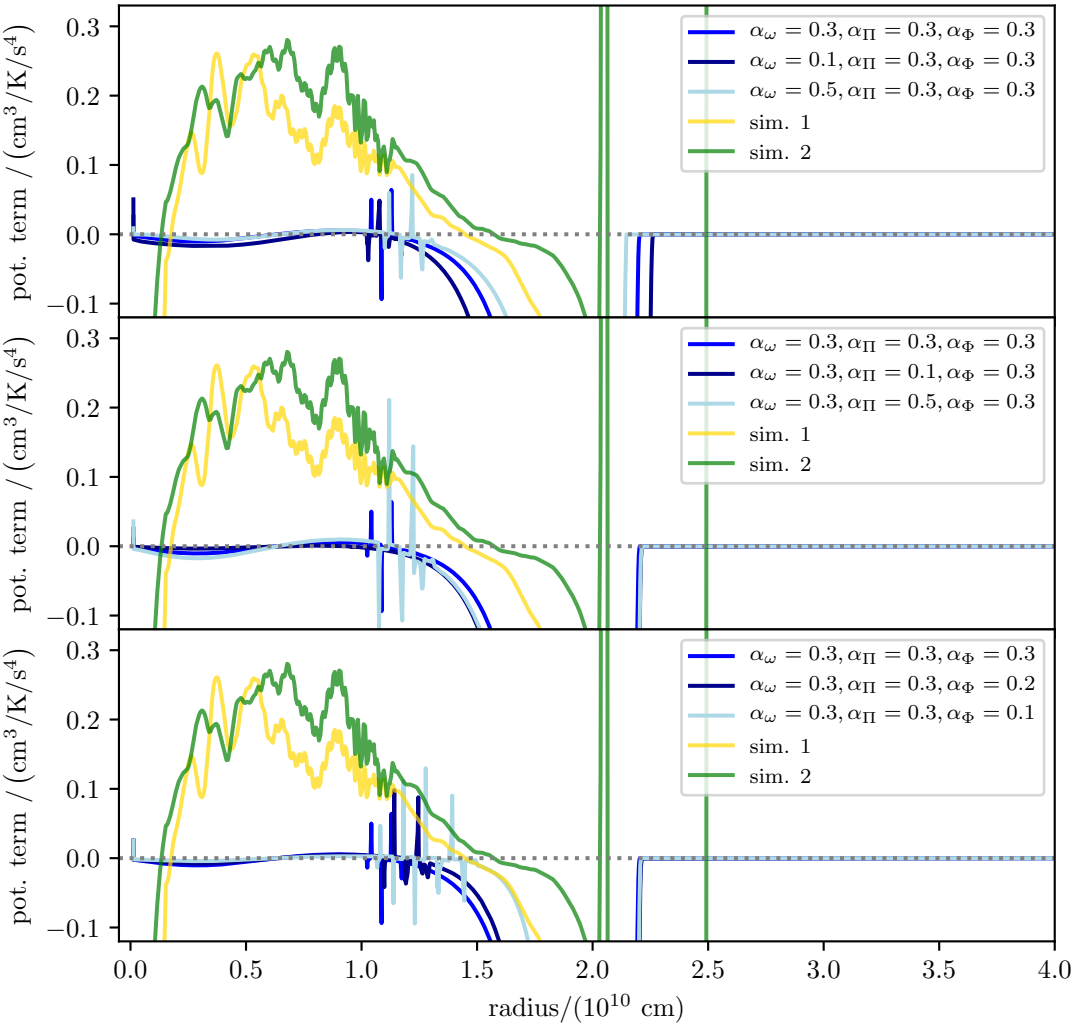

Figure 5.18: As Fig. 5.17, but for the potential term of convective flux equation of the 3-equation model.

α_Φ mainly increases the radial extent of the superadiabatic or close to adiabatic region. As this parameter does not impact on the extent of the TKE as discussed in Sec. 4.3.1 its tuning potential can be in principle exploited to reproduce the radial extent of the superadiabatic region in the simulations. As already described above, the increase of the parameters α_Π and α_Φ leads to an increasing numerical noise in the 3-equation model, hindering an arbitrary variation of these two parameters. While the convective flux in the bulk of the convection zone remains nearly unchanged when varying the parameters, its value in the overshooting changes. We find that a more extended and deeper region of negative convective flux emerges for increasing α_Π. Decreasing α_ϕ to obtain a larger extent

of the superadiabatic region however counteracts this trend and leads to a shallower and less extended negative convective flux region.

As for the 1-equation model we conclude that the variation of the model parameters allows better reproducing the simulation results. Increasing the non-local term of the convective flux equation improves the agreement with the simulations. We note that a more radially dominated TKE distribution would also increase the magnitude of this term in the bulk of the convection zone. We were not able to reproduce the depth of the negative convective flux in the overshooting zone by changing the model parameters. This seems to be again a more fundamental feature of the 3-equation model. This is reflected by the fact that none of the models in Fig. 5.17 reproduces the negative feature beyond the TKE boundary observed in simulation 1 and 2. It is also not possible to reach the required level of superadiabaticity observed in the simulations, which is potentially overestimated in the simulations as they did not reach perfect thermal equilibrium yet. While one would like to obtain perfect agreement with the simulations, it is by no means guaranteed that these reproduce all features of stellar convection correctly. It seems therefore advisable to concentrate on the most basic, and for stellar models, most relevant quantities, such as the TKE and the convective flux for which we find good agreement.

5.6 Discussion

As we have described in Sec. 5.3 and in Tab. 5.1 the two hydrodynamic simulations discussed in this chapter differ fundamentally in the extent of the TKE. At first glance, this seems puzzling, as we have used the same code and numerical setup for both simulations. Both simulations differ however in their initial model. For simulation 1 a Kuhfuß 3-equation model and for simulation 2 an MLT model including ad hoc overshooting has been used. We have chosen the initial models to have approximately the same convectively mixed core size and the same central hydrogen abundance. Hence, the initial models only differ in their temperature structure that is mapped to the 3D simulations. We conclude that the difference in the TKE extent originates from the difference in the initial temperature structures. In principle, the thermal structure changes self-consistently in the convection zone of the simulation. However, the adjustment of the thermal structure occurs on a much longer timescale than has been simulated here. This means that the simulations did not evolve long enough to become independent of their initial state, and a much longer simulation would be needed to obtain a consistent thermal and velocity structure. It is hence unclear which of the simulations, if at all, produces a physically realistic extent of the TKE. As a consequence, all the comparisons in this chapter do only apply for the simulation results in the present state. We note that alternative definitions of the TKE boundary could be used, leading to different estimates for the extent of the TKE. We found that the horizontal component of the TKE in both simulations extends up to the Schwarzschild boundary. Hence, using this as a criterion to determine the TKE boundary would increase the estimated core size of simulation 1. However, extended convective regions which are horizontally dominated are not expected, such that the TKE in this region

more likely originates from a different physical process than convection. Our choice of the TKE boundary based on the anisotropy profile is further supported by the inspection of the individual terms. The non-local term of the TKE equation drops to zero exactly at the TKE boundary. The same is true for the non-local term of the convective flux equation. Also, the buoyancy term and the convective flux in general support our choice of the TKE boundary.

The discrepant structure of the TKE profiles obtained from simulation 1 and 2 in comparison to the Kuhfuß models allows us however to draw a conclusion about the initial temperature stratification. If the thermal structure of the initial stellar models were consistent with the convective velocity structure, one would expect that the hydrodynamic simulation would reproduce the convective velocities of the stellar models. This is however not the case, indicating that in both initial stellar models the thermal structure is inconsistent in view of the hydrodynamic simulations analysed here. We have further observed that the entropy profile did adjust already. In simulation 1 it moved outwards while it moved inward in simulation 2 compared to the respective initial models (see Fig. 5.5). This is another indication, that the initial temperature structure was inconsistent with the velocity structure. We expect that on a timescale much longer than our simulation time, i.e. on a thermal timescale, the TKE would extend further out in radius until it eventually reaches a stationary situation with a consistent temperature structure. Alternatively to running simulations long enough to adjust their thermal structure, one could follow the approach of Higl et al. (2021) and use initial stellar models with varying parameters. Similarly, Anders et al. (2022) propose an iterative modification of the thermal structure in their simulations to accelerate their simulations. To reproduce the TKE profile of the 3-equation model with a simulation, the thermal structure of the initial stellar model could be iteratively adjusted to the entropy profile of the simulation by varying α_Π and α_Φ.

Another result of the initial temperature stratification are the features observable beyond a radius of $2.05 \cdot 10^{10}$ cm. A change in behaviour is visible in some terms and also in the isotropy profile. This location coincides with the formal Schwarzschild boundary of the initial stellar models (see Tab. 5.1). The change in the behaviour originates from waves that are launched beyond the Schwarzschild boundary. Due to the relatively low spatial resolution, these waves remain unresolved in our simulation, leading to the spurious TKE beyond our TKE boundary and the feature in the anisotropy profile (Fig. 5.3). As we have shown in Fig. 4.2 the temperature gradient transitions gradually from nearly adiabatic to radiative in the 3-equation model, while this transition is more abrupt in an MLT model. This difference in the initial temperature structure is also still visible in the simulations, for example the gradient of the mean entropies and terms directly related to that, but also the buoyancy term of the convective flux equation and the squared entropy fluctuations Φ show this behaviour.

The RANS data we have computed from the current hydrodynamic simulations show still a rather high level of statistical fluctuations. This can be attributed to the comparatively short analysis time, that only comprises approximately one convective turnover. We find that the sensitivity of the convection model to changing the model parameters is in some cases less than the statistical fluctuations in the simulations. In addition, we

also observed rather substantial fluctuations between different simulations. This renders the calibration of exact parameter values difficult. Therefore, we have limited the above discussion to indicating how the parameter variations in the Kuhfuß models change the individual terms, without giving a final set of calibrated parameters. The situation may improve for longer simulation times, as this will naturally decrease the statistical fluctuations within a simulation. If it remains impossible to tune the parameters of the TCM to match the simulations for even longer simulations, this might point at more fundamental shortcomings in the convection model. Currently, we see that it is difficult to reproduce the non-local term of the TKE equation and the magnitude of the TKE itself for the same parameters. As pointed out above, this might be caused by neglecting the anisotropic spatial distribution of the TKE in the Kuhfuß model. It could also indicate that terms are missing in the model equation, like for example the pressure fluctuation term, even though we would exclude this from a physical point of view. This mismatch needs to be verified with longer simulation times.

5.7 Conclusions

In this chapter, we have compared 3D hydrodynamic simulations of stellar core convection to results obtained with the Kuhfuß TCM. The simulations have been carried out with the SLH code, a finite volume code, solving the inviscid Euler equations. The code is tailored for low Mach number, nearly hydrostatic conditions, as they are encountered in convective cores of main-sequence stars. To initialise our simulations 1 and 2 we have used two 1D stellar models, a Kuhfuß 3-equation model and an MLT model with ad hoc overshooting. The initial stellar models have been mapped to a 3D wedge geometry. This geometry allows keeping the main features of spherical convection while reducing the computational costs that allow for longer simulation times. We have first directly compared the convective variables ω, Π and Φ and subsequently compared individual terms of the dynamic equations and attempted to calibrate parameters of the convection model.

For stellar structure and evolution the TKE is the most relevant convective quantity, apart from the convective flux, as it is used to determine the convectively induced mixing (see Eq. 2.22). This determines how much fuel a star with a convectively burning core has available, which greatly impacts on the stellar luminosity, age and nucleosynthetic yield. Comparing the TKE obtained from simulation 1 and 2 with the 1- and 3-equation model shown in Fig. 5.2, we find very good agreement in terms of the magnitude, while simulation 2 is in better agreement. In contrast, the TKE obtained from MLT seems to be substantially overestimated. The radial extent of the TKE towards the convective boundary is largely different in simulation 1 and 2. As discussed in the previous section, we associate this with the thermal structure of the simulation that is still adjusting on the simulation timescale. This indicates that the thermal structure of the initial stellar model needs to be slightly modified to match the simulations. Both extents of the TKE as determined from the isotropy profiles of the simulations in Fig. 5.3 extend beyond the boundary of the superadiabatic region as determined from the mean entropy profile,

meaning that an overshooting zone emerges in the simulations. Even though, both TKE extents are smaller than obtained from the Kuhfuß models. Due to the uncertainty in the TKE profiles obtained from the simulations, we can however not conclude whether the TKE extent from the 1- and 3-equation models is incorrect or not. To obtain stationary simulation results, both in terms of the TKE profile and the thermal structure, much longer simulation timescales would be needed. These could finally allow obtaining a more reliable estimate of the radial TKE extent. The spatial distribution of the TKE is very similar in both simulations. As it has been observed in other simulations (e.g. Viallet et al. 2013; Cai 2020; Andrassy et al. 2022) or in a 4-equation Reynolds stress model (Li and Yang 2007) we find that the TKE is not distributed isotropically, but rather is radially dominated in the bulk of the convection zone and becomes horizontally dominated towards the boundaries as expected from simple geometric arguments. The radial location of the decrease of the isotropy is simply shifted outward in simulation 2 compared to simulation 1. To better understand the role of the vertical component of the TKE in the Kuhfuß model a fourth equation for the vertical kinetic energy would need to be introduced such that a self-consistent solution can be computed. Such an equation has for example been introduced in the models by Li and Yang (2001, 2007); Xiong (1979); Canuto (1992) or Canuto and Dubovikov (1998). Introducing an isotropy profile obtained from simulations is however not desirable, as the overshooting distance would again depend on this external input. We note that the isotropy profile observed by Kupka et al. (2018) in simulations of white dwarfs is clearly different from our profile, which we attribute to the different kind of object studied.

As discussed in Sec. 2.3.3 the purpose of the convection model is to provide a theory for the convective flux and the resulting convective temperature gradient for the stellar structure. In Fig. 5.4 we compare the convective flux obtained from the Kuhfuß models and the 3D simulations. The magnitude of the convective flux variable Π is very comparable to the value obtained from the different stellar models. We see indications that it will further adjust to the stellar structure value for longer simulation times. Due to the direct coupling of the stellar structure and convection equations in the Kuhfuß models and the combined implicit solution of these equations in our implementation, the convective flux variable of the convection model will adjust to fulfil Eq. (2.29). Disregarding the minor discrepancy in absolute values, the convective flux variable obtained from the simulations and the 1- and 3-equation models share some common features. The Kuhfuß convection models reproduce a layer of negative convective flux towards the boundary of the turbulent convective region. However, neither the 1- nor the 3-equation model are able to achieve the same extent and depth of this negative convective flux region. This means that according to the simulations, the temperature gradient in the overshooting region is expected to be somewhere in between the result obtained from the 1- and 3-equation model. In simulation 2 the convective flux is a bit more negative in the overshooting zone in agreement with the closer to adiabatic temperature structure as observed in Fig. 5.5. In both simulations, we observe the emergence of a Deardorff layer, despite the different thermal structure in the initial stellar models. Even though the radial extent of the TKE is rather different in both simulations, we conclude that the thermal structure of the overshooting zone is

more complex than predicted by MLT or the 1-equation model. A Deardorff layer and a gradual transition from the nearly adiabatic to the radiative temperature gradient are expected in real systems. Therefore, the convection model should allow for the existence of a Deardorff layer, like it is the case in the 3-equation model. However, the size of this layer seems to be overestimated in the 3-equation model as the radial extent of this layer shrunk, creating a larger superadiabatic region in the bulk of the convection zone of simulation 1. The size of the superadiabatic region in the Kuhfuß 3-equation model can be influenced by changing the parameters α_Π and α_Φ. In the current work, we were not able to achieve the required parameter values due to numerical problems in the 3-equation model, that made the results unreliable. Due to the comparably short simulation time, the question about the radial extent in which the temperature gradient transitions remains unanswered for the moment. As a future direction, we suggest using a stellar model with the Kuhfuß 1-equation theory as an initial model for the hydrodynamic simulation. The very close to adiabatic overshooting zone in the 1-equation model allows testing yet another thermal stratification with 3D simulations.

An important conceptual difference between the TCM and MLT is that individual physical effects can be identified as different terms in the convection model. This allows testing the individual approximations by comparing the individual terms to external sources, e.g. hydrodynamic simulations. As we have pointed out several times before, the non-local terms of the TCM are responsible for the emergence of the overshooting layer and creating some features, like the Deardorff layer, that are not found in local convection models. In Sec. 2.4.1 we have described how the third order moments, constituting the non-local terms, are modelled using the downgradient approximation in the Kuhfuß model, which is a simple diffusion approximation for the non-local fluxes. Given the data of the simulations, we have computed the full third order moments and compared them to their approximated counterparts in the Kuhfuß model. The results are shown in Fig. 5.7, 5.11 and 5.14. Despite the noise, we find a general agreement between the non-local terms of the ω and Π equation between the simulation results and the TCM. For the non-local term of Φ, a meaningful comparison is rendered more difficult due to the increased noise in the simulation data. Our previous discussion about the radial extent of the TKE in both simulations, applies also to the radial extent of the non-local terms, and we will not repeat it here. The magnitude of the non-local terms agrees very well among the simulations and the TCM, which is an encouraging indication for the physical accuracy of the model. Furthermore, the non-local terms and the ω and Π profiles as obtained from the simulations are consistent with each other, indicating that the approximation for the non-local terms of the Kuhfuß model is appropriate. Given the shape of the non-local terms in the simulations, the smooth decrease towards the boundary, as observed in the 3-equation model, seems more likely than an abrupt cut-off as in the 1-equation model. This is in agreement with the shallower negative convective flux region observed in the simulations. The physical accuracy of the non-local terms is very important for the TCM. We point out that we obtain the same functional form of the non-local terms, despite the differences in radial extent, for both simulations, such that this conclusion seems to be independent of the initial model.

Another important term for the convection model is of course the buoyancy term, modelled in the Boussinesq approximation. Comparing the buoyancy terms of the simulations and the TCM allows us to test this approximation and identify whether they correctly represent the driving of the convective motions. By comparing Figs. 5.8 and 5.4 we find that the buoyancy term of the Kuhfuß ω equation could be correctly inferred from the convective flux variable Π, confirming the Boussinesq approximation. For the buoyancy term of the TKE equation, we further find a reasonable agreement of the order of magnitude of this term between the simulations and the solution of the TCM, following the discussion of the convective flux variable Π. The buoyancy term of the convective flux equation cannot be reproduced owing to the large statistical fluctuations in the entropy fluctuations obtained from the simulation. The potential terms of the convective flux and entropy fluctuation equation are proportional to the entropy gradient and hence the thermal structure of the convection zone. Here, the same discussion as for the thermal structure applies, indicating the need for a more extended region with a higher superadiabatic temperature gradient. Using the 3D data, we compute the terms that have been neglected in the derivation of the Kuhfuß models. We find that most terms that have been neglected are indeed very small compared to the terms included in the model. The pressure fluctuation terms are the only exception in this respect, as they show a non-negligible magnitude in our simulations. On physical grounds they are expected to scale as Ma^2 and with the density stratification of the background model and hence should be small. We therefore consider these to be an artefact of the 3D simulation.

We have varied some parameters of the Kuhfuß model attempting to better reproduce the simulation results. For the TKE equation, both in the 1- and 3-equation model, the non-local and the dissipation parameter α_ω and C_D play the most important role. Decreasing (increasing) the dissipation parameter substantially increases (decreases) the absolute value of the TKE. At the same time, it increases (decreases) the size of the convective core. The variation of the absolute value of the TKE also changes the magnitude of the non-local term accordingly. Due to the uncertainty in the radial extent of the TKE in the simulations, calibrating the model parameters to the radial extent seems questionable. The convective fluxes obtained from the 1- and 3-equation model are largely determined by the stellar structure and do not change notably when varying the model parameters. Instead, the temperature gradient adjusts such that the required convective flux is transported. As discussed above, this is a result of the direct coupling of the stellar structure and convection equations. Large variations of the convective flux are also not expected as this would strongly change the overall stellar structure, which can be excluded by observations. The convective flux also determines the buoyancy term of the TKE equation, such that this term is mostly determined by the stellar structure as well. Only in the overshooting zone, the different convection models allow the convective flux variable to vary more independently, as radiative energy transport plays a greater role in this region. The non-local parameters α_Π and α_Φ have only minor impact on the size of the convective core as described in Sec. 4.3.1. They can however be used to change the thermal structure of the 3-equation model.

Our comparison of the Kuhfuß models with 3D simulations shows that the TKE equa-

tion of the 1- and 3-equation model represents the results of the hydrodynamic simulations rather accurately. To reproduce the thermal structure of the simulations, featuring a Deardorff layer, a TCM with a high enough physical complexity, like the 3-equation model, is required. We find the buoyancy, non-local, and potential terms of the 3-equation model to be in agreement with the simulation results, which is an important indication for the physical accuracy of the 3-equation model. The assumption of fully isotropic turbulence in the Kuhfuß model is clearly at odds with our simulations. We therefore suggest using a 4-equation TCM in the future to include the vertical TKE as a fourth variable. To draw conclusions about the thermal structure in the overshooting zone, we suggest following an iterative approach and use initial models with different thermal structures until the simulation consistently reproduces the thermal and velocity structure of the TCM.

Chapter 6

Conclusions

Stellar structure and evolution models play a key role in many fields of astrophysics, for example to determine stellar ages, compute nucleosynthetic yields, characterise exoplanet systems, model the chemical evolution of large populations of stars or describe the late stages of stellar evolution preceding the final fate of the star. To obtain reliable results for all these applications, accurate theoretical models are required. One of the processes that needs to be described by stellar models is convection, the transport of energy and matter by bulk fluid motions. In stars, convection has a large impact on the mixing of chemical elements as well as determining the thermal structure. In nuclear burning regions of the stars, this has a direct impact on the luminosity, lifetime and nucleosynthetic yield. Convection in stellar envelopes affects the radius of the star, that is important for describing binary interactions, and also impacts on the surface composition of the star. The most commonly used theory to describe convection in stars, the so-called mixing length theory (MLT), employs crude assumptions of the underlying physics and is known to underestimate the size of convectively mixed regions. To account for this underestimation of the convective region, parametrised ad hoc chemical mixing descriptions at convective boundaries are introduced. The parameters of these descriptions are calibrated for specific conditions, and the applicability of the same parameter to all circumstances remains uncertain. Most fundamentally, the problems of describing stellar convection are related to the turbulent nature of the flows in the stellar interior. In this work, we have extended and applied a turbulent convection model (TCM) in stellar evolution calculations. The TCM describes the turbulent convective flows in an effective way, that allow for a physically more realistic description of convection. We show that the TCM computes the radial extent of the convective regions in better agreement with observations. In addition, TCMs also allow predicting the thermal structure of the entire convection zone, something which is not possible using MLT. This is a substantial step towards a more realistic description of convection in stellar models.

The effects of turbulence occur on the smallest spatial and temporal scales, which are in stark contrast to the large spatial and temporal scales of stellar structure and evolution. To resolve these small scales would require enormous computational costs, which are beyond feasibility for stellar evolution calculations. Due to the stochastic nature of the turbulent

flows, they can be described using statistical methods. While flow variables measured at single points as a function of time fluctuate randomly, temporal or spatial averages converge to finite values. This led to the development of TCMs, that describe the effects of turbulence without resolving any of the fine structure. The key ingredient of TCMs is to develop models for the different turbulent processes, e.g. turbulent transport or turbulent dissipation. One of the first models to describe the effects of turbulence in general is the MLT developed by Prandtl (1925). The MLT got further adopted for stellar evolution by Biermann (1932) and Böhm-Vitense (1958) and is still the most commonly used model for stellar convection. The TCM by Kuhfuß (1987) used in this work has been developed for stellar structure and evolution calculations. A simplified version of this model, solving only for the turbulent kinetic energy (TKE) of the flow, has been implemented into the GARching STellar Evolution Code (GARSTEC) initially by Flaskamp (2003). We refer to the simplified model as the 1-equation model. In this work, we have implemented the physically more complete version of this TCM that in addition to the TKE also solves the dynamic equations for the convective flux and entropy fluctuations of the turbulent flow. We refer to this model as the 3-equation model. The Kuhfuß TCM models the turbulent flux using a diffusion approximation, the buoyancy terms are treated in the Boussinesq approximation and for the dissipation of the TKE a Kolmogorov cascade is invoked. The equations of the TCM are solved self-consistently, simultaneously with the stellar structure equations in the implicit Henyey scheme.

Compared to the simplified 1-equation model, the 3-equation model is considered to be physically more complete. However, we have first demonstrated that the original 3-equation model leads to overshooting zones covering the whole stellar object, reproducing results from the original thesis by Flaskamp (2003) (Ch. 3). This behaviour is clearly unphysical and can be ruled out by observations. We have attributed this behaviour to a lack of dissipation of TKE in the original version of the Kuhfuß (1987) TCM, approximated by the Kolmogorov cascade. The physically more complete models by Hanjalić and Launder (1972) or Canuto (1992) compute the dissipation of the TKE with another dynamical equation that takes into account different sources of dissipation. However, these models never got implemented into a stellar structure and evolution code. Most importantly, the latter authors take the dissipation by buoyancy waves in stably stratified regions in their equations into account. The introduction of another dynamical equation naturally increases the theoretical and technical complexity of the model. We therefore derived a simplified dissipation expression taking into account the effects of the physically more complete models (Sec. 3.3.5). We demonstrate that our newly introduced dissipation mechanism leads to physically reasonable extents of the overshooting layer. We have further argued that other effects are expected to have less impact on the overshooting extent than the dissipation term of TKE. In Sec. 3.4 we have shown that in the simplified 1-equation model the negative convective flux, proportional to the superadiabatic temperature gradient, is the most important sink term in the TKE equation. In the more complete 3-equation model the convective flux variable is not forced any more to follow the superadiabatic gradient, such that effectively a sink term, dissipating the TKE was missing and causing the overshooting zone to extend through the whole star. This deficiency has been resolved by our newly

introduced dissipation term.

We have applied the 3-equation model including the new dissipation mechanism to compute the evolution of low- and intermediate-mass main-sequence stars with convective cores (Ch. 4). We find that the application of a TCM has some profound implications for stellar structure and evolution. Most importantly, the turbulent transport terms appearing in the TCM lead to the transport of TKE in the radial direction, increasing the extent of the TKE. Due to the high mixing efficiency of turbulent convection, this leads to an increase of the convectively mixed core size. We show that the resulting core sizes are in qualitative agreement with observations and substantially improve the agreement as compared to MLT models (Fig. 4.13). While the core size in ad hoc overshooting schemes is the result of fine-tuning model parameters, the increase of the convective core size and the emergence of an overshooting zone result from the solution of the TCM equations. The predictions of the TCM can be compared to observations or hydrodynamic simulations. The increase of the chemically mixed core increases the amount of fuel in the stellar centre available for nuclear burning, which substantially increases the luminosity and lifetime of the star. A change of the convective core size on the main sequence leads to further structural changes in later evolutionary phases, for example in the core helium burning phase.

Apart from the size of the convective also the thermal structure of the core boundary is of importance for stellar structure and evolution models. The commonly used ad hoc overshooting schemes do not make predictions about the thermal structure, and the temperature gradient of the overshooting region is assumed to be either adiabatic or radiative. The TCM used in this work allow us to predict the temperature gradient in the overshooting zone through Eq. (2.60). We conclude that the thermal structure of the overshooting zone is much more complex than assumed by MLT or the 1-equation model. While in MLT and the 1-equation model, the sign change is forced to happen at the Schwarzschild boundary due to the parametrisation of the convective flux, the 3-equation model allows for a temperature gradient that changes its sign independent of the Schwarzschild boundary. This for example allows for the emergence of a Deardorff or counter gradient-layer in which energy is transported convectively against an entropy gradient. This is known from other simulations and observations, and therefore a stellar convection model should be in principle able to reproduce such a feature. The comparison to the 1-equation model led us to the conclusion that the convection model needs to have a certain level of physical complexity for such a Deardorff layer to emerge, and at least 3-equations are necessary to achieve that. Concerning the thermal structure, I finally note that convection is less efficient in the 3-equation model than in the 1-equation model leading to the mostly radiative overshooting zone in the 3-equation model. This can for example deduced by comparing the Peclet numbers of both convection models (see Sec. 4.5.1).

The TCM contains a number of approximations and model parameters that need to be tested and chosen appropriately. Modern hydrodynamic codes are able to simulate convective flows under stellar conditions. Even though these hydrodynamic simulations cover only a very small fraction of the lifetime of a star, they allow for a comparison to the results of the TCM. We have computed two three-dimensional hydrodynamic simulations

initialised with a stellar model using the 3-equation model and initialised with an MLT model including ad hoc overshooting. The simulations differ initially mainly in their thermal structure. The absolute values of the TKE of the Kuhfuß 1- and 3-equation models are in very good agreement with both simulations. In contrast, the TKE predicted by MLT is too large by about a factor of four. However, we find that even after turbulent convection has been fully developed, the radial extent of the TKE is different in both simulations. We conclude that this discrepancy is related to the difference in the initial thermal structure. While the Kuhfuß model has an extended subadiabatic region in the bulk of the convection zone, the MLT model is superadiabatic up to the Schwarzschild boundary. From this discrepancy between the TKE of the simulation with the 3-equation model, we conclude that the thermal structure of the 3-equation model is not fully consistent with the TKE profile it predicts. It further shows that the hydrodynamic simulations are not yet thermally relaxed, as the simulation time has been too short. It is however important to note that we find a Deardorff layer in both simulations. The fact that we find this in both simulations despite the different initial thermal structure highlights the physical relevance of this effect. Using the full velocity field of the 3D simulation, we have investigated the spatial distribution of the TKE. Reproducing previous results, we find that the bulk of the convection zone is radially dominated while the flow becomes more horizontally dominated in the overshooting zone. This is clearly at odds with the assumption of fully isotropic turbulence, as done in the Kuhfuß models. This is an important direction for future work to move to a 4-equation model, as for example suggested in the models by Canuto (1992); Xiong (1979) or Li and Yang (2001) that have not yet been implemented in a fully implicit stellar evolution code.

One of the advantages of the TCM compared to MLT is that the different terms can be associated with specific physical effects. Using the hydrodynamic simulations, we analysed the behaviour of the individual terms of the TCM. We find a very good agreement of the individual terms of the 3-equation model with the respective terms of the RANS analysis. Especially the non-local terms of the 3-equation model reproduce the RANS expressions in their functional form. Similarly, the buoyancy terms of the TKE equation is in very good agreement with the simulations. We finally demonstrate the ability of the Kuhfuß TCM to adjust to the simulation results by changing the model parameters. The magnitude of the TKE and the non-local term of the TKE equation can be easily varied by changing the dissipation parameter. Varying the parameter α_ω and α_Π allows changing the magnitude of the non-local terms and improving the agreement with the simulations. However, one has to keep in mind that the convective core size is the decisive factor for stellar structure and evolution and any choice of parameters should be able to reproduce observed convective core sizes. The remaining discrepancy in the magnitude of the non-local terms could be resolved by allowing for an anisotropic distribution of the TKE, as this would increase the magnitude within the bulk of the convection zone. The same applies to the magnitude of the non-local term of the convective flux equation.

This leaves us with pointing out a few valuable future directions following from the present work. The 1- and 3-equation Kuhfuß models have been tested and applied to stars with convective cores. This allows for a range of future applications. Stellar oscillations

probe the conditions at convective boundaries in the deep interior of a star (Silva Aguirre et al. 2013; Pedersen et al. 2018; Michielsen et al. 2021). The comparison of asteroseismic observations to stellar models including the turbulent convection theory will therefore allow us to directly probe the conditions at convective boundaries and test predictions made by the TCM. High precision asteroseismic observations from the *Kepler* space telescope (Koch et al. 2010) are available for different pulsating stars that possess a convective core on the main sequence. Studies have been carried out for g-mode pulsators, e.g. B-type main-sequence stars (Moravveji et al. 2015; Michielsen et al. 2021; Pedersen et al. 2021), γ-Dor stars (Mombarg et al. 2019, 2021) but also p-mode pulsators have been used to put constraints on core overshooting (Deheuvels et al. 2016; Angelou et al. 2020; Noll et al. 2021). For all these cases the stellar modelling could be repeated using stellar models including the TCM to model the convection in the core. Especially, the p-mode and γ-Dor pulsators would cover an interesting mass range for the TCM. As we have pointed out above, the extension of the turbulent convective region beyond the Schwarzschild boundary gradually reduces for decreasing stellar mass. For models using ad hoc overshooting this needs to be implemented by fine-tuning the overshooting parameter (Johnston 2021), while in the TCM this is an outcome of the model equations for fixed model parameters. Constructing best fit models of the aforementioned stars would allow for testing the hypothesis of constant TCM parameters or reveal that modifications as a function of stellar mass are necessary. Across the whole mass range, studying stars in different evolutionary stages would be of interest to test whether the TCM parameters are also independent of stellar evolution. Another important test that can be carried out with asteroseismology concerns the thermal structure of the overshooting zone. As shown by Michielsen et al. (2019) and applied in Michielsen et al. (2021) the pulsation modes are sensitive to the temperature gradient. Modelling a few stars with high precision asteroseismic observations could tentatively allow discerning the 1- or 3-equation models based on the temperature gradient in the overshooting zone. Finally, applying an ensemble analysis across a range of stellar masses using machine learning could provide important constraints on the TCM parameters (e.g. Remple et al. 2021).

The previously suggested applications all concerned stars that possess a convective core. Naturally, the investigation of convection in stellar envelopes is another valuable application for TCM. However, prior to the application, we need to validate the applicability of the 3-equation model for stellar envelopes in the same way as it has been accomplished for the stellar cores. From a technical point of view, the Kuhfuß (1987) TCM would be applicable in the envelope as well. For the 1-equation model this has been initially demonstrated in Flaskamp (2003) and we were able to reproduce this result. For the 3-equation model we are facing numerical problems owing to the larger model complexity that have to be sorted out in future work. From a physical point of view, the Kuhfuß TCM is facing certain limitations that need to be considered. For example, pressure fluctuations are expected to be more important in regions with larger density contrasts as they are encountered in stellar envelopes (Viallet et al. 2013). These terms are not foreseen in the original version of the Kuhfuß (1987) model. As for the dissipation term discussed in Ch. 3 a physical model for these terms may be carried over from the models by Canuto (1992, 1993) and

Canuto and Dubovikov (1998). Also radiative dissipation may become more important in the outer layers of the convective envelope, which could again be taken over from the Canuto models. After clarifying the technical and physical problems, the first application should be the computation of a solar model. From helioseismic observations, very detailed constraints on the overshooting at the base of the convective envelope have been obtained (e.g. Sec. 7.2.1 in Basu 2016). Provided a solar model, helioseismic inversions can be used to study the agreement of the TCM with solar observations, especially in reducing the mismatch of the internal sound speed at the base of the convection zone. This would offer an important test of the temperature gradient profile we found with the 3-equation model for convective cores. For example, Christensen-Dalsgaard et al. (2011) pointed out the importance of a Deardorff layer to reproduce solar observations based on earlier results from Xiong and Deng (2001) or Deng and Xiong (2008). Finally, another application of combined stellar envelope and core convection would be the study of the so-called Kissing instability (van Saders and Pinsonneault 2012; Baraffe and Chabrier 2018).

Apart from using asteroseismology to study the dependence of the parameters on stellar mass or evolutionary stage also our comparison of hydrodynamic simulations could be extended to achieve that. By constructing stellar models in different evolutionary stages to initialise hydrodynamic simulations, this could be done. However, before that, we suggest to make sure that the thermal structure of the TCM is in agreement with the simulations. As outlined above, an iterative procedure could lead to an improved agreement between the stellar model and the simulations and finally obtain a consistent thermal structure in the 1D model and 3D simulation. Another direction in hydrodynamic simulations concerns the dissipation rate of the TKE. By increasing the spatial resolution of the simulations compared to the ones discussed in Ch. 5 one could attempt to resolve the gravity waves and study their dissipation properties. Increasing the simulation even further to also resolve the molecular dissipation scale would shed further light on the dissipation mechanism of TKE.

Finally, it is advisable to work on further extensions of the TCM. We have pointed out above, that the spatial distribution of the TKE may play an important role and that it cannot be computed from the 3-equation model realistically. To obtain a self-consistent solution including the vertical component of the TKE would require moving to a physically more complex 4-equation model for example following Canuto and Dubovikov (1998); Xiong et al. (1997) or Li and Yang (2001). Finally, the dynamic equation to compute the dissipation rate ϵ could be included. As we have carried over the most important features of this equation in Ch. 3 this seems however for the moment less important than the inclusion of the vertical component of the TKE. Additional dynamical equations could be included by following the same principle as for the implementation of the original equations of the TCM in GARSTEC by extending the implicit Henyey scheme. However, any new equation complicates the convergence of the stellar models and requires a rather precise initial guess for all the involved quantities. Nevertheless, this thesis has achieved a substantial step forward in the aim to describe turbulent convection more realistically in a stellar structure and evolution code.

Bibliography

Aerts, C., Christensen-Dalsgaard, J., and Kurtz, D. W. (2010). *Asteroseismology*. Springer, Dordrecht, Heidelberg, London, New York.

Ahlborn, F., Kupka, F., Weiss, A., and Flaskamp, M. (2022). Stellar evolution models with overshooting based on 3-equation non-local theories, II. Main-sequence models of A- and B-type stars. *Astronomy and Astrophysics*. accepted.

Almgren, A. S., Bell, J. B., Nonaka, A., and Zingale, M. (2008). Low Mach Number Modeling of Type Ia Supernovae. III. Reactions. *The Astrophysical Journal*, 684(1):449–470.

Almgren, A. S., Bell, J. B., Rendleman, C. A., and Zingale, M. (2006a). Low Mach Number Modeling of Type Ia Supernovae. I. Hydrodynamics. *The Astrophysical Journal*, 637(2):922–936.

Almgren, A. S., Bell, J. B., Rendleman, C. A., and Zingale, M. (2006b). Low Mach Number Modeling of Type Ia Supernovae. II. Energy Evolution. *The Astrophysical Journal*, 649(2):927–938.

Alongi, M., Bertelli, G., Bressan, A., and Chiosi, C. (1991). Effects of envelope overshoot on stellar models. *Astronomy and Astrophysics*, 244:95.

Anders, E. H., Jermyn, A. S., Lecoanet, D., and Brown, B. P. (2022). Stellar Convective Penetration: Parameterized Theory and Dynamical Simulations. *The Astrophysical Journal*, 926(2):169.

Andrassy, R., Higl, J., Mao, H., Mocák, M., Vlaykov, D. G., Arnett, W. D., Baraffe, I., Campbell, S. W., Constantino, T., Edelmann, P. V. F., Goffrey, T., Guillet, T., Herwig, F., Hirschi, R., Horst, L., Leidi, G., Meakin, C., Pratt, J., Rizzuti, F., Röpke, F. K., and Woodward, P. (2022). Dynamics in a stellar convective layer and at its boundary: Comparison of five 3D hydrodynamics codes. *Astronomy and Astrophysics*, 659:A193.

Angelou, G. C., Bellinger, E. P., Hekker, S., Mints, A., Elsworth, Y., Basu, S., and Weiss, A. (2020). Convective boundary mixing in low- and intermediate-mass stars - I. Core properties from pressure-mode asteroseismology. *Monthly Notices of the Royal Astronomical Society*, 493(4):4987–5004.

Arnett, W. D., Meakin, C., Viallet, M., Campbell, S. W., Lattanzio, J. C., and Mocák, M. (2015). Beyond Mixing-length Theory: A Step Toward 321D. *The Astrophysical Journal*, 809(1):30.

Asplund, M., Amarsi, A. M., and Grevesse, N. (2021). The chemical make-up of the Sun: A 2020 vision. *Astronomy and Astrophysics*, 653:A141.

Baglin, A., Auvergne, M., Barge, P., Deleuil, M., Michel, E., and CoRoT Exoplanet Science Team (2009). CoRoT: Description of the Mission and Early Results. In Pont, F., Sasselov, D., and Holman, M. J., editors, *Transiting Planets*, volume 253, pages 71–81.

Baraffe, I. and Chabrier, G. (2018). A closer look at the transition between fully convective and partly radiative low-mass stars. *Astronomy and Astrophysics*, 619:A177.

Basu, S. (2016). Global seismology of the Sun. *Living Reviews in Solar Physics*, 13(1):2.

Basu, S. and Antia, H. M. (2004). Constraining Solar Abundances Using Helioseismology. *The Astrophysical Journal Letters*, 606(1):L85–L88.

Bellinger, E. P., Basu, S., Hekker, S., and Ball, W. H. (2017). Model-independent Measurement of Internal Stellar Structure in 16 Cygni A and B. *The Astrophysical Journal*, 851(2):80.

Biermann, L. (1932). Untersuchungen über den inneren Aufbau der Sterne. IV. Konvektionszonen im Innern der Sterne. (Veröffentlichungen der Universitäts-Sternwarte Göttingen, nr. 27.). *Zeitschrift für Astrophysik*, 5:117.

Böhm-Vitense, E. (1958). Über die Wasserstoffkonvektionszone in Sternen verschiedener Effektivtemperaturen und Leuchtkräfte. Mit 5 Textabbildungen. *Zeitschrift für Astrophysik*, 46:108.

Bono, G. and Stellingwerf, R. F. (1993). Cepheid convective models. *Memorie della Società Astronomia Italiana*, 64:559.

Bono, G. and Stellingwerf, R. F. (1994). Pulsation and Stability of RR Lyrae Stars. I. Instability Strip. *The Astrophysical Journal Supplement*, 93:233.

Boussinesq, J. (1903). *Théorie analytique de la chaleur*, volume 2. Gauthier-Villars, Paris.

Bressan, A. G., Chiosi, C., and Bertelli, G. (1981). Mass loss and overshooting in massive stars. *Astronomy and Astrophysics*, 102(1):25–30.

Cai, T. (2020). Upward Overshooting in Turbulent Compressible Convection. III. Calibrate Parameters for One-dimensional Reynolds Stress Model. *The Astrophysical Journal*, 891(1):77.

Canuto, V. M. (1992). Turbulent Convection with Overshooting: Reynolds Stress Approach. *The Astrophysical Journal*, 392:218.

Canuto, V. M. (1993). Turbulent Convection with Overshooting: Reynolds Stress Approach. II. *The Astrophysical Journal*, 416:331.

Canuto, V. M. (1997). Compressible Turbulence. *The Astrophysical Journal*, 482(2):827–851.

Canuto, V. M. (2011). Stellar mixing. I. Formalism. *Astronomy and Astrophysics*, 528:A76.

Canuto, V. M. (2011). Stellar mixing. V. Overshooting. *Astronomy and Astrophysics*, 528:A80 (4 pp.).

Canuto, V. M. and Dubovikov, M. (1996). A dynamical model for turbulence. I. General formalism. *Physics of Fluids*, 8:571–586.

Canuto, V. M. and Dubovikov, M. (1998). Stellar Turbulent Convection. I. Theory. *The Astrophysical Journal*, 493:834–847.

Canuto, V. M., Minotti, F., Ronchi, C., Ypma, R. M., and Zeman, O. (1994). Second-Order Closure PBL Model with New Third-Order Moments: Comparison with LES Data. *Journal of Atmospheric Sciences*, 51(12):1605–1618.

Carlos, M., Meléndez, J., Spina, L., dos Santos, L. A., Bedell, M., Ramirez, I., Asplund, M., Bean, J. L., Yong, D., Yana Galarza, J., and Alves-Brito, A. (2019). The Li-age correlation: the Sun is unusually Li deficient for its age. *Monthly Notices of the Royal Astronomical Society*, 485(3):4052–4059.

Castellani, V., Giannone, P., and Renzini, A. (1971). Induced Semi-Convection in Helium-Burning Horizontal-Branch Stars II. *Astrophysics and Space Science*, 10(3):355–362.

Chan, K. L. and Gigas, D. (1992). Downflows and Entropy Gradient Reversal in Deep Convection. *The Astrophysical Journal Letters*, 389:L87.

Chan, K. L. and Sofia, S. (1989). Turbulent Compressible Convection in a Deep Atmosphere. IV. Results of Three-dimensional Computations. *The Astrophysical Journal*, 336:1022.

Chan, K. L. and Sofia, S. (1996). Turbulent Compressible Convection in a Deep Atmosphere. V. Higher Order Statistical Moments for a Deeper Case. *The Astrophysical Journal*, 466:372.

Christensen-Dalsgaard, J., Monteiro, M. J. P. F. G., Rempel, M., and Thompson, M. J. (2011). A more realistic representation of overshoot at the base of the solar convective envelope as seen by helioseismology. *Monthly Notices of the Royal Astronomical Society*, 414:1158–1174.

Claret, A. and Torres, G. (2019). The Dependence of Convective Core Overshooting on Stellar Mass: Reality Check and Additional Evidence. *The Astrophysical Journal*, 876(2):134.

Constantino, T. and Baraffe, I. (2018). Significant uncertainties from calibrating overshooting with eclipsing binary systems. *Astronomy and Astrophysics*, 618:A177.

Couch, S. M., Chatzopoulos, E., Arnett, W. D., and Timmes, F. X. (2015). The Three-dimensional Evolution to Core Collapse of a Massive Star. *The Astrophysical Journal Letters*, 808(1):L21.

Daly, B. J. and Harlow, F. H. (1970). Transport equations in turbulence. *Physics of Fluids*, 13(11):2634—2649.

Davidov, B. I. (1961). On the statistical dynamics of an incompressible turbulent fluid. *Dokl. Akad. Nauk. SSSR*, 136:47–50.

Davidson, P. A. (2015). *Turbulence: An introduction for scientists and engineers*. Oxford university press, Oxford.

Deardorff, J. W. (1961). On the direction and divergence of the small-scale turbulent heat flux. *Journal of Meteorolgy (later on: Journal of Atmospheric Sciences)*, 18:540–548.

Deardorff, J. W. (1966). The Counter-Gradient Heat Flux in the Lower Atmosphere and in the Laboratory. *Journal of Atmospheric Sciences*, 23(5):503–506.

Deheuvels, S., Brandão, I., Silva Aguirre, V., Ballot, J., Michel, E., Cunha, M. S., Lebreton, Y., and Appourchaux, T. (2016). Measuring the extent of convective cores in low-mass stars using Kepler data: toward a calibration of core overshooting. *Astronomy and Astrophysics*, 589:A93.

Deheuvels, S., García, R. A., Chaplin, W. J., Basu, S., Antia, H. M., Appourchaux, T., Benomar, O., Davies, G. R., Elsworth, Y., Gizon, L., Goupil, M. J., Reese, D. R., Regulo, C., Schou, J., Stahn, T., Casagrande, L., Christensen-Dalsgaard, J., Fischer, D., Hekker, S., Kjeldsen, H., Mathur, S., Mosser, B., Pinsonneault, M., Valenti, J., Christiansen, J. L., Kinemuchi, K., and Mullally, F. (2012). Seismic Evidence for a Rapidly Rotating Core in a Lower-giant-branch Star Observed with Kepler. *The Astrophysical Journal*, 756(1):19.

Deng, L. and Xiong, D. R. (2008). How to define the boundaries of a convective zone, and how extended is overshooting? *Monthly Notices of the Royal Astronomical Society*, 386:1979–1989.

Dumont, T., Palacios, A., Charbonnel, C., Richard, O., Amard, L., Augustson, K., and Mathis, S. (2021). Lithium depletion and angular momentum transport in solar-type stars. *Astronomy and Astrophysics*, 646:A48.

Edelmann, P. V. F. (2014). *Coupling of nuclear reaction networks and hydrodynamics for application in stellar astrophysics*. PhD thesis, Max-Planck-Institut für Astrophysik, Technische Universität München.

Edelmann, P. V. F., Horst, L., Berberich, J. P., Andrassy, R., Higl, J., Leidi, G., Klingenberg, C., and Röpke, F. K. (2021). Well-balanced treatment of gravity in astrophysical fluid dynamics simulations at low Mach numbers. *Astronomy and Astrophysics*, 652:A53.

Edelmann, P. V. F., Ratnasingam, R. P., Pedersen, M. G., Bowman, D. M., Prat, V., and Rogers, T. M. (2019). Three-dimensional Simulations of Massive Stars. I. Wave Generation and Propagation. *The Astrophysical Journal*, 876(1):4.

Edelmann, P. V. F., Röpke, F. K., Hirschi, R., Georgy, C., and Jones, S. (2017). Testing a one-dimensional prescription of dynamical shear mixing with a two-dimensional hydrodynamic simulation. *Astronomy and Astrophysics*, 604:A25.

Ferguson, J. W., Alexander, D. R., Allard, F., Barman, T., Bodnarik, J. G., Hauschildt, P. H., Heffner-Wong, A., and Tamanai, A. (2005). Low-Temperature Opacities. *The Astrophysical Journal*, 623(1):585–596.

Feuchtinger, M. U. (1999a). A nonlinear convective model for radial stellar pulsations. I. The physical description. *Astronomy and Astrophysics Supplement Series*, 136:217–226.

Feuchtinger, M. U. (1999b). A nonlinear convective model of pulsating stars. II. RR Lyrae stars. *Astronomy and Astrophysics*, 351:103–118.

Flaskamp, M. (2003). *Nichtlokale und zeitabhängige Konvektion in Sternen*. PhD thesis, Max-Planck-Institut für Astrophysik, Technische Universität München.

Freytag, B., Ludwig, H. G., and Steffen, M. (1996). Hydrodynamical models of stellar convection. The role of overshoot in DA white dwarfs, A-type stars, and the Sun. *Astronomy and Astrophysics*, 313:497–516.

Fryxell, B., Olson, K., Ricker, P., Timmes, F. X., Zingale, M., Lamb, D. Q., MacNeice, P., Rosner, R., Truran, J. W., and Tufo, H. (2000). FLASH: An Adaptive Mesh Hydrodynamics Code for Modeling Astrophysical Thermonuclear Flashes. *The Astrophysical Journal Supplement*, 131(1):273–334.

Gabriel, M., Noels, A., Montalbán, J., and Miglio, A. (2014). Proper use of Schwarzschild Ledoux criteria in stellar evolution computations. *Astronomy and Astrophysics*, 569:A63.

Gilet, C., Almgren, A. S., Bell, J. B., Nonaka, A., Woosley, S. E., and Zingale, M. (2013). Low Mach Number Modeling of Core Convection in Massive Stars. *The Astrophysical Journal*, 773(2):137.

Gizon, L. and Birch, A. C. (2012). Helioseismology challenges models of solar convection. *Proceedings of the National Academy of Science*, 109:11896–11897.

Grevesse, N. and Noels, A. (1993). Cosmic abundances of the elements. In Prantzos, N., Vangioni-Flam, E., and Casse, M., editors, *Origin and Evolution of the Elements*, pages 15–25.

Grossman, S. A. (1996). A theory of non-local mixing-length convection - III. Comparing theory and numerical experiment. *Monthly Notices of the Royal Astronomical Society*, 279(2):305–336.

Guillard, H. and Viozat, C. (1999). On the behaviour of upwind schemes in the low mach number limit. *Computers & Fluids*, 28(1):63–86.

Hanasoge, S., Gizon, L., and R., S. K. (2016). Seismic sounding of convection in the sun. *Annual Review of Fluid Mechanics*, 48:191–217.

Hanjalić, K. and Launder, B. E. (1972). A Reynolds stress model of turbulence and its application to thin shear flow. *Journal of Fluid Mechanics*, 52:609–638.

Hanjalić, K. and Launder, B. E. (1976). Contribution towards a Reynolds-stress closure for low-Reynolds-number turbulence. *Journal of Fluid Mechanics*, 74:593–610.

Henyey, L., Vardya, M. S., and Bodenheimer, P. (1965). Studies in Stellar Evolution. III. The Calculation of Model Envelopes. *The Astrophysical Journal*, 142:841.

Henyey, L. G., Forbes, J. E., and Gould, N. L. (1964). A New Method of Automatic Computation of Stellar Evolution. *The Astrophysical Journal*, 139:306.

Henyey, L. G., Wilets, L., Böhm, K. H., Lelevier, R., and Levee, R. D. (1959). A Method for Automatic Computation of Stellar Evolution. *The Astrophysical Journal*, 129:628.

Herwig, F. (2005). Evolution of Asymptotic Giant Branch Stars. *Annual Reviews of Astronomy and Astrophysics*, 43(1):435–479.

Higl, J. (2019). *Multi-Dimensional Simulations of Convective Core Hydrogen Burning*. Dissertation, Technische Universität München, München.

Higl, J., Müller, E., and Weiss, A. (2021). Calibrating core overshooting parameters with two-dimensional hydrodynamical simulations. *Astronomy and Astrophysics*, 646:A133.

Higl, J., Siess, L., Weiss, A., and Ritter, H. (2018). An analysis of the TZ Fornacis binary system. *Astronomy and Astrophysics*, 617:A36.

Holt, S. E., Koseff, J. R., and Ferziger, J. H. (1992). A numerical study of the evolution and structure of homogeneous stably stratified sheared turbulence. *Journal of Fluid Mechanics*, 237:499–539.

Horst, L., Edelmann, P. V. F., Andrássy, R., Röpke, F. K., Bowman, D. M., Aerts, C., and Ratnasingam, R. P. (2020). Fully compressible simulations of waves and core convection in main-sequence stars. *Astronomy and Astrophysics*, 641:A18.

Horst, L., Hirschi, R., Edelmann, P. V. F., Andrássy, R., and Röpke, F. K. (2021). Multidimensional low-Mach number time-implicit hydrodynamic simulations of convective helium shell burning in a massive star. *Astronomy and Astrophysics*, 653:A55.

Iglesias, C. A. and Rogers, F. J. (1996). Updated Opal Opacities. *The Astrophysical Journal*, 464:943.

Jao, W.-C., Henry, T. J., Gies, D. R., and Hambly, N. C. (2018). A Gap in the Lower Main Sequence Revealed by Gaia Data Release 2. *The Astrophysical Journal Letters*, 861(1):L11.

Johnston, C. (2021). One size does not fit all: Evidence for a range of mixing efficiencies in stellar evolution calculations. *Astronomy and Astrophysics*, 655:A29.

Jones, W. P. and Launder, B. E. (1972). The prediction of laminarization with a two-equation model of turbulence. *International Journal of Heat and Mass Transfer*, 15:301–314.

Jørgensen, A. C. S., Mosumgaard, J. R., Weiss, A., Silva Aguirre, V., and Christensen-Dalsgaard, J. (2018). Coupling 1D stellar evolution with 3D-hydrodynamical simulations on the fly - I. A new standard solar model. *Monthly Notices of the Royal Astronomical Society*, 481(1):L35–L39.

Joyce, M. and Chaboyer, B. (2018a). Classically and Asteroseismically Constrained 1D Stellar Evolution Models of α Centauri A and B Using Empirical Mixing Length Calibrations. *The Astrophysical Journal*, 864(1):99.

Joyce, M. and Chaboyer, B. (2018b). Not All Stars Are the Sun: Empirical Calibration of the Mixing Length for Metal-poor Stars Using One-dimensional Stellar Evolution Models. *The Astrophysical Journal*, 856(1):10.

Käpylä, P. J., Rheinhardt, M., Brandenburg, A., Arlt, R., Käpylä, M. J., Lagg, A., Olspert, N., and Warnecke, J. (2017). Extended Subadiabatic Layer in Simulations of Overshooting Convection. *The Astrophysical Journal Letters*, 845(2):L23.

Khan, S., Hall, O. J., Miglio, A., Davies, G. R., Mosser, B., Girardi, L., and Montalbán, J. (2018). The Red-giant Branch Bump Revisited: Constraints on Envelope Overshooting in a Wide Range of Masses and Metallicities. *The Astrophysical Journal*, 859(2):156.

Kippenhahn, R., Weigert, A., and Hofmeister, E. (1967). Methods for Calculating Stellar Evolution. *Methods in Computational Physics*, 7:129–190.

Kippenhahn, R., Weigert, A., and Weiss, A. (2012). *Stellar Structure and Evolution*. Springer, Heidelberg, Dordrecht, London, New York.

Koch, D. G., Borucki, W. J., Basri, G., Batalha, N. M., Brown, T. M., Caldwell, D., Christensen-Dalsgaard, J., Cochran, W. D., DeVore, E., Dunham, E. W., Gautier, Thomas N., I., Geary, J. C., Gilliland, R. L., Gould, A., Jenkins, J., Kondo, Y., Latham, D. W., Lissauer, J. J., Marcy, G., Monet, D., Sasselov, D., Boss, A., Brownlee, D., Caldwell, J., Dupree, A. K., Howell, S. B., Kjeldsen, H., Meibom, S., Morrison, D., Owen,

T., Reitsema, H., Tarter, J., Bryson, S. T., Dotson, J. L., Gazis, P., Haas, M. R., Kolodziejczak, J., Rowe, J. F., Van Cleve, J. E., Allen, C., Chandrasekaran, H., Clarke, B. D., Li, J., Quintana, E. V., Tenenbaum, P., Twicken, J. D., and Wu, H. (2010). Kepler Mission Design, Realized Photometric Performance, and Early Science. *The Astrophysical Journal Letters*, 713(2):L79–L86.

Kolmogorov, A. N. (1941). The local structure of turbulence in incompressible viscous fluid for very large Reynolds numbers. [in russian.]. *Dokl. Akad. Nauk. SSSR*, 30:301–305.

Kolmogorov, A. N. (1942). Equations of turbulent motion of an incompressible fluid. *Izv. Akad. Nauk SSSR, Seria fizicheska*, VI:56–58. Translated from Russian and published within D. B. Spalding 1991.

Kolmogorov, A. N. (1962). A refinement of previous hypotheses concerning the local structure of turbulence in a viscous incompressible fluid at high reynolds number. *Journal of Fluid Mechanics*, 13:82—85.

Kolmogorov, A. N. (1968). Local structure of turbulence in an incompressible viscous fluid at very high reynolds numbers. *Soviet Physics Uspekhi*, 10(6):734–746.

Kuhfuß, R. (1986). A model for time-dependent turbulent convection. *Astronomy and Astrophysics*, 160:116–120.

Kuhfuß, R. (1987). *Ein Modell für zeitabhängige Konvektion in Sternen*. Dissertation, Technische Universität München, München.

Kupka, F. (1999a). Computing Solar and Stellar Overshooting with Turbulent Convection Models. First Tests of a Fully Non-Local Model. In Gimenez, A., Guinan, E. F., and Montesinos, B., editors, *Theory and Tests of Convection in Stellar Structure:*, volume 173, page 157.

Kupka, F. (1999b). Turbulent Convection: Comparing the Moment Equations to Numerical Simulations. *The Astrophysical Journal*, 526:L45–L48.

Kupka, F. (2007). Some open questions concerning the modelling of non-locality in Reynolds stress type models of stellar convection. In Kupka, F., Roxburgh, I., and Chan, K. L., editors, *Convection in Astrophysics*, volume 239, pages 92–94.

Kupka, F. (2009). Turbulent convection and numerical simulations in solar and stellar astrophysics. In Hillebrandt, W. and Kupka, F., editors, *Interdisciplinary Aspects of Turbulence*, volume 756 of *Lecture Notes in Physics*, pages 49–105. Springer, Berlin.

Kupka, F. (2020). Thermal convection in stars and in their atmosphere. In M. Rieutord, I. Baraffe, Y. L., editor, *Multi-Dimensional Processes In Stellar Physics*, pages 69–110. EDP Sciences Proceedings, Les Ulis.

Kupka, F., Ahlborn, F., and Weiss, A. (2022). Stellar evolution models with overshooting based on 3-equation non-local theories, I. Physical basis and the computation of the dissipation rate. *Astronomy and Astrophysics*. accepted.

Kupka, F. and Hillebrandt, W. (2009). An introduction to turbulence. In Hillebrandt, W. and Kupka, F., editors, *Interdisciplinary Aspects of Turbulence*, volume 756 of *Lecture Notes in Physics*, pages 1–20, Berlin. Springer.

Kupka, F. and Montgomery, M. H. (2002). A-star envelopes: a test of local and non-local models of convection. *Monthly Notices of the Royal Astronomical Society*, 330:L6–L10.

Kupka, F. and Muthsam, H. J. (2007a). Probing Reynolds stress models of convection with numerical simulations: I. Overall properties: fluxes, mean profiles. In Kupka, F., Roxburgh, I., and Chan, K. L., editors, *Convection in Astrophysics*, volume 239, pages 80–82.

Kupka, F. and Muthsam, H. J. (2007b). Probing Reynolds stress models of convection with numerical simulations: II. Non-locality and third order moments. In Kupka, F., Roxburgh, I., and Chan, K. L., editors, *Convection in Astrophysics*, volume 239, pages 83–85.

Kupka, F. and Muthsam, H. J. (2007c). Probing Reynolds stress models of convection with numerical simulations: III. Compressibility modelling and dissipation. In Kupka, F., Roxburgh, I., and Chan, K. L., editors, *Convection in Astrophysics*, volume 239, pages 86–88.

Kupka, F. and Muthsam, H. J. (2008). Analysing the Contributions in Moment Equations of Reynolds Stress Models of Convection with Numerical Simulations. In Deng, L. and Chan, K. L., editors, *The Art of Modeling Stars in the 21st Century*, volume 252, pages 463–464.

Kupka, F. and Muthsam, H. J. (2017). Modelling of stellar convection. *Living Reviews in Computational Astrophysics*, 3(1):1.

Kupka, F., Zaussinger, F., and Montgomery, M. H. (2018). Mixing and overshooting in surface convection zones of DA white dwarfs: first results from ANTARES. *Monthly Notices of the Royal Astronomical Society*, 474(4):4660–4671.

Landau, L. D. and Lifshitz, E. M. (2007). *Hydrodynamik*, volume VI of *Lehrbuch der theoretischen Physik*. Verlag Harri Deutsch, Frankfurt am Main.

Lanford, O. E. (1982). The strange attractor theory of turbulence. *Annual Review of Fluid Mechanics*, 14(1):347–364.

Langer, N., El Eid, M. F., and Fricke, K. J. (1985). Evolution of massive stars with semiconvective diffusion. *Astronomy and Astrophysics*, 145(1):179–191.

Langer, N., Fricke, K. J., and Sugimoto, D. (1983). Semiconvective diffusion and energy transport. *Astronomy and Astrophysics*, 126(1):207.

Launder, B. E., Reece, G. J., and W., R. (1975). Progress in the development of a reynolds-stress turbulence closure. *Journal of Fluid Mechanics*, 68:537—566.

Li, T., Bedding, T. R., Huber, D., Ball, W. H., Stello, D., Murphy, S. J., and Bland-Hawthorn, J. (2018). Modelling Kepler red giants in eclipsing binaries: calibrating the mixing-length parameter with asteroseismology. *Monthly Notices of the Royal Astronomical Society*, 475(1):981–998.

Li, Y. (2012). A k-ω Model for Turbulently Thermal Convection in Stars. *The Astrophysical Journal*, 756:37.

Li, Y. (2017). Applications of the k-ω Model in Stellar Evolutionary Models. *The Astrophysical Journal*, 841(1):10.

Li, Y. and Yang, J.-Y. (2001). Anisotropy and Dissipation of Turbulence and Their Effects on Solar Models. *Chinese Journal of Astronomy and Astrophysics*, 1:66–76.

Li, Y. and Yang, J. Y. (2007). Testing turbulent convection theory in solar models - I. Structure of the solar convection zone. *Monthly Notices of the Royal Astronomical Society*, 375:388–402.

Liou, M.-S. (1996). A Sequel to AUSM: AUSM $^+$. *Journal of Computational Physics*, 129(2):364–382.

Liou, M.-S. (2006). A sequel to AUSM, Part II: AUSM $^+$-up for all speeds. *Journal of Computational Physics*, 214(1):137–170.

Liou, M.-S. and Steffen, C. J. (1993). A New Flux Splitting Scheme. *Journal of Computational Physics*, 107(1):23–39.

Lorenz, E. N. (1963). Deterministic non-periodic flow. *Journal for atmospheric sciences*, 20:130.

Maeder, A. and Mermilliod, J. C. (1981). The extent of mixing in stellar interiors: evolutionary models and tests based on the HR diagrams of 34 open clusters. *Astronomy and Astrophysics*, 93:136–149.

Magic, Z., Serenelli, A., Weiss, A., and Chaboyer, B. (2010). On Using the Color-Magnitude Diagram Morphology of M67 to Test Solar Abundances. *The Astrophysical Journal*, 718(2):1378–1387.

Magic, Z., Weiss, A., and Asplund, M. (2015). The Stagger-grid: A grid of 3D stellar atmosphere models. III. The relation to mixing length convection theory. *Astronomy and Astrophysics*, 573:A89.

Meakin, C. A. and Arnett, D. (2007). Turbulent Convection in Stellar Interiors. I. Hydrodynamic Simulation. *The Astrophysical Journal*, 667(1):448–475.

Mellor, G. L. and Yamada, T. (1982). Development of a Turbulence Closure Model for Geophysical Fluid Problems (Paper 2R0808). *Reviews of Geophysics and Space Physics*, 20:851.

Michielsen, M., Aerts, C., and Bowman, D. M. (2021). Probing the temperature gradient in the core boundary layer of stars with gravito-inertial modes. The case of KIC 7760680. *Astronomy and Astrophysics*, 650:A175.

Michielsen, M., Pedersen, M. G., Augustson, K. C., Mathis, S., and Aerts, C. (2019). Probing the shape of the mixing profile and of the thermal structure at the convective core boundary through asteroseismology. *Astronomy and Astrophysics*, 628:A76.

Miczek, F. (2013). *Simulation of low Mach number astrophysical flows*. PhD thesis, Max-Planck-Institut für Astrophysik, Technische Universität München.

Miczek, F., Röpke, F. K., and Edelmann, P. V. F. (2015). New numerical solver for flows at various Mach numbers. *Astronomy and Astrophysics*, 576:A50.

Mironov, D. V. (2009). Turbulence in the lower troposphere: Second-order closure and mass-flux modelling frameworks. In Hillebrandt, W. and Kupka, F., editors, *Interdisciplinary Aspects of Turbulence*, volume 756 of *Lecture Notes in Physics*, pages 161–221. Springer, Berlin.

Mocák, M., Meakin, C., Campbell, S. W., and Arnett, W. D. (2018). Turbulent mixing and nuclear burning in stellar interiors. *Monthly Notices of the Royal Astronomical Society*, 481(3):2918–2932.

Moeng, C.-H. (1984). A Large-Eddy-Simulation Model for the Study of Planetary Boundary-Layer Turbulence. *Journal of Atmospheric Sciences*, 41(13):2052–2062.

Mombarg, J. S. G., Van Reeth, T., and Aerts, C. (2021). Constraining stellar evolution theory with asteroseismology of γ Doradus stars using deep learning. Stellar masses, ages, and core-boundary mixing. *Astronomy and Astrophysics*, 650:A58.

Mombarg, J. S. G., Van Reeth, T., Pedersen, M. G., Molenberghs, G., Bowman, D. M., Johnston, C., Tkachenko, A., and Aerts, C. (2019). Asteroseismic masses, ages, and core properties of γ Doradus stars using gravito-inertial dipole modes and spectroscopy. *Monthly Notices of the Royal Astronomical Society*, 485(3):3248–3263.

Montgomery, M. H. and Kupka, F. (2004). White dwarf envelopes: further results of a non-local model of convection. *Monthly Notices of the Royal Astronomical Society*, 350(1):267–276.

Moravveji, E., Aerts, C., Pápics, P. I., Triana, S. A., and Vandoren, B. (2015). Tight asteroseismic constraints on core overshooting and diffusive mixing in the slowly rotating pulsating B8.3V star KIC 10526294. *Astronomy and Astrophysics*, 580:A27.

Mosumgaard, J. R., Ball, W. H., Silva Aguirre, V., Weiss, A., and Christensen-Dalsgaard, J. (2018). Stellar models with calibrated convection and temperature stratification from 3D hydrodynamics simulations. *Monthly Notices of the Royal Astronomical Society*, 478(4):5650–5659.

Muthsam, H. J., Göb, W., Kupka, F., and Liebich, W. (1999). Interacting convection zones. *New Astronomy*, 4(5):405–417.

Muthsam, H. J., Göb, W., Kupka, F., Liebich, W., and Zoechling, J. (1995). A numerical study of compressible convection. *Astronomy and Astrophysics*, 293:127–141.

Muthsam, H. J., Kupka, F., Löw-Baselli, B., Obertscheider, C., Langer, M., and Lenz, P. (2010). ANTARES - A Numerical Tool for Astrophysical RESearch with applications to solar granulation. *New Astronomy*, 15(5):460–475.

Navier, C. L. M. H. (1822). Memoire sur les lois de mouvement des fluides. *Memoires de l'academie des sciences de l'institut de france*, 6:389.

Noll, A., Deheuvels, S., and Ballot, J. (2021). Probing core overshooting using subgiant asteroseismology: The case of KIC10273246. *Astronomy and Astrophysics*, 647:A187.

Nonaka, A., Almgren, A. S., Bell, J. B., Lijewski, M. J., Malone, C. M., and Zingale, M. (2010). MAESTRO: An Adaptive Low Mach Number Hydrodynamics Algorithm for Stellar Flows. *The Astrophysical Journal Supplement*, 188(2):358–383.

Pedersen, M. G., Aerts, C., Pápics, P. I., Michielsen, M., Gebruers, S., Rogers, T. M., Molenberghs, G., Burssens, S., Garcia, S., and Bowman, D. M. (2021). Internal mixing of rotating stars inferred from dipole gravity modes. *Nature Astronomy*.

Pedersen, M. G., Aerts, C., Pápics, P. I., and Rogers, T. M. (2018). The shape of convective core overshooting from gravity-mode period spacings. *Astronomy and Astrophysics*, 614:A128.

Pietrinferni, A., Cassisi, S., Salaris, M., and Castelli, F. (2004). A Large Stellar Evolution Database for Population Synthesis Studies. I. Scaled Solar Models and Isochrones. *The Astrophysical Journal*, 612(1):168–190.

Pinsonneault, M. (1997). Mixing in Stars. *Annual Reviews of Astronomy and Astrophysics*, 35:557–605.

Pope, S. B. (2000). *Turbulent Flows*. Cambridge University Press, Cambridge.

Prandtl, L. (1925). Bericht über Untersuchungen zur ausgebildeten Turbulenz. *Zeitschrift für angewandte Mathematik und Mechanik*, 5:136–139.

Prandtl, L. (1932). Meteorologische Anwendungen der Strömungslehre. *Beiträge zur Physik der freien Atmosphäre (Bjerknes-Festschrift)*, 19:188.

Prandtl, L. (1945). Über ein neues Formelsystem für die ausgebildete Turbelenz. *Nachrichten der Akademie der Wissenschaften zu Göttingen. Mathematisch-physikalische Klasse*, 1:6–19.

Remple, B. A., Angelou, G. C., and Weiss, A. (2021). Determining fundamental parameters of detached double-lined eclipsing binary systems via a statistically robust machine learning method. *Monthly Notices of the Royal Astronomical Society*, 507(2):1795–1813.

Renzini, A. (1987). Some embarrassments in current treatments of convective overshooting. *Astronomy and Astrophysics*, 188(1):49–54.

Reynolds, O. (1883). An experimental investigation pf the circumstances which determine whether the motion of water shall be direct or sinuous, and of the law of resistance in parallel channels. *Philosophical transactions of the royal society*, 174:935–982.

Reynolds, O. (1894). On the dynamical theory of incompressible viscous flows and the determination of the criterion. *Philosphical Transactions of the Royal Society London Series A*, 186:123–161.

Richardson, L. (1922). Weather prediction by numerical process. *Quarterly Journal of the Royal Meteorological Society*, 48(203):282–284.

Ricker, G. R., Winn, J. N., Vanderspek, R., Latham, D. W., Bakos, G. Á., Bean, J. L., Berta-Thompson, Z. K., Brown, T. M., Buchhave, L., Butler, N. R., Butler, R. P., Chaplin, W. J., Charbonneau, D., Christensen-Dalsgaard, J., Clampin, M., Deming, D., Doty, J., De Lee, N., Dressing, C., Dunham, E. W., Endl, M., Fressin, F., Ge, J., Henning, T., Holman, M. J., Howard, A. W., Ida, S., Jenkins, J. M., Jernigan, G., Johnson, J. A., Kaltenegger, L., Kawai, N., Kjeldsen, H., Laughlin, G., Levine, A. M., Lin, D., Lissauer, J. J., MacQueen, P., Marcy, G., McCullough, P. R., Morton, T. D., Narita, N., Paegert, M., Palle, E., Pepe, F., Pepper, J., Quirrenbach, A., Rinehart, S. A., Sasselov, D., Sato, B., Seager, S., Sozzetti, A., Stassun, K. G., Sullivan, P., Szentgyorgyi, A., Torres, G., Udry, S., and Villasenor, J. (2015). Transiting Exoplanet Survey Satellite (TESS). *Journal of Astronomical Telescopes, Instruments, and Systems*, 1:014003.

Rogers, T. M. (2015). On the differential rotation of massive main-sequence stars. *The Astrophysical Journal Letters*, 815:L30 (5 pp.).

Rogers, T. M., Lin, D. N. C., McElwaine, J. N., and Lau, H. H. B. (2013). Internal gravity waves in massive stars: angular momentum transport. *The Astrophysical Journal*, 772:21 (19 pp.).

Röpke, F. K., Berberich, J., Edelmann, P. F. V., Horst, L., Jones, S. W., Michel, A., and Botto Poala, A. (2018). Towards Multidimensional Hydrodynamic Simulations of Stars. In *NIC Symposium 2018*, volume 49 of *NIC Series*, pages 115 – 122, Jülich. NIC Symposium 2018, Jülich (Germany), 22 Feb 2018 - 23 Feb 2018, Forschungszentrum Jülich GmbH, Zentralbibliothek.

Rotta, J. (1951). Statistische Theorie nichthomogener Turbulenz. *Zeitschrift für Physik*, 129(6):547–572.

Roxburgh, I. W. (1978). Convection and stellar structure. *Astronomy and Astrophysics*, 65:281–285.

Roxburgh, I. W. (1989). Integral constraints on convective overshooting. *Astronomy and Astrophysics*, 211:361–364.

Roxburgh, I. W. (1992). Limits on convective penetration from stellar cores. *Astronomy and Astrophysics*, 266(1):291–293.

Roxburgh, I. W. and Kupka, F. (2007). Mixing length model of convection in stellar cores. In Kupka, F., Roxburgh, I., and Chan, K. L., editors, *Convection in Astrophysics*, volume 239, pages 98–99.

Ruelle, D. and Takens, F. (1971). On the nature of turbulence. *Communications in Mathematical Physics*, 20:167–192.

Salaris, M. and Cassisi, S. (2015). Stellar models with mixing length and T(τ) relations calibrated on 3D convection simulations. *Astronomy and Astrophysics*, 577:A60.

Salaris, M. and Cassisi, S. (2017). Chemical element transport in stellar evolution models. *Royal Society Open Science*, 4(8):170192.

Saltzman, B. (1962). Finite amplitude free convection as an initial value problem—i. *Journal of Atmospheric Sciences*, 19(4):329 – 341.

Sander, J. (1998). Dynamical Equations and Turbulent Closures in Geophysics. *Continuum Mechanics and Thermodynamics*, 10(1):1–28.

Saslaw, W. C. and Schwarzschild, M. (1965). Overshooting from Stellar Convective Cores. *The Astrophysical Journal*, 142:1468.

Schwarzschild, K. (1906). Über das Gleichgewicht der Sonnenatmosphäre. *Nachrichten von der Gesellschaft der Wissenschaften zu Göttingen, Mathematisch-Physikalische Klasse*, 195:41–53.

Schwarzschild, M. and Härm, R. (1958). Evolution of very massive stars. *The Astrophysical Journal*, 128:348–360.

Serenelli, A., Weiss, A., Cassisi, S., Salaris, M., and Pietrinferni, A. (2017). The brightness of the red giant branch tip. Theoretical framework, a set of reference models, and predicted observables. *Astronomy and Astrophysics*, 606:A33.

Shaviv, G. and Salpeter, E. E. (1973). Convective Overshooting in Stellar Interior Models. *The Astrophysical Journal*, 184:191–200.

Silva Aguirre, V., Ballot, J., Serenelli, A. M., and Weiss, A. (2011). Constraining mixing processes in stellar cores using asteroseismology. Impact of semiconvection in low-mass stars. *Astronomy and Astrophysics*, 529:A63.

Silva Aguirre, V., Basu, S., Brandão, I. M., Christensen-Dalsgaard, J., Deheuvels, S., Doğan, G., Metcalfe, T. S., Serenelli, A. M., Ballot, J., Chaplin, W. J., Cunha, M. S., Weiss, A., Appourchaux, T., Casagrande, L., Cassisi, S., Creevey, O. L., García, R. A., Lebreton, Y., Noels, A., Sousa, S. G., Stello, D., White, T. R., Kawaler, S. D., and Kjeldsen, H. (2013). Stellar Ages and Convective Cores in Field Main-sequence Stars: First Asteroseismic Application to Two Kepler Targets. *The Astrophysical Journal*, 769:141.

Snellman, J. E., Käpylä, P. J., Käpylä, M. J., Rheinhardt, M., and Dintrans, B. (2015). Testing turbulent closure models with convection simulations. *Astronomische Nachrichten*, 336(1):32–52.

Spada, F., Demarque, P., Basu, S., and Tanner, J. D. (2018). Improved Calibration of the Radii of Cool Stars Based on 3D Simulations of Convection: Implications for the Solar Model. *The Astrophysical Journal*, 869(2):135.

Spalding, D. B. (1991). Kolmogorov's Two-Equation Model of Turbulence. *Proceedings of the Royal Society of London Series A*, 434(1890):211–216.

Spiegel, E. A. and Veronis, G. (1960). On the Boussinesq Approximation for a Compressible Fluid. *The Astrophysical Journal*, 131:442.

Spruit, H. C. (2015). The growth of helium-burning cores. *Astronomy and Astrophysics*, 582:L2.

Stellingwerf, R. F. (1982). Convection in pulsating stars. I. Non linear hydro-dynamics. *The Astrophysical Journal*, 262:330–338.

Stokes, G. G. (1845). On the theories of the internal friction of fluids in motion, and of the equilibrium and motion of elastic solids. *Transactions of the Cambridge philosophical society*, 8:287–305.

Stokes, G. G. (2009). *On the Theories of the Internal Friction of Fluids in Motion, and of the Equilibrium and Motion of Elastic Solids*, volume 1 of *Cambridge Library Collection - Mathematics*, page 75–129. Cambridge University Press.

Strutt, J. W. (1916). On convection currents in a horizontal layer of fluid, when the higher temperature is on the under side. *The London, Edinburgh, and Dublin Philosophical Magazine and Journal of Science*, 32(192):529–546.

Taylor, G. I. (1923). Stability of a viscous liquid contained between two rotating cylinders. *Philosophical Transactions of the Royal Society of London. Series A, Containing Papers of a Mathematical or Physical Character*, 223(605-615):289–343.

Tennekes, H. and Lumley, J. L. (1972). *A First Course in Turbulence*. M.I.T. Press.

Tiedtke, M. (1989). A Comprehensive Mass Flux Scheme for Cumulus Parameterization in Large-Scale Models. *Monthly Weather Review*, 117(8):1779.

Timmes, F. X. and Swesty, F. D. (2000). The Accuracy, Consistency, and Speed of an Electron-Positron Equation of State Based on Table Interpolation of the Helmholtz Free Energy. *The Astrophysical Journal Supplement*, 126(2):501–516.

Trampedach, R., Stein, R. F., Christensen-Dalsgaard, J., Nordlund, Å., and Asplund, M. (2014). Improvements to stellar structure models, based on a grid of 3D convection simulations - II. Calibrating the mixing-length formulation. *Monthly Notices of the Royal Astronomical Society*, 445(4):4366–4384.

Tremblay, P. E., Ludwig, H. G., Freytag, B., Fontaine, G., Steffen, M., and Brassard, P. (2015). Calibration of the Mixing-length Theory for Convective White Dwarf Envelopes. *The Astrophysical Journal*, 799(2):142.

Turner, J. S. (1986). Turbulent entrainment - The development of the entrainment assumption, and its application to geophysical flows. *Journal of Fluid Mechanics*, 173:431–471.

van Saders, J. L. and Pinsonneault, M. H. (2012). An ^{3}He-driven Instability near the Fully Convective Boundary. *The Astrophysical Journal*, 751(2):98.

Verma, K., Raodeo, K., Basu, S., Silva Aguirre, V., Mazumdar, A., Mosumgaard, J. R., Lund, M. N., and Ranadive, P. (2019). Helium abundance in a sample of cool stars: measurements from asteroseismology. *Monthly Notices of the Royal Astronomical Society*, 483(4):4678–4694.

Viallet, M., Goffrey, T., Baraffe, I., Folini, D., Geroux, C., Popov, M. V., Pratt, J., and Walder, R. (2016). A Jacobian-free Newton-Krylov method for time-implicit multidimensional hydrodynamics. Physics-based preconditioning for sound waves and thermal diffusion. *Astronomy and Astrophysics*, 586:A153.

Viallet, M., Meakin, C., Arnett, D., and Mocák, M. (2013). Turbulent Convection in Stellar Interiors. III. Mean-field Analysis and Stratification Effects. *The Astrophysical Journal*, 769(1):1.

Viallet, M., Meakin, C., Prat, V., and Arnett, D. (2015). Toward a consistent use of overshooting parametrizations in 1D stellar evolution codes. *Astronomy and Astrophysics*, 580:A61.

Viani, L. S. and Basu, S. (2020). Examining the Relationship Between Convective Core Overshoot and Stellar Properties Using Asteroseismology. *The Astrophysical Journal*, 904(1):22.

Viani, L. S., Basu, S., Ong J., M. J., Bonaca, A., and Chaplin, W. J. (2018). Investigating the Metallicity-Mixing-length Relation. *The Astrophysical Journal*, 858(1):28.

Vitense, E. (1953). Die Wasserstoffkonvektionszone der Sonne. Mit 11 Textabbildungen. *Zeitschrift für Astrophysik*, 32:135.

Weiss, A., Hillebrandt, W., Thomas, H.-C., and Ritter, H. (2004). *Cox & Giuli's Principles of Stellar Structure. Extended Second Edition.* Cambridge Scientific Publishers, Cambridge.

Weiss, A. and Schlattl, H. (2008). GARSTEC – the Garching Stellar Evolution Code. The direct descendant of the legendary Kippenhahn code. *Astrophysics and Space Science*, 316:99–106.

Wilcox, D. C. (1988). Reassessment of the scale-determining equation for advanced turbulence models. *AIAA Journal*, 26(11):1299–1310.

Wuchterl, G. (1995). Time-dependent convection on self-adaptive grids. *Computer Physics Communications*, 89:119–126.

Wuchterl, G. and Feuchtinger, M. U. (1998). A simple convection model for selfgravitating fluid dynamics. Time- dependent convective energy transfer in protostars and nonlinear stellar pulsations. *Astronomy and Astrophysics*, 340:419–430.

Xiong, D. R. (1978). Stochastic theory of turbulent convection in pulsating variables. *Chinese Astronomy*, 2(1):118–138.

Xiong, D. R. (1979). A statistical theory of the non-local convection. *Acta Astronomica Sinica*, 20:238–245.

Xiong, D. R. (1986). The evolution of massive stars using a non-local theory of convection. *Astronomy and Astrophysics*, 167:239–246.

Xiong, D. R. (2021). Convection Theory and Relevant Problems in Stellar Structure, Evolution and Pulsation Stability Part II. Turbulent Convection and pulsation Stability of Stars. *Frontiers in Astronomy and Space Sciences*, 7:96.

Xiong, D. R., Cheng, Q. L., and Deng, L. (1997). Nonlocal Time-dependent Convection Theory. *The Astrophysical Journal Supplement Series*, 108:529–544.

Xiong, D. R. and Deng, L. (2001). The structure of the solar convective overshooting zone. *Monthly Notices of the Royal Astronomical Society*, 327:1137–1144.

Xiong, D. R., Deng, L., and Zhang, C. (2015). Turbulent convection and pulsation stability of stars - I. Basic equations for calculations of stellar structure and oscillations. *Monthly Notices of the Royal Astronomical Society*, 451:3354–3365.

Xiong, D. R., Deng, L., and Zhang, C. (2018). Turbulent convection and pulsation stability of stars - III. Non-adiabatic oscillations of red giants. *Monthly Notices of the Royal Astronomical Society*, 480(2):2698–2703.

Xiong, D. R., Deng, L., Zhang, C., and Wang, K. (2016). Turbulent convection and pulsation stability of stars - II. Theoretical instability strip for δ Scuti and γ Doradus stars. *Monthly Notices of the Royal Astronomical Society*, 457(3):3163–3177.

Zahn, J. P. (1991). Convective penetration in stellar interiors. *Astronomy and Astrophysics*, 252:179–188.

Zeman, O. and Lumley, J. L. (1976). Modeling buoyancy driven mixed layers. *Journal of Atmospheric Sciences*, 33:1974–1988.

Zeman, O. and Tennekes, H. (1977). Parametrization of the turbulent energy budget at the top of the daytime atmospheric boundary layer. *Journal of Atmospheric Sciences*, 34:111–123.

Zhang, Q. S. (2016). A Simple Scheme to Implement a Nonlocal Turbulent Convection Model for Convective Overshoot Mixing. *The Astrophysical Journal*, 818:146.

Zhang, Q. S. and Li, Y. (2012). Turbulent Convection Model in the Overshooting Region. I. Effects of the Convective Mixing in the Solar Overshooting Region. *The Astrophysical Journal*, 746:50.

Acknowledgements

First and foremost, I would like to thank my supervisor Achim Weiss for his support in carrying out this scientific work and writing this dissertation, but also for encouraging my scientific interests outside the actual thesis project. It was always possible to ask him for advice or support. I am especially grateful for his guidance through the particularly difficult times of the pandemic and his confidence in my work. Secondly, I would like to thank my collaborators Friedrich Kupka for his contribution to Chapters 3 and 4 and Johann Higl for his contribution to Chapter 5, without whom this work would not have been possible. I would also like to thank my collaborators Saskia Hekker, Sarbani Basu and Earl Bellinger, with whom I have successfully worked on projects not covered in this thesis and who I could always ask for their advice. I would like to thank the Max Planck Institute for Astrophysics for supporting my thesis project by creating a positive working atmosphere and providing all the necessary organisational requirements. Special thanks go to our secretaries and the IT group for their support. My thanks also go to the current and former members of the stellar group, with whom I have had many interesting scientific and non-scientific discussions.

I would like to thank my office mate Liliya Imasheva for many enjoyable discussions about the joys and sorrows in the life of a PhD student. Ich möchte mich bei meinen Eltern bedanken, die mich immer in allen Belangen unterstützt haben und die Voraussetzungen geschaffen haben meine Interessen bis hin zur Fertigstellung dieser Arbeit zu verfolgen. Ein besonderer Dank gilt auch meiner Freundin, die mich trotz der großen Entfernung ermutigt hat meinem Wunsch zu folgen und diese Stelle anzutreten und in vielen Dingen außerhalb der wissenschaftlichen Arbeit unterstützt hat. Abschließend möchte ich mich auch beim Ensemble Roggenstein bedanken, die mich sehr herzlich in ihren Reihen aufgenommen haben und regelmäßig für eine sehr willkommene Ablenkung gesorgt haben.